Durham University

# Durham E-Theses

## *Failure of polyhedral sandwich domes*

I. Smith

**How to cite:**

Smith, I. (1978) Failure of polyhedral sandwich domes. Masters thesis, Durham University.

**Use policy**

The full-text may be used and/or reproduced, and given to third parties in any format or medium, without prior permission or charge, for personal research or study, educational, or not-for-profit purposes provided that:

- a full bibliographic reference is made to the original source
- a https://etheses.durham.ac.uk/id/eprint/9252/ is made to the metadata record in Durham E-Theses
- the full-text is not changed in any way

The full-text must not be sold in any format or medium without the formal permission of the copyright holders.

Please consult the full Durham E-Theses policy for further details.

Academic Support Office, The Palatine Centre, Durham University, Stockton Road, Durham, DH1 3LE
e-mail: e-theses.admin@durham.ac.uk Tel: +44 0191 334 6107
https://etheses.durham.ac.uk

# FAILURE OF POLYHEDRAL

# SANDWICH DOMES

by

I. Smith

A thesis submitted for the degree of M.Sc.

The copyright of this thesis rests with the author. No quotation from it should be published without his prior written consent and information derived from it should be acknowledged.

Department of Engineering Science,
University of Durham

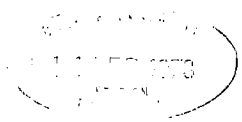

## SUMMARY

Polyhedral sandwich domes of the same span but different heights were tested, so that their elastic behaviour and ultimate failure could be studied. A detailed practical investigation was made into the structural characteristics of the joints.

A finite element technique was used to produce a numerical simulation of the elastic behaviour of the laboratory models. The numerical models were found to give a close simulation of the overall deformation and stress characteristics of the laboratory models, but simulation of the stress characteristics in the panel faces was not good.

In conclusion, recommendations were made concerning the design of polyhedral sandwich domes.

ACKNOWLEDGEMENTS

Firstly I must express my thanks to my supervisor, Dr. G.M. Parton of the Department of Engineering Science, University of Durham, for his guidance and encouragement. My gratitude extends to the members of the academic and technical staff of the Department of Engineering Science, University of Durham, for all the guidance and assistance which I have received.

Thanks must also be expressed to the staff of Durham University Computer Unit and the staff of Durham University Library.

Finally, I thank Miss J. Campbell and Mrs. J. Henderson for typing the manuscript.

CONTENTS

# 1. INTRODUCTION

The work in this thesis is part of the continuous programme of research in the Department of Engineering Science at the University of Durham into the structural behaviour of sandwich shells. The prime motivation behind this programme of work has been the interest in this type of structure shown by Dr. Parton and other members of the department.

The work of Elliott (3) covered the preliminary stages in the long term project to construct domes from arrangements of identical flat triangular sandwich panels. He made experimental investigations to study the behaviour of sandwich beams, consisting of a core of low elastic modulus and faces of relatively high elastic modulus under bending, torsional, and axial compressive loads. He compared his experimental results with simple analytical methods and thus confirmed their validity.

Bettess (2) used the finite element method to analyse a number of dome structures. He developed a triangular plate bending element to which was added a plane stress component, together with suitable apparatus for making transformations at plate boundaries. This element was used in the numerical analysis of three tetrahedral domes, a square pyramid, a hexagonal dome, and a sixteen faced four segment dome, all of which had been investigated experimentally by either Bettess or Parton (12). Agreement varied between very good and moderate.

Following the work of Bettess, Manos (10) developed seven sandwich plate bending finite elements, using two different variational approaches, the "displacement formulation" and the "mixed formulation", from which he selected four to be extended for the development of sandwich dome models. The resulting models were compared with experimental results, from five sandwich dome models, obtained by Manos and other workers at the University

1978

of Durham (Parton and Bettess). He concluded that'..... the developed numerical models, when selectively applied in the most appropriate way, with regard to their special characteristics and the nature of the problem, produce reliable results'.

All the above work was in conjunction with, and simultaneous to the work of Parton (12), who began his work on polyhedral sandwich shells in 1966. He developed several families of structures which could be constructed from assemblies of identical flat sandwich plates. 'Examples of three of these families were constructed pyramids, polyhedral domes and polyhedral vaults which were tested and their behaviour studied under static loading'. Parton developed several types of three dimensional finite elements which he used in the simulation of the laboratory models. 'A particularly detailed treatment was given to the pyramidal structures. The numerical models were found to give a close simulation of the structures and brought a better understanding of their deformation and stress characteristics, especially with respect to the effects at the joints'. He also included a practical study of the stiffness, and strength of the joints.

It was the work performed by Parton on sixteen faced, four segment polyhedral sandwich domes which provided the starting point from which the work described in this thesis was begun.

The geometry of the sixteen faced four segment domes which are considered, is developed from the 'regular dodecahedron' which has rhomboid facets. All the corners of a regular rhombohedron are spherically conformant, but when the shape is flattened the 'mid-height' corners are inside the sphere, and the base is of course above the sphere's diameter. If the 'mid-height' corners are moved out radially to the spherical surface the rhomboid facets are folded into two triangles which are still identical.

The last extension which can be performed and still produce identical facets is achieved by moving the centre of the first fold out to the sphere. This produces the four-segment dome shape shown in Fig. 1.1.

The development of the geometry follows that by Parton,(12), whose dome topology computer programme has been used to calculate the dimensions of the domes studied in this project.

It can be seen from Fig. 1.2 that as the ratio:rise:base radius,(h/r), is increased a significant increase occurs in the quantity of material required to construct a dome with a given base radius.

For the following reasons it is desirable to keep the ratio h/r as low as possible;

1. To keep the quantity of material required to construct a dome to a minimum. The saving could be considerable if, as was envisaged by Parton, domes of this type were produced on a mass production basis.
2. To keep the selfweight of the roof structure to a minimum.
3. Bearing in mind the cost of heating, it reduces the volume to be heated, and also the area over which heat losses can occur.

Domes of the type considered in this project will be subjected to three types of stresses due to applied loads, membrane stresses, shearing stresses, and bending stresses. In general the membrane action will be greater the lower the ratio h/r. The extent to which bending action will effect the structure as a whole will depend upon the ratio h/r,(5). Five groups of parameters affect the stiffness of domes of this type constructed from sandwich panels. They are geometry, joint stiffness, and stiffness with respect to membrane forces, bending and transverse shear.

Geometric stiffness is that imparted to the dome by virtue of the relative inclinations of its facets, and the inclination of the facets

to the load. This kind of stiffness is effective in resisting displacement due to bending, regardless of whether or not that bending is due to direct transverse loading or membrane thrust and/or bending at the edges of the facets, (panels).

Joint stiffness in sandwich panel structures with butt joints is a function of the joint angle, varying from almost complete moment transfer for a flat plate, to almost a simple hinge for high joint angles. Where moment transfer occurs it will tend to reduce mid panel deflections.

It should be borne in mind that shear displacements are significant in sandwich constructions of the type used in this project, and that their overall effect will be reduced the higher the value of ratio h/r.

The requirement is to find the optimum ratio h/r for a sixteen faced, four segment dome bearing in mind the interaction of all the above factors.

The following objectives were defined prior to the commencement of the work described in this thesis:

1. To study the effects upon the structural behaviour of spherically conformant 16 faced, 4 segment,domes, due to changes in ratio h/r.
2. To compare the above with that predicted by a numerical model using a finite element technique, and hence determine the extent to which that numerical model can be relied upon to predict the behaviour of these domes.
3. To determine the load carrying capacity and modes of failure for the various values of ratio h/r
4. To form some definite conclusions concerning the choice of an optimimum ratio h/r.

In order to attain the above objectives it was decided to build a series of model domes constructed of sandwich type material. These models were all to be spherically conformant sixteen faced, four segment

domes of the type described. The only variable was to be the value of ratio h/r.

The range of ratio h/r was not predetermined, only the starting point. The first and highest dome had a h/r ratio of Ø.6. This was the ratio used by Parton (12), who built and tested two similar model domes which proved to be geometrically stable.

It was anticipated that once ratio h/r had been reduced below a certain level, the structure as a whole would become unstable. For this reason the next two domes were chosen to have ratios h/r = Ø.3 and Ø.2 respectively. Finally a fourth dome was constructed which had a ratio h/r = Ø.5.

Concurrent with the tests upon the model domes, numerical models were constructed to simulate their behaviour.

As a result of work performed by other workers at the University of Durham, (2,10,12), it was realised that the role of the joints was very important. Joint tests were therefore carried out upon sample specimens of the joints used in the laboratory models, so as to give an improved understanding of their function in the complete structure.

# Typical 16 Faced, Four Segment Polyhedral Dome (h/r = 0.6)

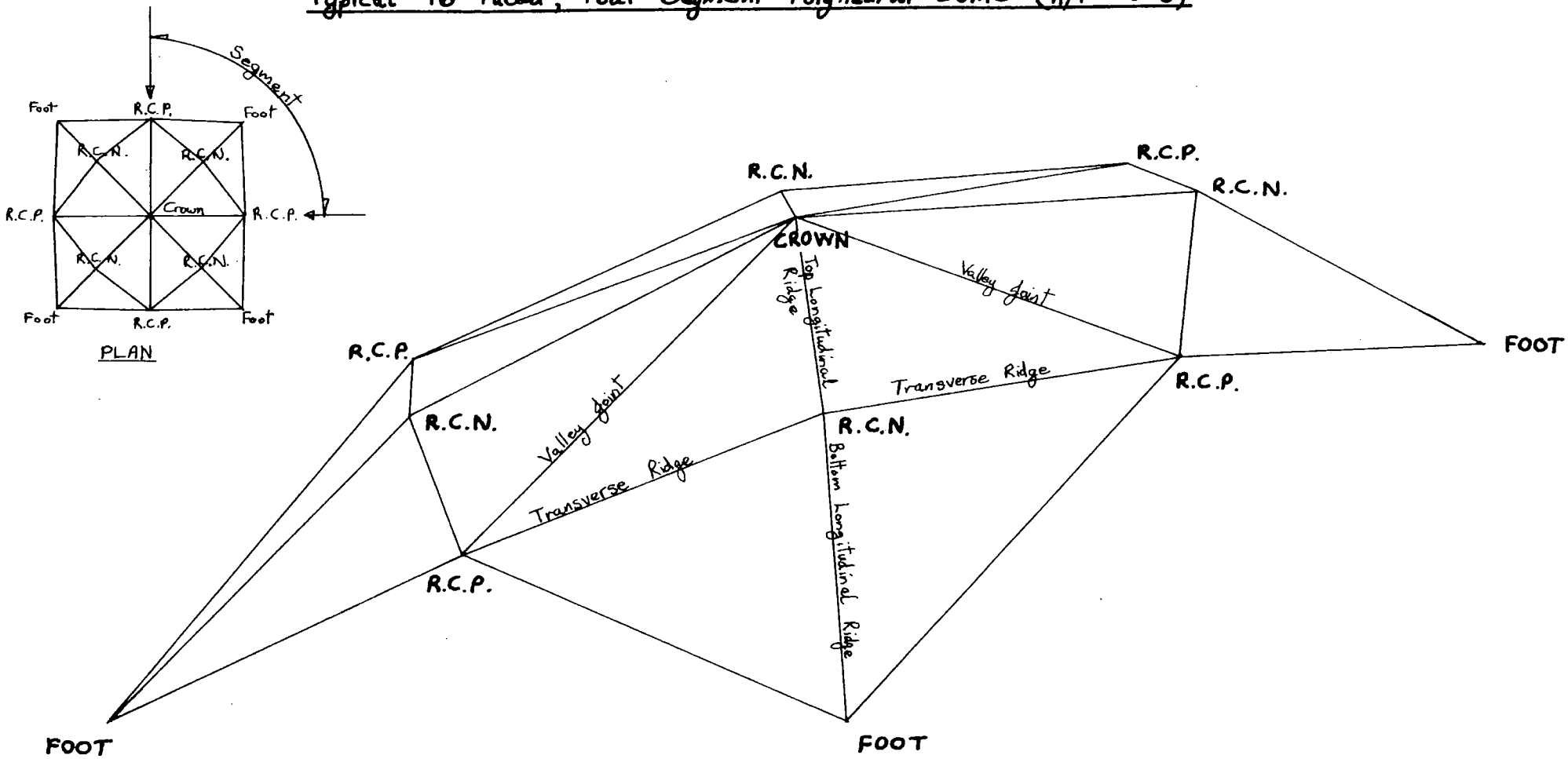


R.C.P. – Rhomb Corner Projection

R.C.N. – Rhomb Centre Node

h – Rise

r – Base Radius

FIG 1.

FIG. 1.2

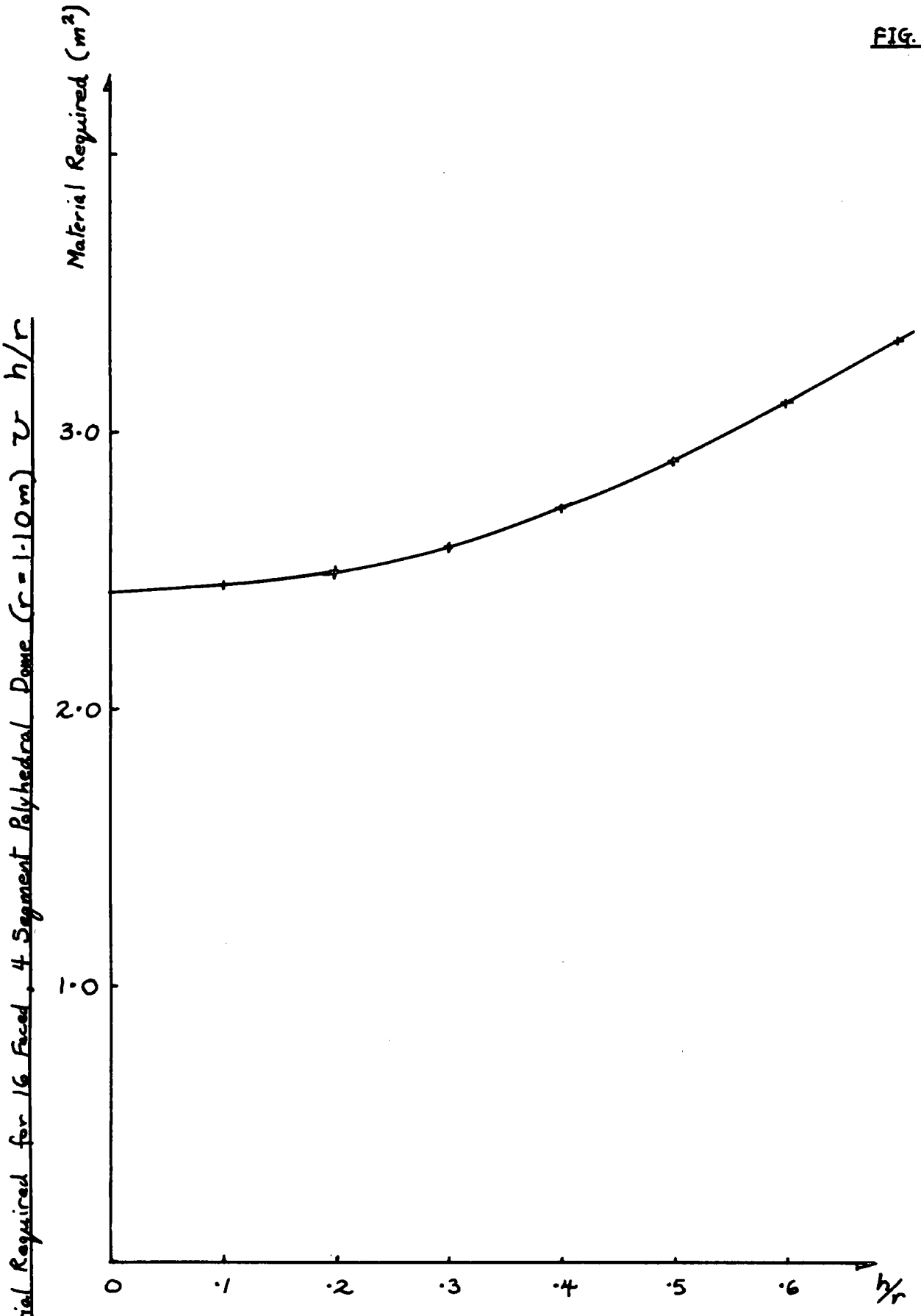
Material Required for 16 Facet, 4 Segment Polyhedral Dome (r = 1·10m) vr h/r
Material Required (m²)
3·0
2·0
1·0
0
·1
·2
·3
·4
·5
·6
h/r

## 2. MATERIALS AND CONSTRUCTION TECHNIQUES

### 2.1 Sandwich Properties

The advantages of sandwich type construction are well documented, (1,3,12,13), and are therefore not reiterated.

The following two assumptions have been made throughout the work described in this thesis:

1. All bending and membrane action is resisted by the panel faces, and stress is assumed to be constant across the depth of the faces.
2. The core resists all shear forces, and shear stress is assumed to be constant across the depth of the core.

These two assumptions have been shown (1,3,13) to be tenable for sandwich panels of the type used by the author, for which the thickness of the core is large compared with the thickness of the faces, and the elastic modulus of the faces is large compared with the elastic modulus of the core.

When choosing the materials from which the panels were to be constructed, the prime consideration was that the ratios of the core and face elastic moduli and thicknesses should be approximately the same as for a full size prototype.

### 2.2 Materials

The face material for all the sandwich domes was 'perstorp' plastic laminate with a nominal thickness of 1 mm, which is made from resin impregnated craft paper.

The face material had the following elastic constants:

| | |
|---|---|
| Elastic moduli in tension | $E_{T1} = E_{T2} = 2.743 \times 10^{10} N/m^2$ |
| Elastic moduli in bending | $E_{B1} = E_{B2} = 1.673 \times 10^{10} N/m^2$ |
| Poisson's ratio | $\mu_1 = \mu_2 = 0.280$ |
| Ultimate tensile stress | $\sigma_{uT} = 72.2 \times 10^6 N/m^2$ |
| Dimensional stability of faces; within $\pm$ 2% mean | |

The core material for all the sandwich domes was 'purlboard' with a nominal thickness of 12.7 mm, which consists of an expanded polyurethane core with two thin card faces. This core material was chosen partially because it was readily available, but primarily because it had been shown by other workers (2,10,12) to be a suitable core material for the type of models which were to be built.

The core material had the following properties:

Shear Modulus $G_{core} = 1{\cdot}449 \times 10^6$ N/m$^2$.

Dimensional stability of core; within $\pm$ 4% mean.

It was desired to attain a high span:depth ratio for the completed sandwich panels, in order that the largest possible prototype could be modelled.

The type of adhesive used was immaterial provided an adequate bond was achieved between the faces and the core. The adhesive should have no pronounced viscoelastic properties. Therefore rubber based adhesives were not suitable.

The adhesive used was "Aerolite 332' a urea-formaldehyde adhesive, with a powder hardener 'type W.148', which is a woodworking adhesive suitable for fixing veneers and laminates.

All the elastic constants for the above materials were derived from laboratory tests performed by the author, using techniques developed by other workers at Durham University, (3,12).

## 2.3 Model Dimensions

The size of the test bed upon which the domes were constructed dictated that the models should be not greater than 1.6 Øm square, (section 3.2). Using the "Dome Topology Program' developed by Parton (12) it was found that the best cutting efficiency for a standard 2.44 m x 1.22 m sandwich board was achieved using a series of domes with a base radius of 1.1Ø m.

Twelve dome faces could be cut from a single sandwich board, for domes of this base radius for which the ratio $h/r \leqslant 0.6$

## 2.4 Construction Method

### 2.4.1 Panel Construction

The panels were constructed by bonding two perstorp faces to a purlboard core, using the aerolite 332 adhesive.

During the manufacture of dome 1 the panels were subjected to a pressure of approximately 0.10 $MN/m^2$, and the panels of subsequent domes to a pressure of approximately 0.20 $MN/m^2$. The adequacy of the resulting bonds has since come into question, and in retrospect these pressures seem inadequate, (manufacturers recommended pressures for applying veneers and thin decorative laminated plastics to plywood, blockboard, etc., are 0.35 - 0.42 $MN/m^2$). Pressures greater than 0.20 $MN/m^2$ were not used in the manufacutre of the sandwich boards becuase they were found to produce excessive permanent deformation in the core. However this type of problem is unlikely to be acute in large scale sandwich domes as a much more rigid core material would be used in their construction, e.g. expanded polyvinyl chloride, and the faces could be expected to have much higher local stiffness.

### 2.4.2 Construction of Segments

Sandwich panels, which formed the individual faces of the polyhedral sandwich domes, were cut to shape using a circular saw and the edges bevelled to the correct mitre angles using an electric planing machine.

The segments of the domes were constructed by glueing together the four constituent panels, on a timber former which ensured that they mated in the correct configuration. The panels were butt jointed using a resin based woodworking adhesive. The internal segment joints were completed by applying a 50 mm wide G.R.P. coverstrip to both surfaces of the joints.

These G.R.P. coverstrips consisted of a single layer of 50 mm fabric reinforcement bonded using polyester resin.

The internal sement joints were those which are subsequently referred to as ridge joints.

Timber edge beams were attached to that edge of each bottom panel which was not to be connected to another panel, i.e. the edge between the R.C.P. and the segment foot, (Fig. 2.1). It was necessary to stiffen the free edges of the bottom panels so as to prevent excessive displacements in the vicinity of these edges. The benefit from such members is most marked when loads are applied directly to the bottom panels. In a full scale sandwich dome this stiffening would probably be provided by the structure to which the dome was attached.

2.4.3 Erection of Domes

The segments were supported at their bases by the feet arrangements described in Section 3.4, and at the crown by a temporary support of adjustable height. The central support was adjusted so as to produce a small gap along the inter segment joints, (valley joints, Fig. 1.1). The segments were then brought together by lowering the central support.

The valley joints were completed in situ, and are discussed fully in Section 4.2

## Edgebeams Dome 1

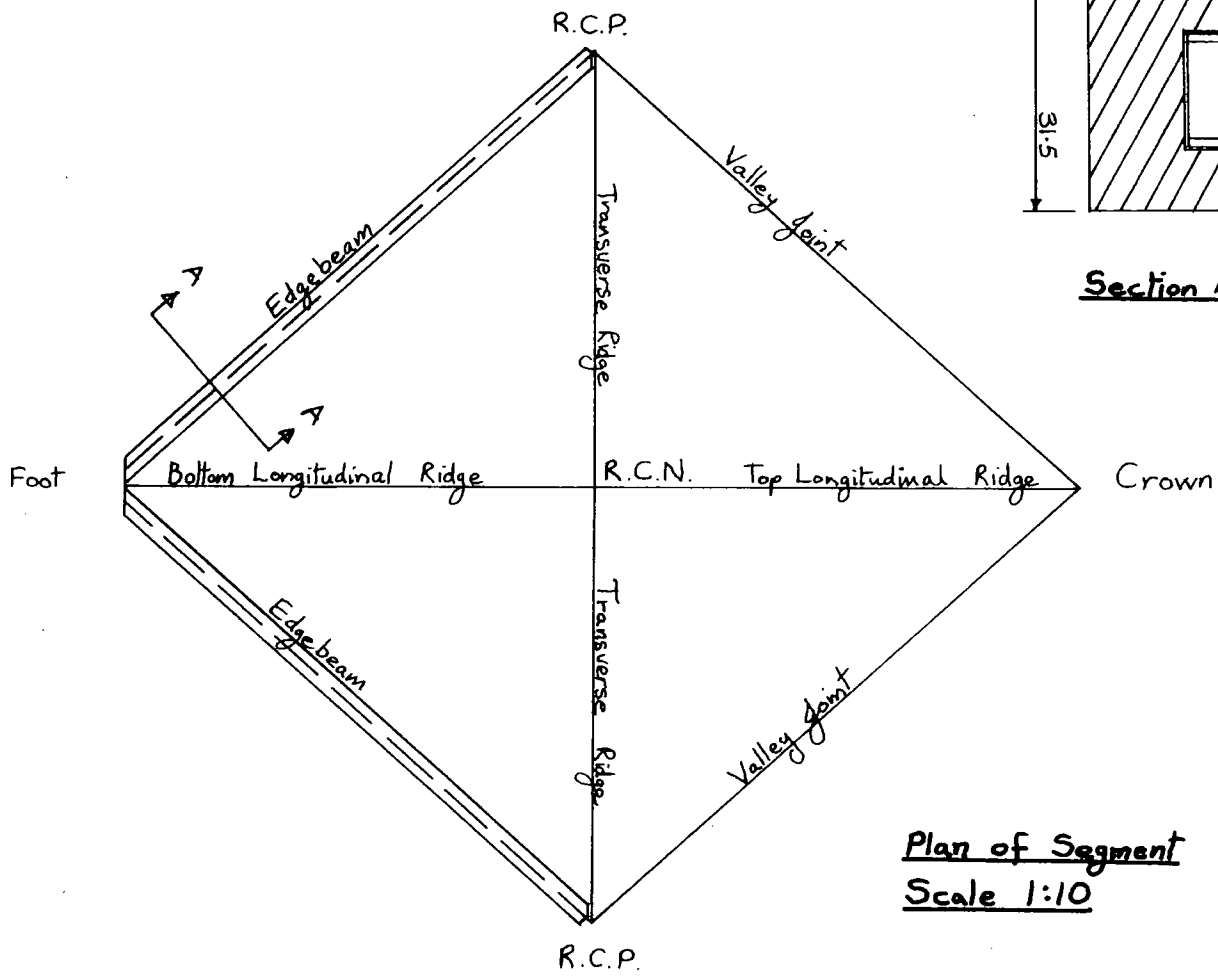


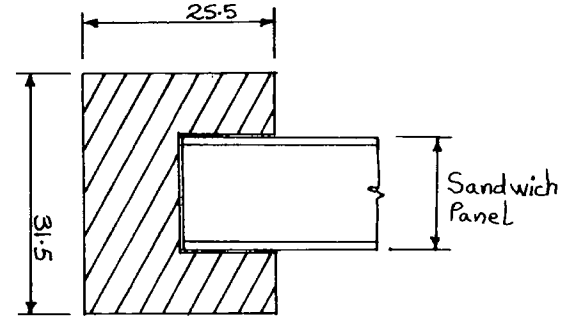


Section AA through edgebeam

Plan of Segment
Scale 1:10

FIG. 2.1

## 3. DOME TESTING APPARATUS

### 3.1 Loading System (for tests to destruction)

#### 3.1.1 Choice of Loading System (for tests to destruction)

From the outset it was realised that it was difficult to simulate the service loading conditions for polyhedral shells. Previous experience (12) had shown that the most critical condition for shell failure could be achieved most readily by applying "inward" loads over the upper panel surfaces. A symmetrical loading system was chosen because in most cases the service loads would have an approximately symmetrical pattern. It was decided to load the top panels only as it was felt that this would be most likely to induce a general instability due to downward loading (12).

Throughout all the loading tests performed the load was applied at the panel centroids via three point loading crabs the feet of which formed an equilateral triangle with 100 mm sides. The feet transmitted the load to the surface of the panels over an area 38 mm in diamter, Fig. 3.1 shows the orientation of the loading crabs relative to the panel edges.

A choice existed between a system of vertical or a system of radial loads. The nett effect of both types of loading would be to force the crown and load points in towards the centre of the dome, as shown by Parton (12), and Manos (10). The behaviour of the domes would be similar in both cases. The radial loading system was chosen for two main reasons. Firstly because wind loading is assumed to act normal to the surface of a structure, and the domes approximate to spheres. Secondly, because equal loads could be applied simultaneously to each of the eight top panels via tensioned cables using a single hydraulic jack. (A much more complicated arrangement would be required for a vertical loading

system which was to be capable of applying all eight loads simultaneously).

A further choice existed with regard to the loading of the domes. The sandwich panels exhibit visco-elastic behaviour. Two types of loading sequence could be used to study the behaviour of the domes. Instantaneous loads could be applied, the loading being released once elastic displacements had been recorded. The magnitude of the load would then be increased and the procedure repeated until a load intensity at which the dome failed was reached. Alternatively a load could be applied continuously, the magnitude being increased once increases in displacements due to time dependent effects had substantially ceased. This would be continued until the dome failed.

The two different load sequences would almost certainly lead to different modes of failure. A general failure of the structure is most likely to occur when viscous effects are allowed to develop, causing a relaxation of local stress concentrations due to instantaneous loads. It was therefore decided that the second alternative should be adopted.

Instantaneous displacements were extracted from a continuous record of displacement with time since the application of the load, which enabled an approximation to be made to the elastic behaviour, (i.e assuming that the total displacements are small).

It should be remembered that, when considering the stability of a structure, it is the worst possible loading situation which must be considered.

3.1.2 Use of Loading System (for tests to destruction)

Fig. 3.2 shows the general arrangement which was used to load the domes to destruction. To enable the load to be applied radially, the line of action of the load cables was varied by adjusting the radius of the outer ring of pulleys.

The most difficult problem in using the loading system was ensuring that the tension in all of the load cables was the same. To ensure that this was so, the following procedure was followed:

1. Using the selfweight of the load hanger and the hydraulic jack, the tension screws at the load crabs, (Fig. 3.2) were adjusted so that the top plate of the load hanger was level. At the same time care was taken to ensure that the top of the load cell just cleared the bottom of the loading beam.
2. A load was applied and maintained, approximately 200 N/Panel. The lengths of the cables were equal to within $\pm$ 2% mean. The tension $T_i \propto 1/L_i^2$, therefore e the error in $T_i$ due to variations in the length of cable $\leqslant$ 4%.
3. The load cables were vibrated, and provided the tension in all of the cables was the same, their natural frequencies $f_i$ would be the same. The tension in the cables was adjusted by means of the tension screws at the load crabs. Tension $T_i \propto f_i^2$, therefore setting an arbitrary value of $\pm$ 5% from mean as a tuning accuracy, the total variation in $T_i \leqslant$ 10% from mean. This was an acceptable limit for two reasons. Firstly, slight variations in the symmetry of the loading should be of relatively minor importance, as demonstrated by Manos (10). Secondly, once the cables are in tension all subsequent load increments should be equally distributed, provided the load cables behave elasticly, the load hanger remains vertical, the cable lengths are approximately equal, and the dome structure deforms symmetrically. As the load intensity is increased the magnitude of any asymmetry in the loading should be reduced.
4. Once the cable frequencies have been balanced loading can commence.

It was found that for 2.08 mm diameter cable variations in the natural frequency f could be easily detected to within $\pm$ 5% for a load

intensity of 200 N/Panel.

With a loading system of this nature the lines of action of the applied loads remain constant except for movement due to displacement of the load points. Therefore no corrections are required to the displacement readings provided the load point displacements are small.

### 3.1.3 Determination of the Natural Frequency of the Load Cables

#### 3.1.3.1 Dome 1

The cable frequencies were determined by matching the source frequency against a signal of constant frequency produced by a waveform generator, using a procedure similar to that employed by Madeiros (9). The vibrations from the cable were picked up using an ordinary crystal microphone, and fed via an audio amplifier onto the Y axis of an oscilloscope. A signal of constant frequency was fed onto the X axis of the oscilloscope from the waveform generator. When the two frequencies were matched an elliptical Lissajous figure was formed on the screen of the oscilloscope. Madeiros gives a detailed account of the interpretation of the Lissajous figures. Due to the effects of resonance in the dome it was found that the best results were obtained by first defining half the source frequency. This had the added advantage that the waveform generator could be read more accurately at lower frequencies, (logarithmic scale).

Due to the damping effect by the dome upon the cable vibrations it was found necessary to sustain the note using a 'double base' bow.

The dome structure acted as a sounding board amplifying the note produced by the cable vibrations to the extent where the pitch could be clearly detected by the unaided ear.

#### 3.1.3.2 Dome 2

It was found during the balancing of the load in the cables of dome 1,

that the frequencies could be matched as accurately by ear as when using an oscilloscope and waveform generator. The frequencies of the cables of dome 2 were therefore merely matched by ear. It was now not necessary to sustain the note by bowing, the cables were vibrated by means of plucking at their midpoint to produce the first harmonic.

3.1.3.3 Domes 3 and 4

In the case of domes 3 and 4 heavier cables were used,3.04 mm diameter. This had the advantage of a much reduced cable extension, which increased the amount of dome displacement that could be accommodated by the loading arrangement. This was of particular advantage with the more flexible domes. The heavier cable had a much reduced natural frequency, compared with the 2.08 mm diameter cable used for domes 1 and 2, for the same load intensity. It was no longer possible to match the cable frequencies satisfactorily by ear.

A simple but effective solution was found using an electromagnet connected to a waveform generator. The electromagnet was placed a small distance, (5-10mm), from the centre of the cable, and the frequency of the current varied using the generator. The cable began to resonate when the generator frequency was a multiple of the cable's natural frequency. Resonance of the cable could be detected by both the unaided ear and the naked eye. With experience an observer can soon find which harmonic he has detected.

It was estimated that the natural frequency of a cable could be measured to within $\pm$ 5% at a load intensity of 200 N/Panel.

In the case of each model the cables were checked at regular intervals to identify the development of any asymmetry in the load distribution.

## 3.2 The Test Bed

Fig. 3.3 shows the layout of the test bed upon which the domes were constructed. The test bed consisted of two sturdy laboratory benches, arranged so that a pair of opposite sides of the dome spanned the length of the benches, with the dome straddling a space between. The benches served to raise the models from the ground, providing sufficient clearance below the dome for the loading arrangement, and for general working convenience. The benches were held together using a dexion frame which completely encircled them, and was located just below the level of the working surface.

While testing dome 3, additional dexion framing was provided between the bases of the benches to prevent overturning due to large outward horizontal thrust at the feet of the dome.

## 3.3 Dial Gauge Configuration

### 3.3.1 Dome 1

In Fig. 3.4 dial gauges 1 to 8 constitute the dial gauge configuration used for dome 1. The dial gauges measured displacements to the nearest 0.01 mm, and were supported on a substantial dexion framing which covered the dome. Displacement at a load point was measured along the line of the load cable.

### 3.3.2 Dome 2

As a result of observations made during the testing of dome 1, gauges 9, 10 and 11 were added. Gauges 10 and 11 were added to measure horizontal displacement along the base diagonals. It was thought that with a dome of low h/r ratio, there might occur a significant amount of outward radial yielding of the feet in the horizontal plane.

### 3.3.3 Dome 3

Following observations made while testing domes 1 and 2 it was decided that the displacement of a third load point should be monitored as a check upon the symmetry of the domes behaviour. Load point 7 was chosen as this was on the side of the dome remote from load points 1 and 2.

### 3.3.4 Dome 4

During load series 1 and 2, (Section 6.3.4), the dial gauge configuration was the same as for dome 3.

As dome 4 was the final dome in the series it was decided to measure the displacements of several additional points during load series 3, (Section 7.4.1). Additional dial gauges were located along the edges of panels 1 and 9 in order to observe the bending along these edges. Displacement readings were taken at each of the three feet of the loading crabs at load points 1 and 2, so that the magnitude of the translation of the line of the loads could be observed.

Fig. 3.5 shows the revised dial gauge configuration for load series 3.

## 3.4 Dome Feet

Using a downward symmetrical loading arrangement the only horizontal reaction at the feet should be radially outward. It was decided that the dome supports should satisfy the following requirements:

1. No moment transfer from the dome to the supporting structure .
2. No outward radial movement to be permitted .
3. Elastic adjustment to be permitted tangential to the base circle.

The feet were bolted to the test bed, (Section 3.2).

### 3.4.1 Foot Arrangement Dome 1

Fig. 3.6 shows the foot arrangement which was used for dome 1. This arrangement functioned satisfactorily in the case of dome 1.

It was realised that the ultimate horizontal thrust would be much greater for dome 2 than for dome 1. The feet were strengthened as shown in Fig. 3.7, but these strengthening precautions proved inadequate and two of the feet failed, as shown in the photograph, (Fig. 3.7), at a load intensity of 1019 N/Panel. The principal reason why the feet proved inadequate was that the strength of the structure had been underestimated.

3.4.2 Revised Foot Arrangement Domes 2,3 and 4

Fig. 3.8 shows the revised foot arrangement for dome 2, which was also used when testing domes 3 and 4. This substantially stronger arrangement has proved completely satisfactory.

3.5 Assessment of Loading System (for tests to destruction)

In general the loading system performed well. The final arrangement as used in the tests on domes 3 and 4 proved highly satisfactory.

A problem which arose was the provision of adequate fastenings at either end of the load cables. The first clamping system adopted was to crimp copper tubing, with an internal diameter slightly larger than that of the cable, onto the cable using a vice. This system failed twice while testing dome 1, (Section 7.1.1). As dome 2 was expected to be weaker than dome 1 a similar system was adopted using a double layer of copper tubing and a heavy duty crimping machine. The cable was knotted at the load crab end in addition to the copper clamps. Unfortunately a failure occurred at the load hanger end of one of the cables, (Section 7.2.1). These failures were more of an inconvenience than a disaster, and merely resulted in the loading having to be restarted on completion of repairs. A satisfactory solution was found by the time dome 3 was tested. A bulldog type of clip was used, in conjunction with a heavier cable.

Following the test to destruction on dome 2, it was found necessary

to strengthen the pulley platform, (Fig. 3.2), by the addition of 3mm steel plates to both faces.

---

This loading system has much to recommend it and modified versions could be used for testing other similar types of models.

---

## 3.6 Laboratory Conditions

All tests upon the model domes were performed in a laboratory which had no external walls. It was assumed that there were no significant variations in temperature, relative humidity and air pressure at any stage during the period covering the test programme. This assumption was based upon the experience of previous workers at the University of Durham, Bettess (2), and Parton (12), who, working under similar conditions with similar types of materials in the same laboratory, had monitored the temperature and relative humidity over a long period and found that there was not much variation in either.

FIG 3·1

# Orientation of Loading Crabs Relative to the Panel Edges (Dome 1)

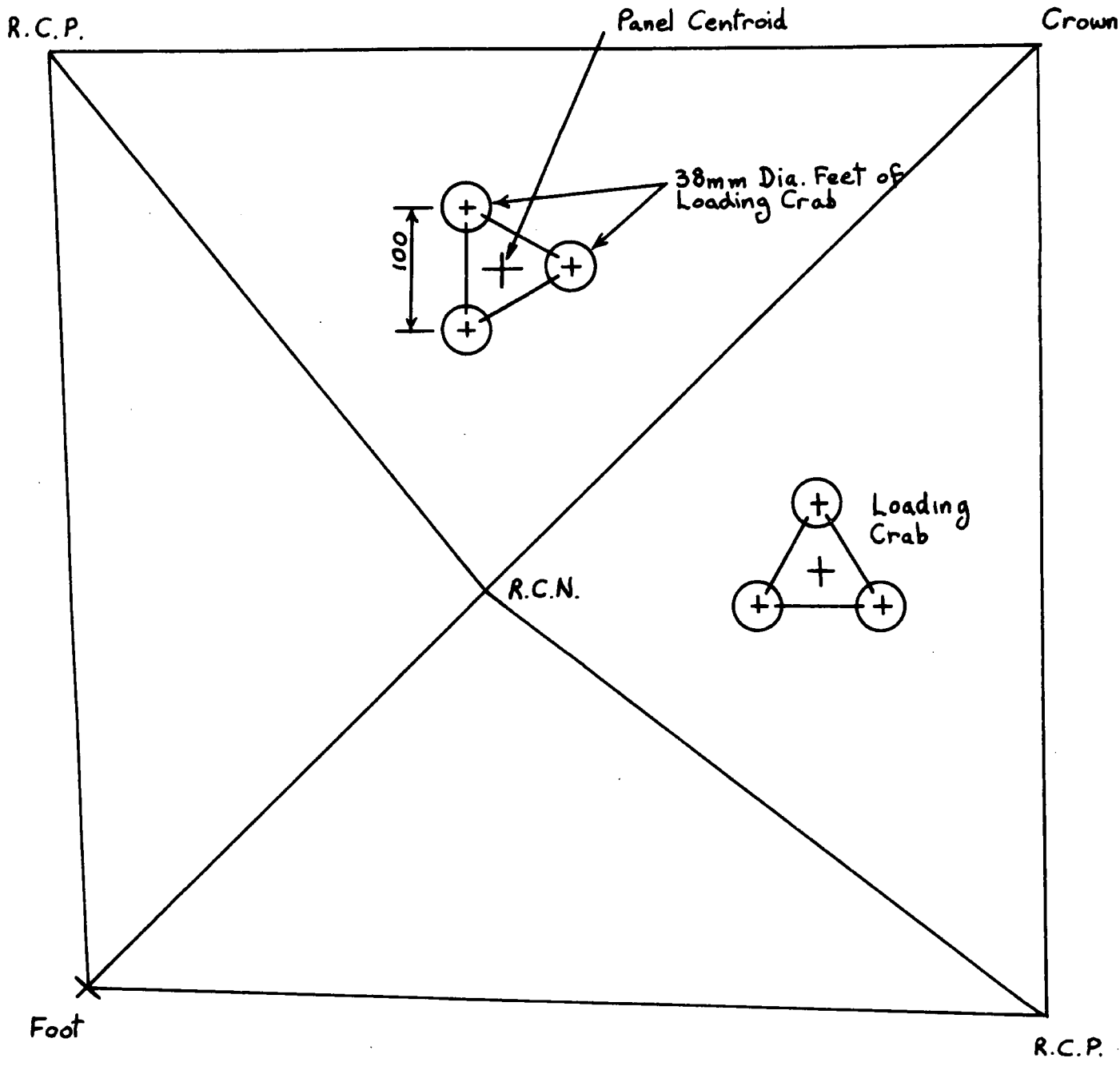


Scale 1:5

# Loading Arrangement

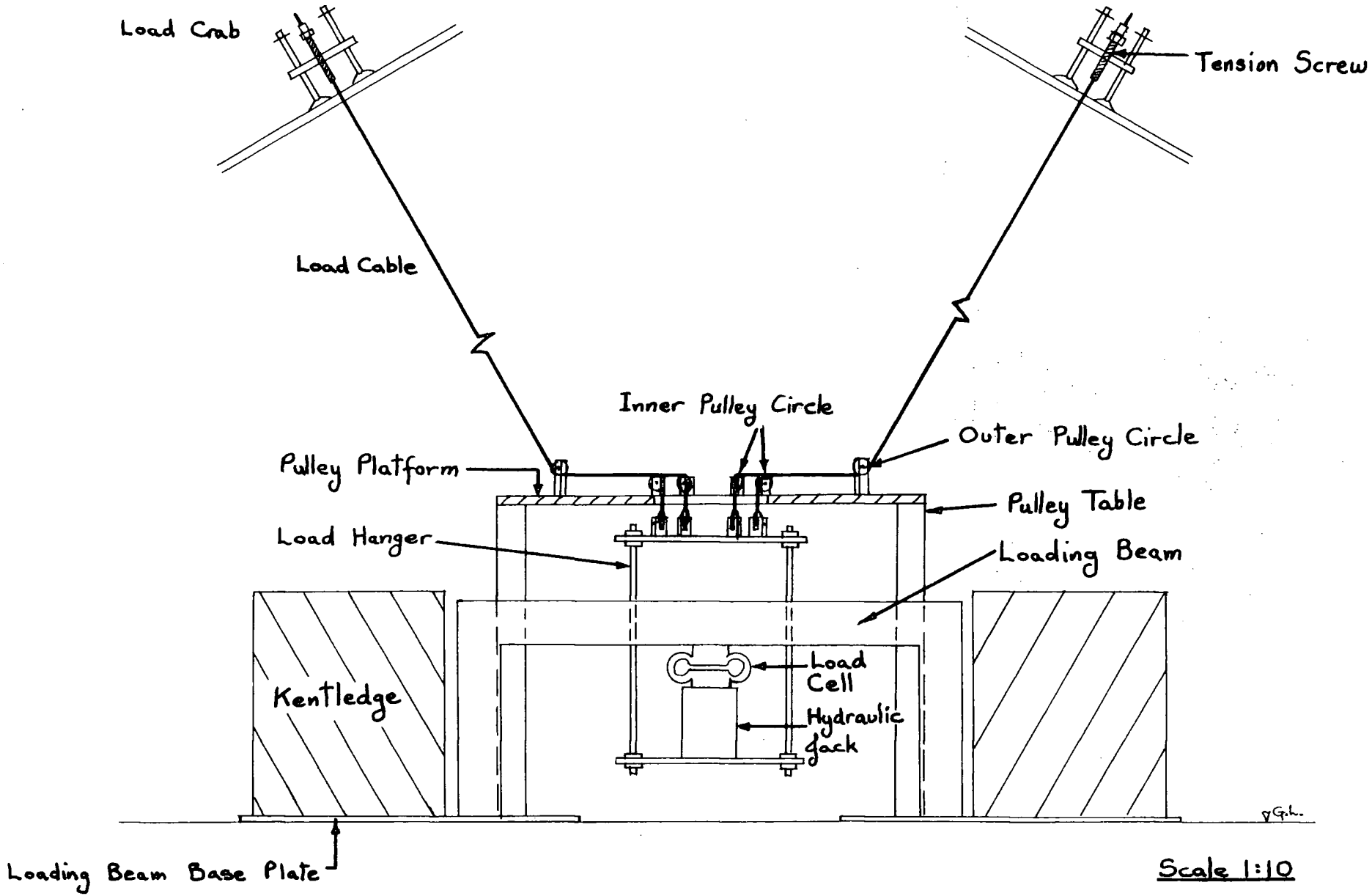


Scale 1:10

FIG. 3.2

# Test Bed Layout

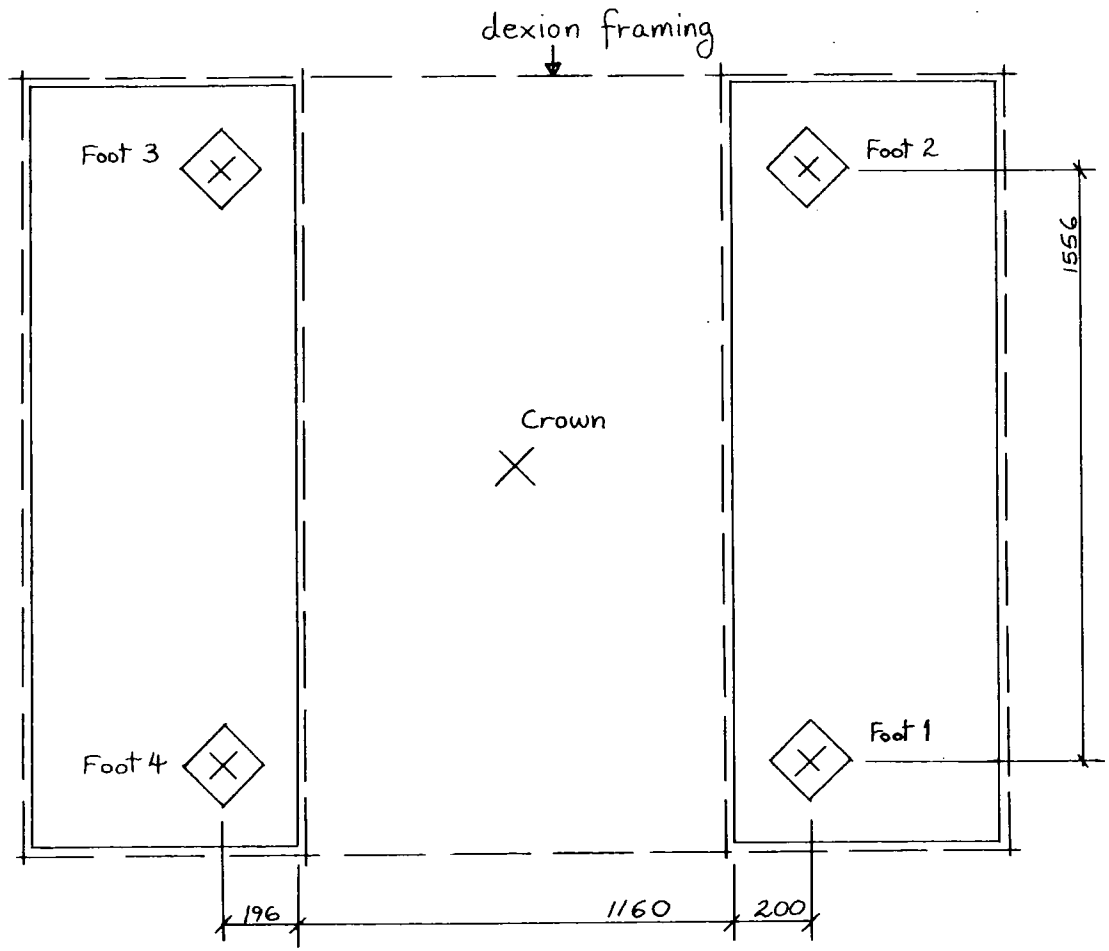


Scale 1:20

FIG 3.3

FIG. 3.4

## Dial Gauge Configuration Domes 1, 2 & 3

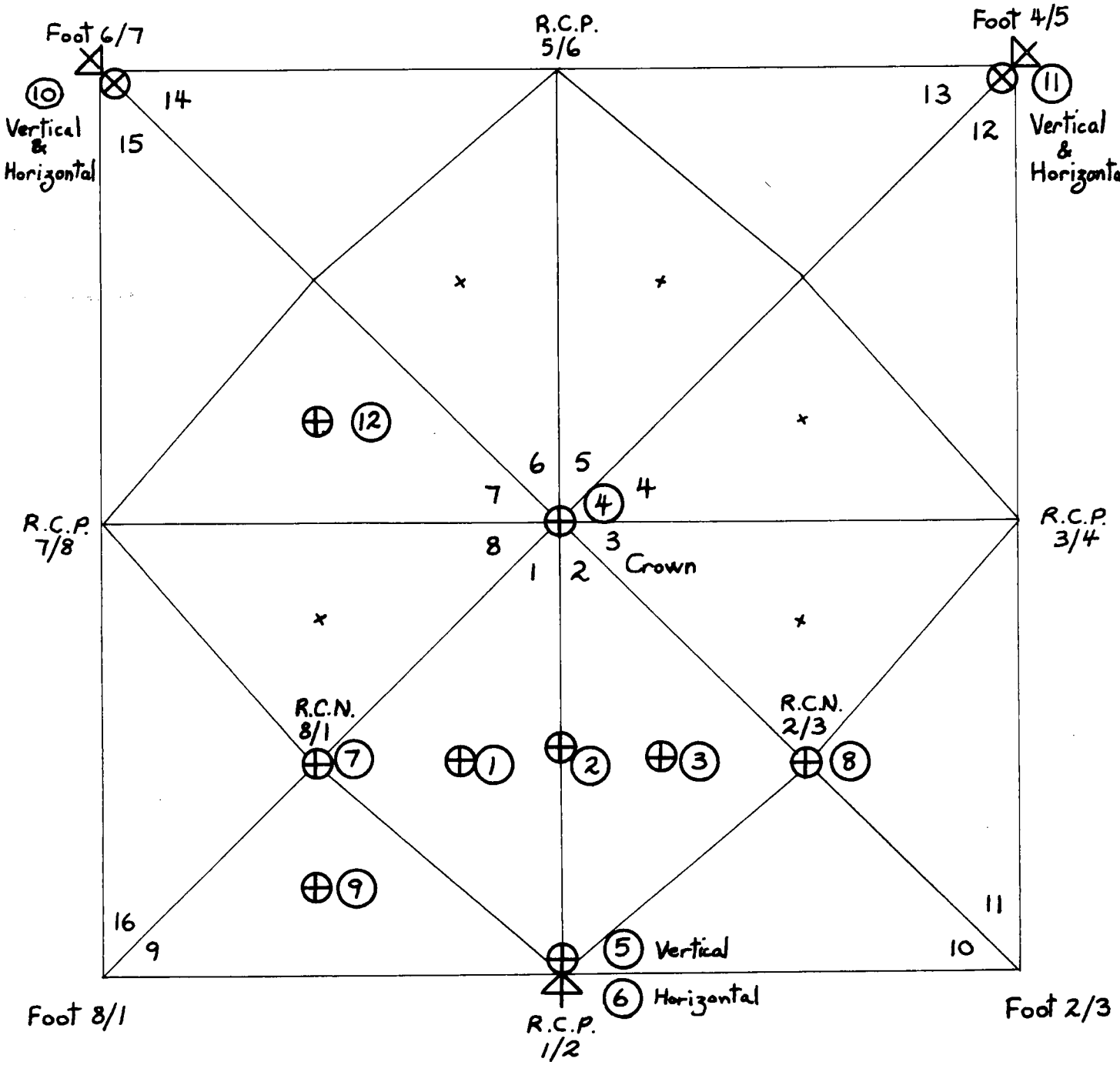


1 - 16 Panel Numbers

(1) - (12) Gauge Numbers

⊕ & ⏃ Gauge Locations

FIG. 3.5

## Dial Gauge Configuration Dome 4

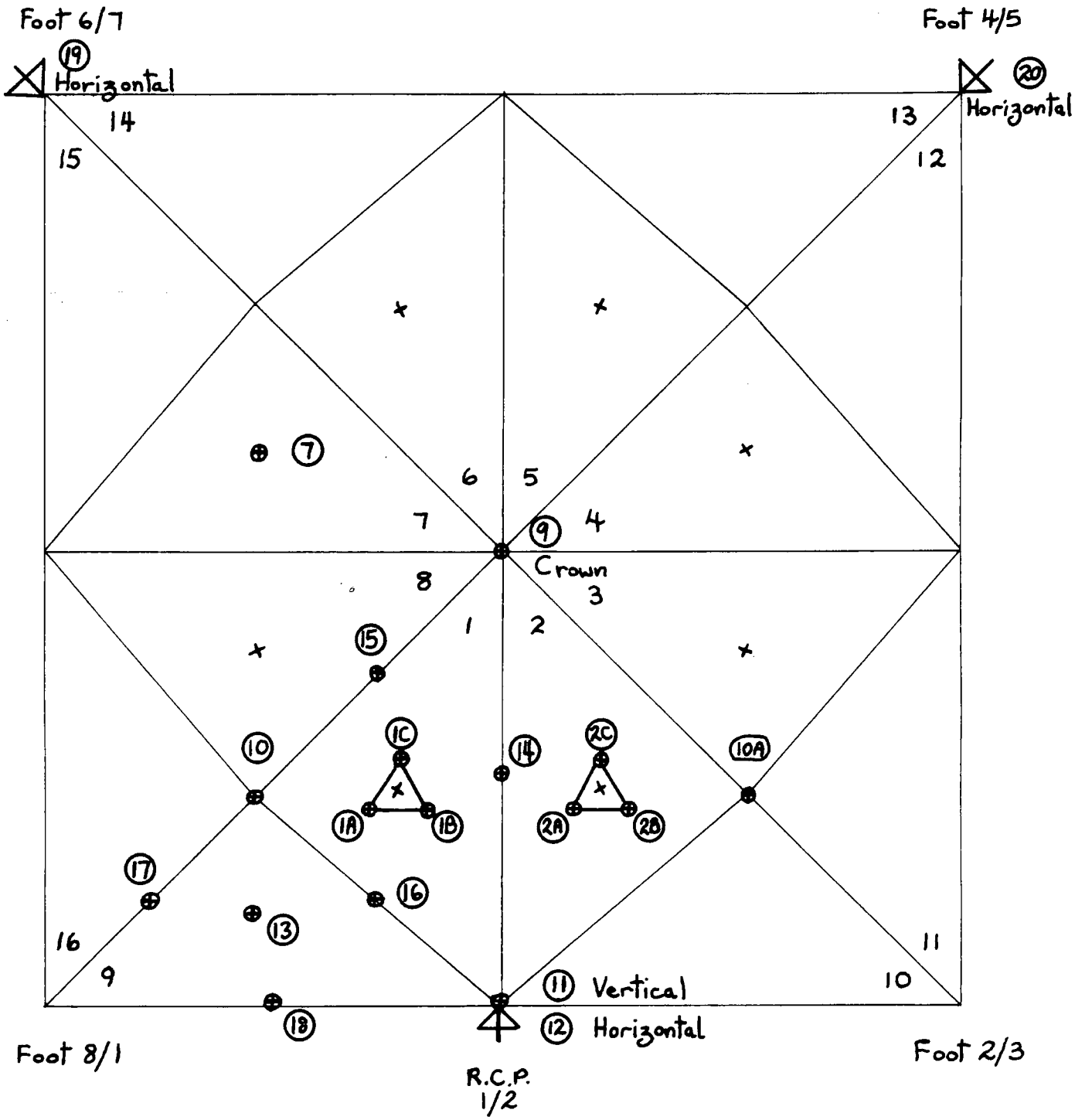


1 - 16 Panel Numbers

(1A) - (20) Gauge Numbers

⊕ & ⏃ Gauge Locations

# Foot Arrangement Dome 1

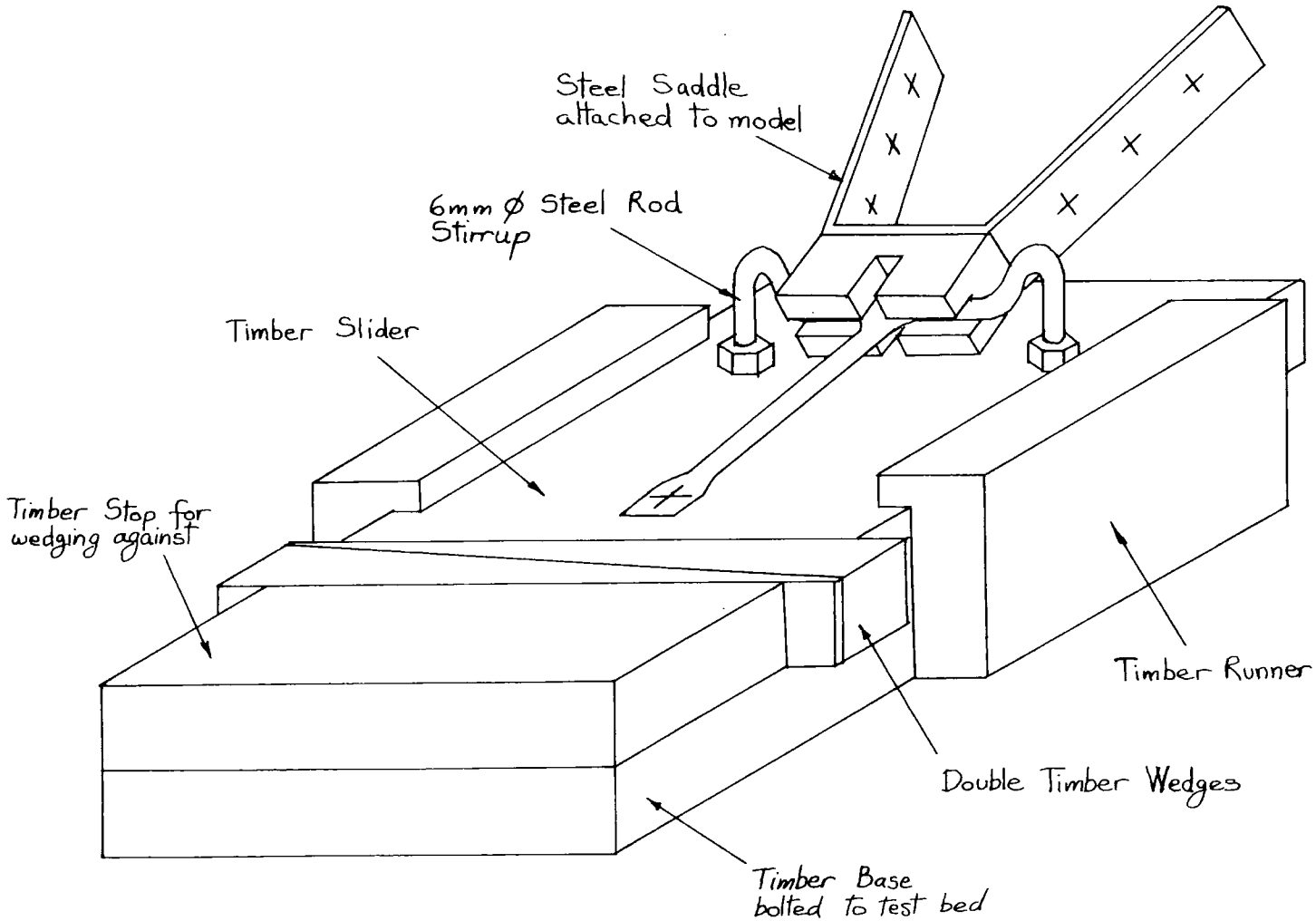


Scale 1:2

FIG.3.6

Modified Foot Arrangement Dome 2 (First test to destruction) showing Mode of Failure

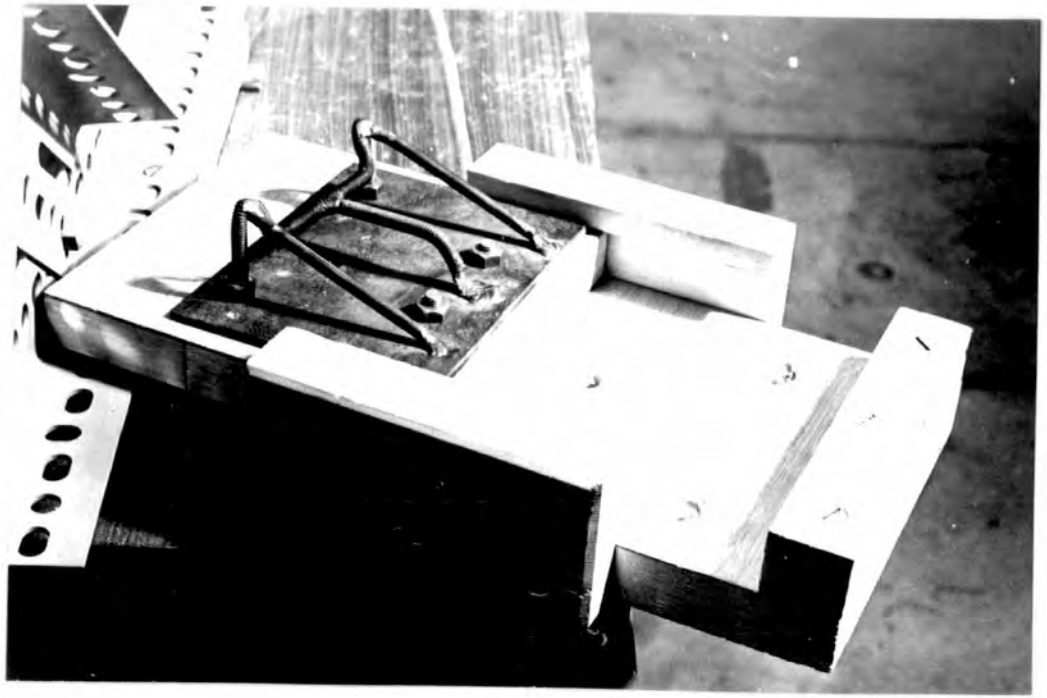

FIG. 3.7

# Foot Arrangement Domes 2 (repeat load series 3), 3 & 4

FIG. 3·8

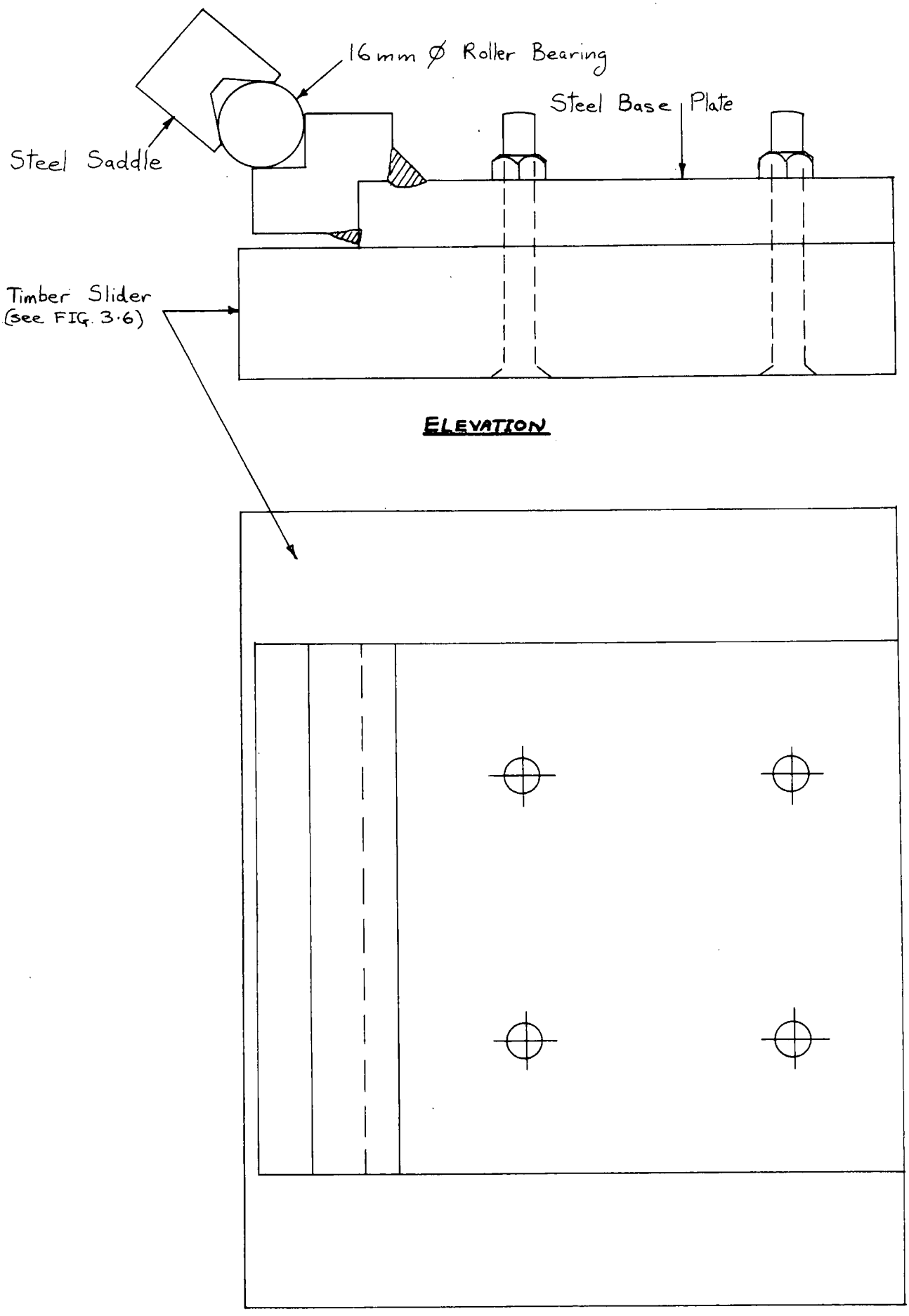


ELEVATION

PLAN

Scale 1:1

## 4. JOINTS

As mentioned in Section 1.0, the joints have a considerable influence upon the structural behaviour of the domes. In this section the characteristics of the joints used in the model domes will be discussed.

### 4.1 Butt Joints with G.R.P. Coverstrips

Fig. 4.1 shows the construction of the butt joints which have been used for the internal segment joints of all the domes that have been constructed. A series of tests were carried out upon test lengths of sandwich panel which contained this type of butt joint.

#### 4.1.1 Tension Tests on Butt Joints with G.R.P. Coverstrips

Three flat 100 mm wide specimens were tested to destruction, two were constructed using the type of glass fibre bandage used in the construction of dome 1 and the third using the type of bandage used in subsequent domes. The polyester resin used was the same in each case. The tension tests were performed using a "Denison Testing Machine", the load being applied as rapidly as possible so as to reduce the effects of time dependent deformation, (duration of each test approximately 2 minutes).

Table 4.1 summarises the results of these tests.

In each case failure was due to shearing of the face/coverstrip bond. The ultimate strength of the joint in tension depended upon the quality of this bond, which had an average ultimate shear strength of $1.44 \times 10^6$ N/m$^2$.

A separate series of tests had shown that the coverstrip had an elastic modulus and ultimate tensile strength of $6.0 \times 10^9$ N/m$^2$ and $120 \times 10^6$ N/m$^2$ respectively.

#### 4.1.2 Bending Tests on Butt Joints with G.R.P. Coverstrips

Joint specimens 250 mm wide were tested using the arrangement shown in Fig. 4.2 which subjected the joint to pure bending. These tests were

similar to those performed by Parton (12).

Figs. 4.3 and 4.4 show the graphs of Applied Moment (Nm/m) $\upsilon$ Angular Rotation at the Joint ( $\Theta_{RAD} \times 10^{-3}$), for a moment opening, and a moment closing the joint respectively. The rotations shown are those due solely to the joint's flexibility. Figs. 4.5 and 4.6 show the nature of the forces acting at the joint for a moment opening, and a moment closing the joint respectively.

Two major points emerged from these tests: the flexibility of the joints increased with the joint angle and with the magnitude of the applied moment; and the joint is substantially more flexible when the moment is closing the joint.

There are two factors which cause the rotation at the joint due to bending; straining of the coverstrips, and deformation of the core.

For a moment which opens the joint the section is increased due to core flexibility which causes a reduction in the bending stress in the faces at the joint. For a moment which closes the joint the section at the joint is reduced due to core flexibility which causes an increase in the bending stress in the faces at the joint. This deformation due to core flexibility is the main cause of the disparity between the flexibility of a joint when subjected to a moment which opens and a moment which closes the joint.

Elimination of the rotation at a joint depends upon the prevention of rotation due to straining of the coverstrips which, compared to the faces, have a low elastic modulus, and maintaining the depth of the section during bending. The former could be eliminated to a large extent by continuing the face material across the joint, which could be achieved using a material such as G.R.P. for the faces, and the latter could be achieved to a large extent by using a more rigid core material.

Figs. 4.7 and 4.8 show graphs of Ultimate Load (Nm/m) $\gamma$ Joint Angle ($\theta^{\circ}$), and the modes of failure for a moment which opens and a moment which closes the joint respectively. For a moment opening the joint the ultimate load capacity falls sharply with increases in the joint angle above $30^{\circ}$. Core penetration is a potential mode of failure for joint angles $\leqslant 15^{\circ}$, but for joint angles $> 15^{\circ}$ the overwhelming problem is that of a tensile failure of the core material, Fig. 4.5. For a moment closing the joint there is a steady decrease in the ultimate load as the joint angle is increased. For joint angles $\leqslant 15^{\circ}$ core penetration is a problem, but for joint angles $> 15^{\circ}$ shearing of the face/coverstrip bond and/or compressive failure of the core material are the most likely causes of failure, Fig. 4.6.

## 4.2 Valley Joints

As the valley joints were formed in-situ, not only had they to perform their normal functions as joints, but they were also required to act as construction aids during the erection of the domes. Bearing this dual function in mind, several different valley joint assemblies were tried by the author.

### 4.2.1 Dome 1

Fig. 4.9 shows the joint detail which was to be used in dome 1. It was intended that the bottom aluminium coverstrip be fixed at one side of the joint prior to the erection of the dome. The segments of the dome were to be connected, once they had been located in their correct position, by inserting pop rivets in pre-drilled holes at the other side of the joint. However when this was attempted it was soon apparent that this was not a workable solution.

The edges of the panels which met at the valley joints were not straight. These edges had waviness along their length with amplitudes

of up to 2mm and wavelengths of between 0.5 and 2.0 x joint length. It had been intended that the 'pop rivets' be used to draw the panel edges together so that the top panels were co-planar at the lines of the valleys, but this proved impossible.

Fig. 4.10 shows the joint detail which was actually used. The bolts which pass through the panels were tightened to bring the panels into line and level along the valleys. When the top coverstrips were applied, polyester resin was forced down between the edges of the panels. Upon dismantling the dome it was found that an estimated 30% of the area of the core, and 40% of the length of the bottom faces were randomly bonded across the valley joints by the polyester resin.

The valley joints proved satisfactory during subsequent tests upon the dome, (Sections 6.0 and 7.1.1).

4.2.2 Dome 2

Following the experience gained during the testing of dome 1, and the tests upon butt joints, (Section 4.1), which were performed during the intervening period between the construction of domes 1 and 2, a new valley detail was used when constructing dome 2, Fig. 4.11. Core penetration had been found to be a problem for flat joints such as the valley joints of domes 1 to 4. Such a failure can destroy the coverstrip and/or the core at the compression face of a joint, and can cause core/face bond failure at that face, (Section 7.1.1, Fig. 4.5).

It was considered that the aluminium coverstrips at the underside of the valley joints of dome 1 had little structural significance in the completed dome, and they were therefore omitted from dome 2.

A shear connector strip was inserted between the panels as shown in Fig. 4.11. The segments were lowered together so that they closed

onto the strip which was to transfer cross plate shear across the valley joints, and prevent core penetration. Two aluminium tie strips were placed across the joints, one adjacent to each end of the valleys. These tie strips were fastened to the panels at either side of the joint using 6 mm diameter bolts. The dome segments were then pulled into line and level by tightening these bolts. The joints were completed by applying G.R.P. coverstrips to their top faces. During the application of these coverstrips polyester resin was forced down between the edges of the panels and the shear connector strips. A length of drafting tape along the bottom face of the joint acted as a resin trap. The carpet tacks in the shear connector strips, Fig. 4.11, were observed to tear the core material along the line of the joints when the segments were brought together during the erection of the dome. For this reason it was considered that the polyester resin was the main ingredient in the successful shear connection which was achieved.

When dome 2 was tested to destruction the valley joints performed perfectly satisfactorily, until at a load intensity of 864 N / Panel the valley joints began to fail in tension at their bottom faces due to bending across these joints. The test to destruction was stopped when two of the dome's feet failed at a load intensity of 1019 N / Panel. As the dome was not damaged, apart from randomly distributed tensile fractures along approximately 20% of the undersides of the valley joints, it was repaired and retested, (Section 7.2.1).

The valley joints were repaired by inverting the dome and applying a G.R.P. cover strip to their bottom faces. The value of adequate coverstrips had been clearly demonstrated.

No further problems were encountered with respect to these joints.

4.2.3 Domes 3 and 4

Fig. 4.12 shows the valley joint detail used when constructing domes 3 and 4. It was the same as for dome 2 following the provision of a bottom coverstrip, except that the shear connector strip was replaced by a plain aluminium anti-penetration strip.

This joint detail proved to be satisfactory during the tests upon domes 3 and 4, (Sections 6.0 and 7.0).

4.2.4 Valley Joint Stiffness

The valley joints, which incorporated aluminium strips, had a significant stiffening effect against cross plate displacement in the top panels adjacent to these joints. The stiffening effect of these joints has therefore been included for in the numerical analyses for domes 1 to 4, (Section 8.0).

4.3 Buckling of Ridge Joints

In domes 2 and 3 the top longitudinal ridge joints failed due to buckling adjacent to their R.C.Ns., (Figs. 7.6 and 7.11). In both cases the buckling was located between a line passing between adjacent load crabs on either side of the ridge and the R.C.N. of a failed ridge. The buckling in the top longitudinal ridges was located closer to the R.C.Ns. in dome 3 than in the case of dome 2. This indicated that the joint configuration at the R.C.Ns. was less stable in dome 3 than in dome 2. The ability of the ridge joints to resist buckling is a function of the geometric stiffness of the dome, which for a spherically conformant dome is proportional to the ratio h/r.

One of the ridges of dome 4 buckled, but this was as a direct result of a failure in one of the panels associated with that ridge, (Section 7.4.1).

The included angles of the ridges of the domes were as follows:

| | |
|---|---|
| dome 1 | $153.73^{o}$ |
| dome 2 | $164.14^{o}$ |
| dome 3 | $168.96^{o}$ |
| dome 4 | $156.53^{o}$ |

As ridge stability was not a problem in domes 1 and 4, it would appear that the transformation from stable to unstable ridges lies somewhere between the geometries of domes 4 and 2.

Taking into account the performance of the ridges of all the domes, the stability of the ridges is liable to be critical if they have an included angle in excess of $157^{o}$.

4.4 Assessment of Joint Performance

The behaviour of the joints is somewhere between that of a moment transferring joint, and a simple hinge. An almost flat panel joint has a behaviour very close to that of a continuous flat plate. For relatively high joint angles, particularly in the case of a moment closing the joint, the behaviour approaches that of a simple hinge. Thus there is clearly a difficulty in analysing numerically the behaviour of complex structures which incorporate joints of the type studied herein, (Section 8.0).

Two practical considerations have emerged concerning the construction of polyhedral sandwich domes:

1. Butt joints in sandwich panels, which have an included angle in excess of $165^{o}$ should include an anti-penetration strip.
2. If unstiffened ridges have an included angle in excess of $157^{o}$, the failure of the dome will be "triggered" by buckling across this joint.

FIG. 4·1

## Butt Joint

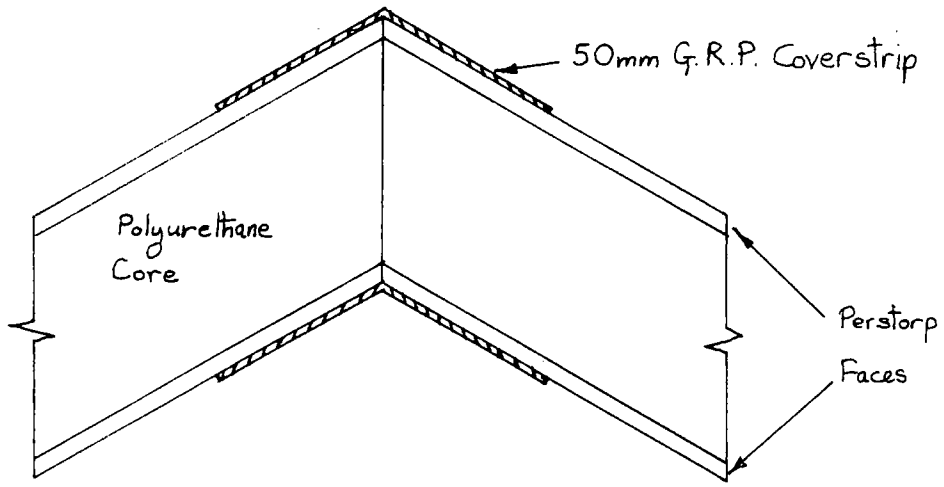


Scale 2:1

FIG. 4·2

## Testing Arrangement for Bending Tests on Butt Joints

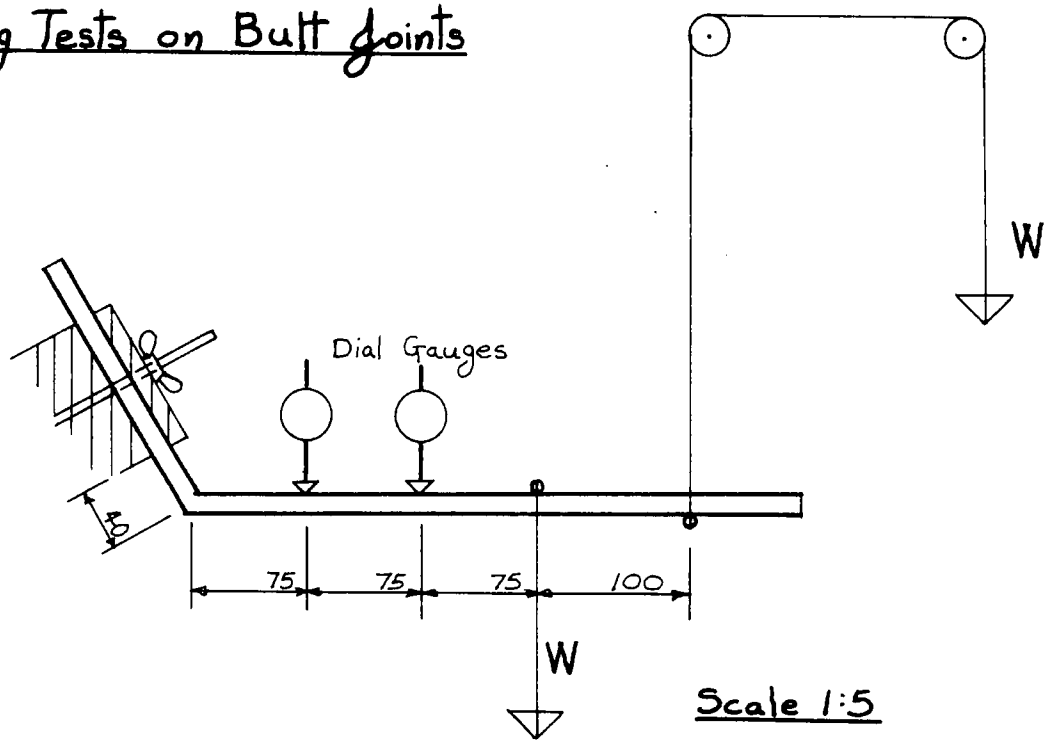


Scale 1:5

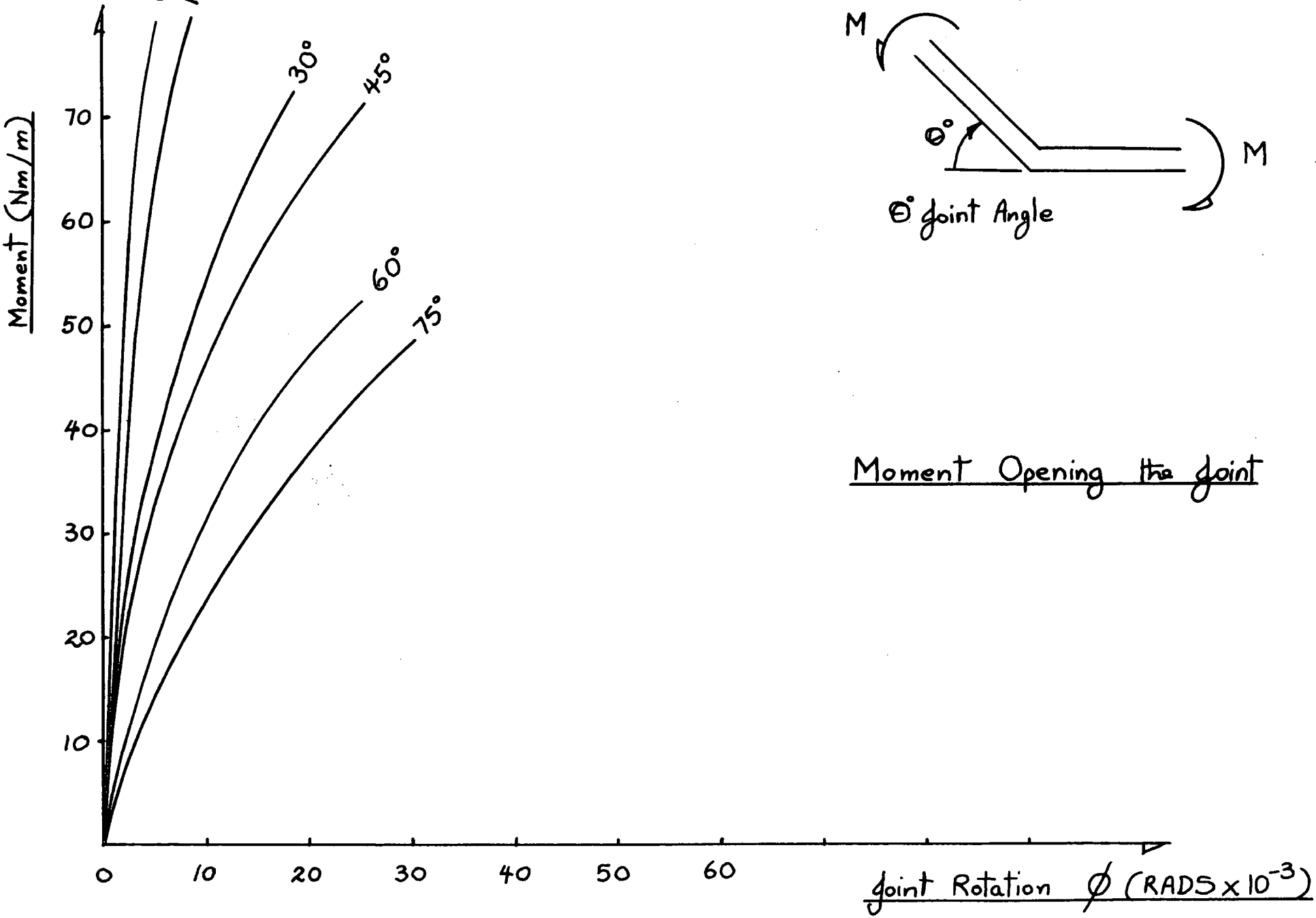





Moment Opening the joint

FIG. 4.3

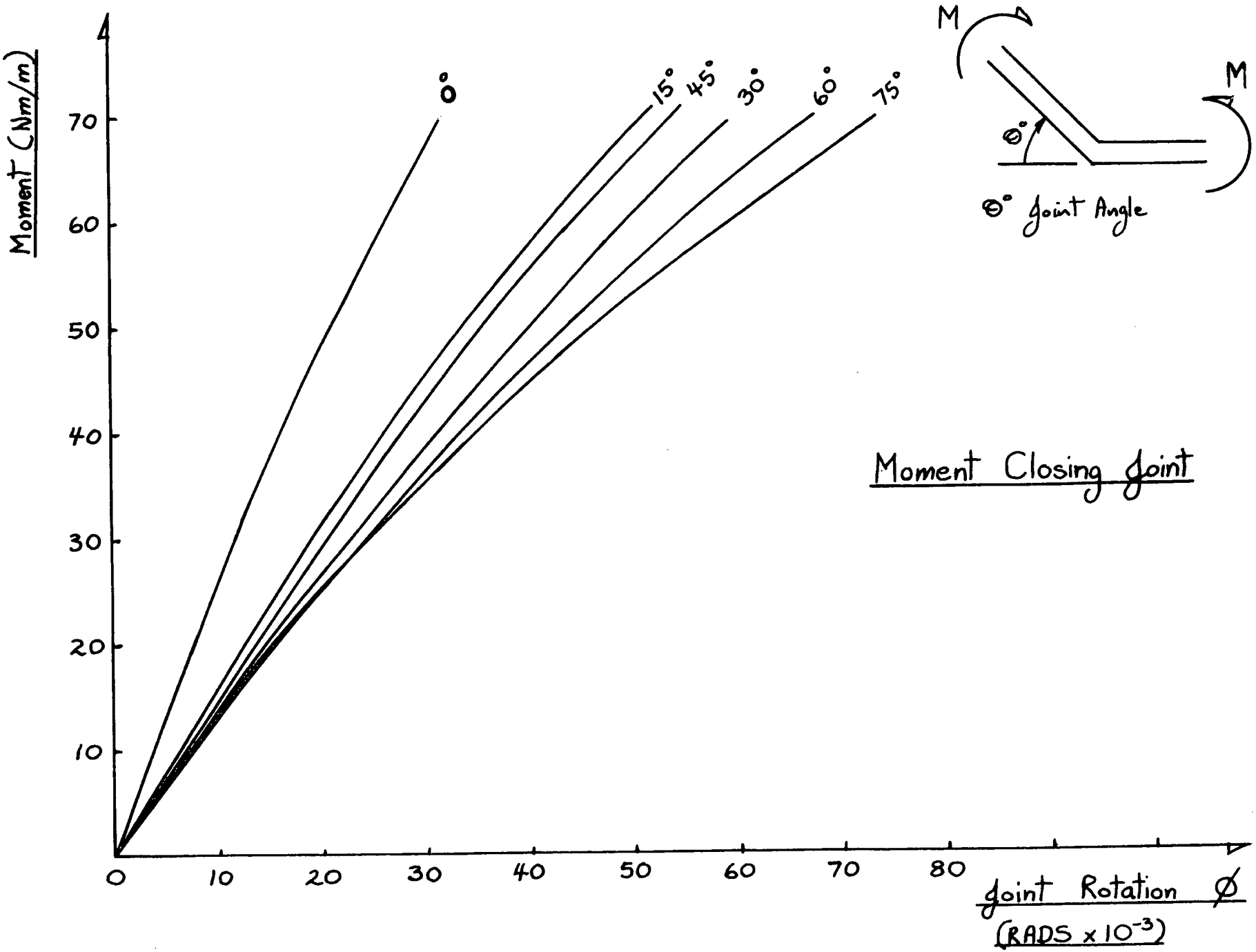
Moment (Nm/m)
70
60
50
40
30
20
10
0
10
20
30
40
50
60
70
80
0°
15°
45°
30°
60°
75°
joint Rotation Ø
(RADS x 10⁻³)
M
M
Θ°
Θ° joint Angle
Moment Closing joint

FIG. 4.4

## Behaviour of Butt Joints Subjected To Pure Bending

### Moment Opening Joint

FIG. 4·5

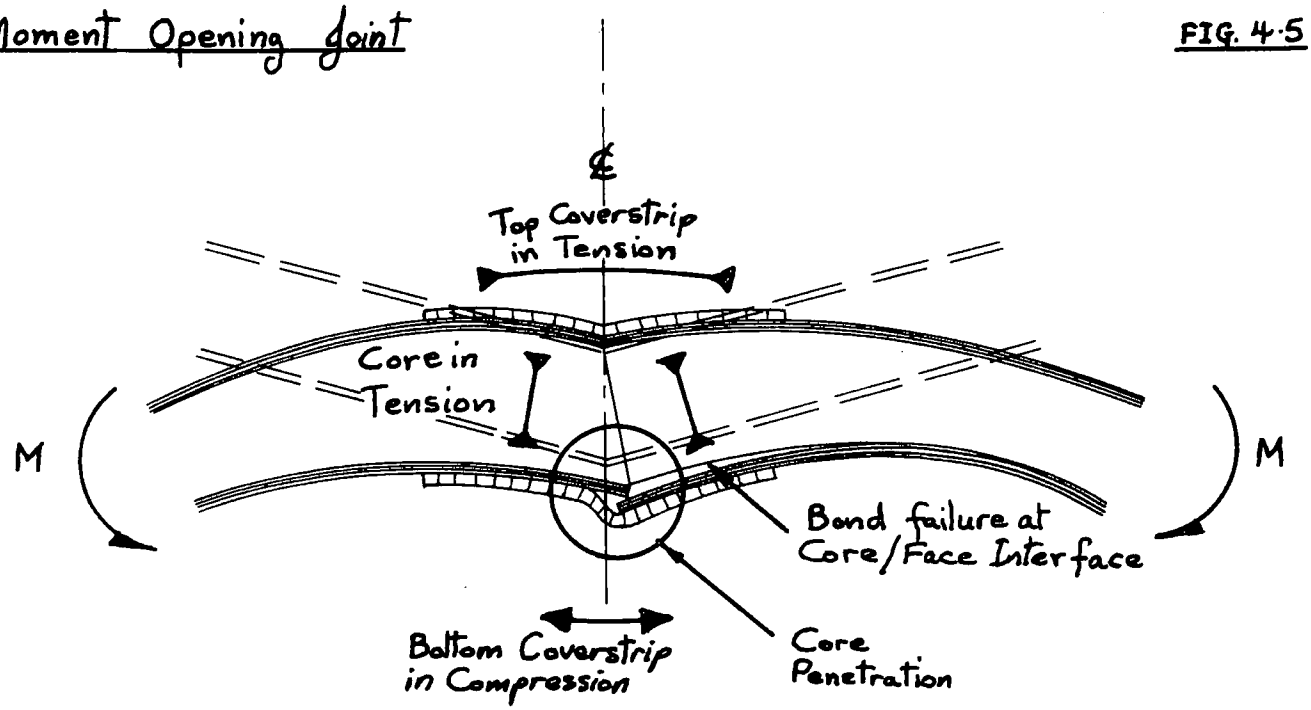


### Moment Closing Joint

FIG. 4·6

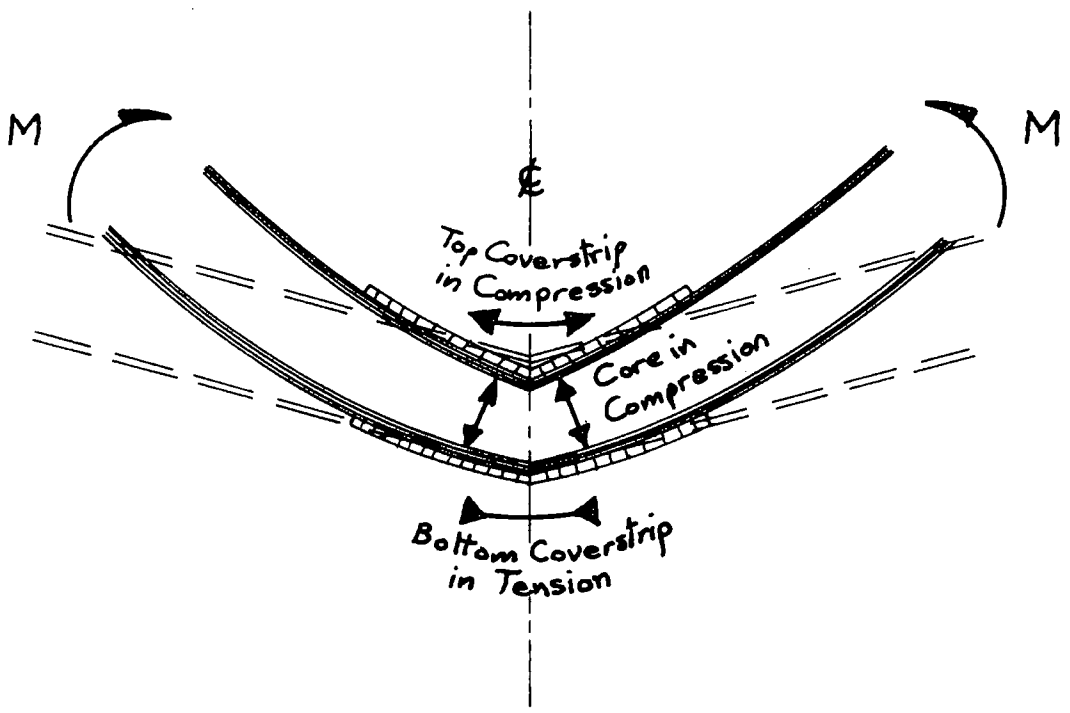

# Ultimate Load v Joint Angle

## Moment Opening Joint

FIG. 4·7

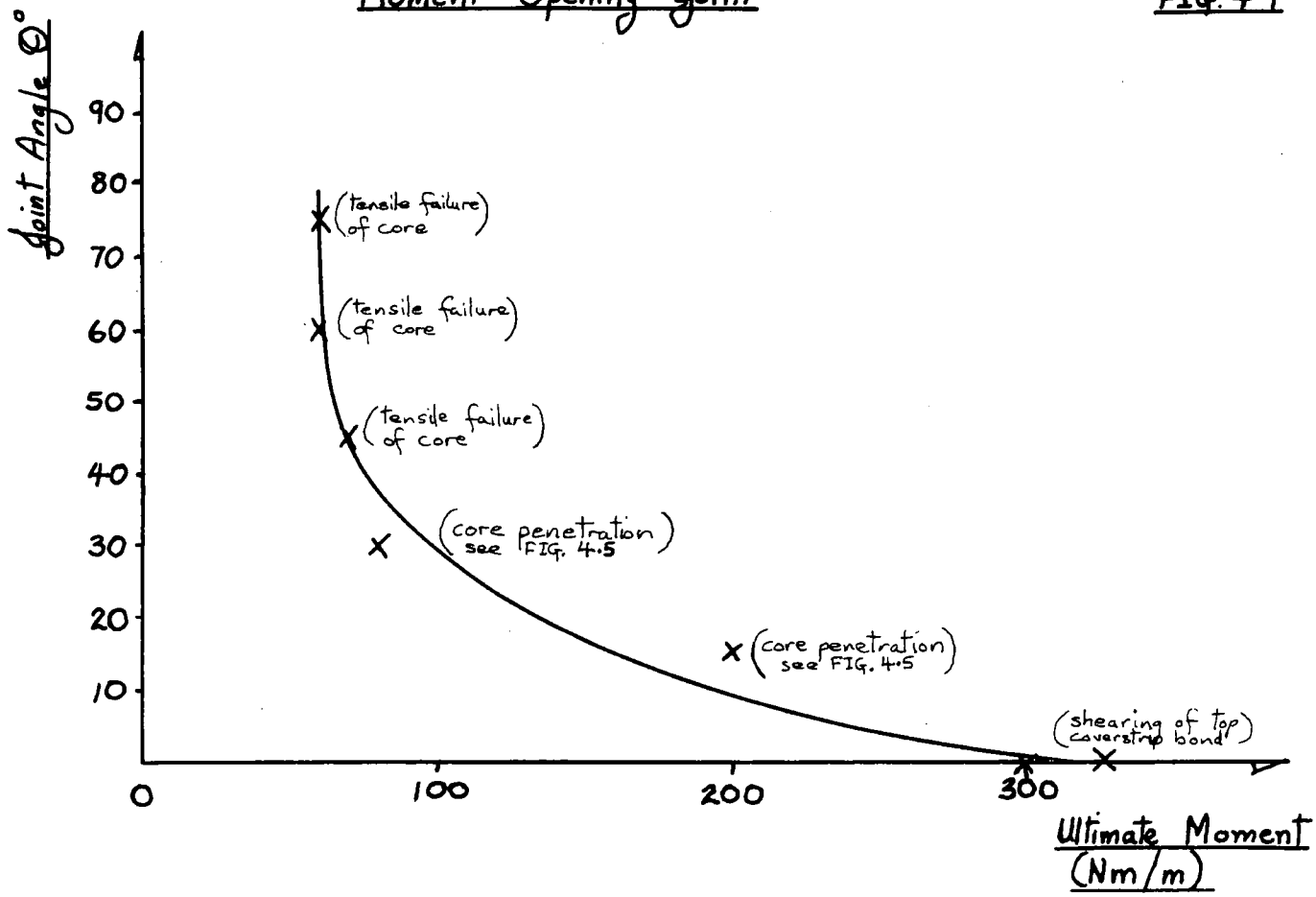


## Moment Closing Joint

FIG. 4·8

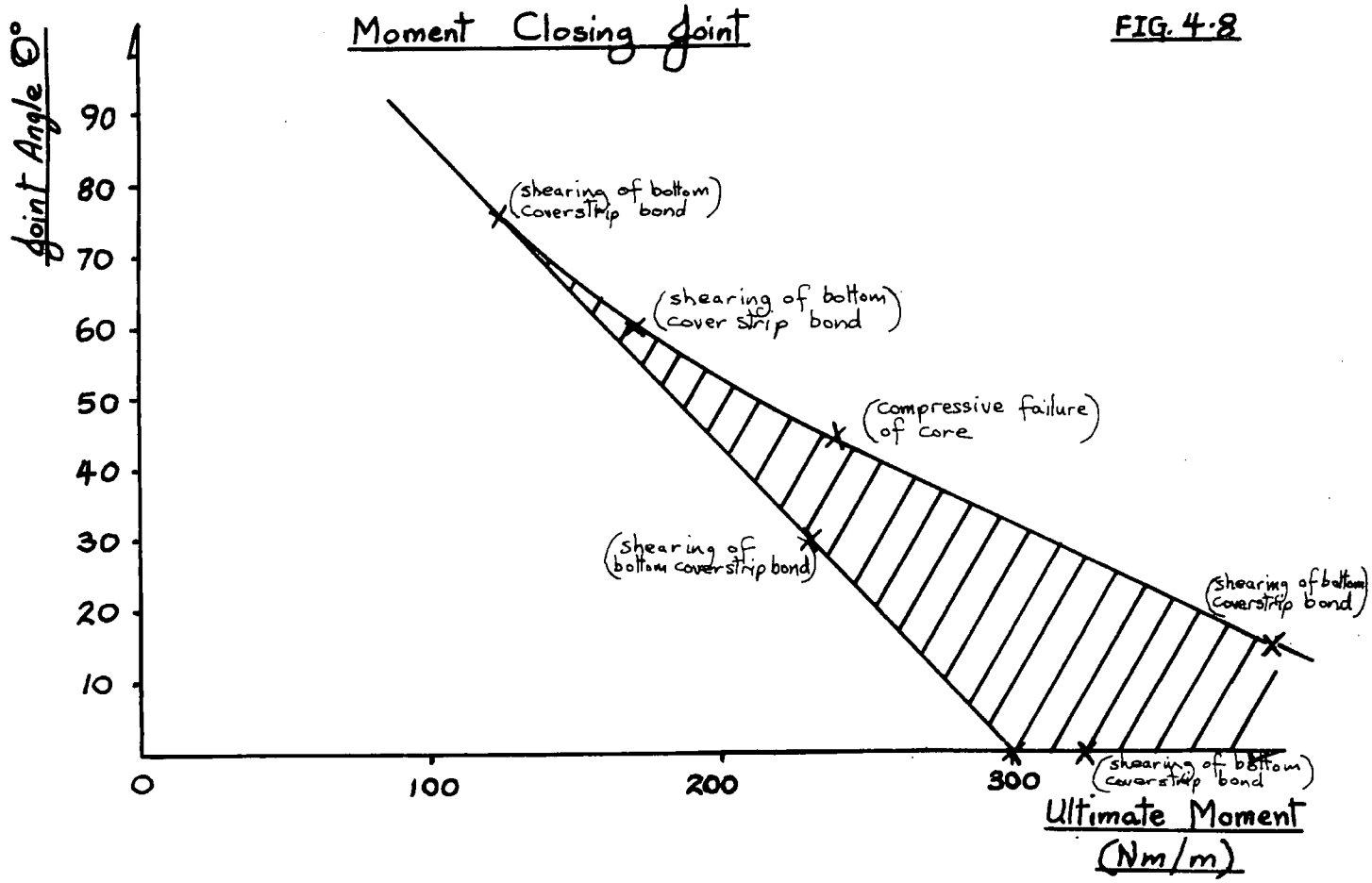

## Proposed Valley Joint Detail Dome 1

FIG. 4·9

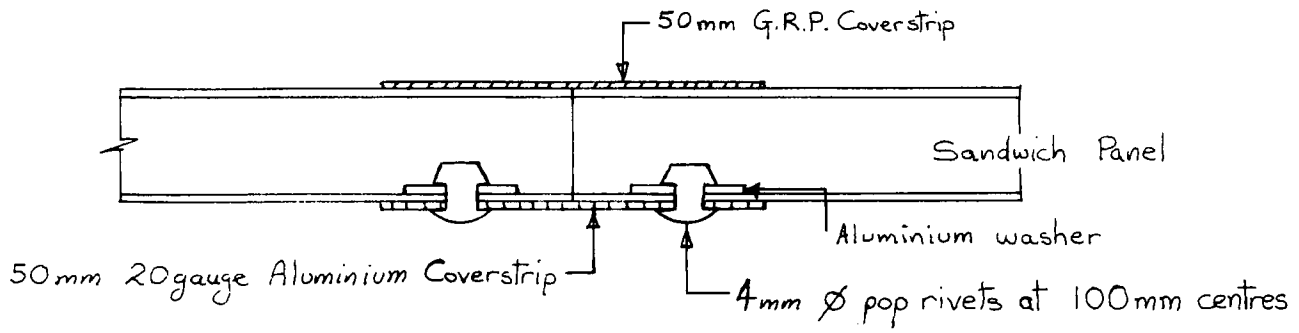


Scale 1:1

## Revised Valley Joint Detail Dome 1

FIG. 4·10

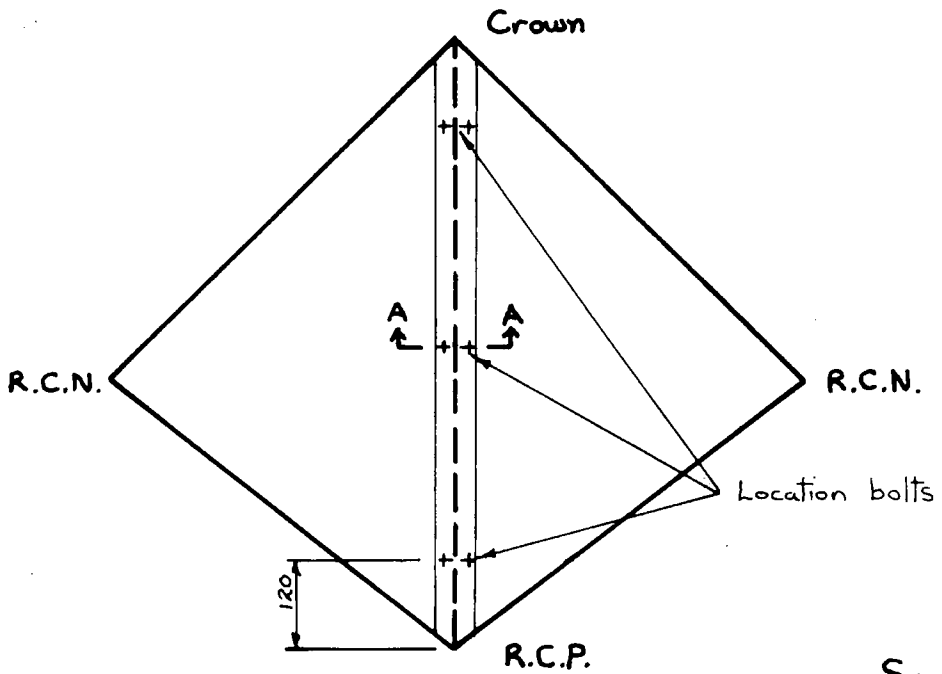


Scale 1:10

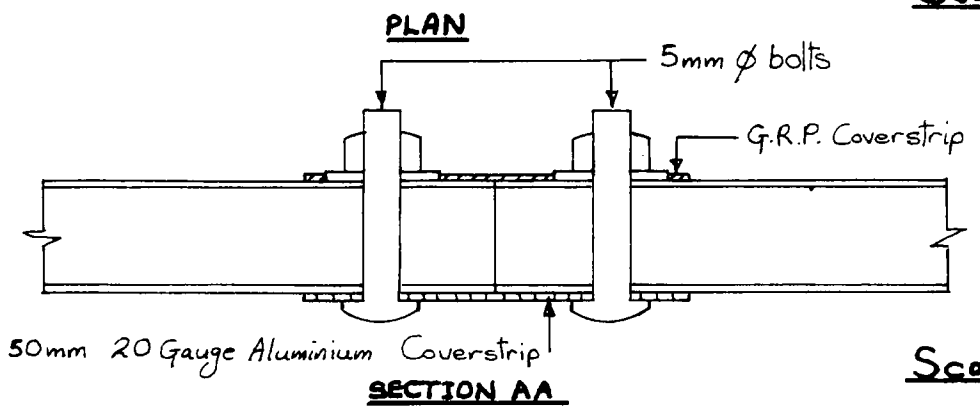


Scale 1:1

# Valley Joint Detail Dome 2

FIG. 4·11

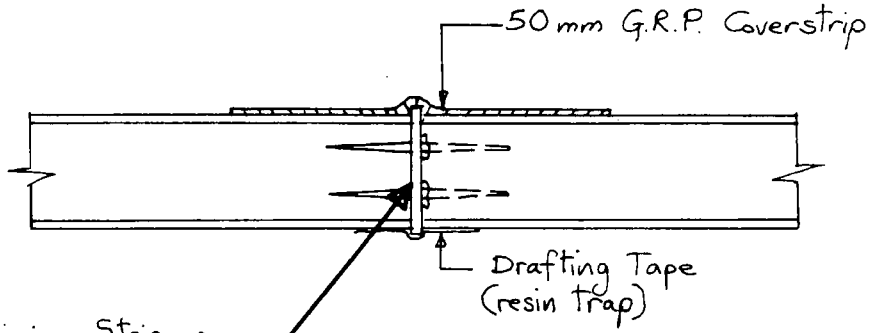


SECTION AA

Scale 1:1

20 Gauge Aluminium Strip with Double Row of 12·7mm Carpet Tacks

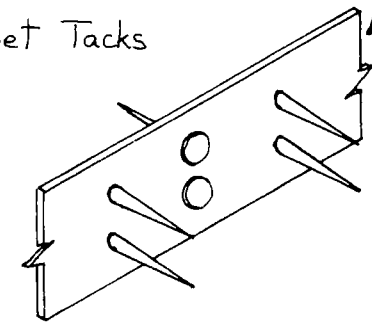

Shear Connector Strip

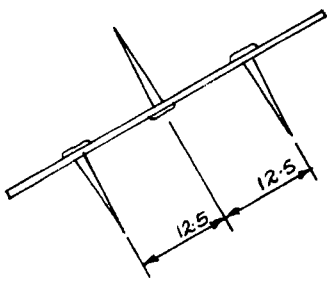


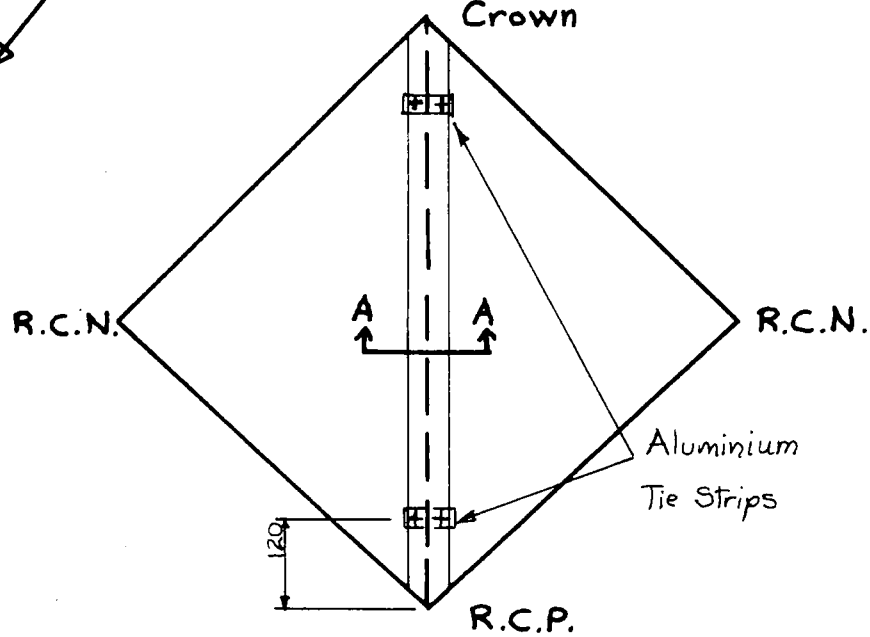


PLAN

Scale 1:10

# Valley Joint Detail Domes 3&4

FIG. 4·12

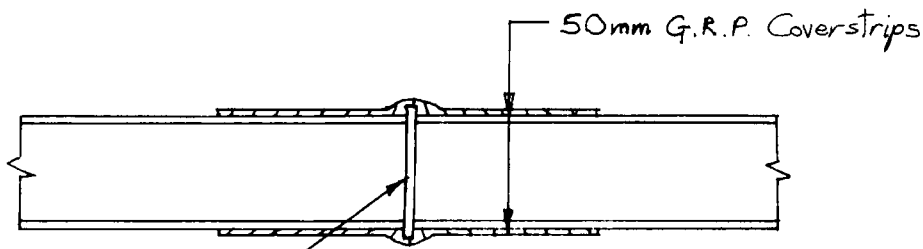


Plain Aluminium Strip
(Anti penetration strip)

Scale 1:1

Tension Tests upon Butt Joints with G.R.P. Coverstrips

| Specimen Number | Thickness of Coverstrip (mm) | Ultimate Load (kN) | Ultimate Shear Stress Face/Coverstrip Bond ($10^6 N/m^2$) | Mode of Failure |
|---|---|---|---|---|
| 1 | 0·56 | 6·8 | 1·36 | Shearing of Face/Coverstrip Bond |
| 2 | 0·42 | 7·8 | 1·54 | ditto |
| 3 | 0·40 | 7·1 | 1·42 | ditto |
| Average | 0·46 | 7·2 | 1·44 | |

TABLE 4·1

## 5. SANDWICH STRUTS

From the work performed by the author and other workers, (2, 10, 12), it was apparent that panel shortening in polyhedral sandwich shells constructed from the type of sandwich materials used by the author, is significant. In-plane deformation caused by in-plane loading has a significant effect upon the overall deformation of complex sandwich structures such as the polyhedral sandwich domes built by the author, (Section 8.0).

It was therefore decided to test a series of sandwich struts, made from the same sandwich material that the author had used to construct his domes, to determine the magnitude of elastic axial displacement due to in-plane loading.

### 5.1 Test Procedure

The struts that were tested were 51 mm wide with lengths between 300 mm and 900 mm, based on a 100 mm module. The longest strut was approximately equal to the maximum panel dimension in any of the model domes that were tested, (859.2 mm, dome 1).

Prior to testing the profile of each strut was measured to identify the magnitude of any initial transverse deformation.

The struts were tested to destruction using the arrangement shown in Fig. 5.1. Both ends of the specimen were seated in a 'V' shaped notch to simulate a pin joint. Care was taken to ensure that the load was applied along the centroidal axis of the strut. The load was applied as quickly as possible, to keep the effects of time dependent deformation to a minimum, using a hydraulic ram, (each strut test lasted approximately 5 minutes).

As the tests proceeded graphs were plotted of load (P) v axial displacement ($\delta x$), and load (P) v transverse displacement at the mid point of the strut ($\delta\omega$ at $x = 0$).

## 5.2 Theoretical Analysis

There are three possible modes of failure for sandwich struts, (1, 3, 13).

1. Elastic Euler type buckling, (long struts).
2. Shearing of the core before the buckling load is reached, (very long struts).
3. Wrinkling due to local instability in the faces before the buckling load is reached, (short struts).

### 5.2.1 Euler type elastic buckling of struts

The struts tested by the author all exhibited Euler type elastic buckling.

Two methods are described below for determining $P_{max}$, the maximum axial load for the strut due to overall buckling of the strut.

(a) It has been shown (1, 3), that the buckling load for a sandwich strut is given by the 'Modified Euler Theory' and that:

$$P_{max} = P_E = \frac{1}{\frac{L^2}{\pi^2 EI} + \frac{1}{G_c A_s}} \qquad (i)$$

where: $P_E$ = Euler buckling load

$A_s$ = b (t + f)

EI = Flexural stiffness

$G_c$ = Shear Modulus of Core

b = Strut width

t = Core thickness

f = Face thickness

L = Strut length

(b) If a strut is assumed to have an initial bow described by equation (ii), Fig. 5.2,it has been shown (13) that:

$$\omega = \frac{4 W_o}{a L \sin \frac{aL}{2}} \left(\cos a x - \cos \frac{aL}{2}\right) \qquad \text{(iii)}$$

where:

$$a^2 = \frac{P}{EI \left(1 - P/G_c A_s\right)}$$

$P$ = Axial load .

$P_{max}$ for a strut can be found from equation (iii) using a trial and error method in conjunction with equations (iv) and (v). Equation (iii) is only valid for loads approaching the buckling load (13).

5.2.2 Shearing of Core

This type of failure does not occur in relatively short struts such as those that were tested by the author. It has been shown (13) that:

$$P_{max} = \frac{\tau_{max} A_s L}{4 W_o} \quad \text{if} \quad a L \leqslant \pi \qquad \text{(iv)}$$

and

$$P_{max} = \frac{\tau_{max} A_s L}{4 W_o} \sin \frac{a L}{2} \quad \text{if} \; a L > \pi \qquad \text{(v)}$$

$\tau_{max}$ for the core can be determined from experimental tests upon long struts by substituting for $P_{max}$ in one of the above equations.

5.2.3 Wrinkling type instability in faces

It can be shown using the equations for wrinkling type instability presented by Allen (1), that for the struts tested by the author buckling could only occur due to an Euler type instability. Therefore wrinkling type instabilities have not been considered in this investigation.

5.2.4 Axial displacement due to transverse displacements in struts

For a perfect strut in which no buckling occurs the axial displacement due to compressive stress is given by:

$$\delta_{xc} = -\frac{P L}{E_{fc} A_f} \qquad \text{(vi)}$$

where: $E_{fc}$ = Elastic modulus of faces in compression

$A_f$ = Area of faces .

If it is assumed the deflected shape of the strut is described by equation (vii), then the axial displacement due to buckling can be calculated in the following manner:

The change in the length of a strut due to transverse displacement is given by:

$$\delta_{xB} = -\int_0^L (ds - dx)$$

and provided $\left(\frac{d\omega}{dx}\right)^n >> 0 \quad \text{for} \quad n > 2$

$$\delta_{xB} = -2\int_0^{L/2} \left[ \left\{ 1 + \left(\frac{d\omega}{dx}\right)^2 \right\}^{\frac{1}{2}} - 1 \right] dx$$

$$\doteq -\int_0^{L/2} \left(\frac{d\omega}{dx}\right)^2 dx$$

The transverse displacement is assumed to be of the form:

$$\omega = \Delta \cos \frac{\pi x}{L} \qquad \text{(vii)}$$

where: $\Delta$ = total transverse displacement at the mid point , (x = 0)

$$\frac{d\omega}{dx} = -\frac{\pi}{L}\,\Delta \sin \frac{\pi x}{L}$$

Therefore

$$\delta_{xB} = -\int_{o}^{L/2} \left(\frac{\pi}{L}\,\Delta \sin \frac{\pi x}{L}\right)^2 dx$$

$$= -\int_{o}^{L/2} \left(\frac{\pi^2}{L^2}\,\Delta^2 \sin^2 \frac{\pi x}{L}\right) dx$$

$$= -\frac{\pi^2}{L^2}\,\Delta^2 \left(\frac{x}{2} - \frac{\sin \frac{2\pi x}{L}}{4\pi/L}\right)_{o}^{L/2}$$

$$= -\frac{\pi^2}{4L}\,\Delta^2 \qquad \text{(viii)}$$

Therefore total axial displacement for a sandwich strut is given by:

$$\delta_x = \delta_{xC} + \delta_{xB}$$

$$= -\frac{PL}{E_{fc} A_f} - \frac{\pi^2}{4L}\,\Delta^2 \qquad \text{(ix)}$$

$\Delta$ can be calculated from the 'Perry Robertson Formula' for axially loaded struts, Fig. 5.13, and it can be shown that the transverse elastic displacement due to buckling at an axial load P is given by:

$$\omega = \frac{PC_o \cos \frac{\pi x}{L}}{P_E - P} \qquad \text{(x)}$$

where $P_E$ is the 'Euler Buckling Load', equation (i).

Therefore

$$\Delta = C_o + \frac{PC_o}{P_E - P} \qquad \text{(xi)}$$

## 5.3 Experimental Results

Two sets of sandwich struts were tested. One set of struts was cut parallel to each axis of the orthogonal sandwich board from which the struts were cut, Table 5.1.

The graphs Figs. 5.3 to 5.8 show the experimental load/displacement relationships for the struts. The graphs Figs. 5.9 and 5.10 show a comparison between experimental buckling loads and those calculated using the 'Modified Euler Theory', equation (i).

Table 5.1 shows, values of $W_o$ which were measured in the laboratory, the tangent modulus at P = 0 for the experimental elastic axial displacement, and the factor by which this exceeds the theoretical elastic axial displacement for a perfect strut, equation (vi), for each strut. The theoretical elastic axial displacements for perfect struts, equation (vi) were calculated on the assumption that $E_{fC}$ was equal to the apparent elastic modulus of the faces in bending.

## 5.4 Comparison of experimental and theoretical results

It can be seen from Figs. 5.9 and 5.10 that the 'Modified Euler Theory', equation (i), gives an excellent approximation of the buckling loads for the sandwich struts for which the slenderness ratios were in the range 40 to 130. This coincides with the findings of Elliott (3) who considered sandwich struts with slenderness ratios in the range 100 to 190. The buckling loads predicted using equation (iii) were not as reliable as those predicted using the 'Modified Euler Theory'.

Figs. 5.11 and 5.12 show a comparison for two typical struts between experimental load/axial displacement relationships, and the corresponding theoretical relationships derived from equation (ix). It was assumed when calculating the theoretical axial displacements that

$E_{fC}$ was equal to the elastic modulus of the faces derived from bending tests, (Section 2.2), and as a result the experimental axial displacement is greatly under-estimated by equation (ix), (Figs. 5.11 and 5.12). For struts such as 4 WR for which the initial transverse deformation is small, the axial displacement due to buckling is small compared to the axial displacements due to compression at loads which are significantly less than the buckling load, (Fig. 5.11). The significance of the axial displacement due to buckling is dependent upon the magnitude of the initial transverse deformation of the strut.

For loads which were significantly less than their buckling loads, most of the struts exhibited approximately linear load/axial displacement relationships.

Figs. 5.3 to 5.8 show that,in the case of some of the struts, e.g. 6 AR and 5 WR , there was no significant transverse displacement at the mid point of the strut at load intensities for which there was significant axial displacement. For most of the struts the axial displacement was due primarily to compressive axial strain. Axial displacement due to buckling of the struts was only significant if their initial transverse deformation was large.

The above has led the author to the conclusion that the elastic modulus for the faces in compression is substantially less than the elastic modulus for the faces in bending. This conclusion was reinforced by the results obtained by the author when he performed a series of tensile load/extension tests on specimens of the face material. From these tests he found that the elastic modulus of the faces in tension (average) was equal to 1.64 x the elastic modulus of the faces in bending, (Section 2.2). The values of the constants k in Table 5.1 represent the factor by which the elastic modulus for the faces in bending exceeds the elastic modulus for the faces in compression.

## 5.5. Conclusions for sandwich struts

Axial displacement due to in-plane compressive load was significant, (Table 5.1).

The magnitude of the initial transverse distortion of the struts appeared to be random, (Table 5.1).

Significant cross-plate shear forces were developed in the core due to membrane forces in the plane of the struts, when transverse displacements and/or initial transverse deformation was large.

Equations (ix) and (x) give a good approximation of the displacements of sandwich struts provided that the magnitude of any initial transverse crookedness is known, and that the transverse displacement is described by equations (vii) & (x). The reliability of equations (ix) and (x) depends mainly upon the accuracy with which $W_o$ and $E_{fC}$ are determined.

FIG.5·1

# Test Arrangement for Sandwich Struts

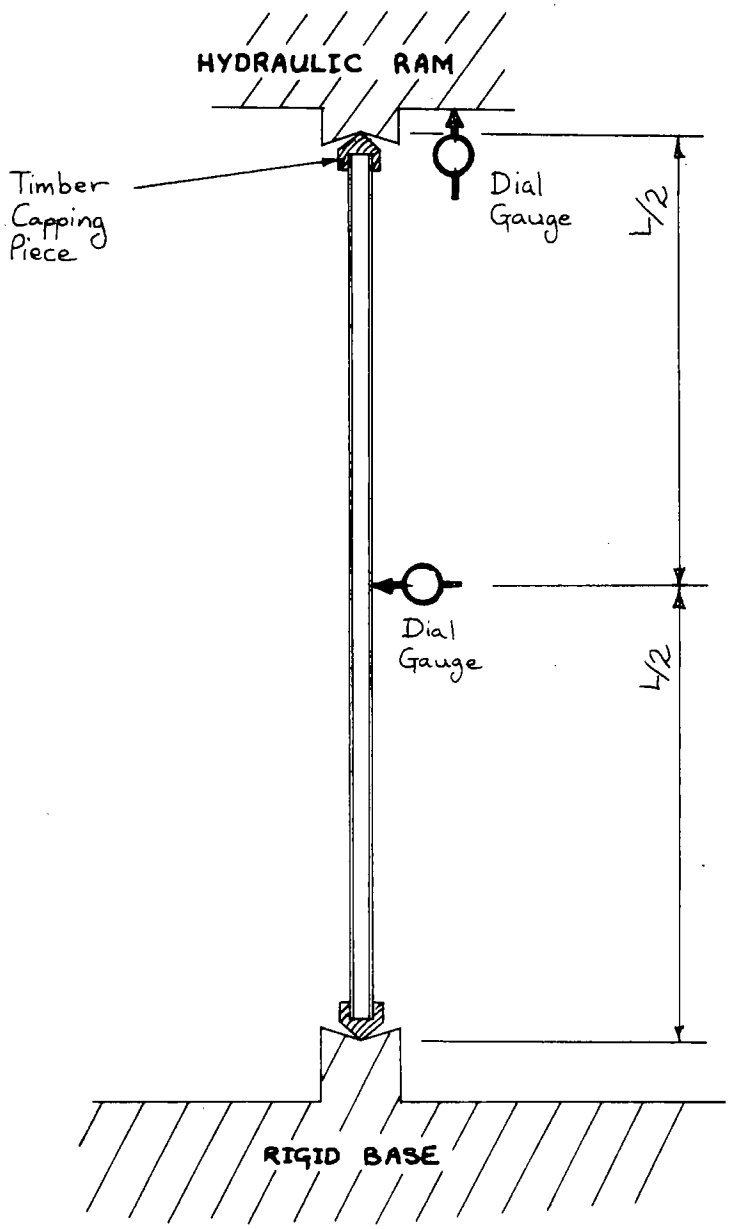


Scale 1:5

FIG. 5·2

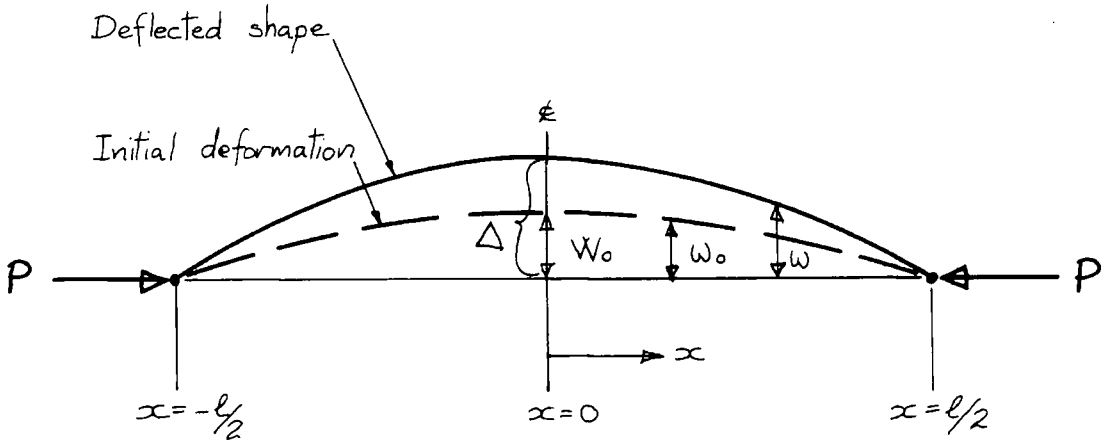


$$\omega_o = W_o\left(1 - \frac{4x^2}{L^2}\right) \qquad \text{(ii)}$$

where: $W_o$ = Initial transverse displacement at mid point, $x = 0$

$\omega_o$ = Initial transverse displacement at a point distant $x$ from the mid point

$\omega$ = Total transverse displacement at a point distant $x$ from the mid point at load P

$\Delta$ = Total transverse displacement at mid point, $x = 0$, at load P

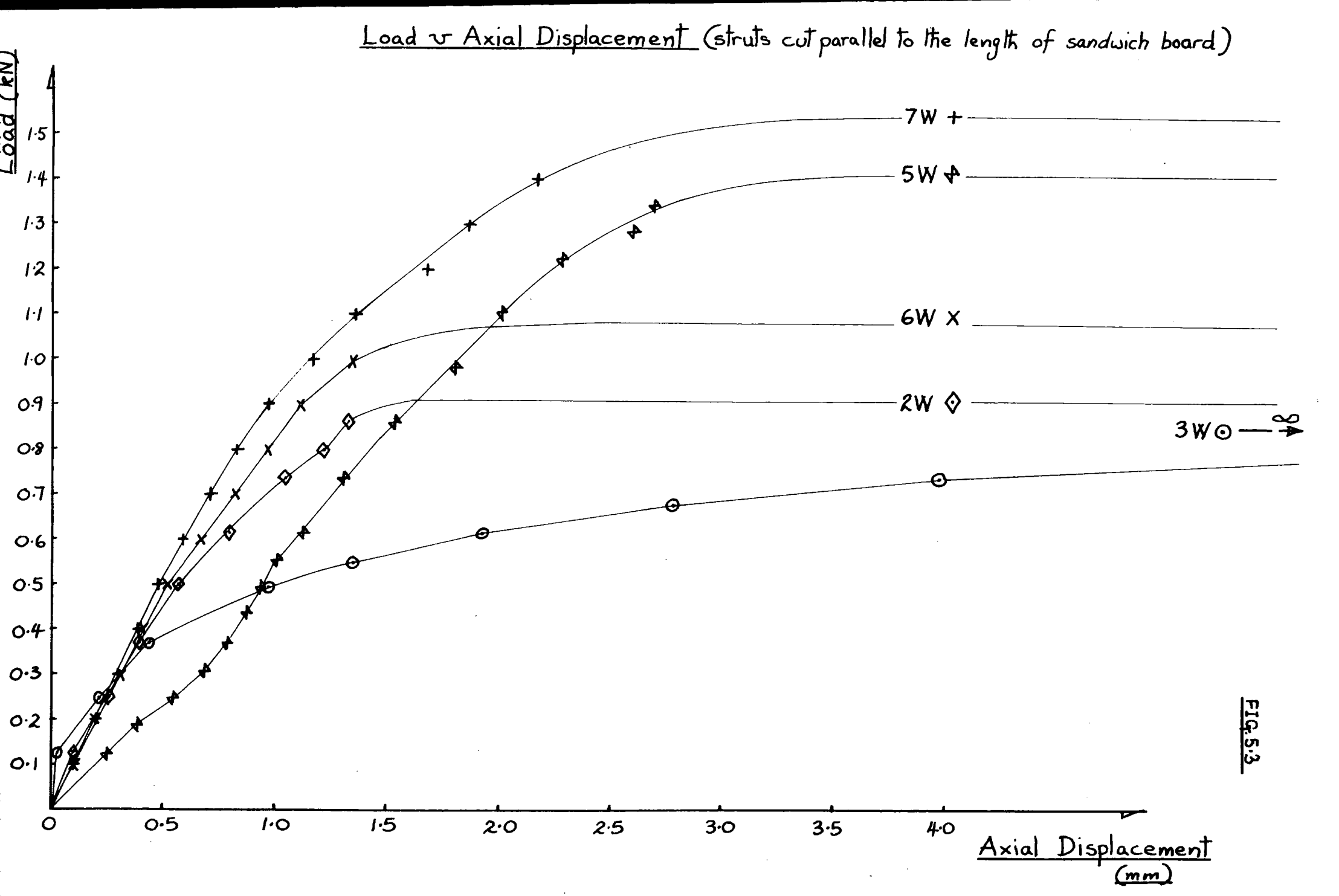
Load v Axial Displacement (struts cut parallel to the length of sandwich board)
Load (kN)
1·5
1·4
1·3
1·2
1·1
1·0
0·9
0·8
0·7
0·6
0·5
0·4
0·3
0·2
0·1
7W +
5W ✱
6W X
2W ◇
3W ⊙
0
0·5
1·0
1·5
2·0
2·5
3·0
3·5
4·0
Axial Displacement (mm)
FIG. 5.3

Load v Axial Displacement (struts cut parallel to the length of the sandwich board)
Repeats

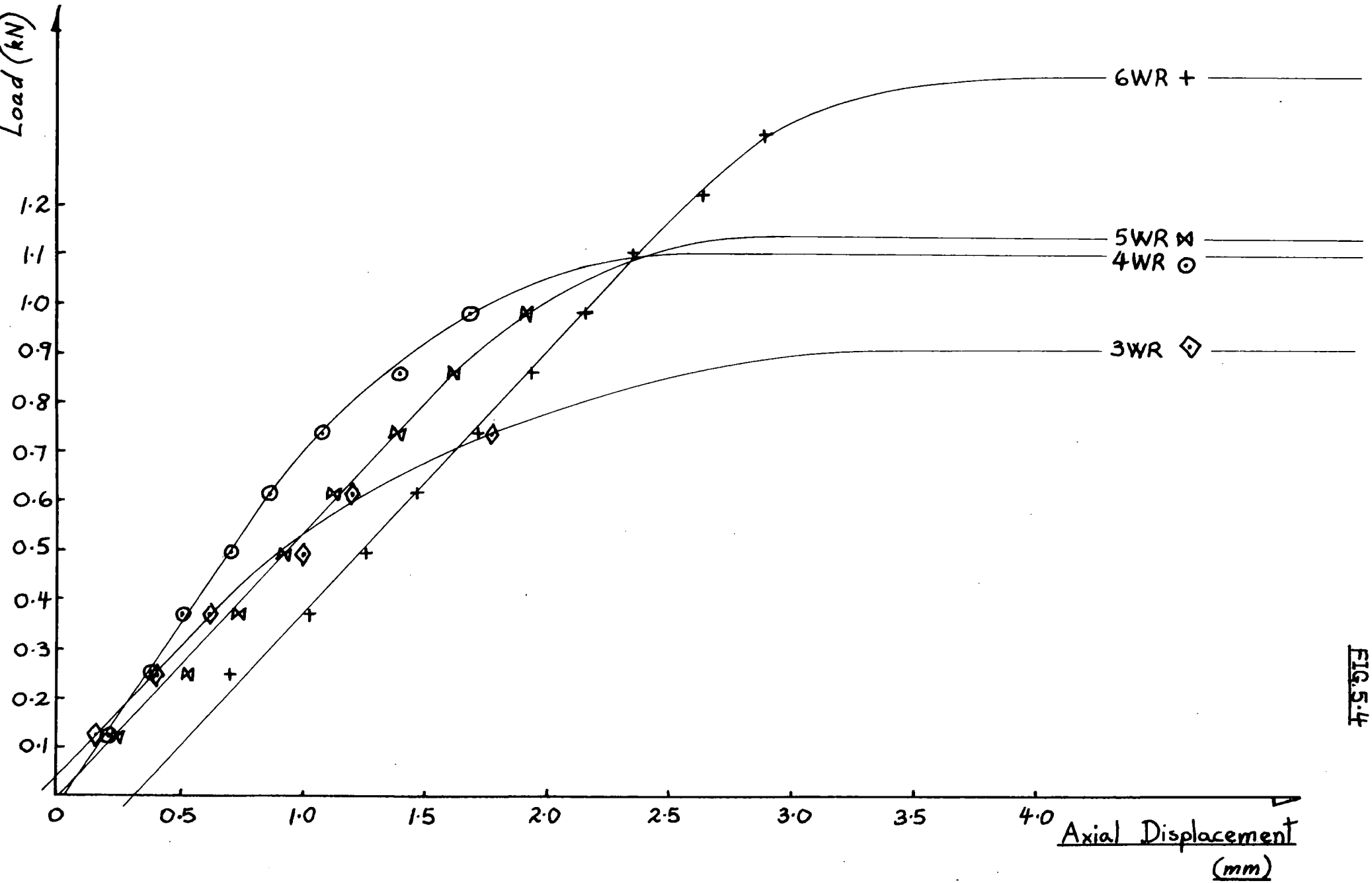


FIG.5.4

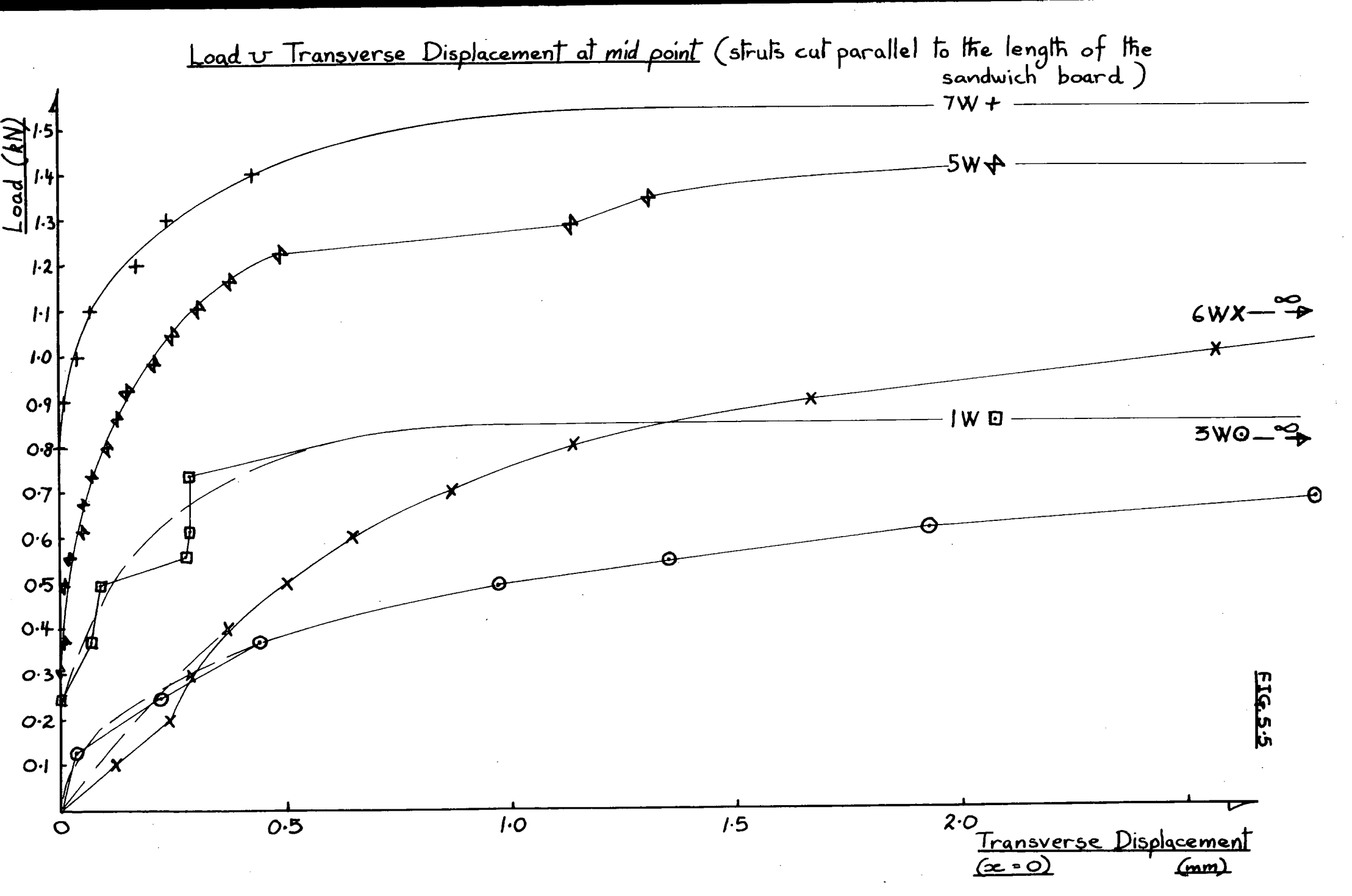
Load υ Transverse Displacement at mid point (struts cut parallel to the length of the sandwich board)
7W +
5W
6WX
1W
3WO
Load (kN)
1·5
1·4
1·3
1·2
1·1
1·0
0·9
0·8
0·7
0·6
0·5
0·4
0·3
0·2
0·1
0
0·5
1·0
1·5
2·0
Transverse Displacement (x = 0) (mm)
FIG.5.5

Load v Transverse Displacement at mid point (struts cut parallel to the length of the sandwich board) Repeats

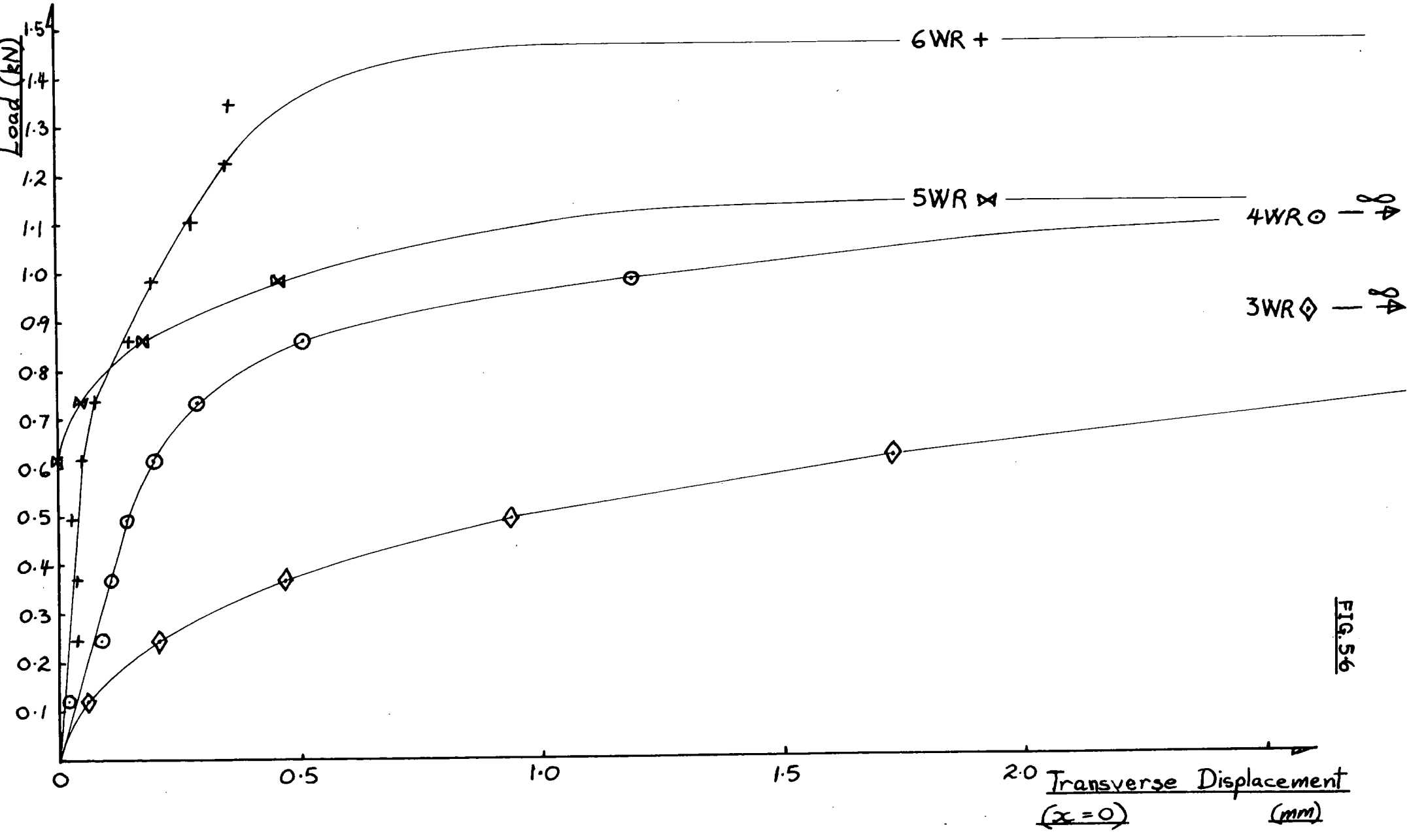


FIG. 5.6

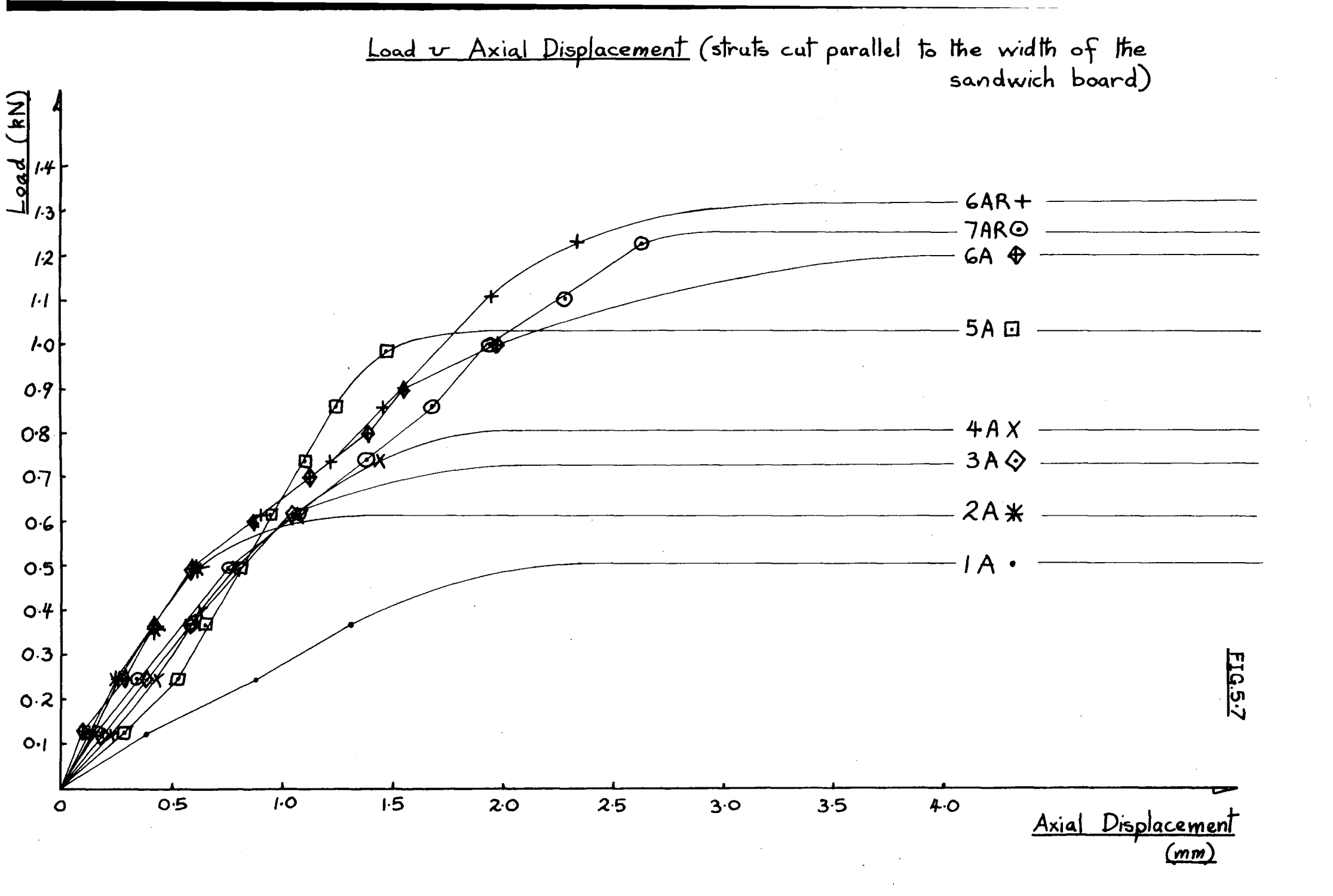
Load v Axial Displacement (struts cut parallel to the width of the sandwich board)
Load (kN)
1.4
1.3
1.2
1.1
1.0
0.9
0.8
0.7
0.6
0.5
0.4
0.3
0.2
0.1
6AR +
7AR ⊙
6A ⊕
5A ⊡
4A X
3A ◇
2A ✳
1A •
0
0.5
1.0
1.5
2.0
2.5
3.0
3.5
4.0
Axial Displacement (mm)
FIG.5.7

Load v Transverse Displacement at mid point (struts cut parallel to the width of the sandwich board)

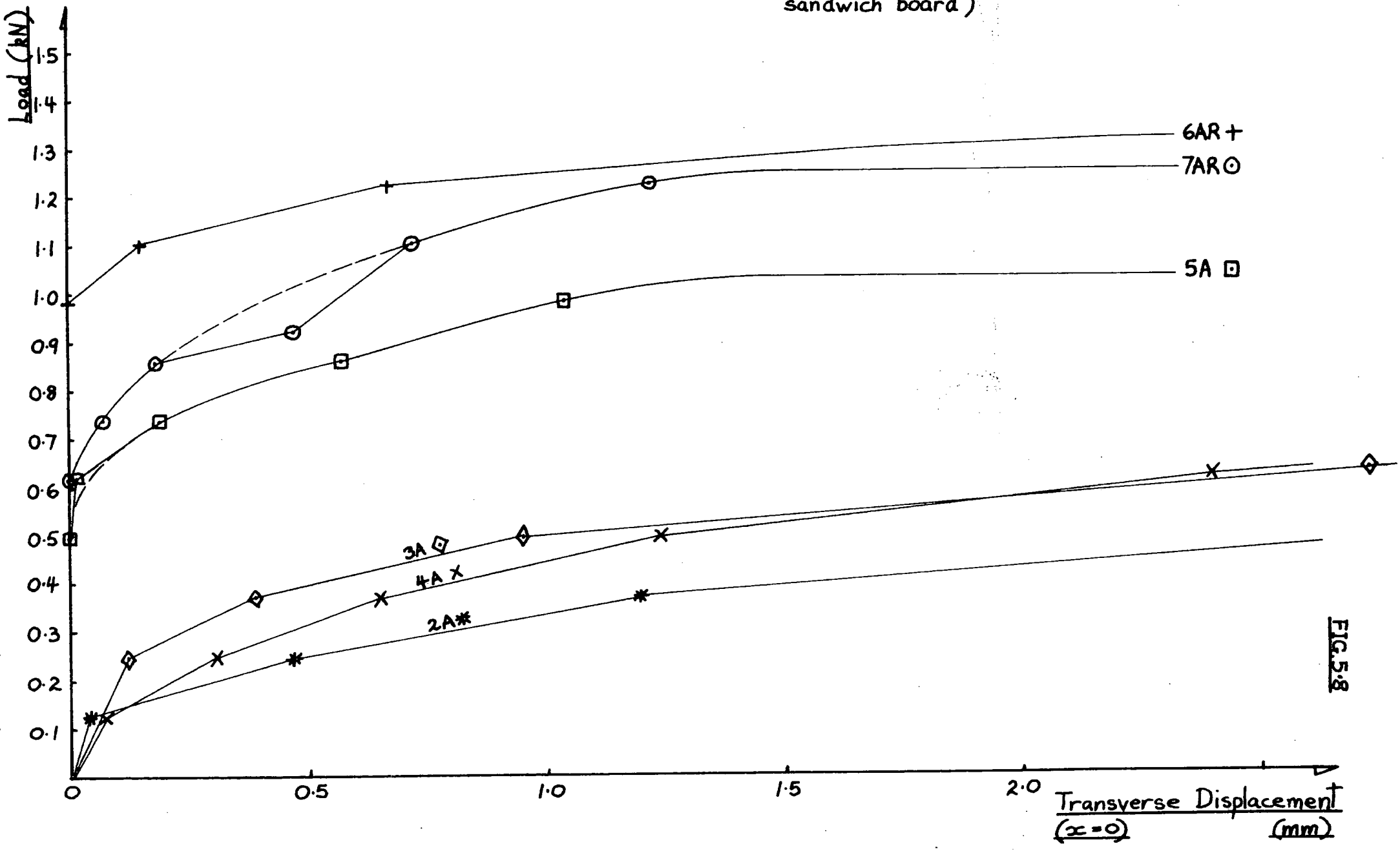


FIG.5.8

## Buckling Loads - Sandwich Struts

FIG. 5·9

(struts cut parallel to the length of the sandwich board)

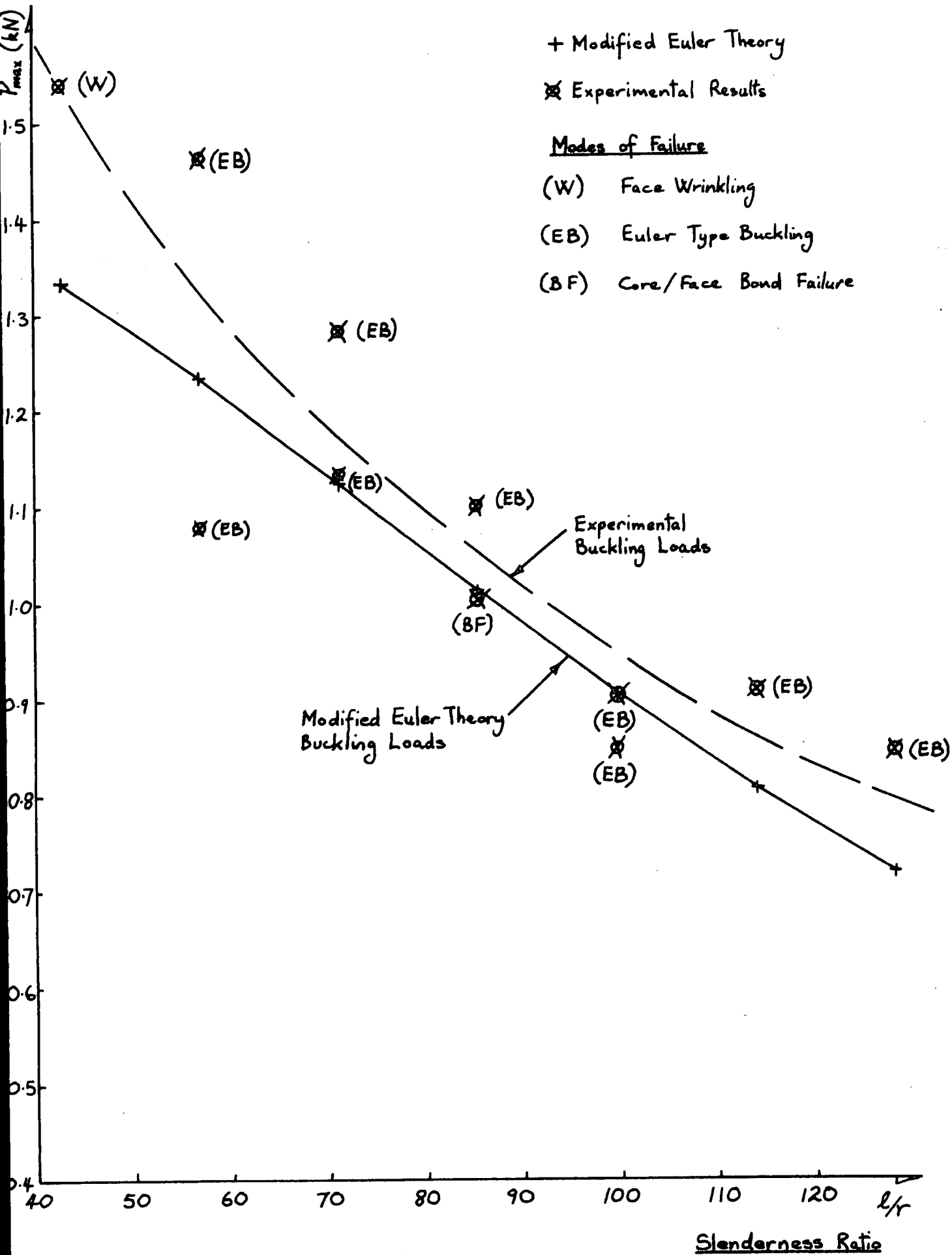

## Buckling Loads - Sandwich Struts

FIG. 5·10

(struts cut parallel to the width of the sandwich board)

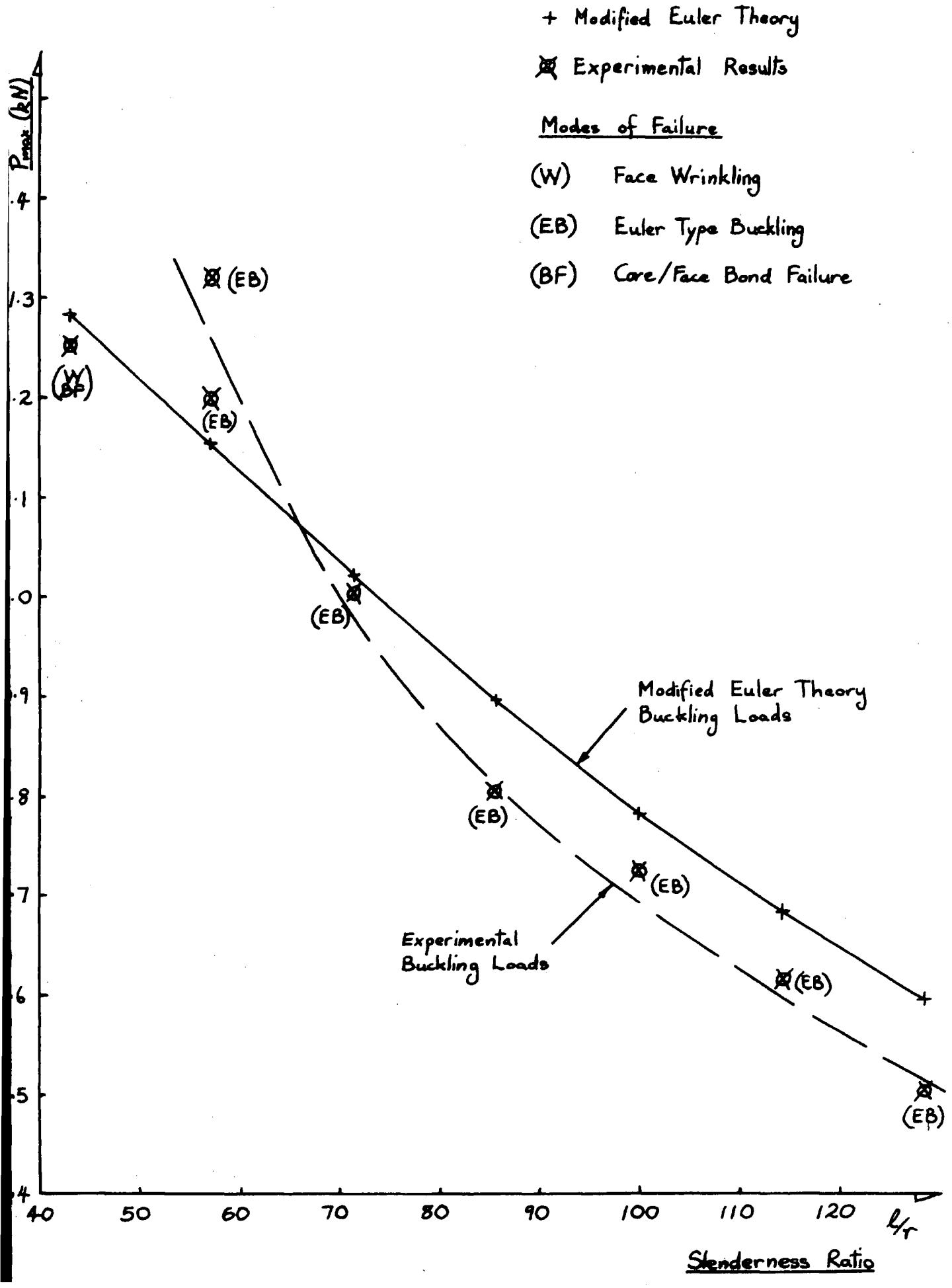

# Load $v$ Axial Displacement - Strut 4WR ($L = 600mm$, $W_o = 1.041mm$)

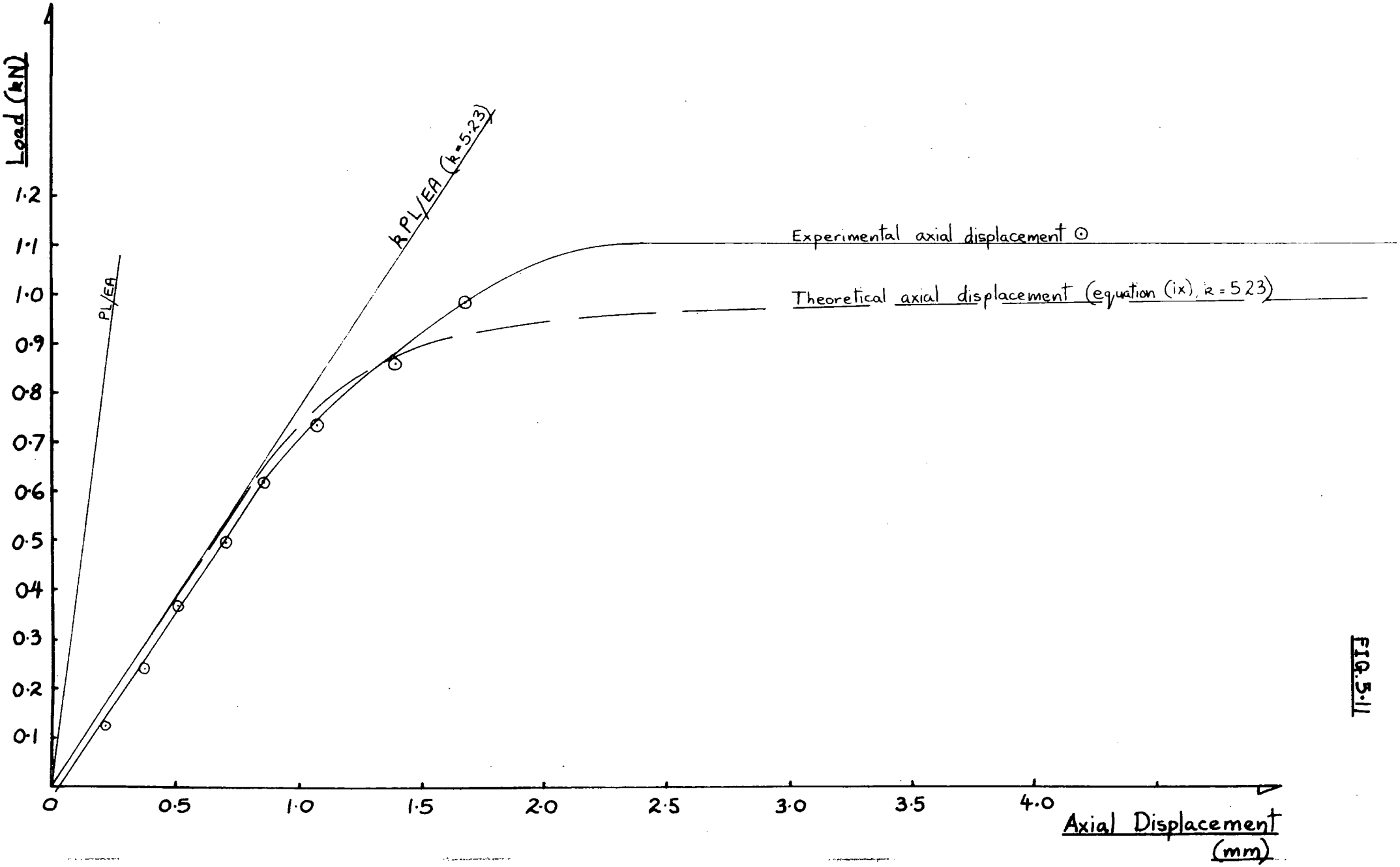


FIG. 5.11

# Load v Axial Displacement - Strut 3A (L = 700 mm, $W_o$ = 3·679mm)

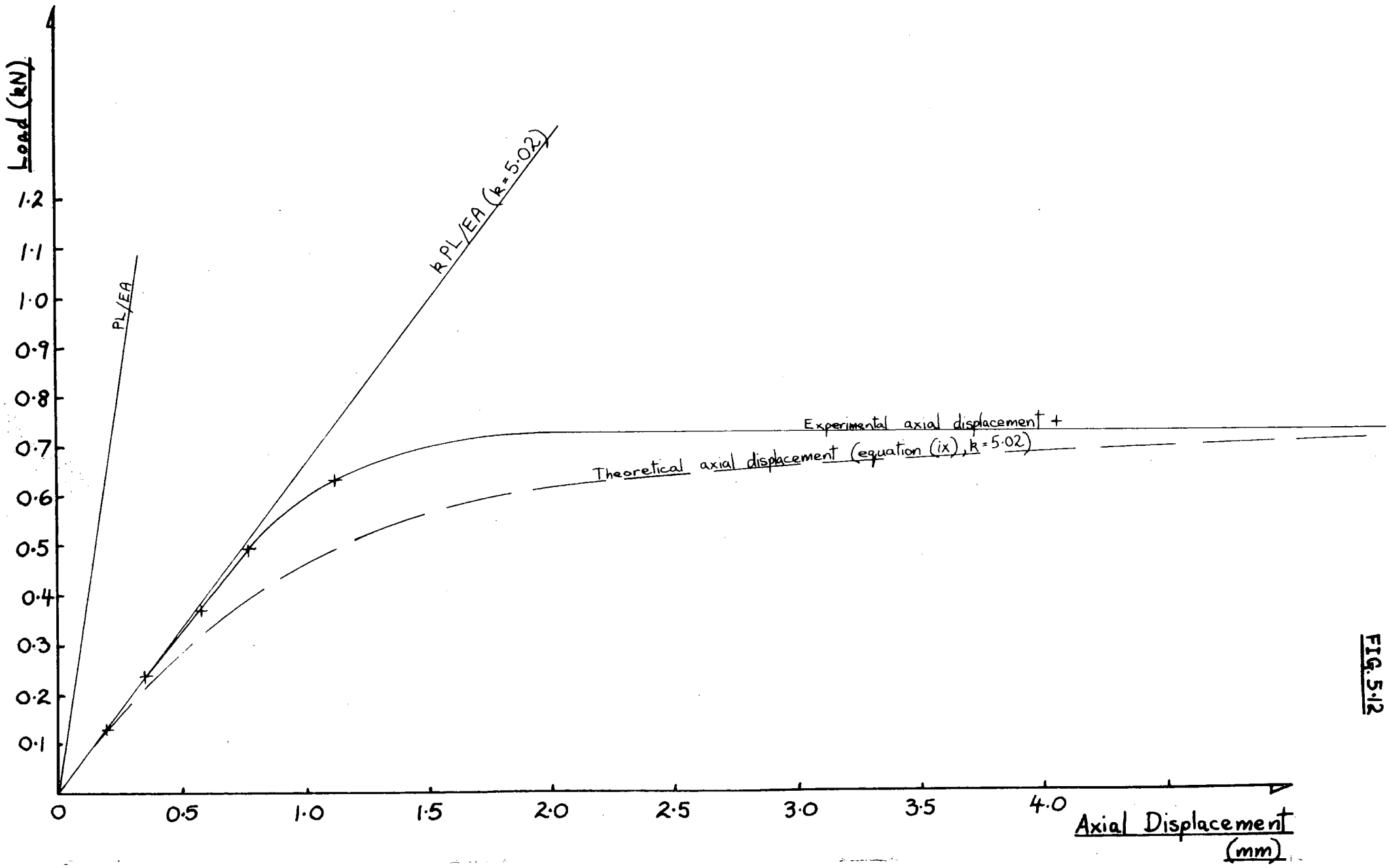


FIG. 5·12

FIG. 5·13

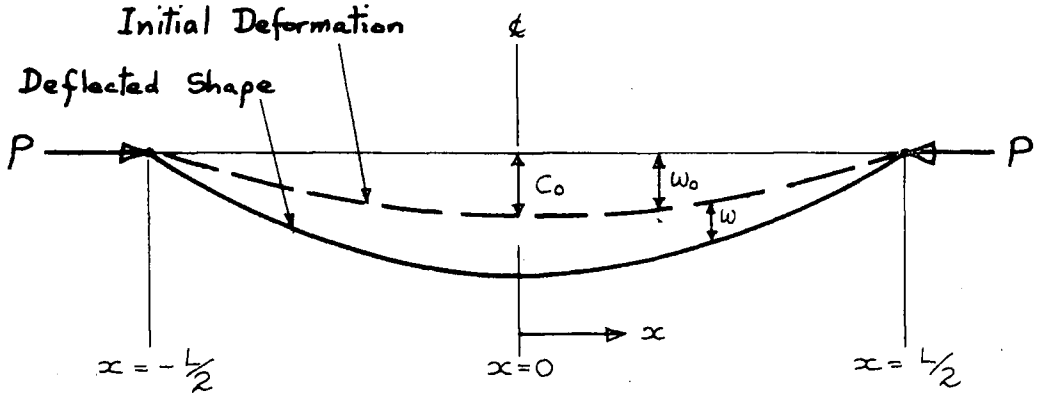


$$w_o = C_o \cos \frac{\pi x}{L}$$

where: $C_o$ = Initial transverse displacement at mid point, $x = 0$

$w_o$ = Initial transverse displacement at a point distant $x$ from the mid point

$w$ = Transverse displacement at a point distant $x$ from the mid point at load P

TABLE 5·1

Experimental Tangent Modulus $\delta_{xT}$ at P=0

(derived from experimental graph $P$ v $\delta_x$)

$$\delta_{xT} = \frac{kPL}{EA}$$ where: E = elastic modulus of faces in bending
A = area of faces

| Strut | L (m) | $W_o$ (mm) | $\delta_{xT}$ (mm x $10^{-3}$/N) | $\frac{PL}{EA}$ (mm x $10^{-3}$/N) | k | $\frac{W_o}{L}$ | |
|---|---|---|---|---|---|---|---|
| 7W | ·3 | 1·280 | ·96 | ·130 | 7·385 | ·0043 | Struts cut parallel to the length of the sandwich board |
| 6W | ·4 | 2·950 | ·96 | ·173 | 5·549 | ·0074 | |
| 6WR | ·4 | 0·620 | 1·91 | ·173 | 11·040 | ·0016 | |
| 5W | ·5 | 1·230 | 1·68 | ·217 | 7·742 | ·0025 | |
| 5WR | ·5 | 0·996 | 1·84 | ·217 | 8·479 | ·0020 | |
| 4WR | ·6 | 1·041 | 1·36 | ·260 | 5·230 | ·0017 | |
| 3W | ·7 | 3·542 | ·24 | ·303 | ·792 | ·0051 | |
| 3WR | ·7 | 3·195 | 1·80 | ·303 | 5·941 | ·0046 | |
| 2W | ·8 | 2·167 | ·96 | ·347 | 2·767 | ·0027 | |
| 7AR | ·3 | 1·212 | 1·52 | ·130 | 11·692 | ·0040 | Struts cut parallel to the width of the sandwich board |
| 6A | ·4 | 1·817 | ·76 | ·173 | 9·393 | ·0045 | |
| 6AR | ·4 | 1·559 | 1·15 | ·173 | 6·647 | ·0039 | |
| 5A | ·5 | 2·340 | 1·07 | ·217 | 4·931 | ·0047 | |
| 4A | ·6 | 1·670 | 1·52 | ·260 | 5·846 | ·0028 | |
| 3A | ·7 | 3·679 | 1·52 | ·303 | 5·017 | ·0053 | |
| 2A | ·8 | 3·651 | 1·52 | ·347 | 4·380 | ·0046 | |
| 1A | ·9 | 4·299 | 3·32 | ·390 | 8·513 | ·0048 | |

Average 6·550

Strut section

## 6. NON-DESTRUCTIVE TESTS ON DOMES

### 6.1 Elastic Loading using a Single Load Point (Load Series 1)

The purpose of load series 1 was to verify that the domes behaved elastically, provided time dependent effects were not allowed to develop, and to check that the domes behaved symmetrically.

Observations were made at a number of displacement points, (i), so as to determine the load/displacement relationships, and hence were found the flexibility influence coefficients, ($f_{ij}$), for a single vertical load acting at, (j), the centroid of one of the top panels. The locations of the displacement points are as detailed in Section 3.3, and their numbering system is shown in Fig. 6.1. Loads were applied using a hydraulic jack, (12).

### 6.2 Elastic Loading using Two Adjacent Load Points (Load Series 2)

The procedure in load series 2 was to load two adjacent top panels simultaneously. The displacements recorded during the load series were used to check that the domes were behaving elastically and that superposition could be assumed to apply. Each combination for loading adjacent top panels was studied in turn.

### 6.3 Results Load Series 1 and 2

#### 6.3.1 Dome 1

Tables 6.1 and 6.2 summarise the results obtained during load series 1 and 2 for dome 1.

Dome 1 behaved elastically, and superposition could be applied. A comparison of results showed that the behaviour of the model in the region of a load was remarkably consistent around the dome. Displacements remote from the load points were variable in magnitude but consistent in direction, their overall pattern suggested that they were

only 'background noise'. The deformation was highly localised, and only those panels adjacent to a loaded panel were affected to a significant extent. If all the top panels were loaded simultaneously, ($\sum_{j=1}^{8} f_{ij}$), 85% of the displacement at a load point would be due to that load, and a further 13% would be due to the loads at the two adjacent top panels, (Fig. 6.2).

There were no signs of any uplift on the side of the dome remote from a load(s). It was apparent, as mentioned in Section 7.1.1, that there was considerable transfer of moment across the valley joints, and that adjacent top panels containing a valley joint behaved essentially as a continuous flat plate. There was no visible evidence of transfer of moment across the ridge joints.

### 6.3.2 Dome 2

Tables 6.3 and 6.4 summarise the results obtained during load series 1 and 2 for dome 2.

All the results indicated that the dome behaved in a linear hookean manner. The correlation between the displacements in load series 1 and load series 2 was poor. Both load series 1 and load series 2 were repeated, but this only served to verify the results obtained previously.

As can be seen from Table 6.4 the displacements produced by loading two panels simultaneously were significantly greater than the combined total of the displacements produced when the same two panels were loaded separately. The correlation between the displacements in load series 1 and load series 2 was best for displacement points adjacent to the load point(s), and worst for displacement points remote from the load point(s). The discrepancy is probably due in large measure to the relatively small magnitude of the displacements in general, and those remote from the load point(s) in particular. Had the magnitude of the

applied load(s) been greater it is probable that the degree of correlation between the displacements in load series 1 and load series 2 would have been greater, (maximum load, load series 1 and 2, 150 N/Panel). It is probable that the correlation between the displacements in load series 1 and load series 2 for domes 1 and 4 is much better than that for domes 2 and 3, because their displacements are more highly localised.

The effect of loads upon remote points was much greater for dome 2 than for dome 1. If all the top panels of dome 2 were loaded simultaneously, $(\sum_{j=1}^{8} f_{ij})$, 70% of the displacement at a load point would be due to that load, and a further 19% would be due to the loads at the two adjacent top panels, (Fig. 6.2).

6.3.3 Dome 3

Tables 6.5 and 6.6 summarise the results obtained during load series 1 and 2 for dome 3.

Dome 3 behaved elastically, the load displacement relationships were highly consistent for the various load points and displacement points. The correlation between the displacements in load series 1 and load series 2 was better than in the case of dome 2. This was probably because of the relatively high magnitude of the flexibility influence coefficients for dome 3 compared with those for dome 2.

Displacements for dome 3 were considerably less localised than those for dome 2. If all the top panels of dome 3 were loaded simultaneously, $(\sum_{j=1}^{8} f_{ij})$, 50.5% of the displacement at a load point would be due to that load, 31.5% would be due to the loads at the two adjacent top panels, and 13.7% would be due to loads at the top panels twice removed, (Fig. 6.2).

As the domes became flatter there was a marked increase in the vertical displacement of the 'Rhomb Corner Projections', which was an

indication that the stresses in the bottom panels were being increased as the rise was reduced.

6.3.4 Dome 4

Tables 6.7 snd 6.8 summarise the results obtained during load series 1 and 2 for dome 4.

Dome 4 behaved elastically and superposition could be applied. The correlation between the displacements in load series 1 and load series 2 was good.

The dome exhibited the type of behaviour observed during the tests upon dome 1, the effects due to loading being highly localised. If all the top panels of dome 4 were loaded simultaneously, $(\sum_{j=1}^{8} f_{ij})$, 80.5% of the displacement at a load point would be due to that load, and a further 13.6% would be due to the loads at the two adjacent top panels, (Fig. 6.2).

During both load series 1 and 2 outward movement occurred at the centroids of the bottom panels of the segments perpendicular to the line of the longitudinal ridge of the loaded segment, (Tables 6.7 and 6.8).

6.4 General observations, Load Series 1 and 2, domes 1 to 4

From the evidence amassed during load series 1 and 2 for domes 1 to 4, the following points emerged:

1. The domes behaved elastically, provided time dependent effects were not allowed to develop. All displacements were recorded within 1st minute following the application of the load(s).
2. The domes all had a high degree of symmetry in their behaviour under load.
3. When the ratio h/r was reduced from 0.6 to 0.3, the loss in the dome's stiffness was not large; but when the ratio h/r was

reduced from 0.3 to 0.2 the loss in the dome's stiffness was large. Fig. 6.3 shows the relationship between the ratio h/r and load point and crown displacements.

4. As the ratio h/r was reduced the general trend was from local deformation to an overall translation of the panels. Fig. 6.2 shows the relationship between the ratio h/r and the extent to which displacement was localised.

5. Moment transfer across the ridge joints appeared to be significant in the case of domes 2 and 3, but not in the case of domes 1 and 4.

6. Dome 4 was less flexible than dome 1, and exhibited a stiffness relative to domes 2 and 3 which one would have expected from dome 1, (Sections 7.0 and 8.0).

# Numbering System for Flexibility Influence Coefficients

FIG. 6·1

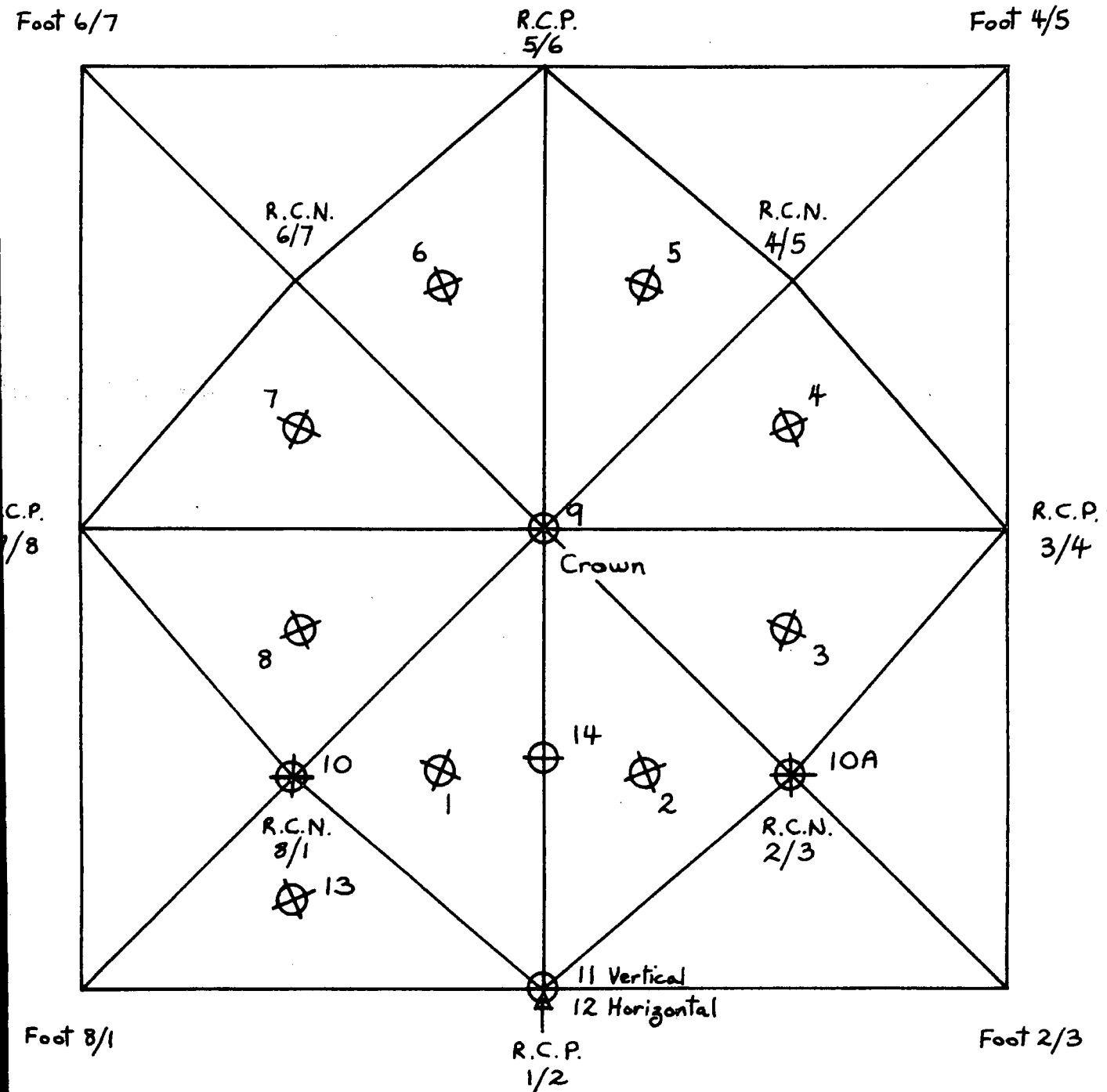


1 - 14 Displacement Points
1 - 8 Load Points

FIG. 6·2

Variation in the ratios of flexibility influence coefficients, due to changes in ratio h/r, for load point 1

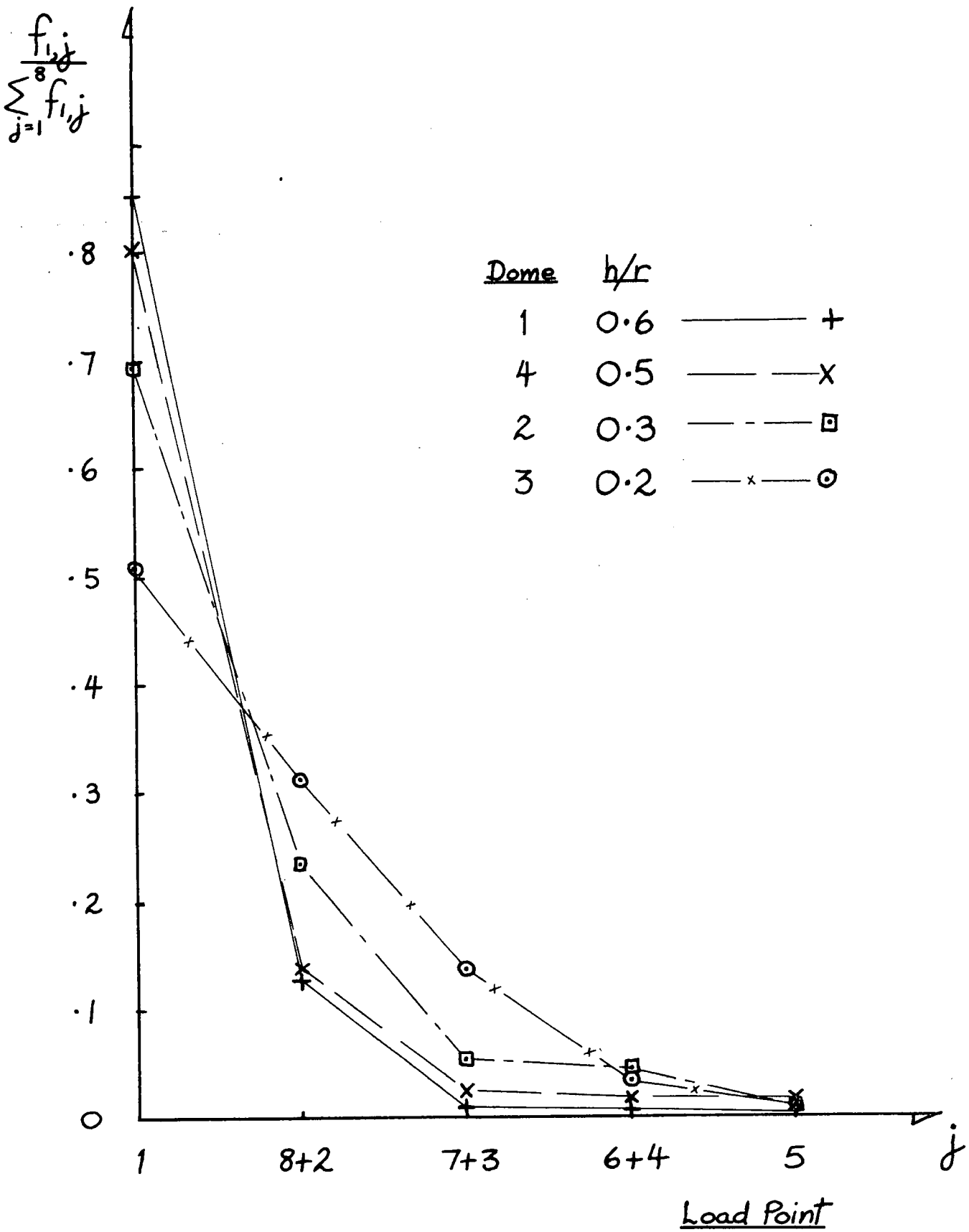

FIG. 6·3

Variation in the displacement at $i$ with change in ratio $h/r$, for the condition where all top panels are loaded with equal vertical loads

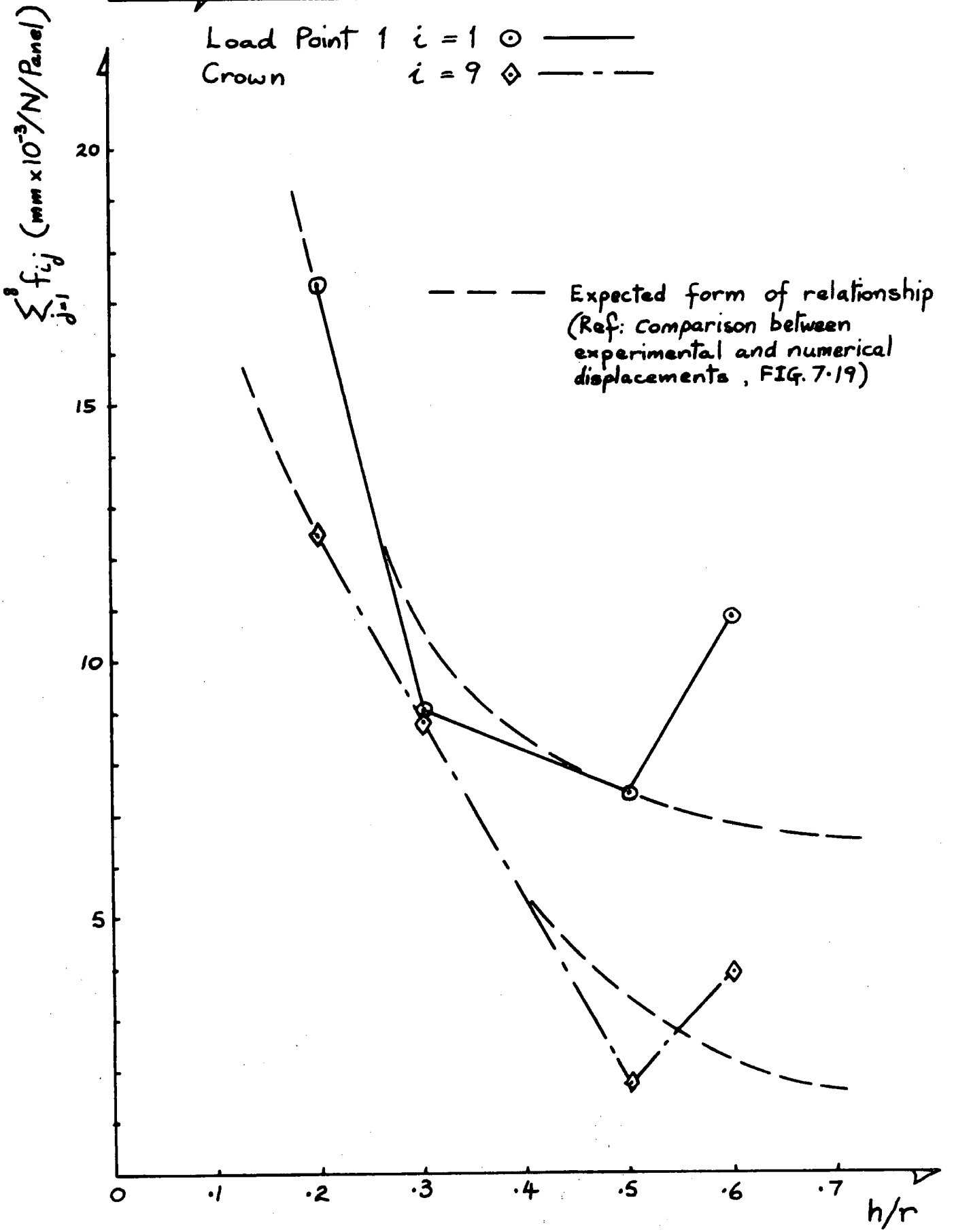

TABLE 6·1

Flexibility Influence Coefficients $f_{i,j}$ mm $\times 10^{-3}$/N DOME 1

Displacement at $i$ due to 1N applied at $j$

| Displacement Point $i$ \ Load Point $j$ | 1 | 2 | 3 | 4 | 5 | 6 | 7 | 8 | $\sum_{j=1}^{8} f_{i,j}$ | Direction $f_{i,k}$ |
|---|---|---|---|---|---|---|---|---|---|---|
| 1 | 9·302 | 1·157 | ·054 | ·033 | ·043 | ·033 | ·054 | ·238 | 10·914 | Vertical |
| 9 | ·499 | ·499 | ·499 | ·499 | ·499 | ·499 | ·499 | ·499 | 3·992 | Radial |
| 10 | ·958 | ·472 | ·067 | ·021 | ·000 | ·169 | ·372 | ·749 | 2·808 | Vertical |
| 14 | 2·905 | 2·905 | ·214 | ·087 | ·122 | ·122 | ·087 | ·214 | 6·656 | Radial |
| 11 | ·739 | ·739 | ·097 | ·000 | ·000 | ·000 | ·000 | ·097 | 1·672 | Vertical |
| 12 | ·295 | ·295 | ·141 | ·000 | ·000 | ·000 | ·000 | ·141 | ·872 | Horiz$^{l}$ |
| 13 | | | | | | | | | | |

TABLE 6·2

Flexibility Influence Coefficients $f_{i,j+k}$ mm $\times 10^{-3}$/N DOME 1

Displacement at $i$ due to, 1N applied at $j$ + 1N applied at $k$

| Displacement Point $i$ \ Load Points $j+k$ | 1+2 | 2+3 | 3+4 | 4+5 | 5+6 | 6+7 | 7+8 | 8+1 | $\sum_{i=1,\ k=j+1}^{8} f_{i,j+k}$ | Direction $f_{i,j+k}$ |
|---|---|---|---|---|---|---|---|---|---|---|
| 1 | 10·194 (10·459) | ·985 (1·211) | ·234 (·087) | ·164 (·076) | ·168 (·076) | ·249 (·087) | ·488 (·292) | 8·342 (9·540) | 20·824 (21·824) | Vertical |
| 9 | ·998 (·998) | ·998 (·998) | ·998 (·998) | ·998 (·998) | ·998 (·998) | ·998 (·998) | ·998 (·998) | ·998 (·998) | 7·984 (7·984) | Radial |
| 10 | 1·379 (1·430) | ·632 (·539) | ·222 (·088) | ·174 (·021) | ·265 (·169) | ·592 (·541) | 1·188 (1·121) | 1·335 (1·707) | 5·787 (5·616) | Vertical |
| 14 | 6·116 (5·810) | 3·256 (3·119) | ·510 (·301) | ·301 (·209) | ·387 (·244) | ·301 (·209) | ·510 (·301) | 3·256 (3·119) | 14·637 (13·312) | Radial |
| 11 | 1·387 (1·478) | 1·276 (·836) | ·092 (·097) | ·000 (·000) | ·000 (·000) | ·000 (·000) | ·092 (·097) | 1·276 (·836) | 4·123 (3·344) | Vertical |
| 12 | ·357 (·580) | ·214 (·436) | ·133 (·141) | ·000 (·000) | ·000 (·000) | ·000 (·000) | ·133 (·141) | ·214 (·436) | 1·051 (1·744) | Horiz$^{l}$ |
| 13 | | | | | | | | | | |

Notes:

1/ All values quoted in Tables 6·1 & 6·2 are average values derived from all the readings taken during load series 1 and 2 respectively.

2/ In Table 6·2, 10·194 = $f_{i,j+k}$ ; (10·459) = $f_{i,j} + f_{i,k}$.

3/ Positive displacements are in towards the centre of the dome.

TABLE 6·3

Flexibility Influence Coefficients $f_{i,j}$ mm x $10^{-3}$/N DOME 2

Displacement at i due to 1N applied at j

| Displacement Point i | Load Point j | | | | | | | | | |
|---|---|---|---|---|---|---|---|---|---|---|
| i \ j | 1 | 2 | 3 | 4 | 5 | 6 | 7 | 8 | $\sum_{j=1}^{8} f_{i,j}$ | Direction $f_{i,j}$ |
| 1 | 6·315 | ·895 | ·260 | ·180 | ·135 | ·240 | ·250 | ·785 | 9·060 | Vertical |
| 9 | 1·110 | 1·110 | 1·110 | 1·110 | 1·110 | 1·110 | 1·110 | 1·110 | 8·880 | Radial |
| 10 | 1·733 | ·845 | ·350 | ·350 | ·350 | ·350 | ·845 | 1·733 | 6·556 | Vertical |
| 14 | 3·000 | 3·000 | ·725 | ·475 | ·500 | ·500 | ·475 | ·725 | 9·400 | Radial |
| 11 | 2·265 | 2·265 | ·555 | ·000 | ·135 | ·135 | ·000 | ·555 | 5·910 | Vertical |
| 12 | 1·630 | 1·630 | ·405 | ·000 | ·000 | ·000 | ·000 | ·405 | 4·070 | Horiz$^{l}$ |
| 13 | 1·270 | ·500 | ·110 | ·000 | ·180 | ·100 | ·300 | ·980 | 3·440 | Normal to Panel |

TABLE 6·4

Flexibility Influence Coefficients $f_{i,j+k}$ mm x $10^{-3}$/N DOME 2

Displacement at i due to, 1N applied at j + 1N applied at k

| Displacement Point i | Load Points j+k | | | | | | | | | |
|---|---|---|---|---|---|---|---|---|---|---|
| i \ j+k | 1+2 | 2+3 | 3+4 | 4+5 | 5+6 | 6+7 | 7+8 | 8+1 | $\sum_{j=1,k=j+1}^{8} f_{i,j+k}$ | Direction $f_{i,j+k}$ |
| 1 | 9·680 (7·210) | 2·850 (1·155) | ·085 (·440) | 1·220 (·315) | 1·120 (·375) | 1·370 (·490) | 2·390 (1·035) | 8·970 (7·100) | 28·450 (18·120) | Vertical |
| 9 | 2·715 (2·220) | 2·715 (2·220) | 2·715 (2·220) | 2·715 (2·220) | 2·715 (2·220) | 2·715 (2·220) | 2·715 (2·220) | 2·715 (2·220) | 21·720 (17·760) | Radial |
| 10 | 2·980 (2·578) | 1·525 (1·195) | ·810 (·700) | ·963 (·700) | ·963 (·700) | 1·525 (1·195) | 2·980 (2·578) | 4·170 (3·466) | 15·916 (13·112) | Vertical |
| 14 | 8·150 (6·000) | 4·990 (3·725) | 1·835 (1·200) | 1·320 (·975) | 1·520 (1·000) | 1·320 (·975) | 1·835 (1·200) | 4·990 (3·725) | 25·960 (18·800) | Radial |
| 11 | 6·720 (4·530) | 3·820 (2·820) | ·710 (·555) | ·200 (·135) | ·500 (·270) | ·200 (·135) | ·710 (·555) | 3·820 (2·820) | 16·680 (11·820) | Vertical |
| 12 | 1·320 (3·260) | 1·420 (2·035) | ·400 (·405) | ·000 (·000) | ·300 (·000) | ·000 (·000) | ·400 (·405) | 1·420 (2·035) | 5·260 (8·140) | Horiz$^{l}$ |
| 13 | 2·900 (1·770) | 1·010 (·610) | ·200 (·110) | ·400 (·180) | ·400 (·280) | 1·010 (·400) | 1·930 (1·280) | 3·160 (2·250) | 11·010 (6·880) | Normal to Panel |

Notes:

1/ All values quoted in Tables 6·3 & 6·4 are average values derived from all the readings taken during load series 1 and 2 respectively.

2/ In Table 6·4, 9·680 = $f_{i,j+k}$ ; (7·210) = $f_{i,j} + f_{i,k}$.

3/ Positive displacements are in towards the centre of the dome.

TABLE 6·5

Flexibility Influence Coefficients $f_{i,j}$ mm x $10^{-3}$/N DOME 3

Displacement at $i$ due to 1N applied at $j$

| Displacement Point $i$ \ Load Point $j$ | 1 | 2 | 3 | 4 | 5 | 6 | 7 | 8 | $\sum_{j=1}^{8} f_{i,j}$ | Direction $f_{i,j}$ |
|---|---|---|---|---|---|---|---|---|---|---|
| 1 | 8·800 | 3·000 | 1·330 | 0·070 | 0·200 | 0·470 | 1·050 | 2·470 | 17·390 | Vertical |
| 9 | 1·560 | 1·560 | 1·560 | 1·560 | 1·560 | 1·560 | 1·560 | 1·560 | 12·480 | Radial |
| 10 | 2·950 | 1·250 | ·400 | ·000 | ·000 | ·400 | 1·250 | 2·950 | 9·200 | Vertical |
| 14 | 5·300 | 5·300 | 1·900 | ·600 | ·300 | ·300 | ·600 | 1·900 | 16·200 | Radial |
| 11 | 5·200 | 5·200 | 1·150 | 1·350 | -·350 | -·350 | 1·350 | 1·150 | 14·700 | Vertical |
| 12 | 0·550 | 0·550 | ·000 | ·050 | -·050 | -·050 | ·050 | ·000 | 1·100 | Horiz$^{l}$ |
| 13 | 3·000 | 1·400 | ·000 | -·500 | -·100 | ·000 | ·600 | 1·300 | 5·700 | Normal to Panel |

TABLE 6·6

Flexibility Influence Coefficients $f_{i,j+k}$ mm x $10^{-3}$/N DOME 3

Displacement at $i$ due to, 1N applied at $j$ + 1N applied at $k$

| Displacement Point $i$ \ Load Points $j+k$ | 1+2 | 2+3 | 3+4 | 4+5 | 5+6 | 6+7 | 7+8 | 8+1 | $\sum_{i=1}^{8} f_{i,j+k}$ $k=j+1$ | Direction $f_{i,j+k}$ |
|---|---|---|---|---|---|---|---|---|---|---|
| 1 | 12·500 (11·800) | 4·600 (4·330) | 2·300 (1·400) | 1·330 (·270) | ·700 (·670) | 2·200 (1·520) | 4·800 (3·520) | 11·600 (11·270) | 40·030 (34·780) | Vertical |
| 9 | 3·700 (3·120) | 3·700 (3·120) | 3·700 (3·120) | 3·700 (3·120) | 3·700 (3·120) | 3·700 (3·120) | 3·700 (3·120) | 3·700 (3·120) | 29·600 (24·960) | Radial |
| 10 | 5·300 (4·200) | 1·800 (1·650) | ·900 (·400) | ·900 (·000) | ·700 (·400) | 2·300 (1·650) | 5·300 (4·200) | 5·500 (5·900) | 22·700 (18·400) | Vertical |
| 14 | 11·800 (10·600) | 7·750 (7·200) | 3·450 (2·500) | 1·500 (·900) | ·300 (·600) | 1·500 (·900) | 3·450 (2·500) | 7·750 (7·200) | 37·500 (32·400) | Radial |
| 11 | 13·000 (10·400) | 7·850 (6·350) | 1·000 (2·500) | ·300 (1·000) | -1·400 (-·700) | ·300 (1·000) | 1·000 (2·500) | 7·850 (6·350) | 29·900 (29·400) | Vertical |
| 12 | ·300 (1·100) | ·000 (·550) | ·000 (·050) | ·000 (·000) | -·200 (-·100) | ·000 (·000) | ·000 (·050) | ·000 (·550) | ·100 (2·200) | Horiz$^{l}$ |
| 13 | 5·400 (4·400) | 1·700 (1·400) | -·200 (-·500) | ·000 (-·600) | -·200 (-·100) | 1·200 (·600) | 6·200 (1·900) | 5·700 (4·300) | 19·800 (11·400) | Normal to Panel |

Notes:

1/ All values quoted in Tables 6·5 & 6·6 are average values derived from all the readings taken during load series 1 and 2 respectively.

2/ In Table 6·6, 12·500 = $f_{i,j+k}$ ; (11·800) = $f_{i,j} + f_{i,k}$.

3/ Positive displacements are in towards the centre of the dome.

TABLE 6·7

Flexibility Influence Coefficients $f_{i,j}$ mm x $10^{-3}$/N DOME 4

Displacement at i due to 1N applied at j

| Displacement Point i | j / i | Load Point j: 1 | 2 | 3 | 4 | 5 | 6 | 7 | 8 | $\sum_{j=1}^{8} f_{i,j}$ | Direction $f_{i,j}$ |
|---|---|---|---|---|---|---|---|---|---|---|---|
| | 1 | 6·020 | ·800 | ·060 | ·070 | ·130 | ·070 | ·110 | ·220 | 7·480 | Vertical |
| | 9 | ·220 | ·220 | ·220 | ·220 | ·220 | ·220 | ·220 | ·220 | 1·760 | Radial |
| | 10 | ·370 | ·070 | ·050 | ·000 | ·000 | ·050 | ·070 | ·370 | ·980 | Vertical |
| | 14 | 1·940 | 1·940 | ·000 | ·100 | ·140 | ·140 | ·100 | ·000 | 4·360 | Radial |
| | 11 | ·350 | ·350 | ·000 | ·000 | ·000 | ·000 | ·000 | ·000 | ·700 | Vertical |
| | 12 | ·200 | ·200 | ·000 | ·000 | ·000 | ·000 | ·000 | ·000 | ·400 | Horiz$^{l}$ |
| | 13 | ·200 | -·200 | --120 | ·000 | ·000 | ·000 | ·000 | ·240 | ·120 | Normal to Panel |

TABLE 6·8

Flexibility Influence Coefficients $f_{i,j+k}$ mm x $10^{-3}$/N DOME 4

Displacement at i due to, 1N applied at j + 1N applied at k

| Displacement Point i | j+k / i | Load Points j+k: 1+2 | 2+3 | 3+4 | 4+5 | 5+6 | 6+7 | 7+8 | 8+1 | $\sum_{\substack{j=1 \\ k=j+1}}^{8} f_{i,j+k}$ | Direction $f_{i,j+k}$ |
|---|---|---|---|---|---|---|---|---|---|---|---|
| | 1 | 6·990 (6·820) | ·670 (·860) | ·100 (·130) | ·130 (·200) | ·100 (·200) | ·110 (·180) | ·300 (·330) | 6·330 (6·240) | 14·730 (14·960) | Vertical |
| | 9 | ·520 (·440) | ·520 (·440) | ·520 (·440) | ·520 (·440) | ·520 (·440) | ·520 (·440) | ·520 (·440) | ·520 (·440) | 4·160 (3·520) | Radial |
| | 10 | ·590 (·440) | ·050 (·120) | ·000 (·050) | ·040 (·000) | ·000 (·050) | ·050 (·120) | ·590 (·440) | 1·020 (·740 | 2·340 (1·960) | Vertical |
| | 14 | 4·260 (3·880) | 1·960 (1·940) | ·200 (·100) | ·200 (·240) | ·250 (·280) | ·200 (·240) | ·200 (·100) | 1·960 (1·940) | 9·230 (8·720) | Radial |
| | 11 | ·540 (·700) | ·220 (·350) | ·180 (·000) | ·000 (·000) | ·000 (·000) | ·000 (·000) | ·180 (·000) | ·220 (·350) | 1·340 (1·400) | Vertical |
| | 12 | ·370 (·400) | ·200 (·200) | ·080 (·000) | ·000 (·000) | ·000 (·000) | ·000 (·000) | ·080 (·000) | ·200 (·200) | ·930 (·800) | Horiz$^{l}$ |
| | 13 | ·120 (·000) | -·200 (-·320) | -·240 (-·120) | ·000 (·000) | ·000 (·000) | ·000 (·000) | ·490 (·240) | ·440 (·440) | ·610 (·240) | Normal to Panel |

Notes:

1/ All values quoted in Tables 6·7 & 6·8 are average values derived from all the readings taken during load series 1 and 2 respectively.

2/ In Table 6·8, 6·990 = $f_{i,j+k}$ ; (6·820) = $f_{i,j} + f_{i,k}$.

3/ Positive displacements are in towards the centre of the dome.

## 7. DESTRUCTIVE TESTS ON DOMES, (Load Series 3)

In load series 3 the domes were tested to destruction using the loading system described in Section 3.1. The load was applied in increments which were multiples of 55.5 N/Panel, i.e. an increase in the total load applied to the dome of 100 lbs. Displacement readings were recorded after the application of each increment of load until there was no significant change in the displacements with time. A further increment of load was then applied.

### 7.1.1 Behaviour of Dome 1 during test to destruction

Dome 1 was loaded with increments of load up to a value of 464 N/Panel, at which stage there was no visible deformation, and time dependent effects had not become significant. The crown, load points and rhomb centre nodes, (R.C.Ns.), all moved in towards the centre of the dome. The rhomb corner projections, (R.C.Ps.), moved down and out. There was no significant movement at the feet.

The load/displacement relationships were not regular, but no explanation could be found for this. When it was attempted to increase the load to 575 N/Panel a sudden failure occurred at three of the load cable clamps adjacent to the load hanger. The load was immediately released.

The dome had suffered no visible damage, the load cables were therefore repaired and testing restarted.

The load was again applied in increments. At an intensity of 853 N/Panel the average elastic displacement of the load points was 5.65 mm, and their average total displacement, including time dependent displacement, was 9.48 mm. The top panels had deflected so that adjacent top panels which contained a valley joint, formed dish shaped depressions which were roughly parabolic in cross-section and extended

across the centre of the valley and around the load crabs, Fig. 7.1. There was no visible deformation in the bottom panels. The top longitudinal ridge joints could be seen to be sagging, and the bottom longitudinal ridge joints could be seen to be hogging, (maximum deflection 1-2 mm). The transverse ridge joints showed no signs of any deformation.

During the application of the load increment from 797 to 853 N/Panel the dome showed signs of stiffening against further deformation. This was probably due to a reduction in the bending moment in the top panels as a result of their deformantion.

At a load intensity of 908 N/Panel the first evidence of a failure was detected. A blister had developed on the top surface of panel 2. The blister was approximately 75 mm x 50 mm and orientated parallel to a line between between load points 1 and 2, butting up to the valley joint, Fig. 7.2. This blister had developed at the point of maximum curvature, at the edge of the dished area which extended over the centre of panels 1 and 2, where the compressive stress in that top face, was greatest. When the dome was dismantled the blister was confirmed as being due to a failure of the core/face bond at that location. The cause of the failure was probably a mixture of tensile failure of the bond normal to the plane of the face, and core penetration, (Sections 2.4.1 and 4.4).

The top panels had developed a pronounced wave-form along the length of the valley joints, as shown in Fig. 7.3, which indicated that the top panels were beginning to buckle.

The bottom panels still showed no signs of any deformation.

The dome had failed but it was decided to continue so as to develop the failure. The failure load was maintained over the weekend, but no significant changes resulted.

The buckling in the top panels became more pronounced when the load was increased, otherwise no significant changes occurred up to a load intensity of 1019 N/Panel, when there was a significant fall off in the load in cables 3 and 4. A marked rise in the rate of increase in the displacement readings indicated that some kind of failure had occurred. Several small areas were found where the core/face bond had failed, most of the top panels exhibited this to some degree, on either their top and/or bottom face(s) in areas where the face(s) were in compression. The size of the blisters varied from approximately 50 to 100 mm diameter.

The first evidence of failure of the bottom panels was also discovered at this stage. Panel 11 had developed a 50 mm wide blister, approximately 300 mm up from the segment foot, which extended completely across the width of the top face. Similar blisters had begun to form in both faces of panel 12. The reason why blisters should form at these particular locations appeared to be that at this location compressive membrane action in the faces was sufficiently concentrated to cause wrinkling, (local buckling of the faces). Below this level the panel faces were being stabilised by the presence of the bottom longitudinal ridges and the edge beams.

It was observed that following the failures occurring when the load was increased to 1019 N/Panel, the dome showed signs of having regained its stiffness following a period during which the dome was left to creep.

Loading continued until at an intensity of 1130 N/Panel load cables 3 and 4 failed in tesnion. As the dome had obviously failed the test was abandoned and all the load was removed to allow the dome to recover.

Fig. 7.4 shows the graphs of the load intensity V elastic displacements for the crown and load points 5 and 6.

### 7.1.2 Recovery and Dismantling of dome 1

Upon removal of the load the dome experienced an instantaneous elastic recovery, (load points 5 and 6 recovering over 80% of their elastic displacements). The dome was then left to recover for four days, after which the dome was dismantled. At this time load points 5 and 6 having recovered over 70% of their total displacements. The rate of recovery had become insignificant, but the dome had already recovered to the extent that an uninformed observer could not detect that the dome had ever been loaded, even the blisters in the faces having disappeared.

When the dome was dismantled it was obvious that the core/face bond had failed in many locations, but it was not possible to determine the exact nature of these failures. It was suspected that they were caused by either, a shear failure; or a tensile bond failure normal to the plane of the face as a result of wrinkling, (1, 13); or a combination of these.

### 7.1.3 Observations on behaviour of dome 1 during test to destruction

From the evidence gathered during load series 3 for dome 1 it would appear that a dome of this nature with ratio $h/r = 0.6$ will fail as a result of a local failure in one or more of the panels. There was no evidence to suggest that either the segments, or the dome itself would become unstable when the dome was subjected to a symmetrical system of loads.

During loading the dome's top panels gained increased stiffness against further displacement due to the form of their deformation. Initially the top panels formed dish shaped depressions as shown in Fig. 7.1. As loading progressed these depressions spread until they extended almost completely across pairs of adjacent top panels

which contained a valley joint. The deformed shape assumed had the effect of reducing the bending moments in these panels. The ridge joints appeared to transmit significant amounts of thrust and shear between adjacent panels, (Section 4.0), but transfer of bending moments did not appear to be significant.

As loading progressed the top panels began to buckle as shown in Fig. 7.3, which resulted in additional stiffening of the top panels against further deformation. The deflected shape of the valley was the same as that predicted by the numerical model, the inflections adjacent to the crown and R.C.P. being due to geometric stiffness at these locations. It was to be expected that when the top panels buckled the mode would be induced by the deflected shape of the valleys. The ridges which were consequently formed across the valley joints stiffened the top panels against bending normal to the line of the valleys.

From load series 3 an indication can be gleaned of the type of failure which would have resulted had the adhesive not failed at the core/face interfaces of the panels. A general buckling of the top panels would probably have continued until some unrecoverable contortion resulted. Due to what appeared to have been a premature failure of dome 1, it was decided to construct another dome of similar h/r, (dome 4, $h/r = 0.5$).

7.2.1 Behaviour of Dome 2 during tests to destruction

Dome 2 was loaded with increments of loading up to an intensity of 331 N/Panel before the first visible deformation occurred in the form of shallow depressions around the load crabs, (approximately 150 mm dia.). As the load was increased to 508 N/Panel dish shaped depressions formed, extending around and between the load crabs of pairs of adjacent top panels which contained a valley joint. All points along the valley joints had experienced a large displacement, relative to the R.C.N.s. The dome as a whole was significantly more flexible than dome 1 . Displacements were due primarily to an overall translation of the panels. The foot of the segment containing panels 4 and 5 had yielded 2.18 mm horizontally, which was cause for concern. The average elastic and total displacements for the load points being 7.10 mm and 8.20 mm respectively.

When the load was again increased the depressions in the top panels spread so as to cover the whole of the combined area of pairs of adjacent top panels which contained a valley joint. A slight outward bowing was visible, in the bottom panels, all the ridge joints, and along the length of the edge beams. Upon increasing the load to 642 N/Panel the dome was observed to stiffen against further deformation.

At a load intensity of 819 N/Panel the undersides of the valley joints could be seen to be expanding, due to tension caused by bending across the width of these joints, but no failure could be detected. The horizontal yield of the foot of the segment containing panels 4 and 5 had increased to 4.80 mm.

Failure occurred at the underside of the valley joints as the load was increased to 908 N/Panel. The bond between the bottom faces had fractured in a random manner along an average of approximately

20% of the length of the joints.

It was decided to continue with the loading so as to develop the failure, but as the load was increased the feet of the segment containing panels 2 and 3, and the segment containing panels 4 and 5 failed , (Section 3.4.1).

Fig. 7.5 shows the graphs of load intensity v elastic displacements for the crown and load points 1 and 2, for the first test to destruction for dome 2.

As the dome appeared to be undamaged apart from the valley joints, it was decided to repair the dome and repeat load series 3 for the dome, (Sections 3.4.2 and 4.2.2).

Loading was restarted following the repair of the dome, but when the loading reached an intensity of 686 N/Panel, the cable clamp on cable 5 adjacent to the load hanger failed. The loading was immediately released and the dome allowed to recover, (Section 3.5).

Having repaired cable 5 loading was again restarted. The behaviour of the dome was similar to that prior to the repairs to the valleys and the strengthening of the feet, but the magnitudes of the displacements were considerably reduced. Horizontal yielding of the feet had been almost completely eliminated. The effect of flexibility at the supports can be appreciated by comparing the graphs of load intensity v elastic displacements for the two foot details used in conjunction with dome 2, Figs. 7.5 and 7.8.

When the load intensity had reached 908 N/Panel, adjacent top panels which contained a valley joint, began to develop the same kind of wave form along the length of the valleys as was observed during the testing of dome 1, but much less pronouced, Fig. 7.3. All the ridge joints and the edgebeams were bowing out from the centre of the dome, (a maximum of 2-3 mm). Time dependent effects had become significant.

As the load intensity was increased deformation of the top panels became more pronounced, but the bottom panels showed no visible signs of any deformation.

While increasing the load intensity to 1186 N/Panel it was observed that the top longitudinal ridges had begun to bow in towards the centre of the dome. A further increment of loading from 1186 to 1241 N/Panel and pairs of adjacent top panels which contained a valley joint had formed continuous dish shaped dperessions over the whole of their combined surface. This indicated that the geometric stiffness at the crown and R.C.P.s, which in conjunction with any joint stiffness produced the inflections at either end of the valleys, had been overcome. There were no signs of any instability at the crown. Time dependent deformation had become large.

The maximum load intensity using the loading system, (1408 N/Panel), was attained without any material failure having occurred, though by this time the deformations were unacceptably large, and would have been well beyond any limit state on deflection. The structure was left to creep, and 180 minutes later failure occurred due to buckling in the top longitudinal ridges between, panels 2 and 3,4and 5, and 6 and 7, Fig. 7.6. There were no other visible failures and the structure continued to sustain the failure load. Loading was maintained and the ridges' failures continued to develop until the buckling extended across the failed ridges from load point to load point, as shown in Fig. 7.7. Even at the most heavily distorted locations there was no indication that the faces and core had separated. The dome was left to creep for twelve days, but a total collapse did not ensue, even though the failure load was maintained throughout.

By means of the author pushing downwards on top of the dome it

was found that the dome had stiffened against further deformation, and was capable of sustaining a substantially greater load without collapsing. The load was released and the dome's recovery monitored.

Fig. 7.8 shows the graphs of load intensity v elastic displacements for the crown and load points, for the second test to destruction for dome 2.

7.2.2. Recovery and Dismantling of dome 2

The dome recovered most of its elastic displacement immediately, (load points 1 and 2, approximately 95%). The dome was then allowed to recover for a period of nine days at the end of which the rate of recovery was very small. Following recovery the only visible damage was the buckling of the top longitudinal ridges between panels 2 and 3, 4 and 5, and 6 and 7. The load points had recovered approximately 70% of their total displacement. When the dome was dismantled there was found to be no significant damage to any of the panels. There were some small random patches of core/face bond failure in most of the panels, but this was not sufficiently developed to have had any significant effect upon the dome's behaviour.

7.2.3 Observations on behaviour of dome 2 during test to destruction

From the evidence gathered during load series 3 for dome 2 it would appear that a dome with ratio $h/r = 0.3$ will fail as a result of instability in the ridge joint(s) of one or more of the segments. There was no evidence that the dome would become liable to general collapse, until one or more of the segments had failed as a result of a local failure, when the dome was subjected to a symmetrical system of loads.

As was expected dome 2 was more flexible than dome 1, but the difference was not as marked as had been expected. Dome 2 sustained a considerably greater ultimate load than dome 1 when retested

following the repair of the valley joints. This was largely a reflection upon the quality of the core/face bond in dome 1. It is probable that when retested dome 2 sustained a substantially higher ultimate load, due to "shakedown", following the application of load during the first test to destruction, than would have been carried had the dome been loaded for the first time, (6).

The graphs of load intensity v elastic displacements, Fig. 7.8, are not linear, which was probably due to changes in the geometry becoming significant. Dome 2 showed a much greater tendency towards overall translation of the panels, and reduced local deformation as compared with dome 1.

Due to the relative geometries of domes 1 and 2, the magnitude of the compressive membrane action in the bottom panels of dome 2 was much greater than in dome 1. The fact that there were no significant areas of bond failure in the bottom panels of dome 2 was a further indication of the relative competance of the core/face bonding for the two domes.

### 7.3.1 Behaviour of Dome 3 during test to destruction

#### 7.3.1.1 Strain Measurements

Due to the geometry of dome 3, it was assumed that stress levels in regions remote from the load points would be higher than for any of the other domes that were tested. For this reason dome 3 was chosen for a comparison between the experimental and numerical stress situations at selected locations on the panel faces.

Fig. 7.9 shows the strain gauge configuration used. Load intensity v elastic strain relationships were determined by applying a specific load intensity to the top panels and measuring the strain at a single rosette, as quickly as possible to eliminate time dependent effects, then releasing the load and allowing the dome to recover. The procedure was repeated for each rosetteat several different load intensities , until all the gauges had been calibrated.

The results that were obtained are discussed in Section 8.5.3.1.

#### 7.3.1.2 Test to destruction

Load was applied in increments as for the previous domes. The most stiking aspect of the dome's behaviour was that local deformation around the load points was much less pronounced than in the case of dome 2. Initially, displacement was due almost completely to translation of the panels. At a load intensity of 464 N/Panel the first visible deformation was observed in the form of shallow dish shape depressions around the loading crabs with a pronounced local depression at each of their feet. The general level of displacement was high compared with the other domes, the elastic displacement at the crown and load points being 4.84 mm and 7.61 mm (average) respectively. Horizontal yield at the feet was not significant.

When the load intensity was increased to 575 N/Panel all the ridge joints, and the edge beams could be seen to be bowing out from the centre of the dome, (maximum 1-2 mm). Time dependent effects had begun to be significant. The graphs of load intensity v elastic displacement, (Fig. 7.12), were not linear, which indicates that changes in the geometry had become large enough to have significant effect upon the magnitude of subsequent changes in the displacements. After the load had been maintained at 575 N/Panel for 144 minutes the top longitudinal ridges were found to be sagging in towards the centre of the dome, (Section 7.2.1), each with a maximum displacement, adjacent to the load crabs, of approximately 2 mm.

As the load intensity was increased the familiar dishing, observed in previous domes, began to spread across the valley joints from the centres of pairs of adjacent top panels which contained the valley joints. The valley joints developed a waveform similar to those encountered in domes 1 and 2, but much less pronounced. Most of the displacement continued to be in the form of an overall translation of the panels. The compressive membrane action in the bottom panels was relatively large, the heaviest concentrations being in the top faces adjacent to the feet. Horizontal yielding of the feet continued to be small.

When the load intensity was increased to 797 N/Panel the first evidence was found that failure had occurred in top panel 6, and bottom panels 9, 10 and 16. All of the failures were due to core/face bond failure,at the top face, which resulted in blistering in the top faces of those panels. The top faces of panels 9, 10, and 16 had blistered adjacent to the edge rails approximately 300 mm up from the feet.

These blisters were between 60 mm and 80 mm in diameter and bore a resemblance to bottom panel failures which occurred in dome 1. Panel 6 exhibited a 70 mm diameter blister situated at the point of maximum curvature in the panel and bore a resemblance to the failure which occurred in the top face of panel 2 of dome 1, but was situated 80 mm in from the line of the valley joint, Fig. 7.10. By this stage the displacements had become large, the elastic displacements for the crown and load points being 11.42 mm and 15.44 mm (average) respectively.

When the load was increased pairs of adjacent top panels which contained a valley joint developed into a general dish shaped depression, the inflections at either end of the valleys disappearing, (Section 7.2.1). The blistering in the panel faces continued to develop, and most of the bottom panels were found to have the same type of failure as had occurred in panels 9,10 and 16. The sagging in the top longitudinal ridges was becoming more pronounced, (Maximum 3-4 mm, at 908 N/Panel). In some locations on these ridges the face/coverstrip bond had failed in shear at the top face.

When the load intensity was increased to 1019 N/Panel there was no sign of any additional failure, other than the continued development of the core/face bond failures at the faces of the top and bottom panels. The bottom panels had a distinct band of blistering across the width of the top faces, approximately 300 mm up from the feet. There were numerous small random patches of blistering in both the top and bottom faces of the bottom panels, particularly along the length of the edge beams. Top panels 7 and 8 had developed failures in their top faces which were similar to that in panel 6. The dome was left to creep overnight, and in the morning two of the top

longitudinal ridges were found to have buckled.

Figure 7.11 shows a typical failure of the longitudinal ridges of dome 3. The ridges between panels 2 and 3, and 4 and 5 had buckled next to the R.C.Ns. These failures were very similar to those which occurred in dome 2, except that they were located closer to the R.C.Ns. The contortions in the panels were much more severe, and both faces had brittle fractures across the width of the joints, but there were no signs of either core penetration or bond failure. The valley joints between panels 1 and 2, and 3 and 4 had failed next to the R.C.Ps. due to tension across the joint, the extent of the failures being greatest at the bottom face due to the bending moments which these joints transferred. The load (1019 N/Panel) was maintained for a further 24 hours, but no noticeable change occurred.

The load intensity was then increased to the maximum for the system (1408 N/Panel), but little change occurred during the next 24 hours. The faces of the panels continued to be peeled from the core, and the tensile failures in the valley joints had extended. The valley joint between panels 5 and 6 had also begun to fail in tension next to the R.C.P. These failures extended for typically 50 mm along the top face, and 200 mm along the bottom face.

The ridge between panels 6 and 7 buckled approximately 49 hours after the load was increased to 1408 N/Panel. This failure was similar to the previous ridge failures, but was less pronounced.

Five days after the failure of the ridge between panels 6 and 7 it was decided to release the load as the dome had stiffened against further deformation. As for dome 2 the structure was capable of sustaining a considerably increased load, following the sustained period of creep, without a total collapse ensuing.

Figure 7.12 shows the graphs of load intensity v elastic displacement for the crown and loading points.

### 7.3.2 Recovery and Dismantling of Dome 3

When the load was released the dome made an instantaneous recovey of approximately half the total displacement. The dome was then allowed to recover for a period of six days before being removed to make way for it's successor. At the end of this period of recovery the dome had regained its initial shape except for the deformation of the top longitudinal ridges, having recovered approximately 75% of it's total displacement. The only visible damage was that to the ridges and the valley joints.

When the dome was dismantled there were found small randomly distributed areas of core/face bond failure in the top panels. The bottom panels exhibited fairly extensive bond failure, particularly in the top faces adjacent to the feet and along the edge beams. It was however doubtful whether these bond failures had any significant effect upon the overall behaviour of the dome.

### 7.3.3 Observations on behaviour of dome 3 during test to destruction

From the evidence gathered during load series 3 for dome 3 it would appear that a dome with $h/r = 0.2$ will fail as a result of instability in the ridge joint(s) of one or more of the segments, or as a result of a local failure in one or more of the panels. There was no evidence that the dome would become generally unstable, until one or more of the segments had failed due to a local failure, when the dome was subjected to a symmetrical system of loads.

As would be expected dome 3 was considerably more flexible than domes 1 and 2. The behaviour of the top panels was very similar to that for dome 2, except that overall translation of the panels was greatly increased, and local deformation was reduced. This behaviour was as expected following observations made during load

series 1 and 2, and from a knowledge of the behaviour of the joints when subjected to bending moments, (Sections 6.3.3 and 4.1.2).

Once again the degree of uniformity in the behaviour of the different panels was surprisingly good.

The failures which occurred in dome 3 were very similar to those which occurred in domes 1 and 2. The ridge joint configuration in dome 3 was much less stable than that of dome 2. This would explain why the buckling occurred directly adjacent to the R.C.Ns.. Had dome 3 been subjected to additional loads on the bottom panels, it is likely that all the ridge joints could have been induced to fail at a relatively low load intensity. The compressive membrane stresses in the bottom panel faces were proportionally large enough for instability in the top faces, (due to wrinkling), to be caused by relatively low loads at the top panels. As for the ridges, had the bottom panels been loaded the situation would have been worse.

### 7.4.1 Behaviour of Dome 4 during test to destruction

Dome 4 was loaded with increments of load up to an intensity of 689 N/Panel before there were any visible signs of deformation. The deformation was in the form of shallow depressions approximately 60 mm diameter around each of the feet of the load crabs. With the aid of a straight edge a very slight dishing was detected in the top panels. This dishing extended completely across the combined surfaces of pairs of adjacent top panels which contained a valley joint. All the displacement points had moved in towards the centre of the dome. The load points had average elastic and total displacements of 4.03 mm and 4.75 mm respectively.

When the load intensity had reached 926 N/Panel the top panels had begun to deform in the manner observed in the previous domes. There had developed a local dishing around the load points which extended across the valleys between adjacent load points. There were slight inflections along the lines of the valleys adjacent to the crown and the R.C.Ps.. These inflections were not as marked as in the case of dome 1. The dome bore a closer resemblance to the deformation observed in dome 2.

The general pattern of the deformation remained the same as the load intensity was increased.

Failure occurred when the load intensity was increased to 1376 N/Panel, due to core/face bond failure at the top faces of top panel 8 and bottom panel 10. Fig. 7.13 shows the extent and location of these failures. Due to their nature and position it is probable that the failure in panel 8 was due to a shear failure of the bond, and the failure in panel 10 was due to a tensile failure of the bond due to wrinkling in the face.

At the failure load the only visible deformation were the dish

shaped depressions in the top panels, which extended across the centre of the valleys. The inflections at either end of the valleys had not become pronounced, as had happened in dome 1. Deformation around the load points was less localised than in dome 1.

Following the above failures the structure was left to creep.

After the dome had crept for 18 hours, no new failures had occurred, but the failures in panels 8 and 10 had increased in magnitude as indicated in Fig. 7.13. All the bottom longitudinal ridges, all the transverse ridges, and all the edge beams could now be seen to be bowing out from the centre of the dome, (maximum 1-2 mm).

The top longitudinal ridge between panels 8 and 1 was detected to be sagging in towards the centre of the dome, 24 hours after the dome had been left to creep. A new failure had developed in panel 12, which was similar to the failure in panel 10.

After a further 18 hours there was no significant change in the overall deformation. Most of the bottom panels had begun to develop wrinkling type failures in their top faces, along the side of the edge beams. The top faces of panels 8, 10, and 12 continued to be peeled from the core material in the regions where bond failure had occurred. There were no signs of any failure in the bottom faces of any of the panels.

When the dome had crept for 48 hours following the first panel failures, the ridge between panels 8 and 1 could be clearly seen to have begun to buckle adjacent to its centre, at the edge of the blister in the top face of panel 8. Fig. 7.14 shows the nature of the buckling which had been induced by the face failure in panel 8. None of the other top longitudinal ridges showed any visible deflection.

After the dome had crept for a total of 114 hours, during which time the load intensity was maintained at 1376 N/Panel, the dishing

across adjacent top panels which contained a valley joint had become more pronounced. The top faces of panels 8,10 and 12 showed no significant change. Most of the bottom panels exhibited wrinkling type failures in the top faces along the side of their edge beams, along the portion of their lengths between 200 mm to 600 mm from the segment feet. There were still no visible failures in the bottom faces of any of the panels. The magnitude of the buckling in the ridge between panels 8 and 1 had increased as shown in Fig. 7.15.

After 120 hours the rate of creep was judged to have become insignificant. As in the case of the other domes the structure had stiffened against further deformation, following relaxation of stress concentrations due to viscous effects. The load was released and the dome allowed to recover.

Fig. 7.16 shows the graphs of load intensity v elastic displacement for the crown and load points 1, 2 and 7.

7.4.2 Recovery and Dismantling of Dome 4

Upon removal of the load the dome recovered all the elastic deformation immediately. After elastic recovery the only visible deformation was a blister in the top face of panel 8, and an indentation in the ridge between panels 8 and 1 where the ridge had failed. After 42 hours the rate of recovery was small; even the deformation adjacent to the centre of ridge 8/1 had almost disappeared. The dome was allowed to recover over a total period of 22 days, at the end of which the dome had recovered approximately 75% of its total deformation.

When the dome was dismantled there was found to be no significant damage to any of the top panels, with the exception of panel 8. The failure of ridge 8/1 was due entirely to bond failure at the top face

of panel 8. There were many small, randomly distributed, areas of bond failure at the faces of the bottom panels, mostly in the top faces, but these were not sufficiently developed to have had any significant effect upon the overall structural behaviour of the dome.

7.4.3 Observations on behaviour of dome 4 during test to destruction

From the evidence gathered during load series 3 for dome 4, it would appear that a dome with ratio h/r = 0.5 will fail as the result of a local failure in one or more of the panels. There was no evidence to suggest that either, the segments, or the dome itself, would become generally unstable when the dome was subjected to a symmetrical system of loads.

Dome 4 was slightly more flexible than dome 1, which was why the top panels did not buckle along the line of the valleys as did the corresponding panels of dome 1. The behaviour of dome 4 was similar to that of dome 2, except that the deformation was more localised.

The ultimate load required to fail dome 4, (1376 N/Panel), was well in excess of that required to fail dome 1, (908 N/Panel), and dome 3, (797 N/Panel), and approximately equal to that required to fail dome 2, (1408 N/Panel). This confirmed the impression which had been gained previously that dome 1 failed prematurely due to the poor quality of the core/face bond. Had the quality of the core/face bonds in general been better it is highly probable that the ultimate loads sustained by domes 1 and 4 would have been substantially greater than that sustained by dome 2.

The core/face bond failures in the top faces of the bottom panels were an indication that they carried substantially greater compressive stresses than the bottom faces of the bottom panels. The buckling in these top faces adjacent to the edge beams, (wrinkling), was caused due to the thrust which was being transferred into those members.

The graphs of load intensity v elastic displacement, Fig. 7.16, were not continuously linear, which indicated that changes in the geometry were significant at high load intensities. It can be seen from the disparity of the load v elastic displacement relationships for the three feet of loading crabs 1 and 2 that there was a translation of the lines of action of the loads, (Fig. 7.16). However this translation was not large, and it would appear reasonable when analysing domes of this type to assume that the lines of action of the loads remained constant.

## 7.5 Time Dependent Deformation of domes during tests to destruction, domes 1 to 4

The creep characteristics of plastics seriously limit their use as structural materials. Creep must always be taken into account in design. No matter how small the stress, whether in compression, tension or shear, creep will occur. In general creep eliminates plastics from consideration as materials to carry primary stresses. Sandwich panels with plastic faces and foamed plastic cores, are therefore only suitable to withstand transient loading systems.

### 7.5.1 Analysis of Time Dependent Deformation, Domes 1 to 4

As mentioned previously in Sections 3.1.1 and 7.0, a continuous record was made of the variation of displacements with time during the tests to destruction for each of the domes 1 to 4. Using these records a study was made of the time dependent displacement for these domes.

The methods used, to analyse the time dependent behaviour of the domes, were similar to those used by Parton (12). Domes 1 and 3 were chosen for detailed analysis of the relationship between the time dependent displacement, ( $\delta_{TDi}$ ), and time, (T), for the load points, (i = 1), and the crown, (i = 9). These two domes were chosen becuase they are at the two extremes of the range of the ratio, h/r for the domes that were tested.

The first analysis performed was to determine whether $\delta_{TDi}$ was proportional to the square root of T, (time in minutes since the application of the load increment being considered). It soon became apparent that, although $\delta_{TDi}$ was proportional to time, the power of T was not one half.

As displacements were proportional to time it was decided to

plot 'log-log graphs', to determine the power of T in the general expression

$$\delta_{TDi} = T^{n_i} \qquad (1)$$

Figs. 7.17 and 7.18 show typical graphs for the variation of $\delta_{TDi}$ with time and the determination of $n_i$ for the load points and crown of dome 3, at a load intensity of 464 N/Panel. Tables 7.1 to 7.4 show the values of $n_i$ for each increment in the load intensities up to the failure loads for domes 1 and 3.

A third analysis was performed to determine the ratio of total displacement to elastic displacement for load points, crown, rhomb centre nodes, and rhomb corner projections for domes 1 to 4. The constants derived are shown in Table 7.5 and represent the ratio of the sum of all the displacements, including any time dependent displacements : the sum of the elastic displacements, for all the increments in load up to and including the maximum load intensity for which displacements were recorded.

7.5.2 Observations on Time Dependent Behaviour of Domes 1 to 4

Analysing the results presented in Tables 7.1 to 7.4 the following points emerged:

1. There was no apparent constant relationship between the time dependent displacements and the time since the application of load increments. Time dependent displacements and the index $n_i$ depend upon the location of displacement point i, the time since the application of load increments, the loading history, the size of the load increment, and the magnitude of the total applied load.

2. There was an increase in the magnitude of the time dependent displacements with the magnitude of the total applied load.

3. There was, for most increments of load, a comparatively short period during which there was a rapid rate of increase in displacements prior to the dome settling down to a steady rate of creep, as can be seen from Fig. 7.17, and Tables 7.1 to 7.4. The general trend appeared to be for the duration of the period of rapid creep to increase with the magnitude of the total applied load.

The conclusion to be drawn from the above is that an analysis of the time dependent displacements based on equations such as equation (1) is of relatively small use to an engineer, unless some constant relationship can be defined (12). What would be required if an accurate analysis were to be performed would be to establish some fundamental approach,based on stress/strain relationship, and the time dependent variations of the strain in the sandwich materials, which could be adapted for incorporation into a numerical model using an approach such as a finite element technique, (4,6). Such an analysis was beyond the scope of the work described in this thesis.

Provided that a dome is geometrically stable and the panel construction is able to resist design loads in accordance with 'CP3' and 'CP110' panels of the type used in domes 1 to 4 will not suffer any permanent structural damage due to time dependent effects under normal service conditions. The most severe service loading conditions are likely to be caused by transient wind loads; however snow and possibly construction or maintenance loads may be relatively prolonged. A designer would need to take into account the possibility of time dependent deformation when calculating displacements for the

serviceability limit state. The constants listed in Table 7.5 give an indication of the maximum range of suitable factors to be applied to the elastic displacements to take account of any time dependent deformation. Suitable values for $C_i$ in equation (2), (see Table 7.5), for a dome of the type and material tested, would seem to be in the range 2.00 to 3.50.

Factors based on the values quoted in Table 7.5 are in fact higher than those that would be needed to be applied in practice. More realistic values for these factors would be based on a dome's working load. The design load for a dome can be derived from the ultimate load using the partial load factors recommended in CP110: Part I: 1972: Section 2.3.3.1 for determining the design loads, (ultimate limit state), for dead and imposed load. The design load $= 1.4\ G_K + 1.6\ Q_K$, where $G_K$ and $Q_K$ represent the characteristic dead load and characteristic imposed loads respectively. For practical purposes $G_K$ was negligible compared to $Q_K$ at the failure load of domes 1 to 4. The ultimate load for these domes can therefore be assumed to correspond to $1.6\ Q_K$. The design working load $Q_K$ can be taken as the failure load $\div 1.6$. The assumption that $G_K$ is negligible compared with $Q_K$ would still be valid for a full scale prototype, built from the same type of sandwich board as the model domes, with a base radius of three to five times that of the models.

Table 7.6 gives values of $C_i$ for domes 1 to 4 based on the assumed working loads calculated in the manner outlined above. As can be seen, the values of the constants are significantly reduced compared to those in Table 7.5. Acceptable values for $C_i$, based on

the working load for the design of a dome of the type and material tested,would be between 1.25 and 2.00. This is due to the fact that the relative magnitudes of time dependent displacements, compared with their corresponding elastic displacements, increase with the applied load.

Values of factors based on $C_i$ would depend upon the geometry of the dome, the type of material, the design life of the structure, and the location. Account should also be taken of the extent to which time dependent deformation is recoverable once loading is removed, and that recovery is aided by the suction effect due to wind loading, (8, 11).

## 7.6 General Observations Resulting from Destructive Tests on Domes 1 to 4

Following the work performed during load series 3 for domes 1 to 4 the following points emerged:

1. Domes 1 and 4 were the most resistant to displacement due to symmetrical loading of the top panels, but the degree by which their stiffnesses exceeded that of dome 2 was surprisingly small. Dome 3 was by far the most flexible (Figure 7.19).
2. For spherically conformant sandwich domes, where ratio $h/r \geqslant 0.2$, the structure as a whole will not become unstable until one or more of the segments has failed locally.
3. The domes tested had a very high degree of symmetry in their behaviour due to a symmetrical system of loads.
4. Under loading the domes were remarkably adept at shedding the effects of that loading, by virtue of the deformed shape assumed, even after failure had occurred.
5. The domes recovered all their elastic and most of their plastic deformation once loading was released.
6. The domes "concealed" all but the largest deformations due to loading.
7. For domes 1 and 4, where the ridges were geometrically more stable, the ultimate load depended upon the ultimate strength of the sandwich materials. For domes 2 and 3, where the ridges were geometrically unstable, the ultimate load depended upon the geometric stiffness of those domes.
8. The stability of the feet of a dome has a significant effect upon the structural behaviour of the dome (Dome 2, Section 7.2.1, Figures 7.5 and 7.8).

9. The edgebeams carried a significant proportion of the thrust in the bottom panels near to the feet of the domes. The general trend was for compressive thrust to be transfered from the longitudinal ridge into the edgebeams, moving down the panels from the R.C.Ns. towards the feet. The increase in the vertical displacements of the R.C.Ns. and R.C.Ps. as the ratio h/r was reduced,was an indication that the amount of compressive thrust in the bottom panels and edge beams was increased.

10. Time dependent effects (notably displacements) were significant at high load intensities.

11. It was apparent from the state of the contortions in the regions of the top panels of domes 2 and 3, where the ridges had buckled, that the panels were capable of withstanding severe deformation without any resulting permanent damage.

12. The quality of the panels from which the polyhedral sandwich domes were constructed was very important in terms of the strength of the core and face materials, the strength of the bond between the core and faces, and any initial deformation.

Figure 7.19 shows the variations in the elastic flexibility influence coefficients for crown, R.C.Ns., R.C.Ps., and load points, with the ratio h/r.

Tables 8.1 to 8.4 show the experimental and theoretical elastic flexibility influence coefficients for domes 1 to 4; load series 3.

## 7.7 Comparison with Behaviour of Polyhedral Sandwich Domes which were tested to Destruction by Other Workers at Durham University

Parton tested two sixteen faced, four segment domes, constructed from sandwich boards with birch ply faces and polyurethane cores, with ratio h/r = o.6, (r = 2.00 m), to destruction. The first dome was spherically conformant, and the second dome was nearly so, (12). The destructive testing in both cases was by the application of concentrated vertical loads at the centroids of a pair of adjacent top panels which contained a valley joint.

Manos constructed a twenty-four faced, six segment dome, with ratio h/r = 0.533, (r = 3.75 m), constructed from sandwich boards with hardboard faces and polyurethane cores, which was modified to a thirty-six faced dome by the addition of dormer sections (10). The purpose of the Manos dome was to determine the elastic influence coefficients for comparison with the numerical analyses which he performed. This dome was destroyed as a "final year undergraduate project" by Pryor (14). The destructive testing was by the application of sandbags, to the whole of the upper surface, which were distributed so as to achieve a uniform downward load.

Each of the above domes was failed using an incremental sequence of loading, during which time dependent deformation was allowed to develop. These tests were therefore suitable for direct comparison with those performed by the author.

Parton observed the following characteristics in the behaviour of the domes which he tested, which reinforce the observations made during the destructive, and non-destructive, tests on the domes in this project.

1. The Parton domes acted very much as though pairs of adjacent top

panels which contained a valley joint were a single quadrilateral flat sheet.

2. Parton observed that his second dome stiffened against further deformation at high load intensities due to the stiffening effect of the deflected shape of the loaded pair of panels. They developed the dish shaped type of depression which was observed in domes tested by the author. There was no buckling along the line of the valley joint between the loaded panels of the Parton domes, as occurred in dome 1 of this project (Section 7.1.1). This may have been because the crowns of the Parton domes were not constrained against movement in the horizontal plane due to symmetrical loading, and also because his board faces were relatively stiffer.

3. Following loading tests upon his first dome, during which strain measurements were taken, Parton observed that significant stresses in an unloaded panel were only produced by load on an adjacent panel, and received very little stress contribution from loads elsewhere. This confirms the pattern of behaviour which was reported for load series 1 and 2 (Section 6.0).

4. From strain measurements on his second dome, Parton observed a stress concentration around the R.C.Ns., which confirms the impression which was gained during the destructive tests on domes 2 and 3, that it was the stability of the R.C.Ns. and not the crown which was critical (Sections 7.2.3 and 7.3.3).

5. Parton performed tests upon his second dome to compare its behaviour before and after the application of the cover strips to the joints. He concluded that, ". . . the enhancement of the moment transfer over the joint was less important than the

general stiffening of the joints, causing them to act as stiffening members along the boundaries". This is of particular relevance to the conclusions which the author reached concerning the representation of the ridge joints in the numerical analyses for domes 1 to 4 (Section 8.0).

6. Parton observed the same general pattern of time dependent deformation as in this project. Because of the relatively long delay which he adopted between successive increments of load (24 hours) the effect of each increment was isolated to a much greater extent. As a result, his work showed much more clearly that the time dependent deformation for an increment of load increased with the magnitude of the total applied load.

7. When the load was released from the Parton domes following failure, the domes recovered to the extent that only slight deformation could be detected in just those panels that had been loaded. All other panels were undamaged.

Failure in the first Parton dome was as a result of a tensile fracture of the valley joint between the loaded top panels adjacent to the R.C.P. As in the case of similar failures which occurred in dome 3 of this project, the failure followed a sustained period of creep (Section 7.3.1). The second Parton dome failed due to tensile fracture of the ridge joints at one of the R.C.Ns. adjacent to the loaded panels. This type of failure is not compatible with those associated with downward symmetrical systems of loads such as were used in this project.

When Pryor tested the Manos dome to destruction, failure was initially due to tensile fractures in the top faces of the panels next to some of the ridge joints and adjacent to the apexes of the segments. Similar failures occurred along the underside of some of

the valley joints. Even though the joints all had 1 mm thick steel cover plates, compression ridges were detected along the top of two of the longitudinal ridge joints. These failures were similar in nature to those observed in domes 2 and 3 (Sections 7.2.1 and 7.3.1.2). The Manos dome collapsed under a total load of 8.1 tonnes, due to failure of four of the supporting columns, and it was therefore not possible to draw any firm conclusions concerning its ultimate mode of failure.

## Deformation Around Load Points Dome 1

FIG. 7·1

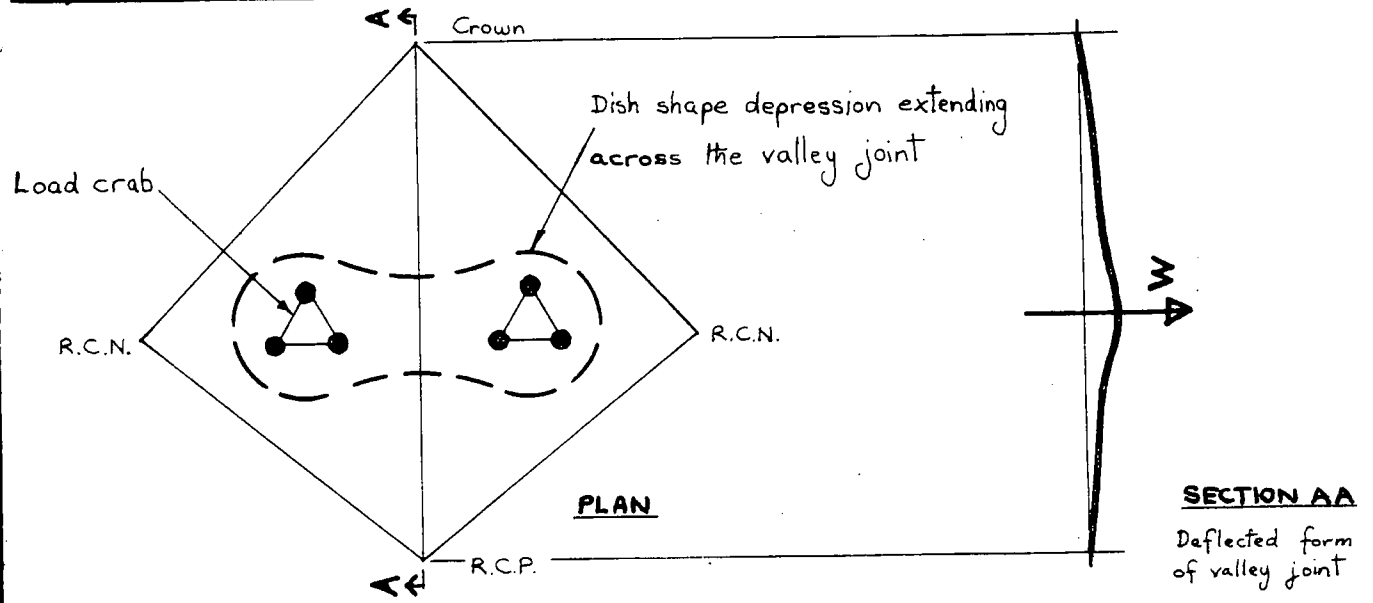


## Failure in Panel 2 Dome 1 (908N/Panel)

FIG. 7·2

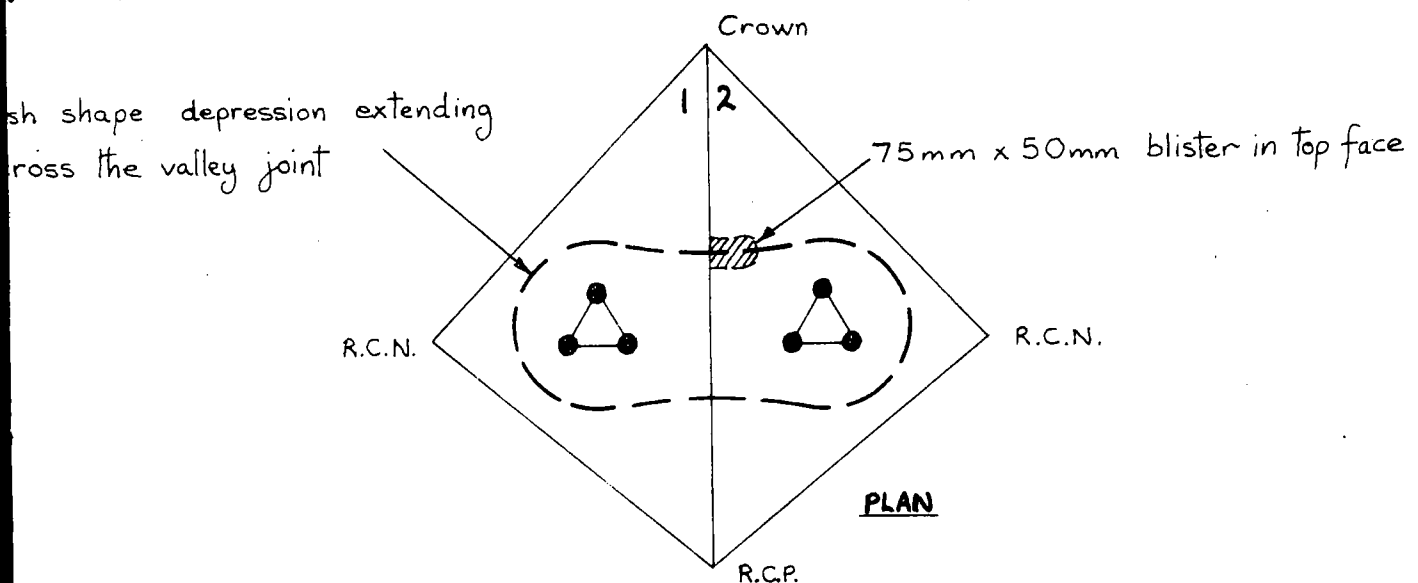


## Buckling of Top Panels Dome 1

FIG. 7·3

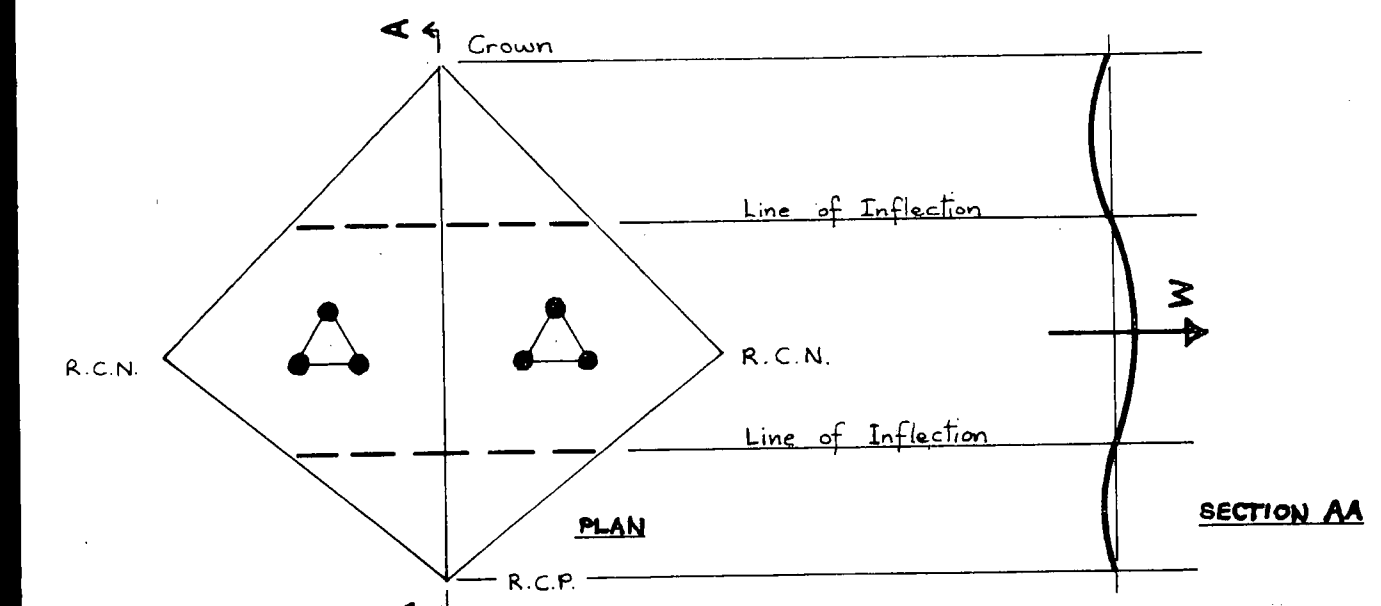

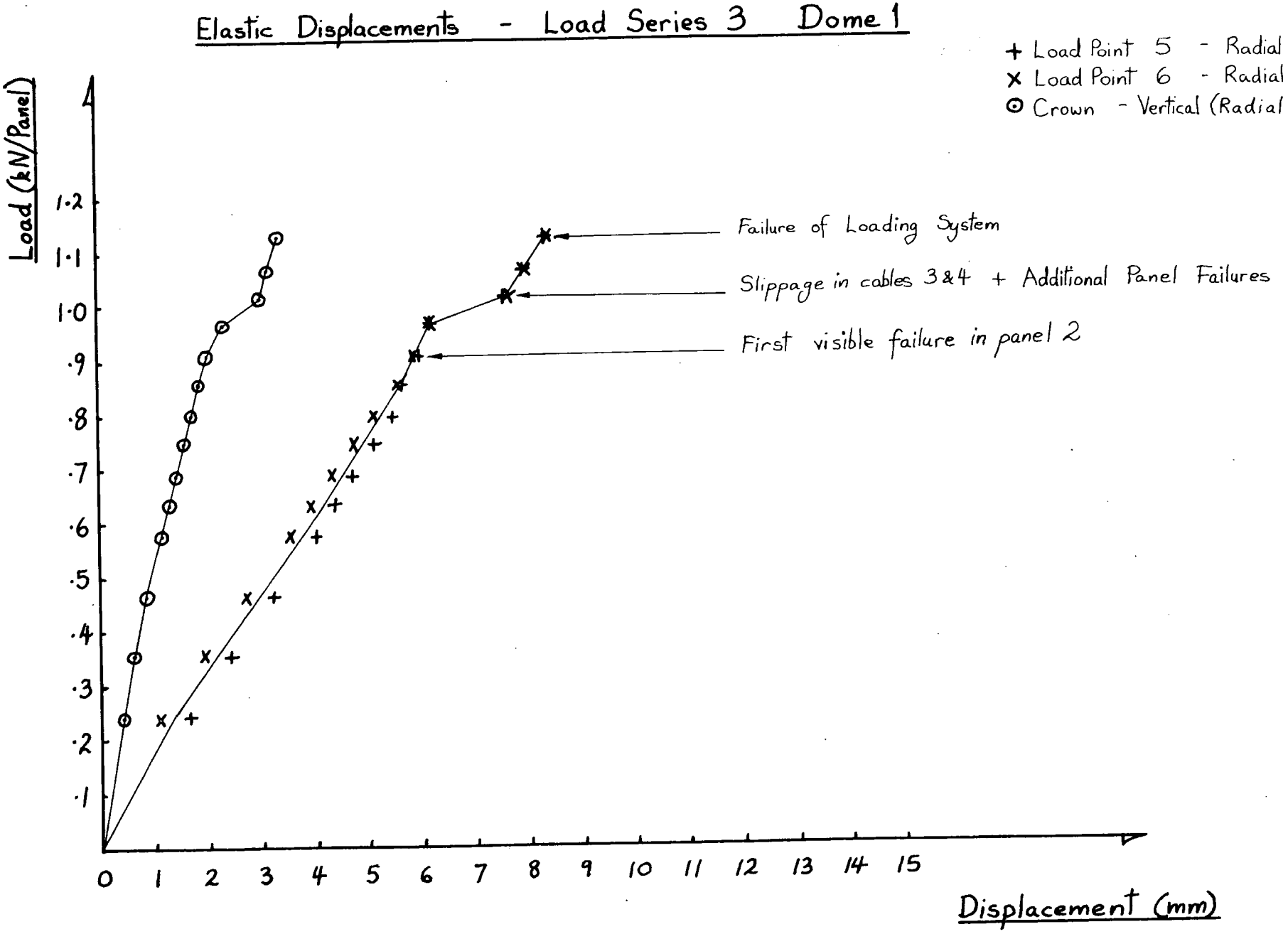
Elastic Displacements - Load Series 3 Dome 1
+ Load Point 5 - Radial
× Load Point 6 - Radial
⊙ Crown - Vertical (Radial)
Load (kN/Panel)
1·2
1·1
1·0
·9
·8
·7
·6
·5
·4
·3
·2
·1
Failure of Loading System
Slippage in cables 3&4 + Additional Panel Failures
First visible failure in panel 2
0 1 2 3 4 5 6 7 8 9 10 11 12 13 14 15
Displacement (mm)

FIG. 7.4

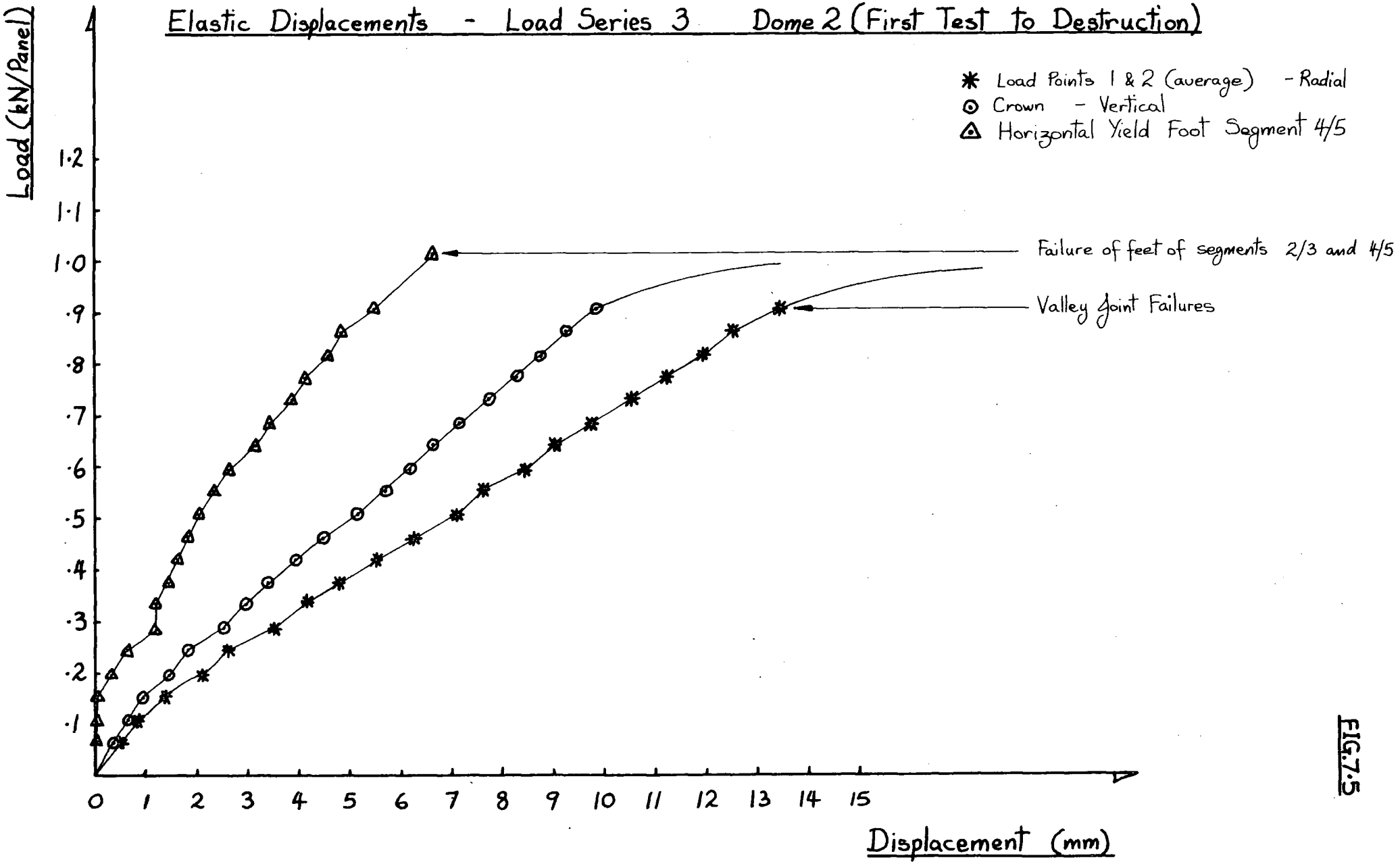
Elastic Displacements - Load Series 3 Dome 2 (First Test to Destruction)
Load (kN/Panel)
1·2
1·1
1·0
·9
·8
·7
·6
·5
·4
·3
·2
·1
0 1 2 3 4 5 6 7 8 9 10 11 12 13 14 15
Displacement (mm)
Load Points 1 & 2 (average) - Radial
Crown - Vertical
Horizontal Yield Foot Segment 4/5
Failure of feet of segments 2/3 and 4/5
Valley Joint Failures

FIG.7.5

FIG. 7·6

## Profiles of Top Longitudinal Ridges Showing Buckling Type Failures

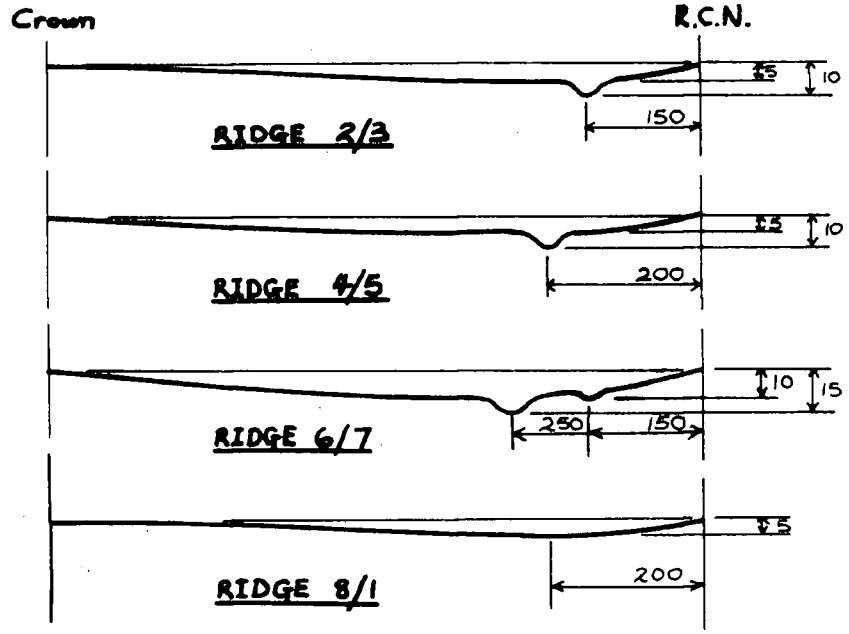


Note:
Displacements represent the situation 21 hrs. after the load was increased to the failure load of 1408 N/Panel.

FIG. 7·7

## Sketch Showing Buckling in Top Longitudinal Ridge 6/7, 21 Hrs. after the load was increased to 1408 N/Panel

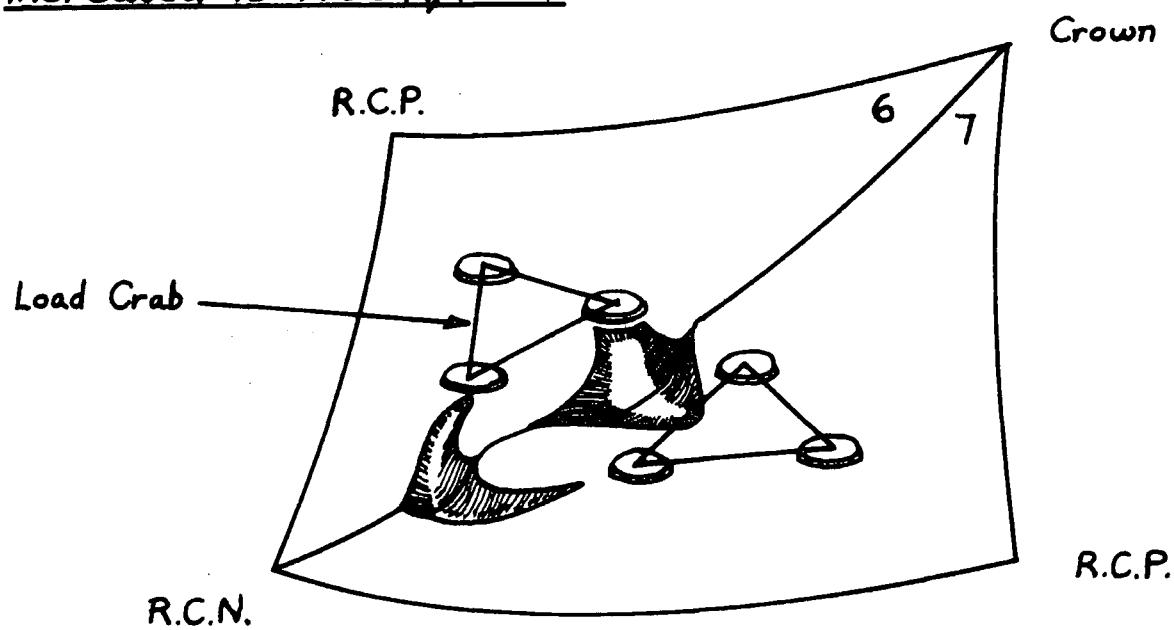

# Elastic Displacements - Load Series 3  Dome 2 (Second Test to Destruction)

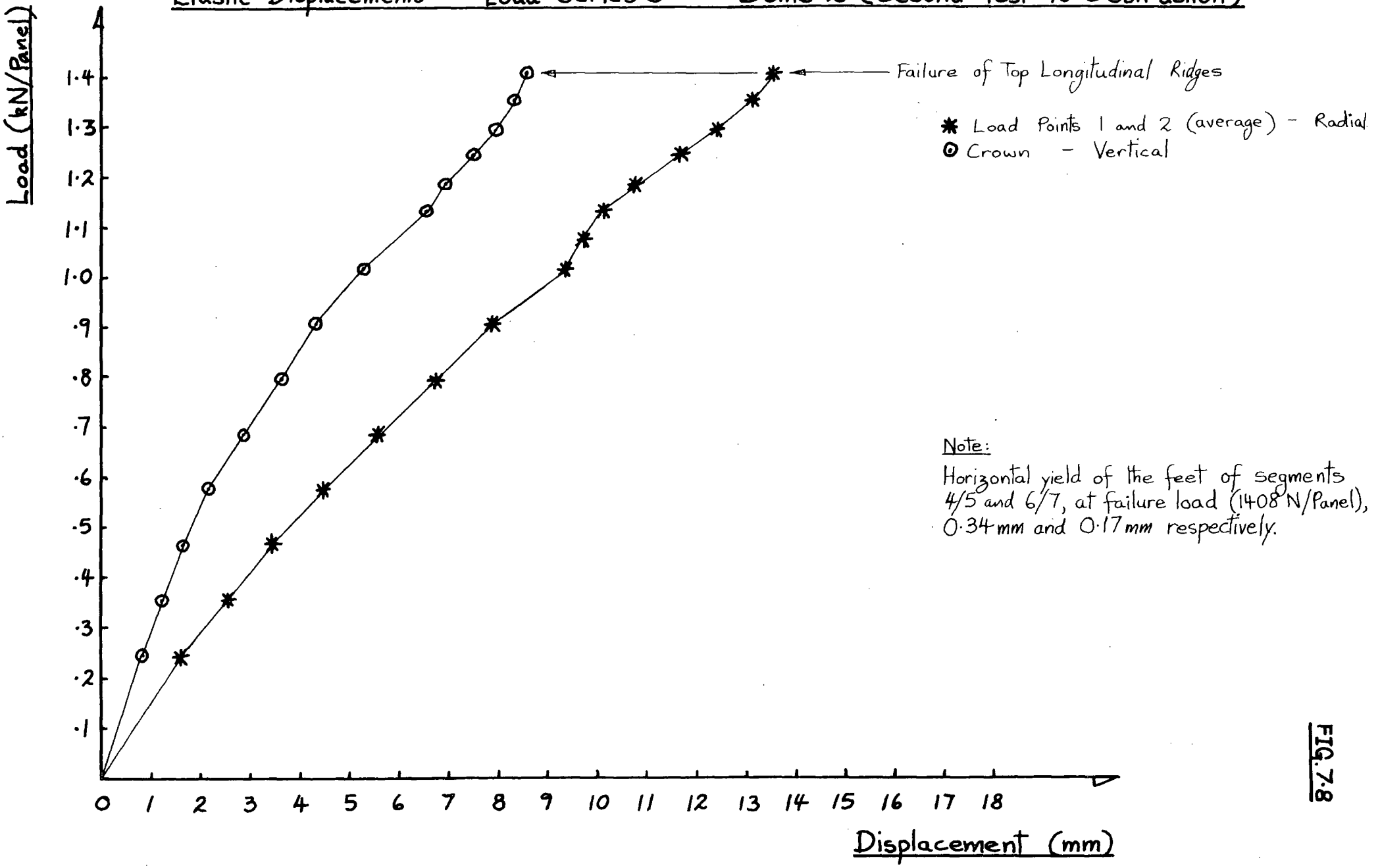


Note:

Horizontal yield of the feet of segments 4/5 and 6/7, at failure load (1408 N/Panel), 0·34 mm and 0·17 mm respectively.

FIG. 7.8

FIG. 7·9

## Location of Strain Rosettes Dome 3

(The strain rosettes are located at the centroids of the elements in the finite element analysis)

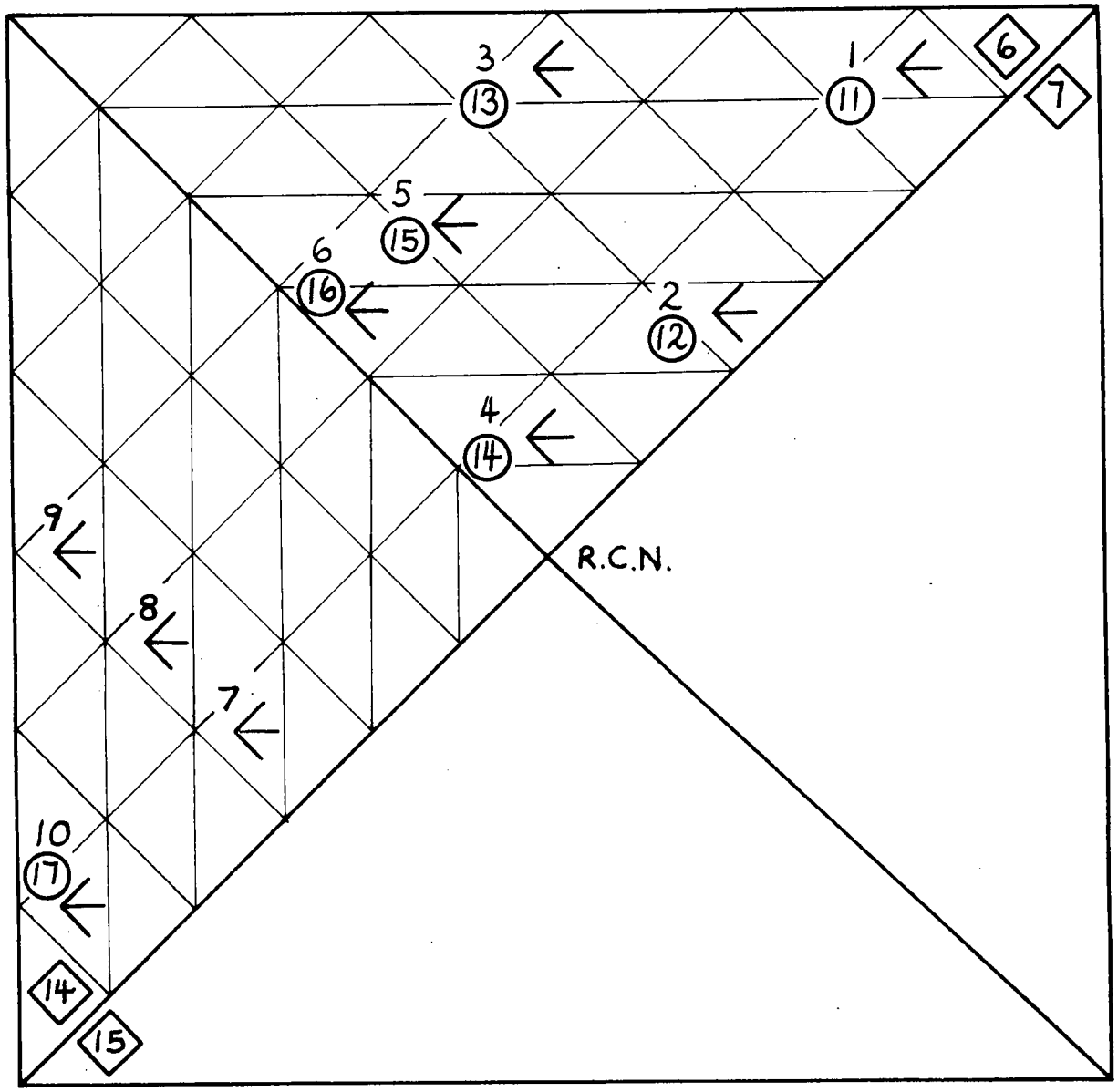


Numbering System

6 Panel Numbers

2 Top Face Rosette

(12) Bottom Face Rosette

Notes:

Gauge type PR 10-11, 45° Rosettes

Gauge Length 10 mm Gauge Resistance 120 ± 0·3 Ω

Gauge Factors; 1, 2·01; 2, 2·01; 3, 2·01.

FIG. 7·10

## Location of Areas of Bond Failure at Top Face Dome 3 at Load 797 N/Panel

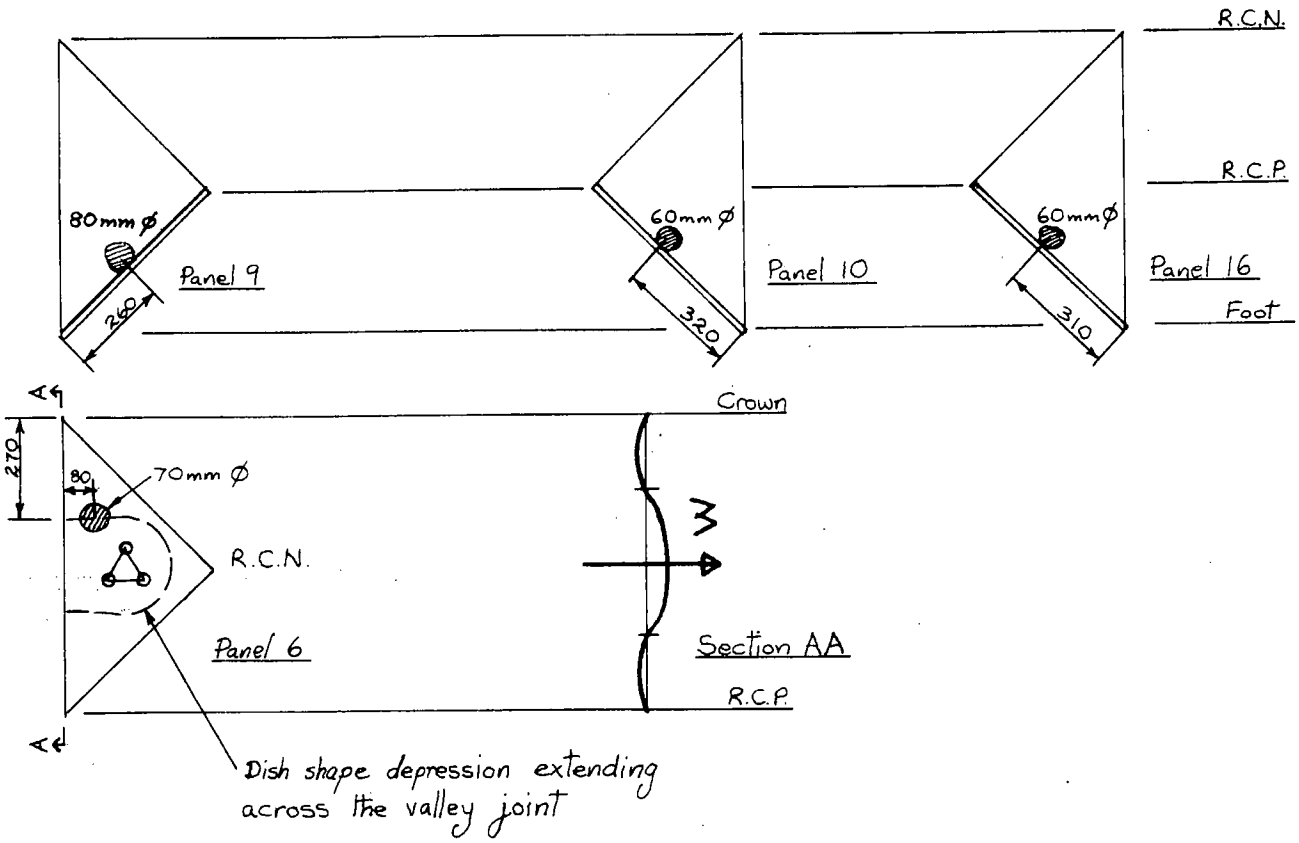


FIG. 7·11

## Top Longitudinal Ridge Failure Dome 3

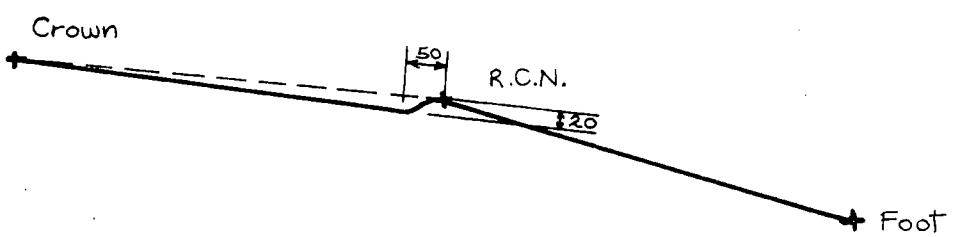


SECTION

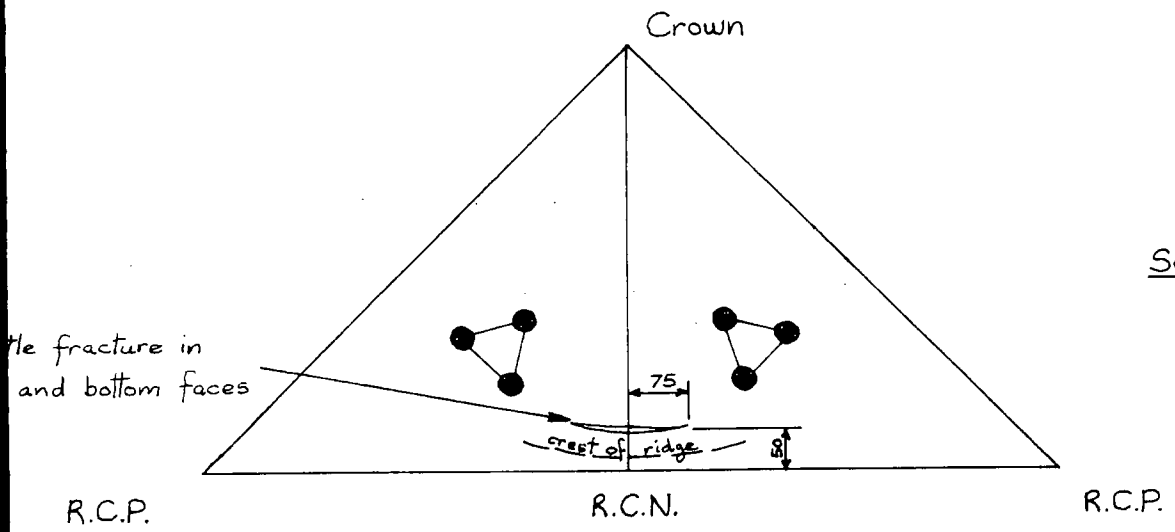


PLAN

Scale 1:10

# Elastic Displacement - Load Series 3 Dome 3

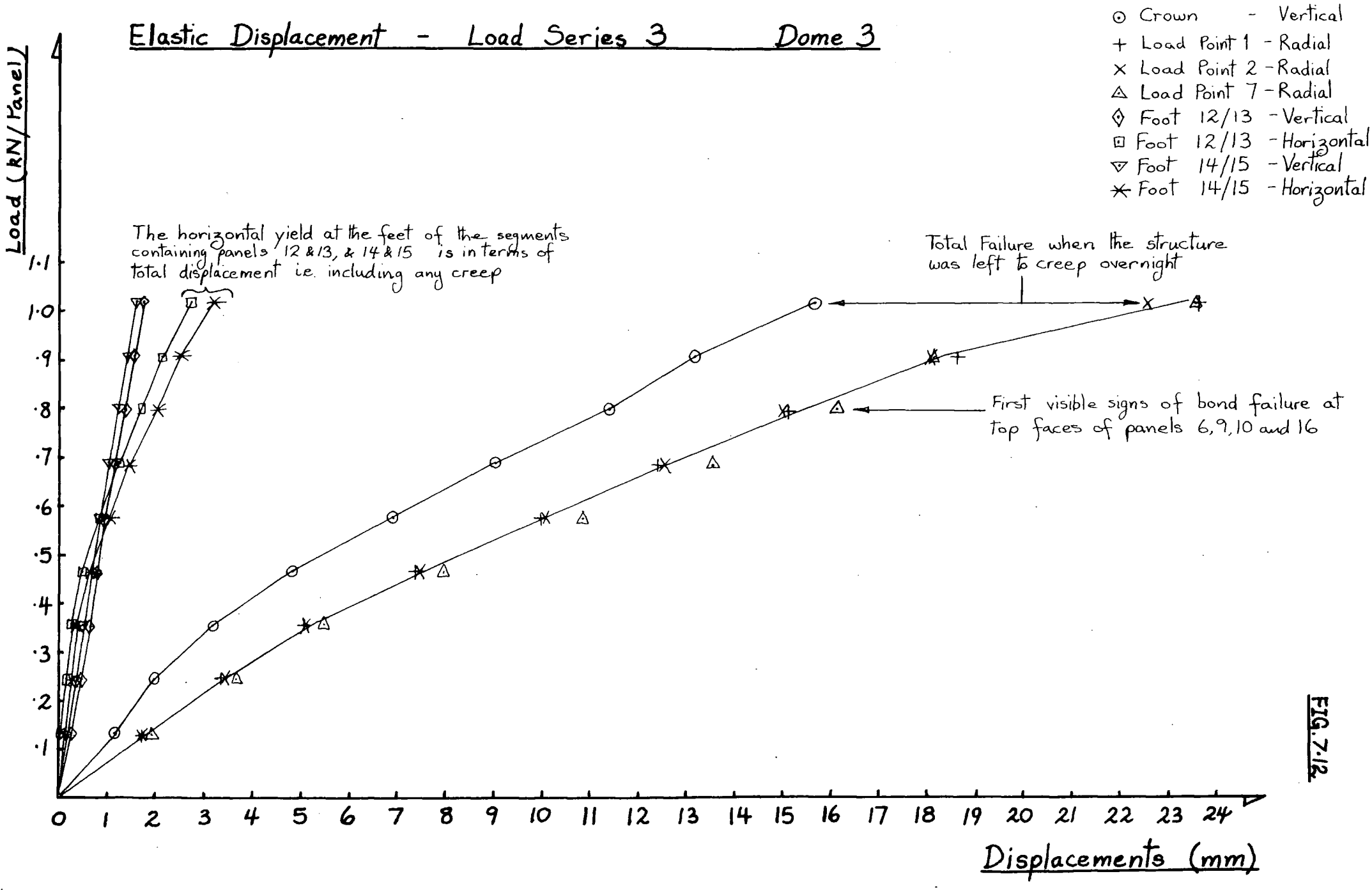


FIG. 7.12.

Bond Failure at Top Face of Panels 8 & 10 Dome 4

Load Series 3 1376 N/Panel

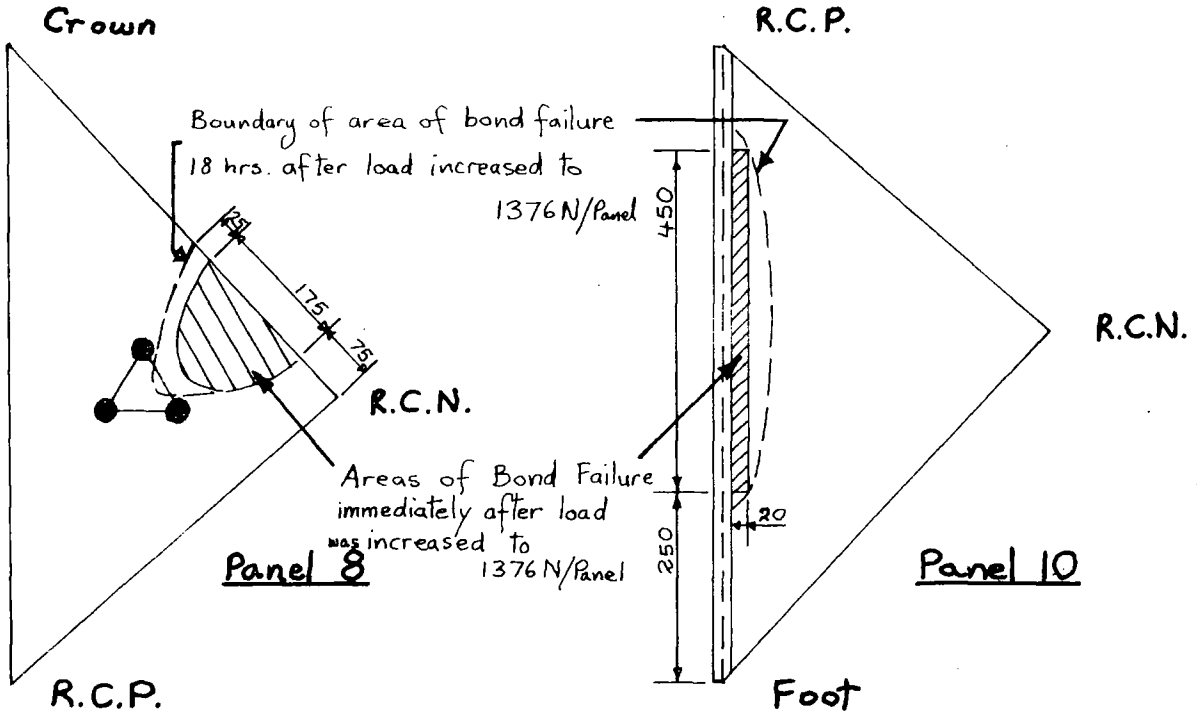


Scale 1:10

FIG. 7.13

FIG. 7·14

Sketch showing Buckling of Ridge Between Panels 8&1

48 Hrs. After Load Increased to 1376 N/Panel

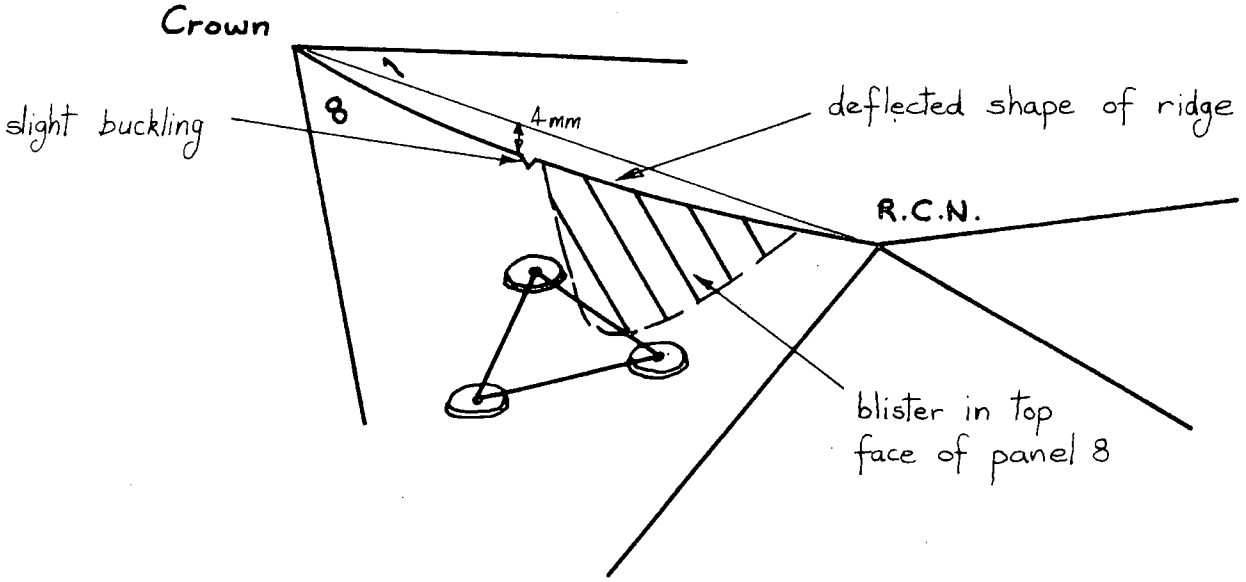


FIG. 7·15

Sketch showing Buckling of Ridge Between Panels 8&1

114 Hrs. After Load Increased to 1376 N/Panel

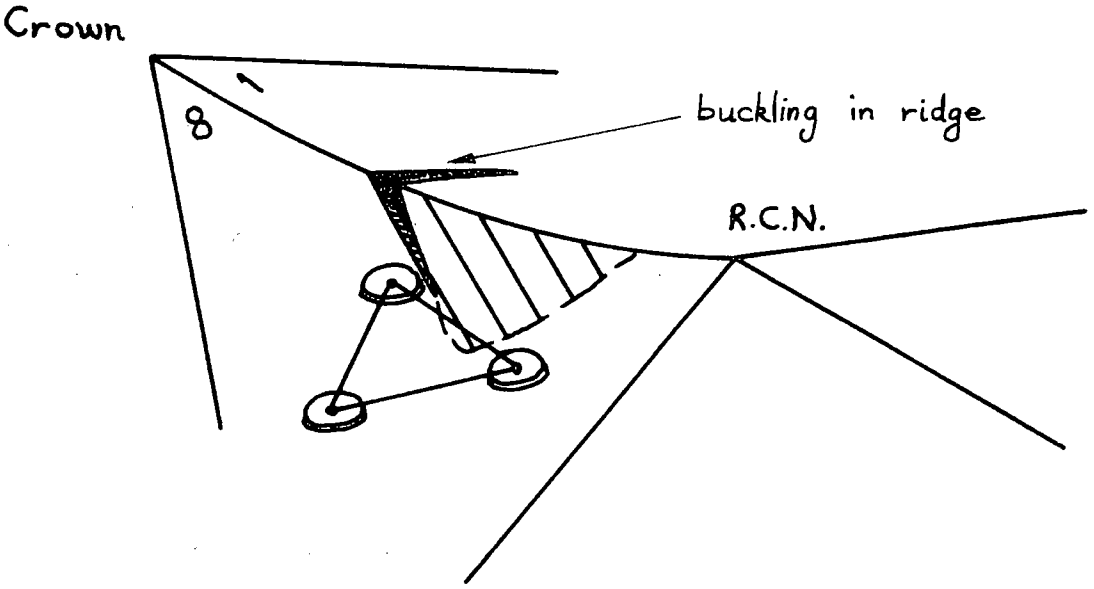

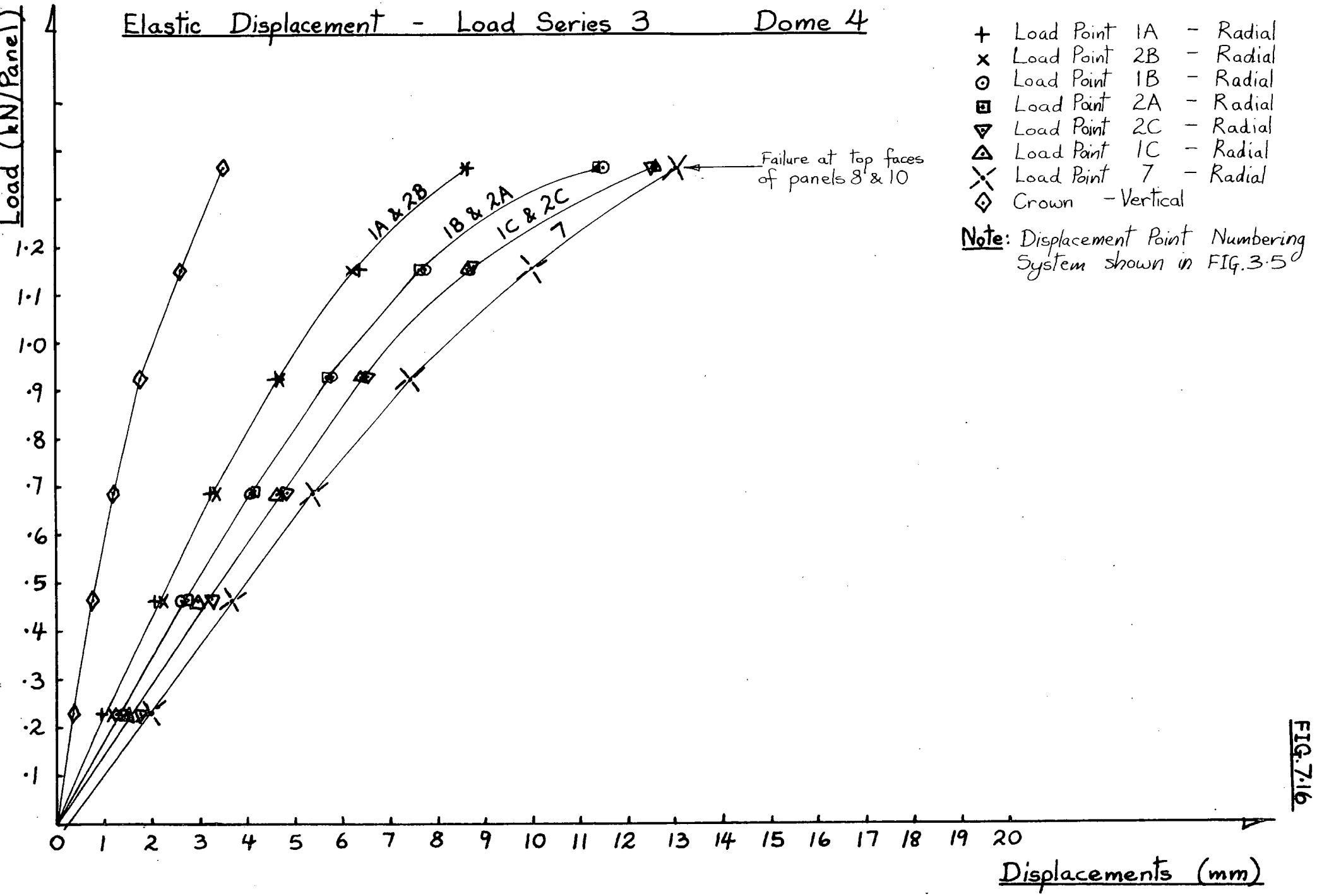
Elastic Displacement - Load Series 3 Dome 4
Load (kN/Panel)
1·2
1·1
1·0
·9
·8
·7
·6
·5
·4
·3
·2
·1
0 1 2 3 4 5 6 7 8 9 10 11 12 13 14 15 16 17 18 19 20
Displacements (mm)
1A & 2B
1B & 2A
1C & 2C
7
Failure at top faces of panels 8 & 10
+ Load Point 1A - Radial
× Load Point 2B - Radial
⊙ Load Point 1B - Radial
⊡ Load Point 2A - Radial
▽ Load Point 2C - Radial
△ Load Point 1C - Radial
Load Point 7 - Radial
◇ Crown - Vertical
Note: Displacement Point Numbering System shown in FIG. 3·5

FIG. 7.16

Displacements due to Increment in Load from 353 to 464 N/Panel

Dome 3

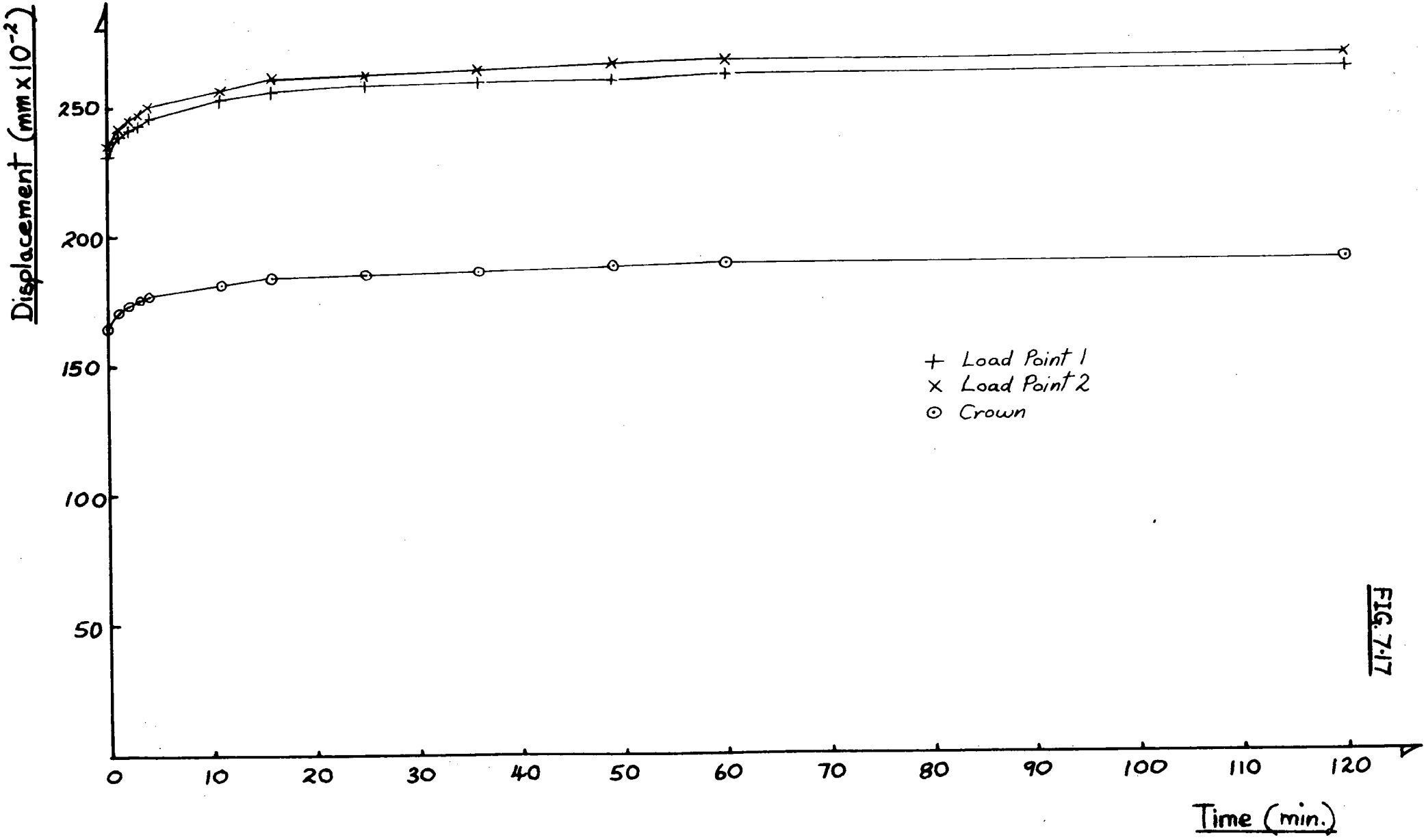


Fig. 7.17

FIG. 7·18

Time Dependent Displacements — Dome 3

Increment in Load from 353 to 464 N/Panel

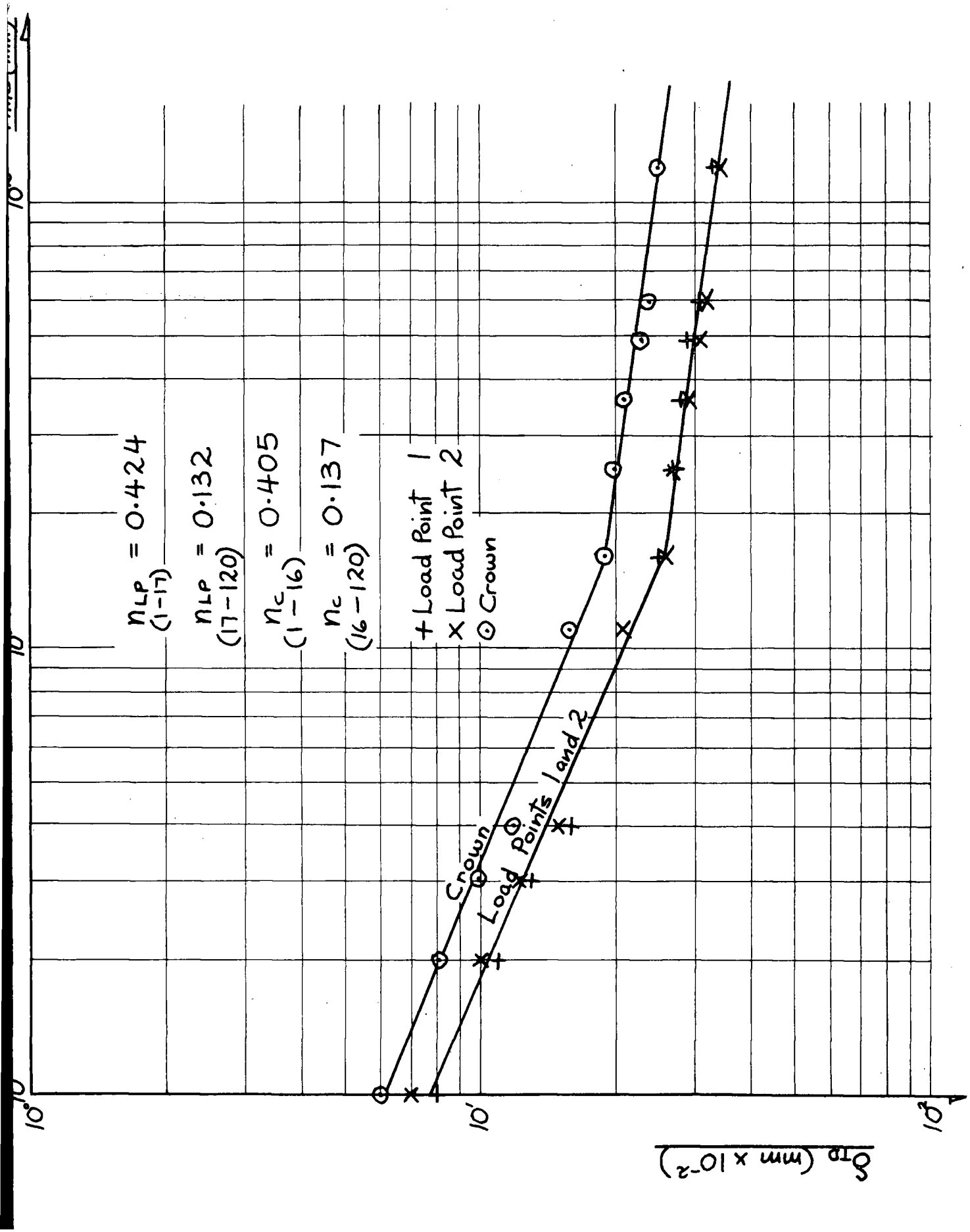

# Experimental & Numerical Flexibility Influence Coefficients
## υ Ratio Rise : Base Radius

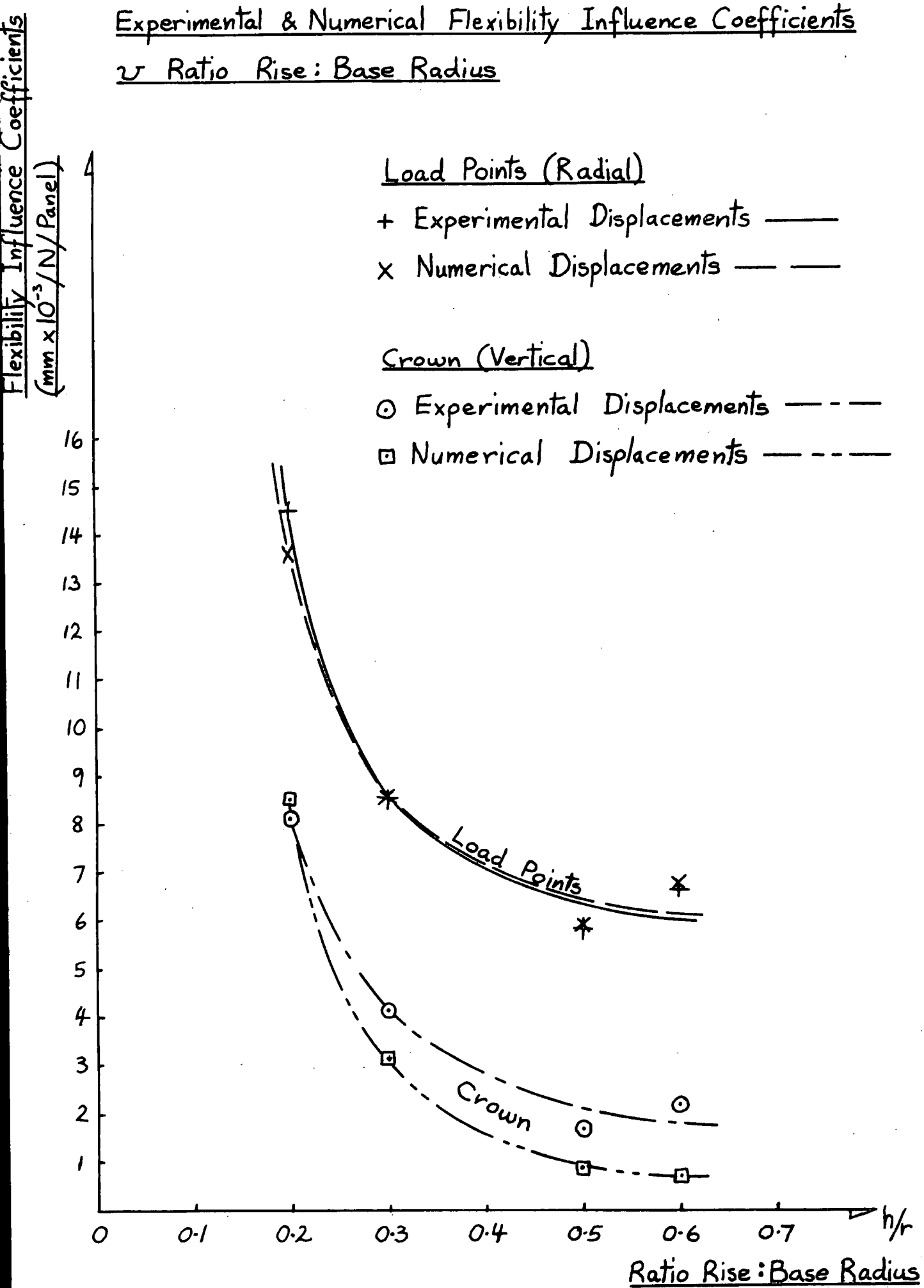

# Experimental & Numerical Flexibility Influence Coefficients
## v Ratio Rise : Base Radius

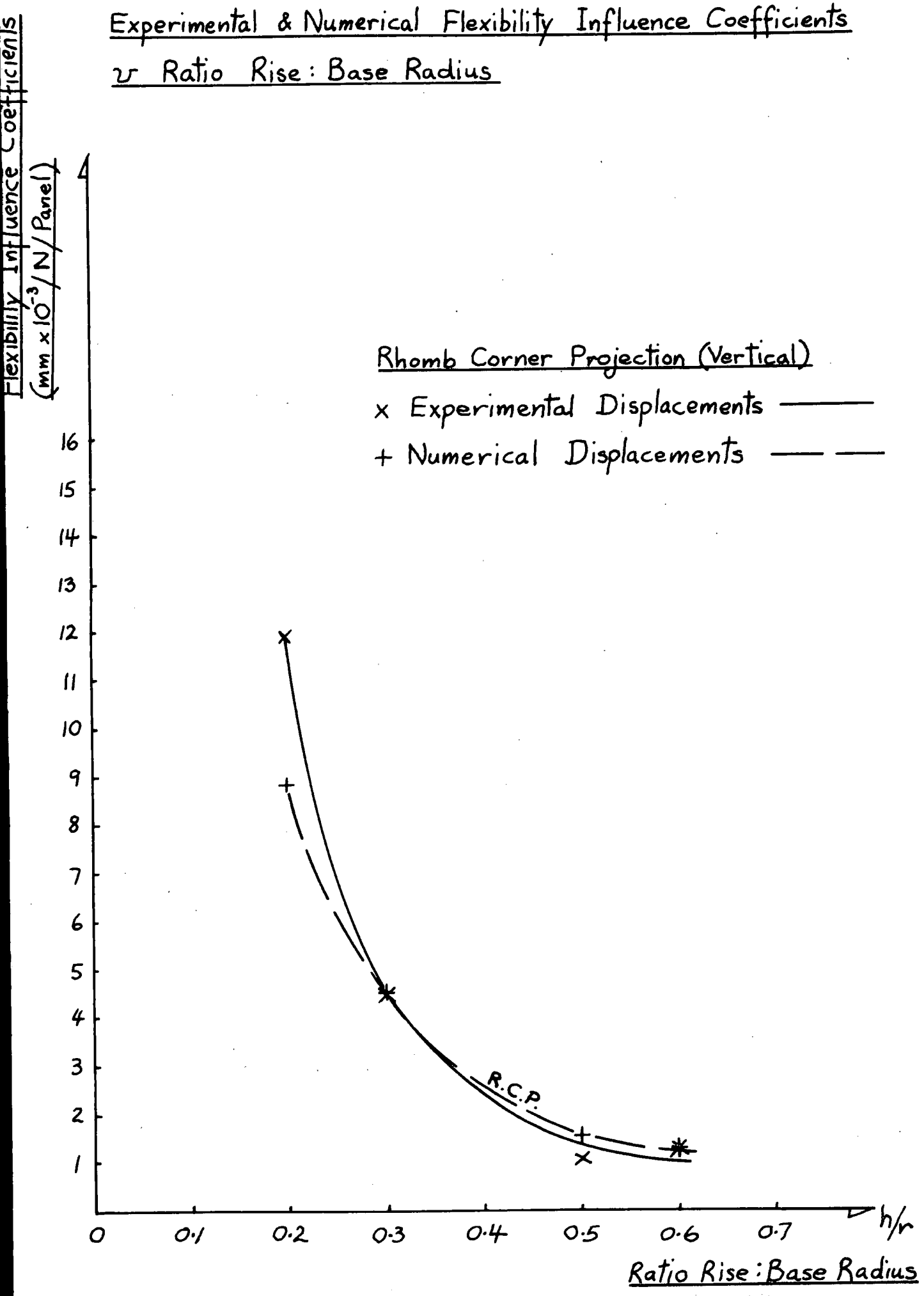

# Experimental & Numerical Flexibility Influence Coefficients
## v Ratio Rise : Base Radius

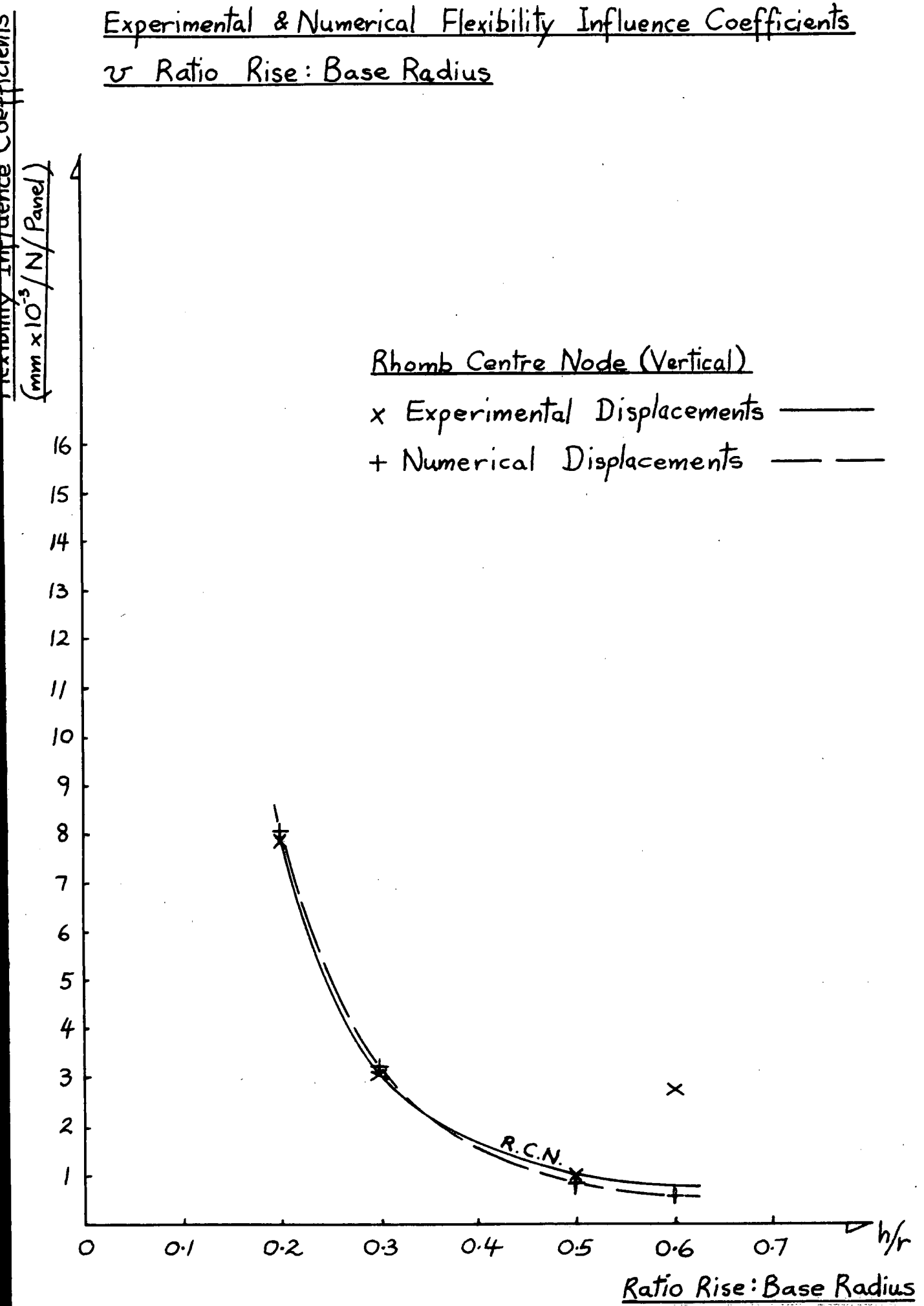

Summary of powers of T
from log-log graphs in general expression

$$\delta_{T.D.i} = T^{n_i}$$

Load Points Dome 1

TABLE 7.1

| Panel Load (N/Panel) | Time Range (mins.) | $n_i$ | Time Range (mins.) | $n_i$ | Remarks |
|---|---|---|---|---|---|
| 242 | 0 - 12 | 0.799 | 12 - 36 | 0.117 | |
| 353 | 0 - 15 | 0.551 | 15 - 36 | 0.000 | |
| 464 | 0 - 36 | 0.677 | | | |
| 575 | 0 - 9 | 0.566 | 9 - 1000 | 0.364 | overnight |
| 686 | 0 - 180 | 0.397 | | | |
| 797 | 0 - 9 | 1.276 | 9 - 1285 | 0.450 | overnight |
| 908 | 0 - 60 | 0.848 | 60 - 3960 | 0.380 | week-end; failure load. |

Crown Dome 1

TABLE 7.2

| Panel Load (N/Panel) | Time Range (mins.) | $n_i$ | Time Range (mins.) | $n_i$ | Remarks |
|---|---|---|---|---|---|
| 242 | 0 - 36 | 0.443 | | | |
| 353 | 0 - 36 | 0.482 | | | |
| 464 | 0 - 36 | 0.650 | | | |
| 575 | 0 - 48 | 0.383 | 48 - 1000 | 0.160 | overnight |
| 686 | 0 - 180 | 0.309 | | | |
| 797 | 0 - 5 | 1.556 | 5 - 1285 | 0.314 | overnight |
| 908 | 0 - 65 | 0.626 | 65 - 3960 | 0.055 | week-end; failure load. |

Note: All displacements in $mm \times 10^{-2}$

Summary of powers of T
from log-log graphs in general expression

$$\delta_{T.D.i} = T^{n_i}$$

Load Points Dome 3

TABLE 7·3

| Panel Load (N/Panel) | Time Range (mins.) | $n_i$ | Time Range (mins.) | $n_i$ | Remarks |
|---|---|---|---|---|---|
| 242 | 0 - 144 | 0·451 | | | |
| 353 | 0 - 1140 | 0·470 | | | overnight |
| 464 | 0 - 1 | 1·890 | 1 - 17 | 0·424 | |
| | 17 - 120 | 0·132 | | | |
| 575 | 0 - 1 | 2·035 | 1 - 180 | 0·433 | |
| 686 | 0 - 1 | 2·160 | 1 - 1200 | 0·357 | overnight |
| 797 | 0 - 1 | 2·000 | 1 - 180 | 0·560 | failure load. |

Crown Dome 3

TABLE 7·4

| Panel Load (N/Panel) | Time Range (mins.) | $n_i$ | Time Range (mins.) | $n_i$ | Remarks |
|---|---|---|---|---|---|
| 242 | 0 - 144 | 0·535 | | | |
| 353 | 0 - 1140 | 0·414 | | | overnight |
| 464 | 0 - 1 | 1·780 | 1 - 16 | 0·405 | |
| | 16 - 120 | 0·137 | | | |
| 575 | 0 - 1 | 1·960 | 1 - 180 | 0·418 | |
| 686 | 0 - 1 | 2·090 | 1 - 1200 | 0·339 | overnight |
| 797 | 0 - 1 | 1·590 | 1 - 180 | 0·562 | failure load. |

Note: All displacements in $mm \times 10^{-2}$

## Ratio Total Displacement at point $i$ : Elastic Displacement at point $i$

$$\delta_i^* = C_i \times \delta_{Ei} \quad \text{(2)}$$

| Dome No. | $h/r$ | Maximum Load Considered (N/Panel) | Total Duration Considered (days) | $C_i$ | | | |
|---|---|---|---|---|---|---|---|
| | | | | Load Points (Radial) | Crown (Vertical) | Rhomb Centre Node (Vertical) | Rhomb Corner Projection (Vertical) |
| 1 | 0·6 | 1075 | 5 | 1·83 | 2·00 | 3·19 | 2·53 |
| 4 | 0·5 | 1376 | 6½ | 1·69 | 2·46 | 1·91 | 1·95 |
| 2 | 0·3 | 1075 | 5 | 1·89 | 1·95 | 1·78 | 2·66 |
| 3 | 0·2 | 1019 | 3 | 2·32 | 1·68 | 2·01 | 2·35 |

$\delta_{Ei}$ = Elastic displacement at point $i$

$\delta_i^*$ = Total displacement at point $i$, (including any time dependent displacement)

$C_i$ = Constant relating $\delta_i^*$ to $\delta_{Ei}$ for point $i$

TABLE 7.5

## Ratio Total Displacement at point $i$ : Elastic Displacement at point $i$ at the Dome's Working Load

$$\delta_i^* = C_i \times \delta_{Ei} \quad \text{(2)}$$

| Dome No. | $h/r$ | Working Load (N/Panel) | Total Duration Considered (days) | $C_i$ | | | |
|---|---|---|---|---|---|---|---|
| | | | | Load Points (Radial) | Crown (Vertical) | Rhomb Centre Node (Vertical) | Rhomb Corner Projection (Vertical) |
| 1 | 0·6 | 570 | 3/4 | 1·42 | 1·32 | 1·44 | 1·29 |
| 4 | 0·5 | 860 | 1 | 1·13 | 1·22 | 1·25 | 1·22 |
| 2 | 0·3 | 880 | 1 | 1·24 | 1·23 | 1·24 | 2·08 |
| 3 | 0·2 | 500 | 1 1/4 | 1·21 | 1·15 | 1·15 | 1·14 |

$\delta_{Ei}$ = Elastic displacement at point $i$

$\delta_i^*$ = Total displacement at point $i$, (including any time dependent displacement)

$C_i$ = Constant relating $\delta_i^*$ to $\delta_{Ei}$ for point $i$

TABLE 7.6

## 8. NUMERICAL WORK

A finite element method has been used to analyse the polyhedral sandwich domes, using the quadratic shape function sandwich element developed by Parton (12). The solution of the overall problem has been performed using the computer program developed by Irons (7), which solves the simultaneous equations derived using stiffness subroutines such as those developed by Parton and other workers at the University of Durham (2,10,12, Collins).

The Parton quadratic shape function sandwich element is compatable along, but not across the inter element boundaries. It is a 'complete' element and therefore converges towards an exact solution from below. This element was used for the following reasons:-

1. The element is based on a very simple idealisation. The faces are supposed to act as thin membranes in plane stress. The core is credited with a shear stiffness, the stiffnesses in the plane of the panel are taken to be zero, and the stiffness normal to the plane of the panel is taken to be infinite, i.e. the faces are constrained by the displacement definition to remain the same distance apart. This has the effect of making the element two dimensional instead of three dimensional.

2. This quadratic element has been shown by Parton (12) to give good agreement with experimental behaviour and analytical solutions, for displacements and stresses, for sandwich panels, such as those used in the work described in this thesis, subjected to loads normal to the plane of the plate.

3. Compared with the more sophisticated of the sandwich elements which have been developed by Manos (10), and Collins at the

University of Durham, the Parton quadratic shape function element although requiring a comparatively high mesh density to achieve the same accuracy, is relatively economic in terms of data preparation and computer solution time. It was found advantageous when analysing the deformation of domes 1 to 4 to have a numerical model with a high number of displacement points.

One modification was made to the stiffness subroutine, 'STIFF' for the 'Parton quadratic shape function element' in order to make it more suitable for use in the analysis of domes 1 to 4. A separate subroutine 'BSTIFF' has been added which enables beam members to be added to any of the element edges. Appendix I contains details of the edge stiffening option, together with a listing of the subroutines for this 'Modified Parton Quadratic Shape Function Sandwich Element'. A separate program 'BFORCE', which calculates the strains and forces in the beam members which were added to the edges of the elements, is described in Appendix II.

## 8.1 Numerical Analysis of Polyhedral Sandwich Domes

A numberical analysis was performed for each dome, which corresponded to the experimental load series 3, (Section 7.0).

### 8.1.1 Numerical Model

The polyhedral sandwich domes were analysed using the two panel finite element model shown in Fig. 8.1, each triangular panel having a 6 x 6 mesh of elements. The mesh density was chosen in the light of the experience of both Parton (12), and the author, and gave a close approximation to the exact numerical solution. The model had two lines of symmetry, one along the longitudinal ridge and the other along the valley joint.

### 8.1.2 Joint Representation

All the ridge joints were assumed to act as simple hinge joints, and the valley joints were assumed to transfer bending moment across, but not along the line of the joint.

#### 8.1.2.1 Ridge Joints

The hinge joint representation of the ridge joints follows the method adopted by Parton (12). Parton has shown that, in the case of the polyhedral sandwich shells that he analysed, the hinge joint analogy gave a close approximation to the experimental behaviour. From the joint tests, (Section 4.1.2), and the behaviour of the model domes tested by the author, (Sections 6.0 and 7.0), it was apparent that the true situation at these joints was somewhere between a simple hinge and a moment transferring joint. It was thought that, for domes with a relatively high ratio h/r, (domes 1 and 4), all the ridge joints would approximate to a simple hinge and, for domes with a relatively low ratio h/r, (domes 2 and 3), the longitudinal ridge joints would approximate to moment transferring joints and the transverse ridges would approximate to simple hinges. However it was found that the optimum solution in the case of all the ratios h/r analysed, (domes 1 to 4), was achieved when the simple hinge analogy was applied to all the ridge joints.

Figs. 8.2 to 8.4 show a comparison for dome 2, (h/r = 0.3), between numerical displacements for an analysis with moment transfer, and an analysis with no moment transfer across the longitudinal ridge joints, where in each case all other parameters are the same. In both cases the transverse ridge joint was represented as a simple hinge (Section 8.5.3.1), and the load was equally distributed between elements 50, 53 and 59 which corresponded to the locations of the three feet of the load crab. As can be seen the simple hinge analogy gives a much

closer approximation to the experimental displacements in the regions adjacent to the longitudinal ridges. The introduction of moment transfer across the longitudinal ridge joints over-stiffened the structure along the line of these joints.

It would seem that ridge joint stiffness does not have a very significant effect upon the stiffness of a complete polyhedral sandwich dome of the type tested.

8.1.2.2 Valley Joints

It has been observed by both Parton (12), and the author that pairs of adjacent top panels which contained a valley joint behaved essentially as a single flat plate. Moment transfer across the valley joints was deemed to be significant and was therefore included in the numerical model. This was achieved by constraining the elements' bottom face nodes along the line of the valley joint, which was a line of symmetry, against displacement normal to the line of the valley joint using 'Legrane Multiplier Constrains' (2).

8.1.3 Load Representation

The load was applied radially to the top panels only, as in the experimental load series 3 (Section 7.0).

It was found that the experimental loading situation was more closely modelled by a U.D.L. across the whole of the top panel, than by concentrating the load at the mid-side nodes of the three elements which corresponded to the locations of the feet of the load crab, (elements 50, 53 and 59). There is some justification for using a U.D.L. type of load representation. The experimental load situation approximated to a U.D.L. over the centre of the top panel. Distribution of the load in the plane of the panel, will occur due to spreading of the load across the thickness

of the panel, and due to local bending effects. Parton (12) found for elements such as his 'Quadratic Shape Function Sandwich Element ', that concentrated loads produced local distortion around the load points, and that a more accurate representation of the experimental behaviour was achieved if the loads were distributed between the nodes of the elements surrounding the load positions.

The optimum solution was found to be a combination of a U.D.L. over the whole of the top panel, plus point loads of $^{1}/_{54}^{th}$ of the total panel load at each of the mid-side nodes of elements 50, 53 and 59. The U.D.L. was simulated by applying $^{1}/_{54}^{th}$ of the total panel load to every mid-side node in the top panel, except those located along the panel edges, (45 No.)

Figs. 8.5 to 8.7 show a comparison for dome 2, between numerical displacements for an analysis with the load equally distributed between the mid-side nodes of elements 50, 53 and 59, and an analysis using the combination of a U.D.L. and point loads described above. All other parameters were the same in each case. The former produced exaggerated transverse displacements around the load points, and underestimated the displacement of points remote from the load points. The latter gave an excellent approximation of displacements for all points except those adjacent to the centre of the valley joint.

### 8.1.4 Edge Stiffening Members

The free edge of the bottom panel, i.e. the edge between the R.C.P. and the foot, was stiffened using an edge beam, (Section 2.4.2). This member was included in the numerical model using the subroutine 'BSTIFF' described in Appendix I.

Stiffening was also applied to the edge of the top panel along the line of the valley joint using 'BSTIFF'. This was to take account

of the stiffening effect of the valley joint, (Section 4.2.4). The numerical models used to calculate the displacements plotted in Figs. 8.2 to 8.7, did not include for the stiffness of the valley joint. The final numerical model for dome 2, the displacement profiles for which are shown in Figs. 8.22 to 8.24, included for the stiffening effect of the valley joint. It can be seen that the valley joint has a significant effect upon the transverse displacement adjacent to that joint.

## 8.2 Propagation of stresses in the faces of polyhedral sandwich domes

Stresses in the faces of polyhedral sandwich domes are propagated due to the following:-

1. Local bending in a loaded panel due to the load at that panel.
2. Overall bending of the segments of the dome.
3. Bending caused by thrust along the edges of the panels at the joints.
4. Transfer of bending moments across the joints.
5. Membrane action.
6. There are local concentrations of stress in the panel faces near to the feet, the nature and magnitude depending upon the way in which the constraint is applied.

## 8.3 Non-linear elastic behaviour of polyhedral sandwich domes

As mentioned in Section 5.0 it was apparent from the work performed by the author and other workers, (2, 10, 12), that in-plane deformation in the panels of polyhedral sandwich shells, constructed from the type of sandwich materials used by the author, is significant. Tables 8.1 to 8.4 show a comparison between the experimental flexibility influence coefficients for domes 1 to 4, load series 3, the corresponding numerical values dervied using a numerical model in which no allowance was made for the variation between the elastic moduli of the faces in

bending and compression, and a numerical model in which allowance was made for the variation between the elastic moduli of the faces in bending and compression. It can be seen from these tables that the effect of in-plane deformation was relatively small in dome 1, (h/r = 0.6), and particularly large in the case of dome 3, (h/r = 0.2). The extent of the in-plane deformation depended upon the magnitude of the compressive membrane stresses in the panels. The extent of the in-plane deformation increased as the ratio h/r was reduced.

Non-linear variations in the displacements with the ratio h/r, Fig. 7.19, are dependent, for loads in towards the centre of the dome, upon (i) variations in the geometric stiffness, i.e. the ratio of bending to membrane stresses in the panels; and (ii) to a lesser extent upon variation in the stiffness of the ridge joints. For loading out from the centre of the dome, in-plane deformation in the panels would be much less important as the membrane stresses would be mostly tensile, ($E_{Tension} \doteqdot 11 \times E_{Compression}$), (Section 5.4).

## 8.4 Approximate method of including for non-linear elastic behaviour in the numerical analysis of polyhedral sandwich domes

The investigation into the behaviour of sandwich struts in Section 5.0 was performed so as to establish the magnitude of the in-plane deformation of sandwich panels due to compressive membrane stresses. It was found that, for the pin ended sandwich panel struts tested, the axial displacement was up to 12 times greater than the predicted using the bending stress/strain relationship for the face material, Table 5.1.

Accuract predictions can be made of plate buckling using a finite element technique, combined with a numerical solution of the resulting eigenvalue problem, using a method such as that described by Holand and Moan (6). An analysis of this type was beyond the scope of the work performed by the author and was therefore not attempted.

An approximate method for including non-linear elastic effects due to in-plane loading in the numerical analyses of polyhedral sandwich domes has been used, in which factors are applied to the elastic bending constants of the shell faces to take account of the composite nature of the stresses in these faces.

Reduction factors have been applied to the elastic moduli of the face material of both faces of the top and bottom panel. The value of these factors depended upon the ratios of the bending to membrane stresses in the panel. As the membrane stresses were mostly compressive in domes 1 to 4, load series 3, the factors which were applied produced relatively large reductions in elastic constants of the faces. When domes of this type are subjected to outward loading, (wind loads), the membrane stresses will be mostly tensile and the factors would exceed unity, ($E_{Tension} > E_{Bending}$), (Section 2.2).

There is no sound theoretical basis for the manner in which reduction factors were applied in the numerical analysis of domes 1 to 4, load series 3. The main justification for the method is that it produces an acceptable approximation to the true solution. The reduction factors have been applied to panels as a whole, i.e. both faces of every element within a panel are assumed to have the same reduced elastic modulus. It can be seen from the principal stresses, Figs. 8.15, 8.20, 8.25 and 8.30, that some of the membrane stresses are tensile. This has been neglected as the effects of tensile membrane stresses are of a secondary nature. There is no explicit allowance in the element formulation for transverse displacement due to in-plane compressive stresses. However in the 'Parton Quadratic Shape Function Sandwich Element' (12), as there is no separation of the membrane stiffness from the bending stiffness, any reduction factor applied to the elastic modulus will increase the strain due to bending stresses

as well as the strain due to membrane stresses. This is not totally undesirable as this makes an implicit allowance for the transver displacement due to plate buckling,provided that the transver displacement in an element due to plate buckling is in the same direction as that due to bending.

There is a high degree of judgement involved in the selection of appropriate reduction factors, and great caution must be exercised in the use of such a method.

No reduction factor was applied to the shear modulus of the core material. From the analysis of sandwich struts, (Section 5.0), it was obvious that there was a significant increase in transverse shear displacement as a result of in-plane loading. There is no explicit allowance for transverse shear displacement due to plate buckling, but there is an increase in the transverse shear strain due to the above mentioned increase in transverse displacement due to bending caused by the reduction in the elastic modulus of the faces.

The elastic modulus of the edge beam was reduced to take account of buckling. This had the effect of increasing axial displacement due to thrust, $P_x$, and the transverse displacement due to the bending moment, $M_y$. No reduction factor was applied to the shear modulus for the edge beam as the torque, $T_x$, was considered to be unaffected by longitudinal buckling of the member.

## 8.5 Comparison of experimental and numerical displacements and stresses, dome 3

### 8.5.1 Numerical model dome 3

The numerical analysis of dome 3 was performed using the numerical model described in Section 8.1, and shown diagrammatically in Fig. 8.1.

The factors applied to the elastic constants were determined by trial and error, and were found to give the closest approximation to the behaviour of the structure as a whole. The factors that were used are listed in Table 8.5.

8.5.2 Comparison of experimental and numerical displacements, dome 3, load series 3.

A comparison of experimental and numerical flexibility influence coefficients for load series 3 is shown in Table 8.3 and Figs. 8.8 to 8.10. It can be seen that the numerical model gives an excellent approximation to the experimental elastic behaviour.

8.5.3 Comparison of experimental and numerical stresses in panel faces, dome 3, load series 3.

8.5.3.1 Experimental Stress Situation in Panel Faces

Figs. 8.11 to 8.14 show the experimental face stresses determined as described in Section 7.3.1.1.

8.5.3.1.1. Top Panels

There was predominantly compressive membrane stresses in the top panels, coupled with bending stresses due to the loads at the top panels. Compressive membrane action was greatest adjacent to and parallel with the longitudinal ridges. There was a general compressive membrane action around the crown. Inflections were formed in the top panels adjacent to the crown, due to the geometric stiffness at that location. A high proportion of the face stresses in the centre of the top panel were due to bending. There was moment transfer across the valley joints, (Section 7.6). Moment transfer across the bottom longitudinal and transverse ridges was not significant. There was a small amount of moment transfer across the top longitudinal ridges. Both the top longitudinal and transverse

ridges sagged in towards the centre of the dome due to the local effects of the loads at the top panels. Shear stresses in the faces were not significant along the lines of symmetry which indicated that the dome was behaving symmetrically.

8.5.3.1.2 Bottom Panels

There were compressive stresses in the faces down the length of the panels. These stresses were greatest adjacent to the longitudinal ridges. Membrane forces were transferred from the panel into the edge beams. The resultant compression in the top faces was radial to the segment feet, (Gauges 7, 8 and 9). As the top faces only were gauged it was not possible to determine the stress situation in the bottom faces of the bottom panels. There was a small tensile stress in the top face approximately parallel to the line of the edge beams. This tensile stress increased moving across the panels from the R.C.N. to the edge beam. There was a disparity between the magnitude of the compressive stresses in the top and bottom faces adjacent to the segment feet, (Gauges 10 and 17). This was probably due to bending induced by compressive thrust along the lines of the transverse ridges.

8.5.3.1.3 General Situation

The overall pattern was one of compressive membrane action around the top of the dome and down the line of the longitudinal ridges, and local bending effects near to the loads.

8.5.3.2 Numerical Stress Situation in Panel Faces

Figs. 8.12 to 8.16 show the numerical stresses determined using the numerical model described in Section 8.5.1.

8.5.3.2.1 Top Panels

There was a general compressive membrane action in the top panels. As in the experimental model there was a small amount of tensile membrane action in the top panels adjacent to the crown. The stress situation in the faces at the centre of the top panels was distorted due to the overall bending in the segments being exaggerated. The stress produced by the segment bending was in opposition to that produced by thrust at the panel edges and the local bending around the loads. The local bending around the loads did not have a predominant effect upon the face stresses in the top panels. The overall form of the top panel deformation was due mainly to transverse shear displacement in the core. As an illustration of the relative importance of the bending and shear displacements in the top panels, a doubling of the core shear modulus produced a 37.5% reduction in the transverse displacement of the panel centroid relative to the panel nodes, while a three-fold reduction in the face elastic modulus produced only a 26% increase in the transverse displacement of the panel centroid relative to the panel nodes.

8.5.3.2.2 Bottom Panels

There were compressive stresses down the length of the panel in both faces of the bottom panel. The magnitude of these compressive stresses was greatest in the top face. The disparity between this compressive stress in the faces was probably due to bending induced by compressive thrust along the line of the transverse ridge. The intensity of the compressive membrane action down the length of the bottom panel was greatest adjacent to the longitudinal ridge. Membrane forces were transferred from the panel into the edge beam. Fig. 8.16 shows the build up of compressive thrust down the length of the edge beam.

Bending and torque in the edge beam was not significant.

There was a small amount of tensile membrane action across the width of the bottom panel.

8.5.3.2.3 General Situation

The overall stress situation in the faces was one of compressive membrane action around the top of the dome and down the longitudinal ridges combined with bending action due to overall segment bending, thrust at the panel edges, and local bending around the loads.

8.5.3.3 Effect of Edge beams

Figs. 8.8 to 8.10 show a comparison between the displacements for the numerical model for dome 3, (Section 8.5.1), and the same numerical model with the edge beam omitted. As can be seen this has a significant effect upon the overall displacement pattern. The panel shortening in the bottom panel particularly along the free edge ,(i.e. the edge to which the edge beam is attached),is greatly increased when the edge beam is omitted. The displacements within the top panel are relatively unaffected by the omission of the edge beam.

Membrane stresses immediately adjacent to the free edge of the bottom panel were reduced when the edge beam was omitted. As a result there was a small increase in the magnitude of the compressive membrane action in the centre of the bottom panel and adjacent to the bottom longitudinal ridges. There was no significant change in the overall stress situation.

The true value of the edge beams is not apparent for a loading situation in which the top panels only are loaded, i.e. where there is no significant crossplate deformation in the bottom panels, (Section 2.4.2, 12).

8.5.4 Comparison of experimental and numerical face stresses, dome 3, load series 3

During the test to destruction on dome 3, it was observed that the ridges and the edge beams bowed out away from the centre of the dome, which indicated that overall bending of the segment was significant. The numerical model over-estimates this effect which causes distortion of the stress situation in the faces of the top and bottom panels. The disparity between the compressive stresses in the top and bottom faces of the bottom panel is under-estimated due to this discrepancy.

Because of the way in which the load was represented in the numerical model the local bending adjacent to the load points is under-estimated.

Although the magnitudes of the compressive membrane stresses in the top and bottom panels were of the same order in the numerical model the factors by which the elastic moduli were reduced were not the same. This was because the numerical model over-estimated the compressive membrane stresses in the top panel. There was some distortion in the numerical model as a result of the disparity in the face stiffnesses on either side of the transverse ridge, but this distortion was not large.

The numerical model over-estimated the stress concentrations in the faces at the crown and segment foot due to the inability to simulate the exact experimental constraint conditions in the numerical model. The finite element mesh is too coarse to give an accurate representation of the stress in the faces in regions where there is rapid change in the stress levels. A more accurate representation of the true stress situation would be gained if the finite element mesh were

to be refined adjacent to the crown, R.C.N., R.C.P., segment foot, load points (load crab feet) and along the line of the edge beam. Discrepancies in these regions are accentuated due to the elements being non-conforming across the inter element boundaries.

Despite the discrepancies mentioned above the numerical analysis does give a reasonable approximation of the general level of the stresses in the panel faces. The level of these stresses is small compared to their ultimate tensile stress, which was measured to be $72.2 \times 10^6$ N/m$^2$, with maximum variations of + 18% and - 50%. The face stresses are unlikely to be critical under service loading conditions. Overall, the stresses in the faces of the bottom panels were modelled reasonably well, but the stress situation in the faces of the top panels was poorly modelled.

As displacement was produced primarily by panel shortening and transverse shear deformation of the core material, the numerical model gave an acceptable approximation to the behaviour of the dome during load series 3, provided that the limitations of the model are recognised.

## 8.6 Numerical models domes 1, 2 and 4

The numerical analyses for domes 1, 2 and 4 were performed using the numerical model described in Section 8.1. The factors applied to the elastic constants are shown in Table 8.5. These factors were selected so as to produce the closest approximation to the experimental behaviour of each structure as a whole.

### 8.6.1 Comparison of experimental and numerical displacements, domes 1, 2 and 4, load series 3

8.6.1.1 Dome 1

Figs. 8.17 to 8.19 show a comparison between experimental and numerical displacements for dome 1. Table 8.1 shows the experimental and numerical flexibility influence coefficients for dome 1.

It can be seen that the numerical model gave a good approximation to the transverse displacements remote from the longitudinal ridges. As was observed during the tests upon dome 1, it was more flexible than would be expected from a comparison with the experimental behaviour of the other domes. Transverse displacements adjacent to the longitudinal ridges were significantly under-estimated by the numerical model. The numerical displacements follow the pattern which would be expected from a comparison with the other domes.

8.6.1.2 Dome 2

Figs. 8.22 to 8.24 show a comparison between experimental and numerical displacements for dome 2. Table 8.2 shows the experimental and numerical flexibility influence coefficients for dome 2.

It can be seen that the numerical model gives an excellent approximation to the experimental displacements.

8.6.1.3 Dome 4

Figs. 8.27 to 8.29 show a comparison between experimental and numerical displacements for dome 4. Table 8.4 shows the experimental and numerical flexibility influence coefficients for dome 4.

The numerical model gives an excellent overall approximation to the experimental displacements. As mentioned in Section 8.5.4, the numerical model under-estimates the local effects in the top panels due to the loads at those panels. The sagging in the top longitudinal ridges due to the local effects of the loads is under-estimated. Fig. 8.31.1

shows that the transverse deflection of the edge beams in the experimental and numerical models is not the same. This is probably caused by the over-estimation in the numerical model of the bending in the bottom panels due to compressive thrust along the transverse ridge, and the inability of the numerical model to simulate the exact constraint conditions at the foot, (Section 8.5.4).

### 8.6.2. Numerical stress situation in the faces of domes 1, 2 and 4

Figs. 8.20, 8.25 and 8.30 show the numerical principal stesses in the panel faces of domes 1, 2 and 4 respectively.

The numerical models for these domes produced the same pattern of face stresses as was produced by the numerical model for dome 3. Presumably the same kind of discrepancies are present compared with the true (experimental) face stress situation as were encountered with the numerical model for dome 3.

There was no great variation in the general level of stresses in the faces of any of the four domes. The bending stresses were of the same order in each case.

The magnitude of the membrane stresses was reduced as the ratio h/r was increased. This variation in the membrane stresses was relfected in the magnitude of the factors applied to the elastic constants for the dome materials, (Table 8.5).

## 8.7 Conclusions : Numerical Work

The numerical models gave a reasonably good approximation to the overall behaviour of the experimental models. The comparison between experimental and numerical face stresses for dome 3 provides the only basis upon which an assessment can be made of the reliability of the numerical values for these stresses. It must be concluded that,although the numerical analyses gave good displacement predictions the face

stresses can only be taken as a guide to the order of magnitude of these stresses in an actual structure.

The accuracy of the numerical displacements depends upon the selection of appropriate factors to be applied to the elastic constants of the dome materials, (Table 8.5). The choice of appropriate factors in an analysis using the 'Parton Quadratic Shape Function Sandwich Element' relies to a high degree upon the judgement of the person performing the analysis, a situation which would not be acceptable for general application.

An improvement to the numerical analysis would be to use an element for which different elastic moduli could be specified for the bending and membrane actions. Experimentally determined values for these moduli could be specified separately, (Sections 2.2 and 5.0). The sandwich element developed by Manos (10) would be suitable for this type of approach. Alternatively the 'Parton Quadratic Shape Function Sandwich Element' could be modified so that the elastic moduli of the top and bottom faces could be specified separately. The appropriate elastic moduli for each face could be selected depending upon whether the stresses in that face were tensile or compressive.

The above improvements would be performed using an iterative solution procedure.

# Numerical Model - Load Series 3

## Load U.D.L. + Point Loads (elements 50, 53 & 59)

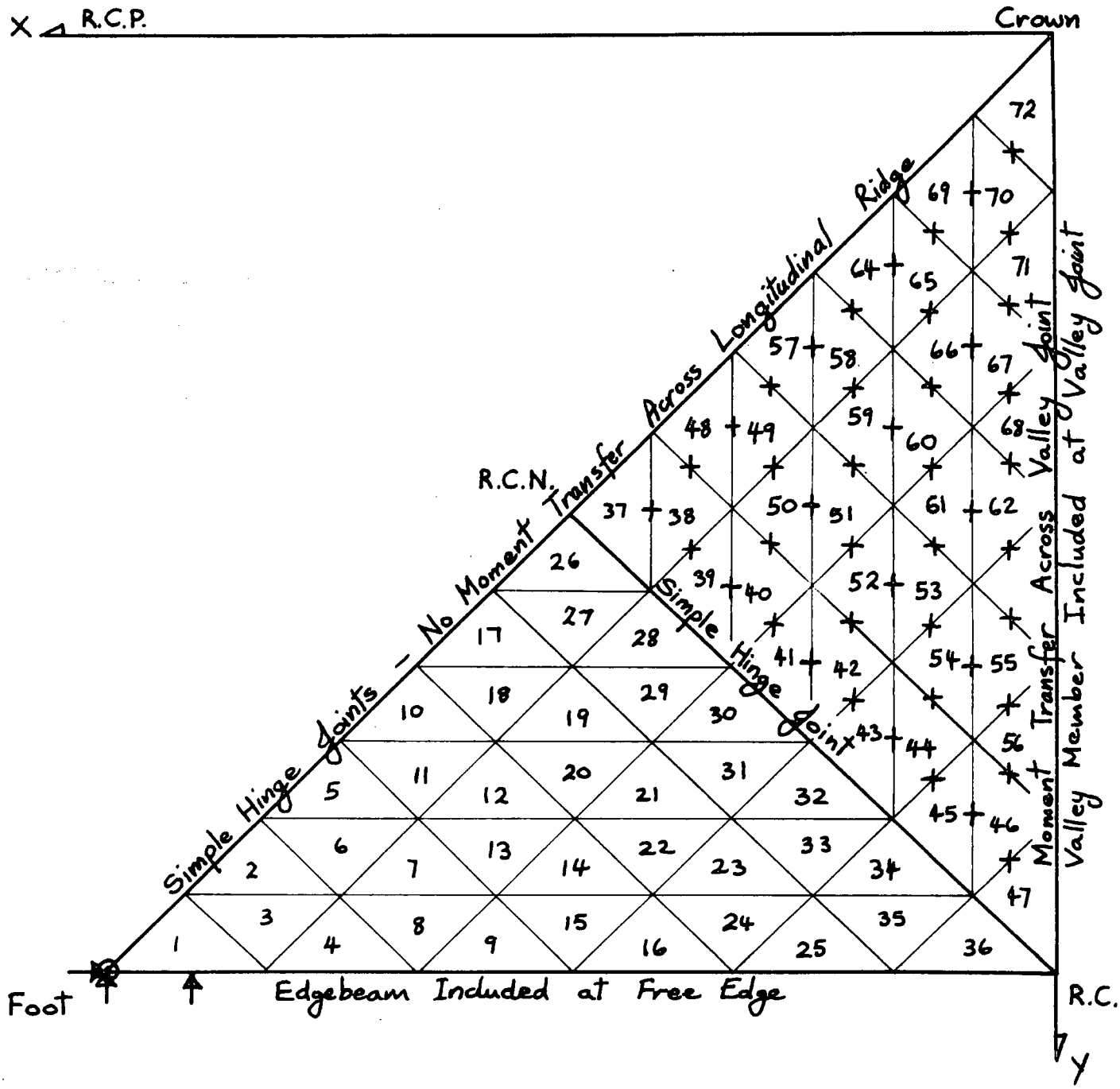


XYZ Global Coordinate System

1 - 72 Element Numbers

\+ Load Points

Foot - Constrained Degree of Freedom

↑ Horizontal

⊙ Vertical

# Numerical Model - Load Series 3

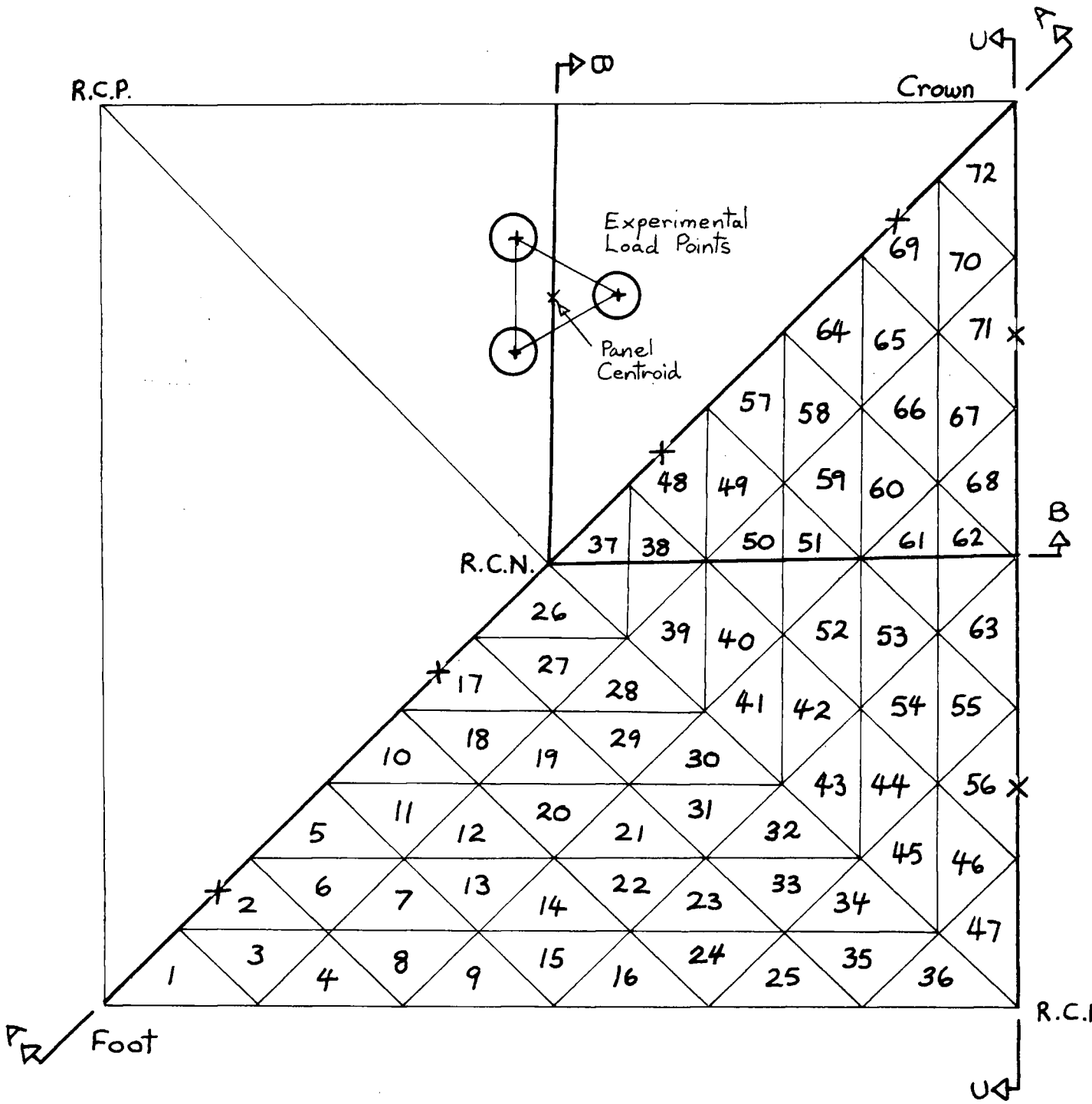


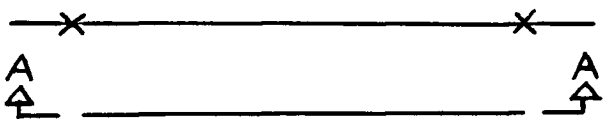


Lines of symmetry

Section Lines

Section AA Dome 2 (Load Series 3)

Displacements mm x $10^{-3}$/N/Panel

Displacement Scale 1000 : 1

All Displacements - Global

⊙ Numerical Model Moment Transfer Across Longitudinal Ridge.

◇ Numerical Model No Moment Transfer Across Longitudinal Ridge.

—⊡— Experimental Results

Note:
In both numerical analyses the radial load is evenly distributed between the mid-side nodes of elements 50, 53 & 59.

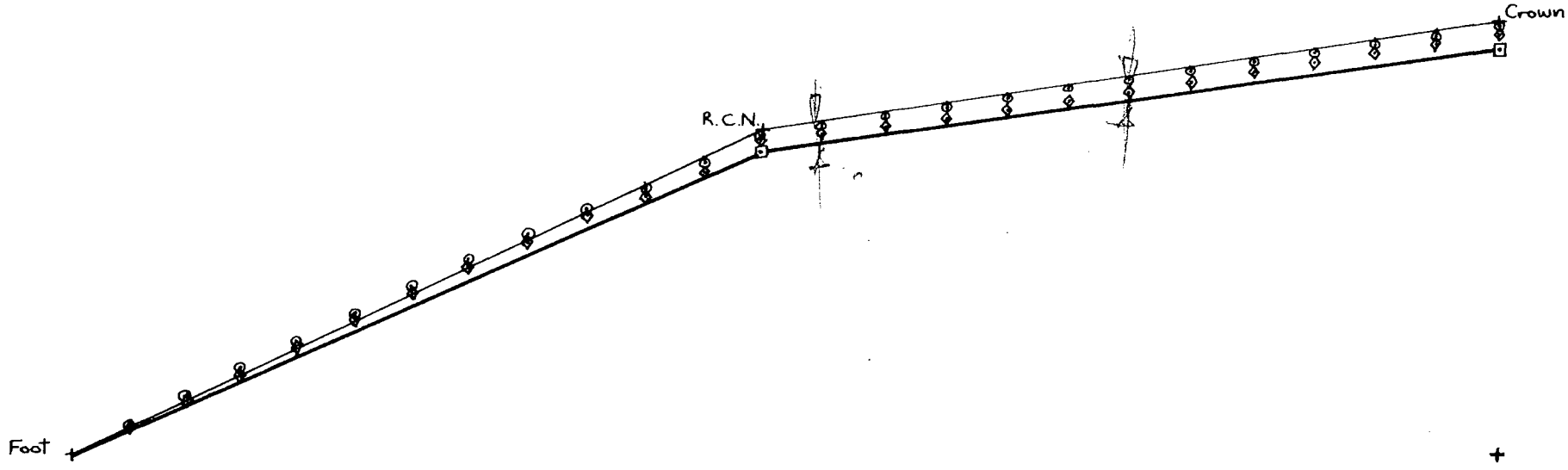


FIG. 8.2

Section BB Dome 2 (Load Series 3)

Displacements mm x $10^{-3}$/N/Panel

Displacement Scale 1000:1

All Displacements - Local Coordinates
(except at panel edges - global)

- ⊙ Numerical Model Moment Transfer Across Longitudinal Ridge
- ◇ Numerical Model No Moment Transfer Across Longitudinal Ridge
- —⊡— Experimental Results

**Note:**
In both numerical analyses the radial load is evenly distributed between the mid-side nodes of elements 50, 53 & 59.

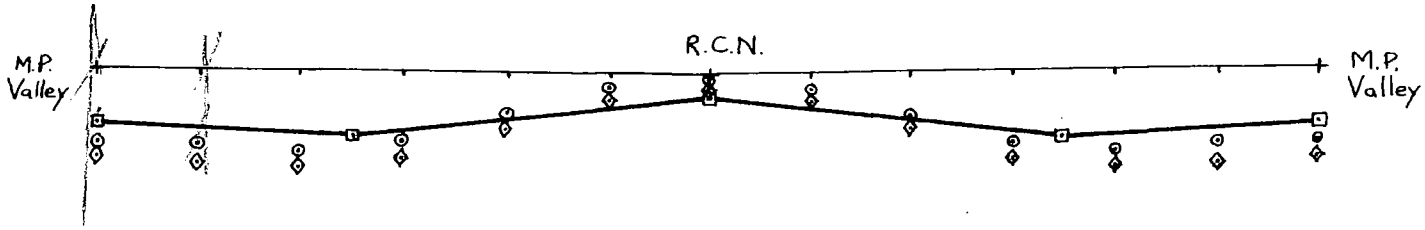


FIG. 6.3

Section CC Dome 2 (Load Series 3)

Displacements mm x $10^{-3}$/N/Panel

Displacement Scale 1000:1

All Displacements - Global

⊙ Numerical Model Moment Transfer Across Longitudinal Ridge

◇ Numerical Model No Moment Transfer Across Longitudinal Ridge

—⊡— Experimental Results

**Note:**
In both numerical analyses the radial load is evenly distributed between the mid-side nodes of elements 50, 53 & 59.

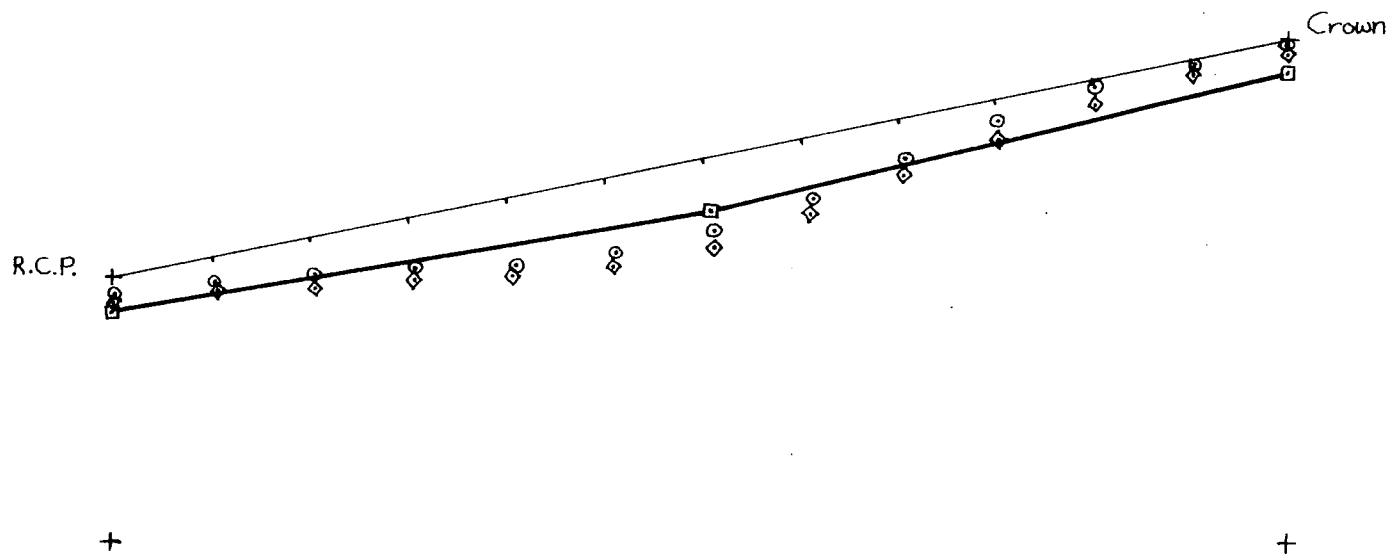


FIG. 84

Section AA Dome 2 (Load Series 3)

Displacements mm x $10^{-3}$/N/Panel

Displacement Scale 1000 : 1

All Displacements - Global

⊙ Numerical Model Point Loads Elements 50, 53 & 59

◇ Numerical Model U.D.L. + Point Loads (elements 50, 53 & 59)

—□— Experimental Results

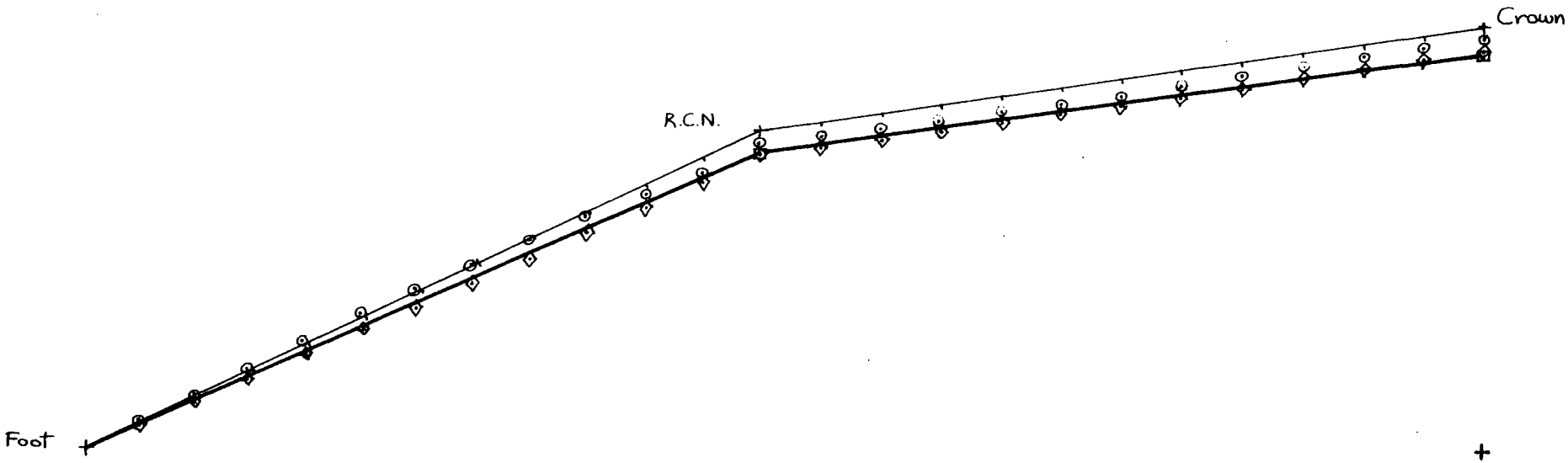


FIG.85

Section BB Dome 2 (Load Series 3)

Displacements mm x $10^{-3}$/N/Panel

Displacement Scale 1000:1

All Displacements - Local Coordinates
(except at panel edges - global)

⊙ Numerical Model Point Loads Elements 50, 53 & 59

◇ Numerical Model U.D.L. + Point Loads (elements 50, 53 & 59)

—□— Experimental Results

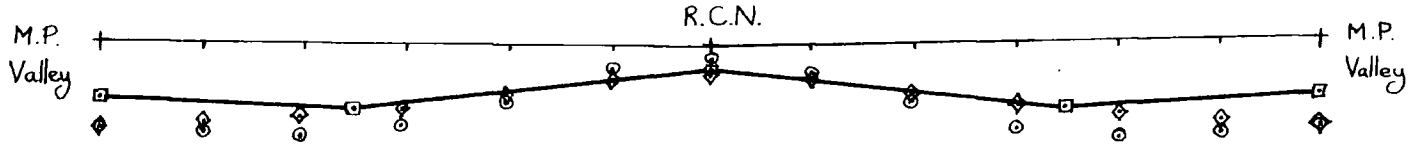


FIG. 8.6

Section CC Dome 2 (Load Series 3)

Displacements mm x $10^{-3}$/N/Panel

Displacement Scale 1000:1

All Displacements - Global

⊙ Numerical Model Point Loads Elements 50, 53 & 59

◈ Numerical Model U.D.L. + Point Loads (elements 50, 53 & 59)

—⊡— Experimental Results

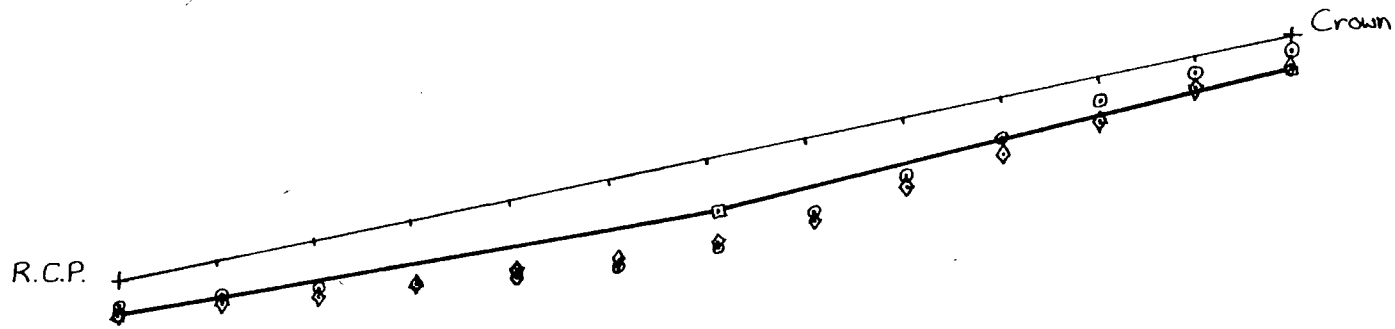


FIG 8.7

Section AA Dome 3 (Load Series 3)

Displacements mm x $10^{-3}$/N/Panel

Displacement Scale 1000 : 1

All Displacements - Global

⊙ Numerical Model

◇ Numerical Model with edgebeam omitted

—□— Experimental Results

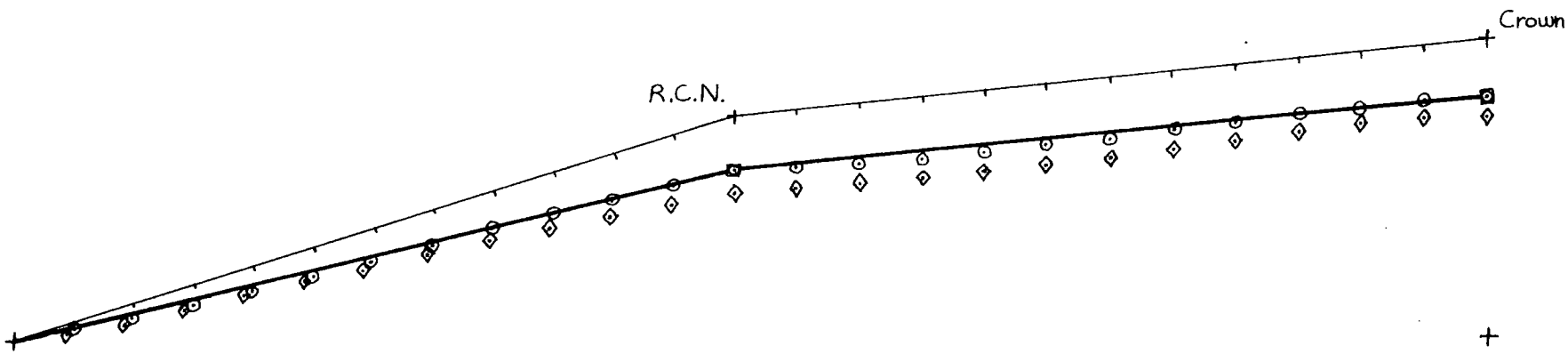


FIG.8.8

Section BB Dome 3 (Load Series 3)

Displacements mm x $10^{-3}$/N/Panel

Displacement Scale 1000:1

All Displacements - Local Coordinates
(except at panel edges - global)

⊙ Numerical Model

◇ Numerical Model with edgebeam omitted

—⊡— Experimental Results

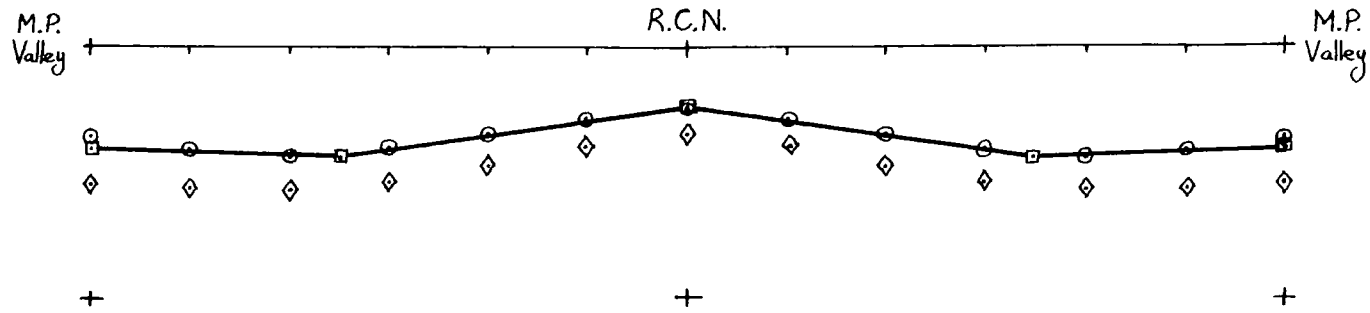


FIG.87

Section CC Dome 3 (Load Series 3)

Displacements mm $\times 10^{-3}$/N/Panel

Displacement Scale 1000 : 1

All Displacements - Global

⊙ Numerical Model

◇ Numerical Model with edgebeam omitted

—□— Experimental Results

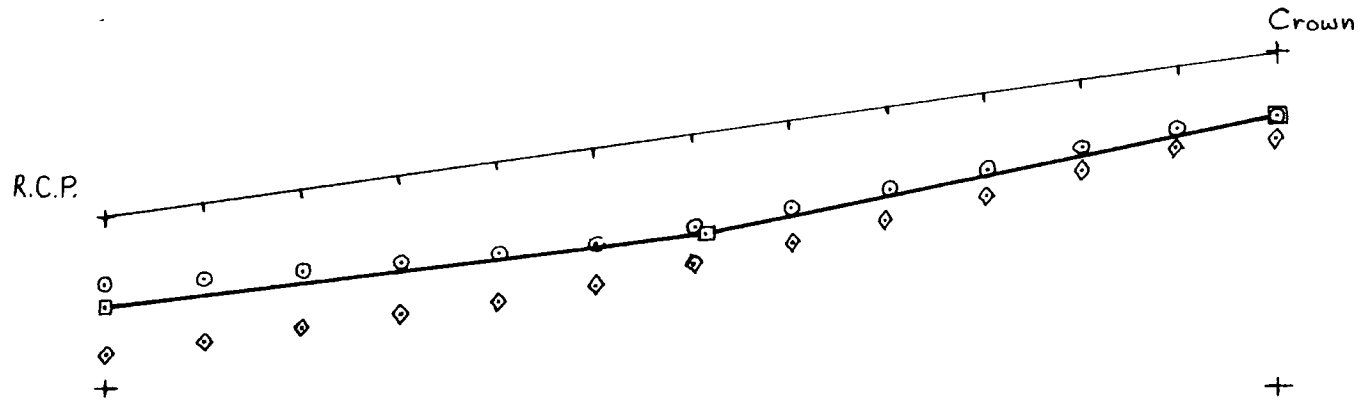


FIG.8-10

FIG. 8·11

## Experimental Principal Stresses Load Series 3 — Dome 3

Tension +ve
Compression -ve
} N x 10³/m²/N/Panel

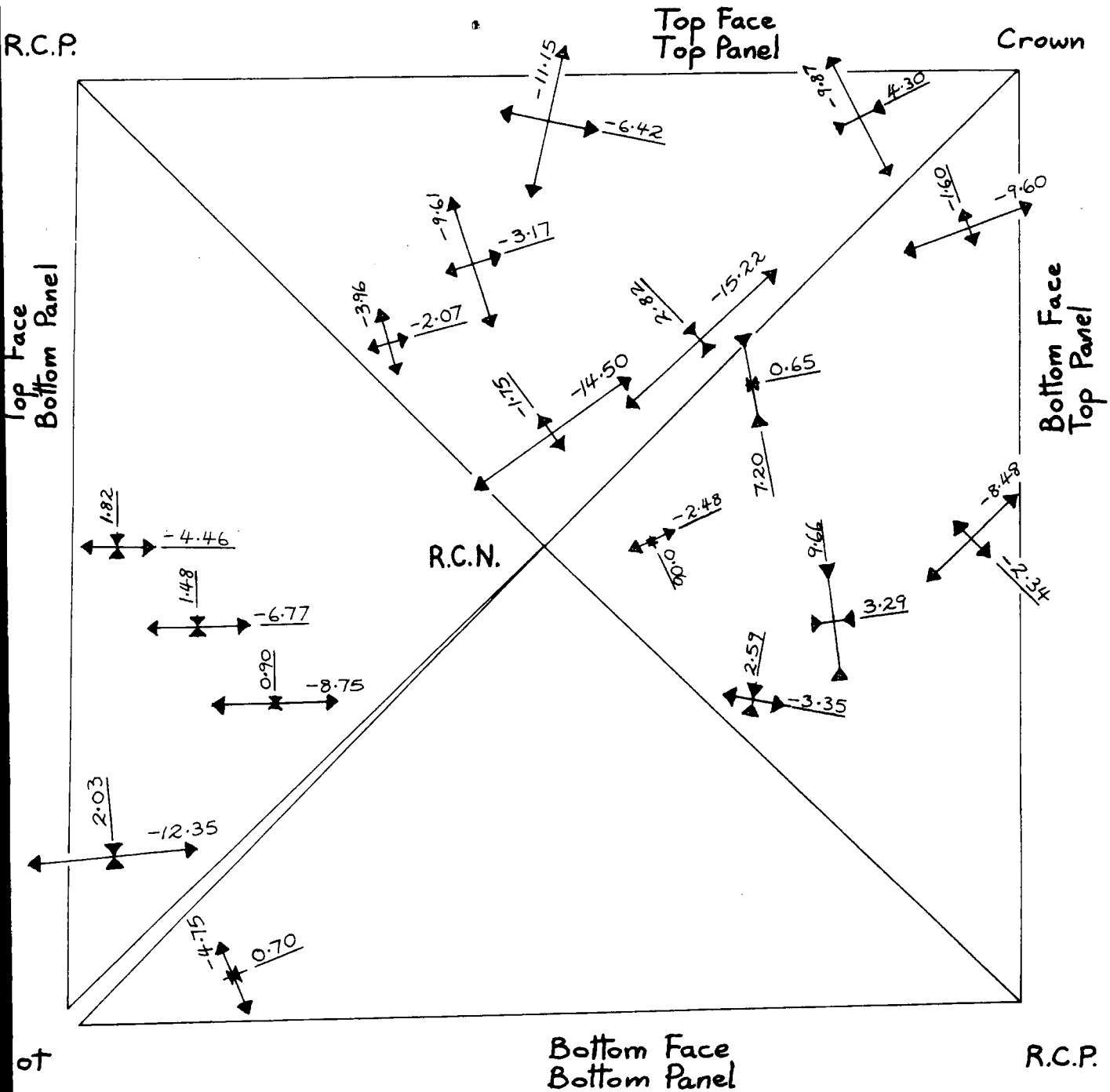

FIG. 8·12

Numerical Stress $\sigma_x$ Load Series 3 ($N \times 10^3/m^2/N/Panel$) Dome 3

Tension +ve

+ -10·79 Experimental Stress

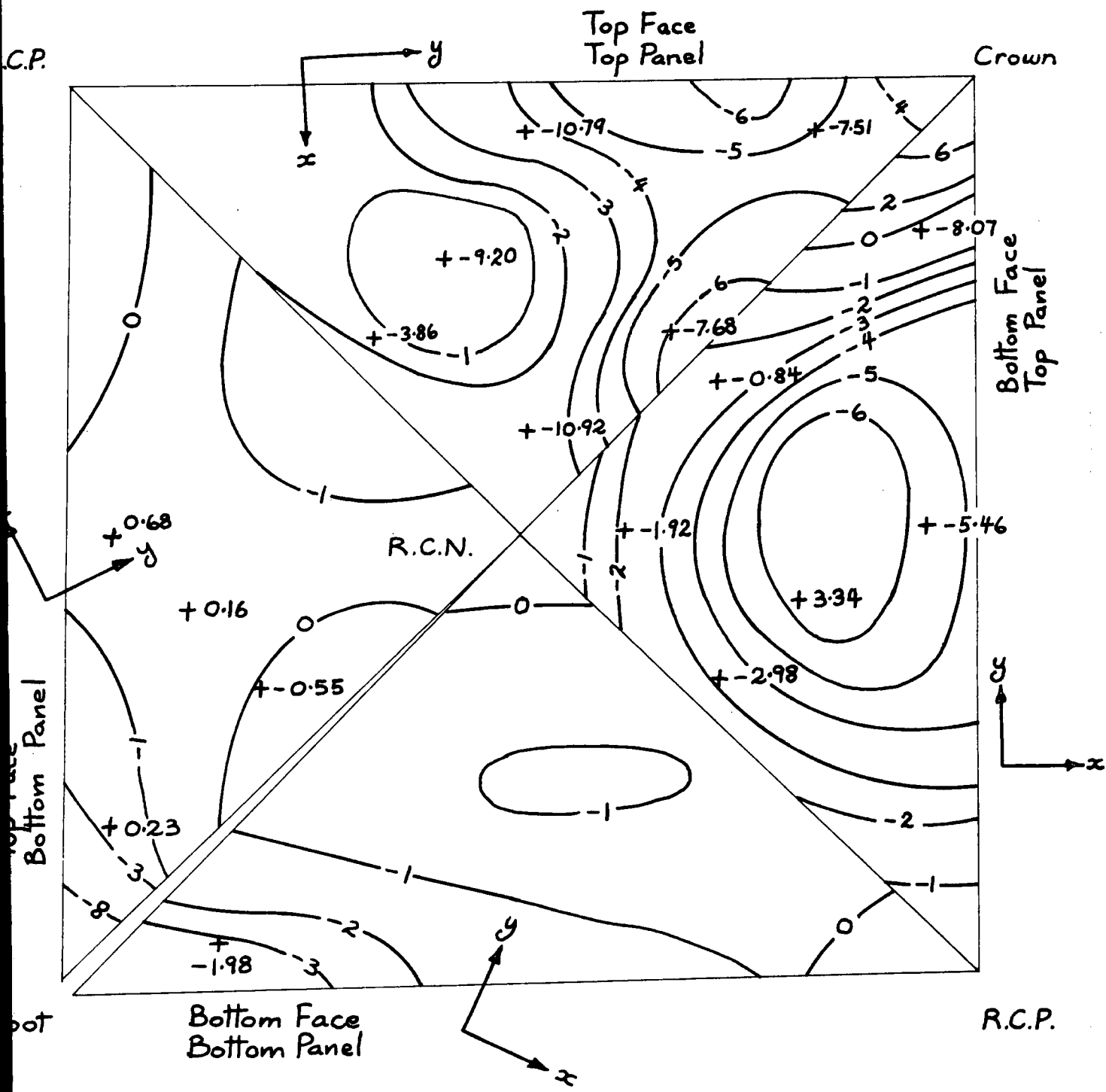

FIG. 8·13

Numerical Stress $\sigma_y$ Load Series 3 ($N \times 10^3/m^2/N/Panel$) Dome 3

Tension +ve

+ - 6·77 Experimental Stress

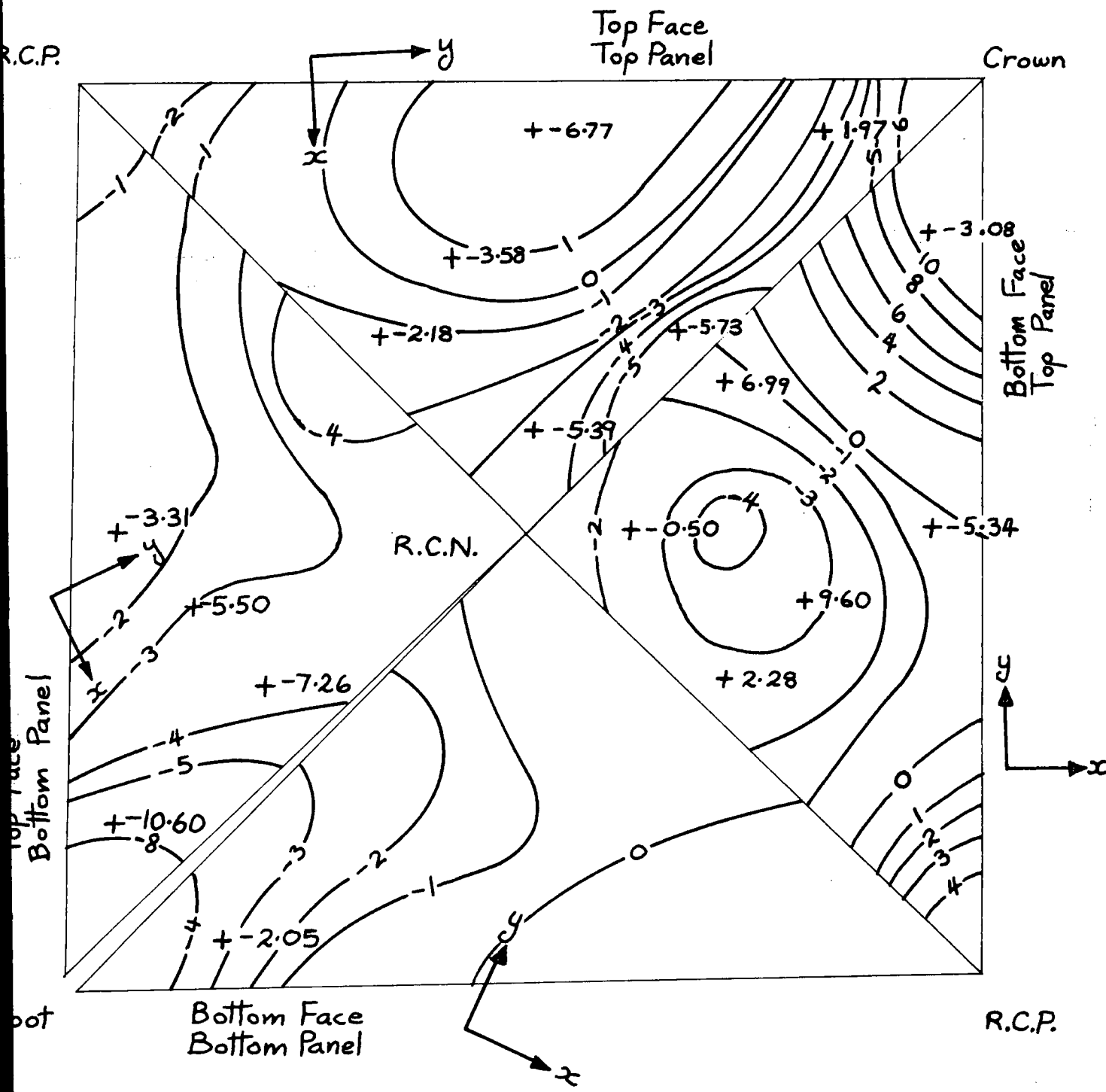

FIG. 8·14

Numerical Stress $\tau_{xy}$ Load Series 3 ($Nx10^3/m^2/N/Panel$) Dome 3

\+ 1·20 Experimental Stress

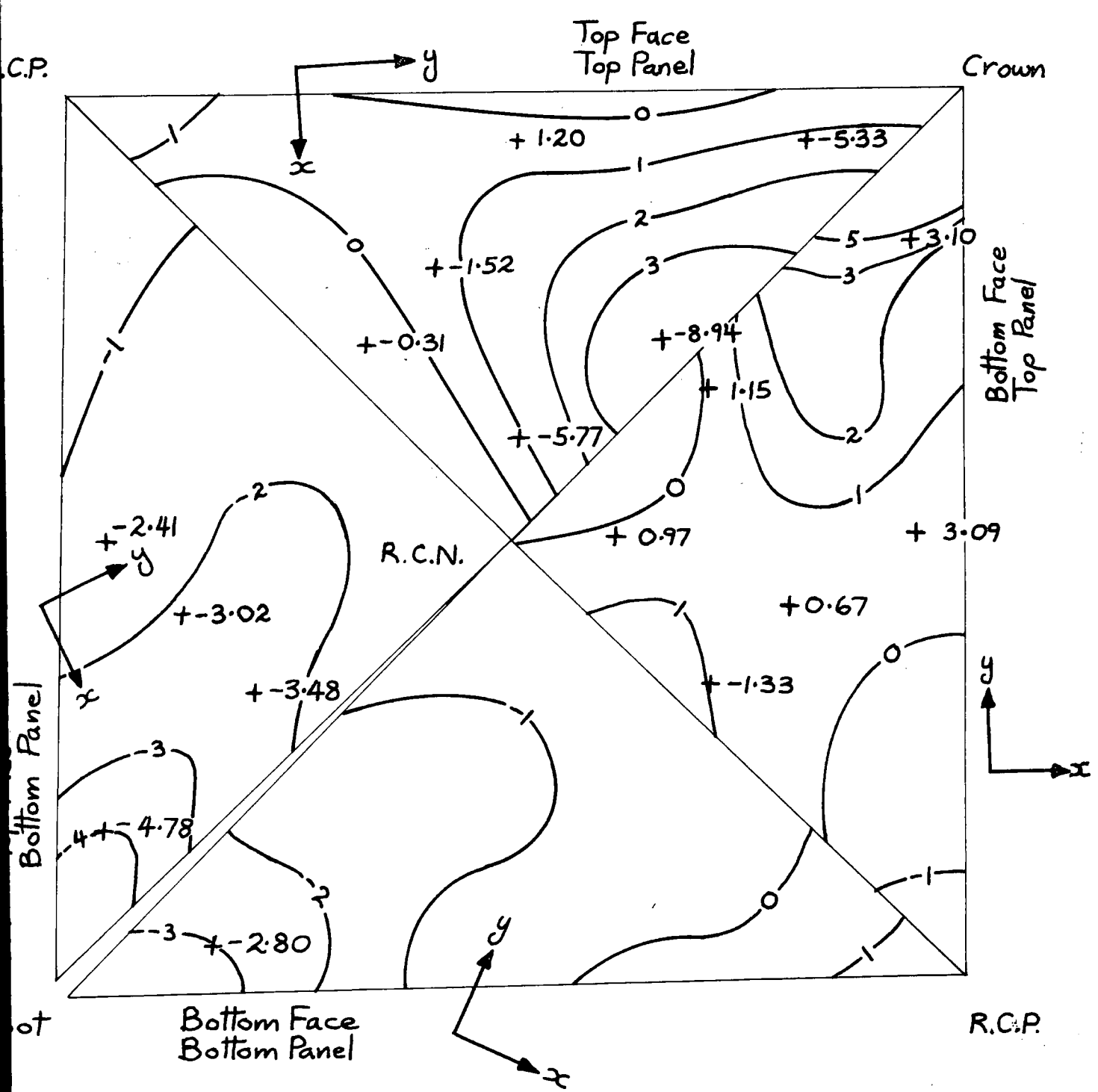

FIG. 8·15

# Numerical Principal Stresses Load Series 3 — Dome3

Tension +ve
Compression −ve
} N×10³/m²/N/Panel

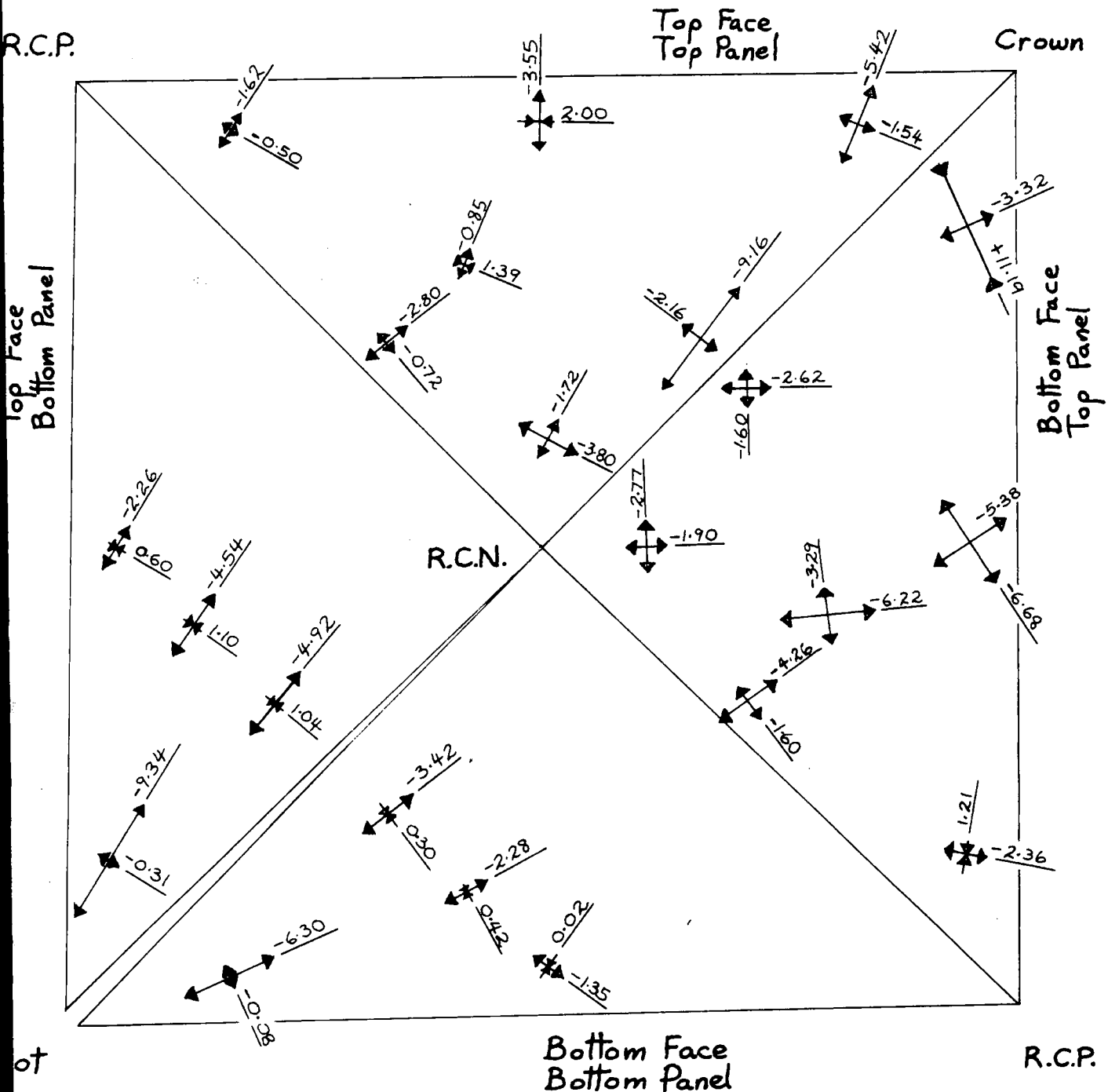

# Numerical Displacements and Forces in Edgebeams
## Load Series 3 Dome 3

FIG. 8·16·1
(1 OF 2)

# Numerical Displacements and Forces in Edgebeams
## Load Series 3 Dome 3

FIG.8·16·2
(2OF2)

Section AA Dome 1 (Load Series 3)

Displacements mm x $10^{-3}$/N/Panel

Displacement Scale 1000:1

All Displacements - Global

⊙ Numerical Model

—⊡— Experimental Results

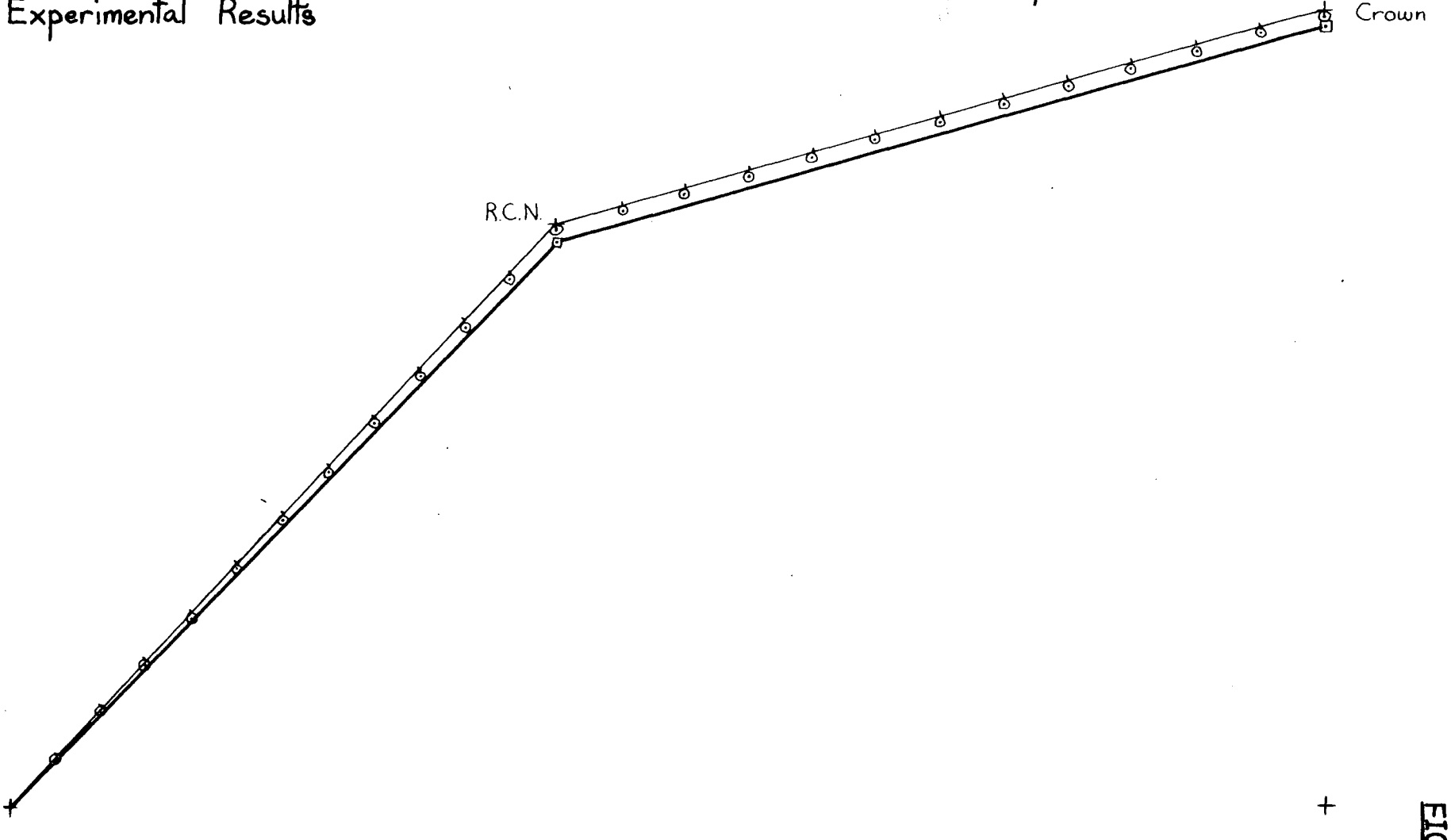


FIG. 8.17

Section BB Dome 1 (Load Series 3)

⊙ Numerical Model

—⊡— Experimental Results

Displacements mm x $10^{-3}$/N/Panel

Displacement Scale 1000:1

All Displacements - Local Coordinates
(except at panel edges - global)

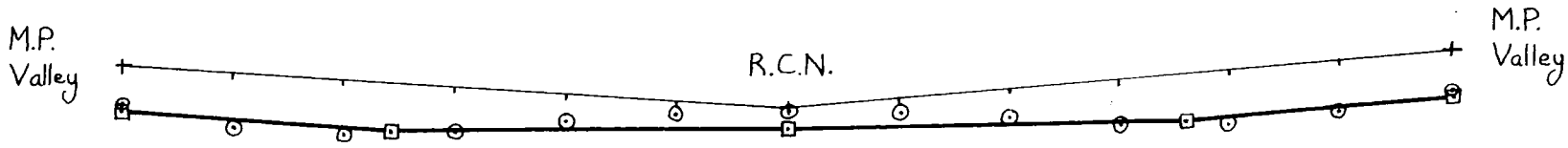


FIG.8.18

Section CC Dome 1 (Load Series 3)

Displacements mm x $10^{-3}$/N/Panel

Displacement Scale 1000:1

All Displacements - Global

⊙ Numerical Model

—⊡— Experimental Results

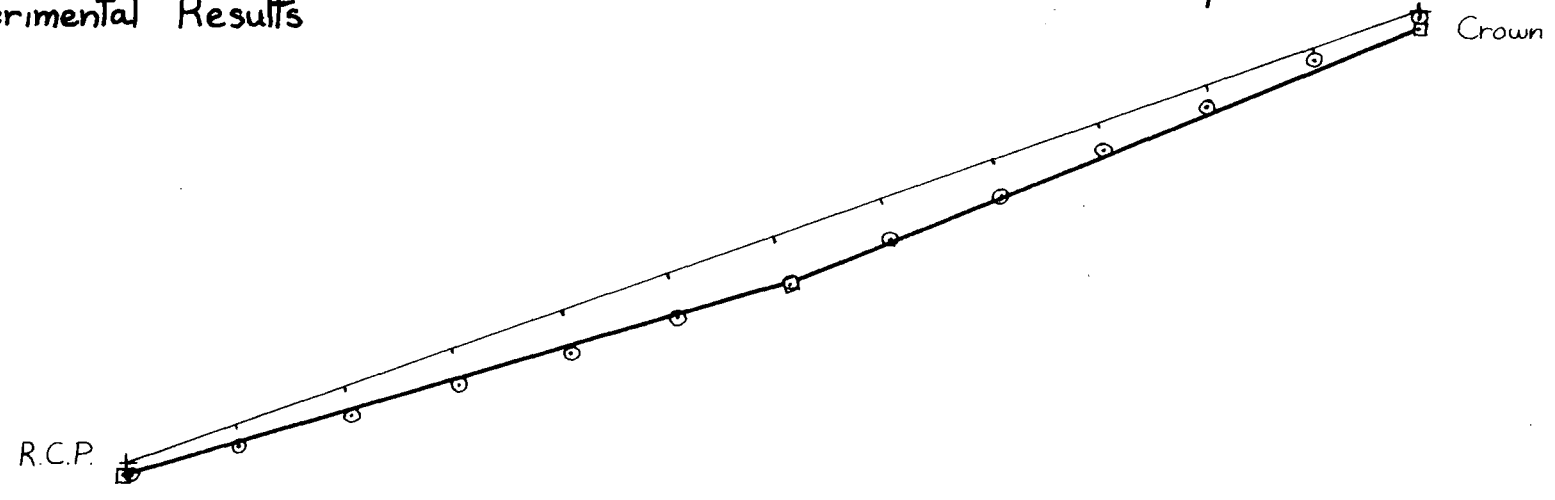


FIG. 8.12

FIG. 8·20

# Numerical Principal Stresses Load Series 3 — Dome 1

Tension +ve
Compression -ve
} $N \times 10^3/m^2/N$/Panel

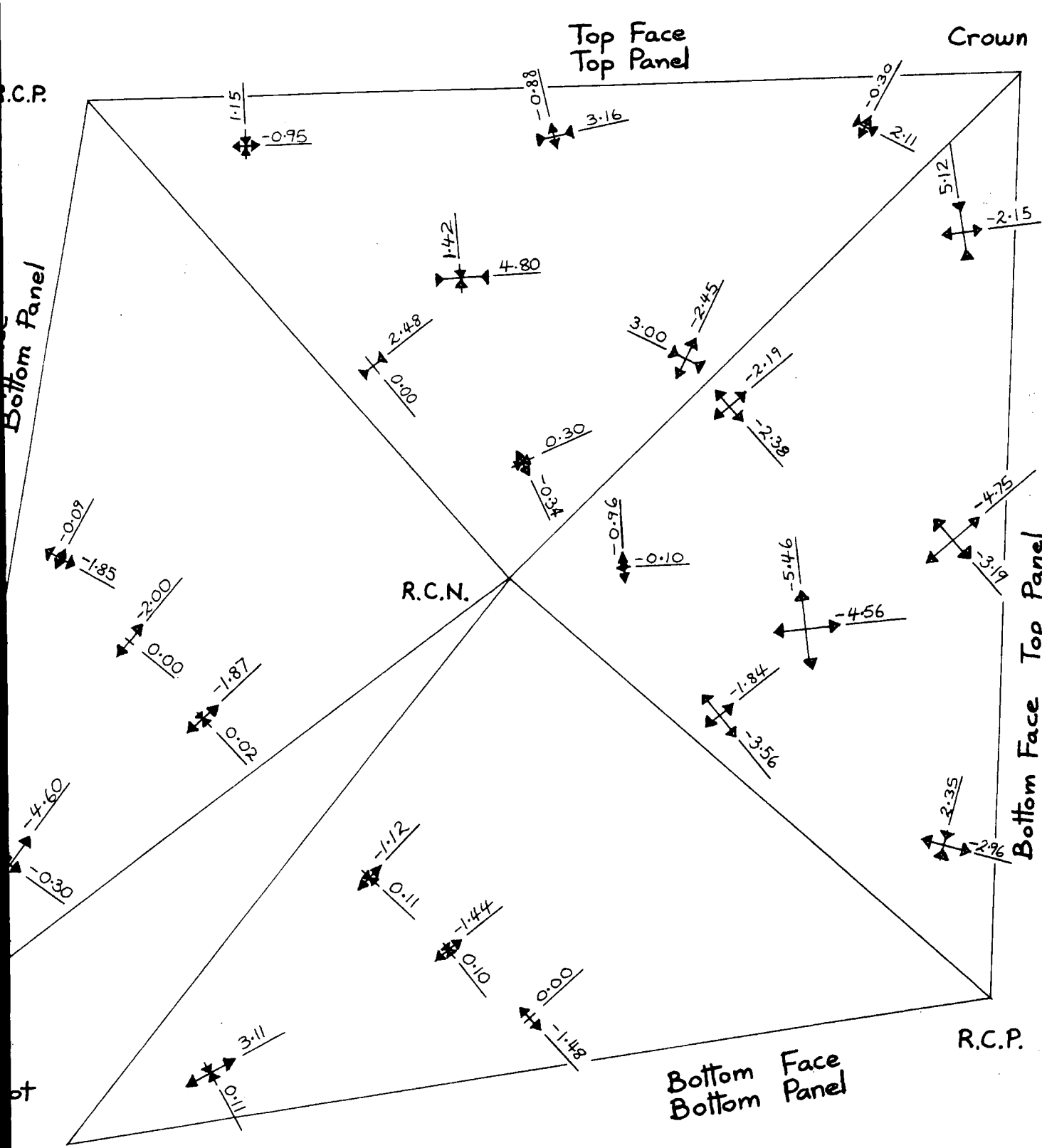

# Numerical Displacements and Forces in Edgebeams
## Load Series 3 Dome 1

FIG.8·21·1
(1 OF 2)

# Numerical Displacements and Forces in Edgebeams
## Load Series 3 Dome 1

FIG. 8·21·2
(2 OF 2)

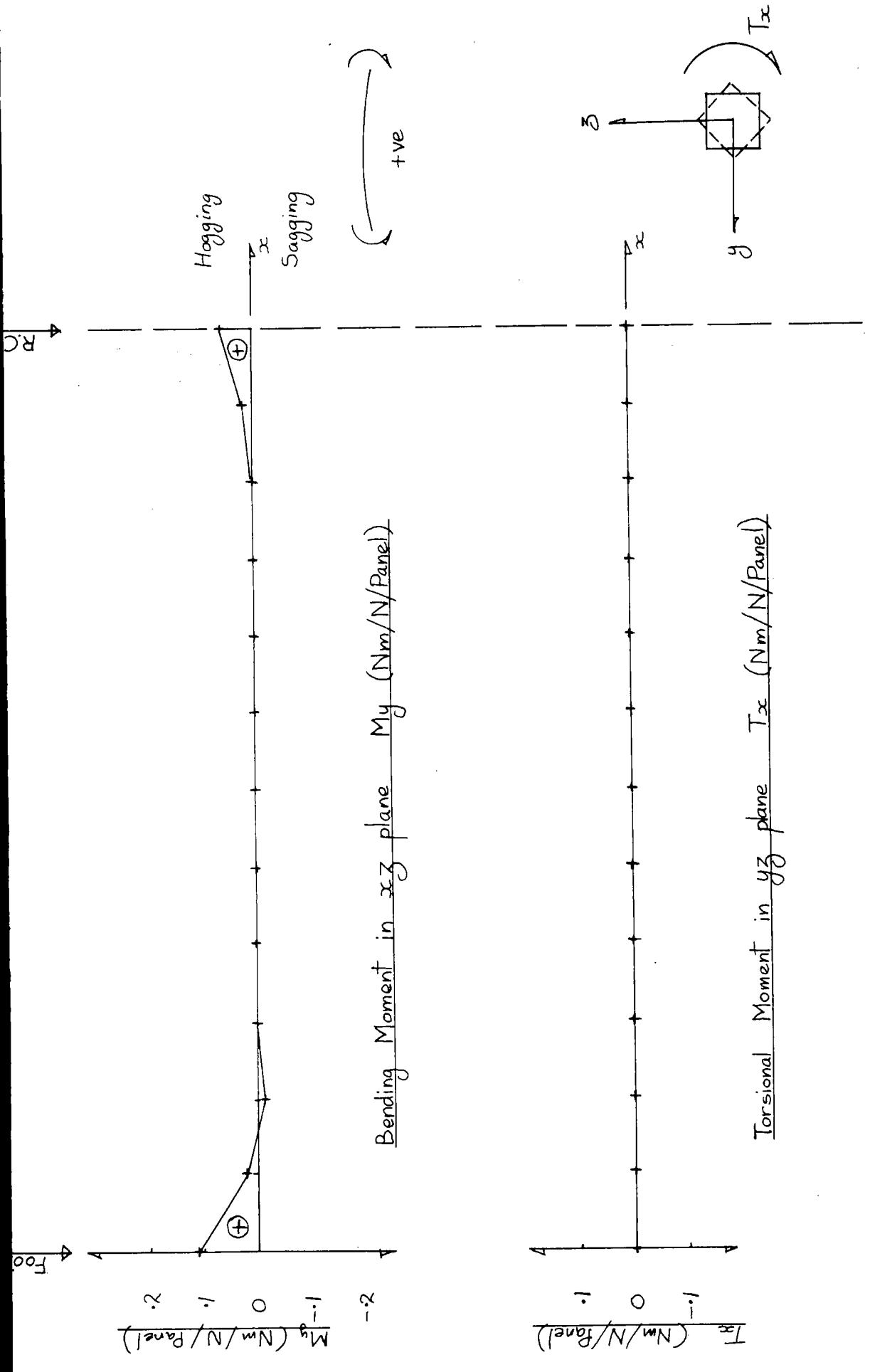

Section AA Dome 2 (Load Series 3)

⊙ Numerical Model

—⊡— Experimental Results

Displacements mm x $10^{-3}$/N/Panel

Displacement Scale 1000:1

All Displacements - Global

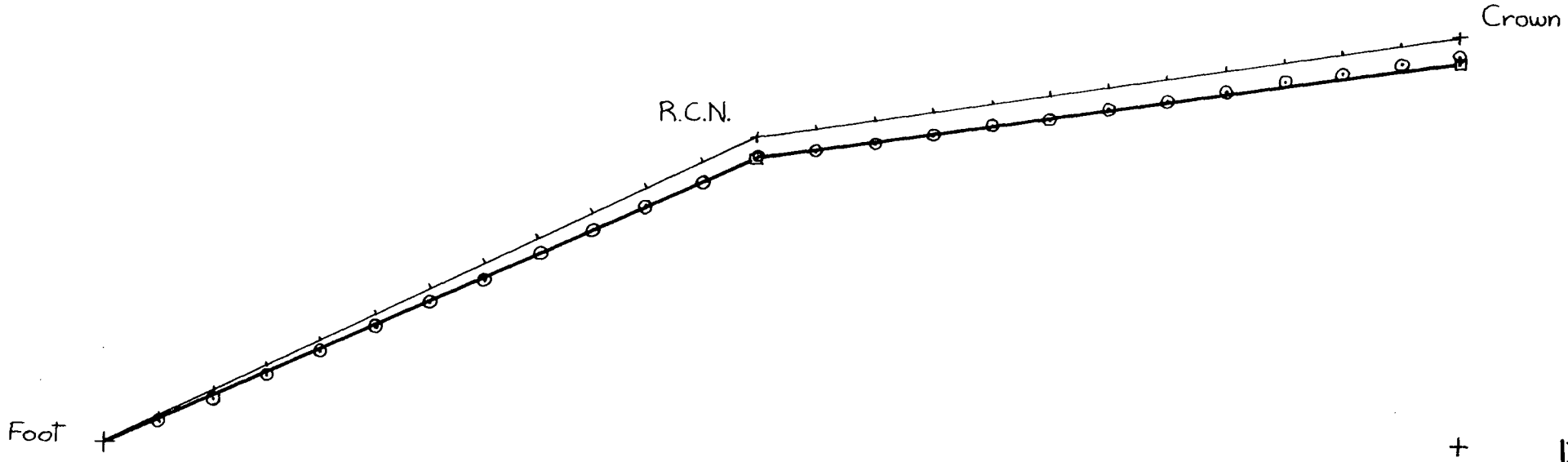


FIG. 8.22

Section BB Dome 2 (Load Series 3)

⊙ Numerical Model

—⊡— Experimental Results

Displacements mm x $10^{-3}$/N/Panel

Displacement Scale 1000:1

All Displacements - Local Coordinates
(except at panel edges - global)

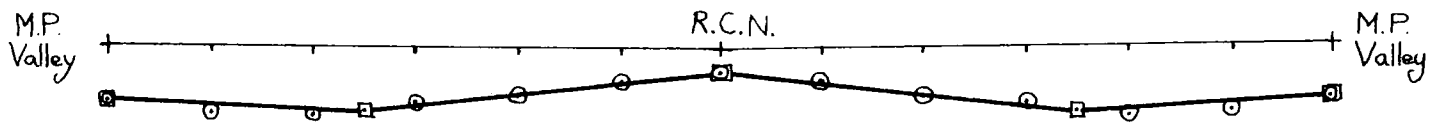


FIG. 8.23

Section CC Dome 2 (Load Series 3)

Displacements mm x $10^{-3}$/N/Panel

Displacement Scale 1000:1

All Displacements - Global

⊙ Numerical Model

—⊡— Experimental Results

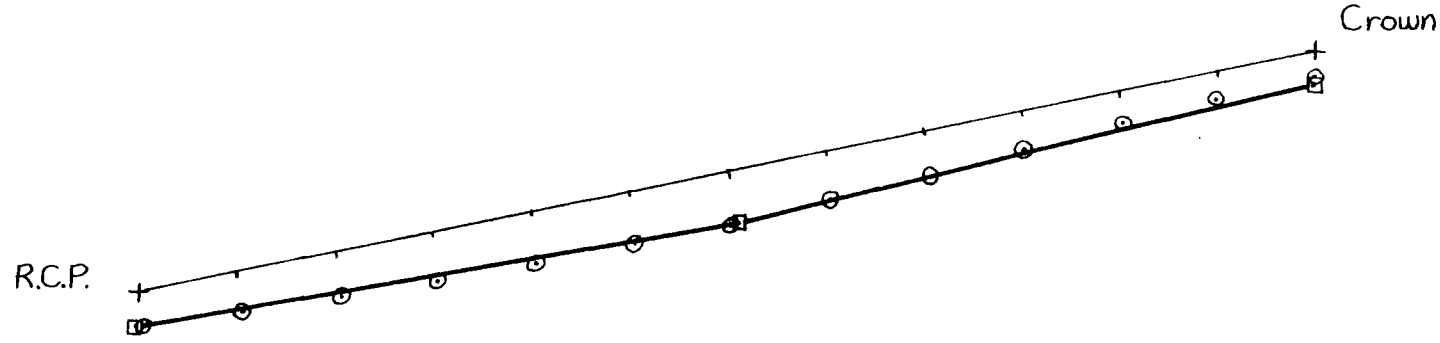


FIG. 8.24

FIG. 8.25

# Numerical Principal Stresses Load Series 3 Dome 2

Tension +ve
Compression -ve
} N×10³/m²/N/Panel

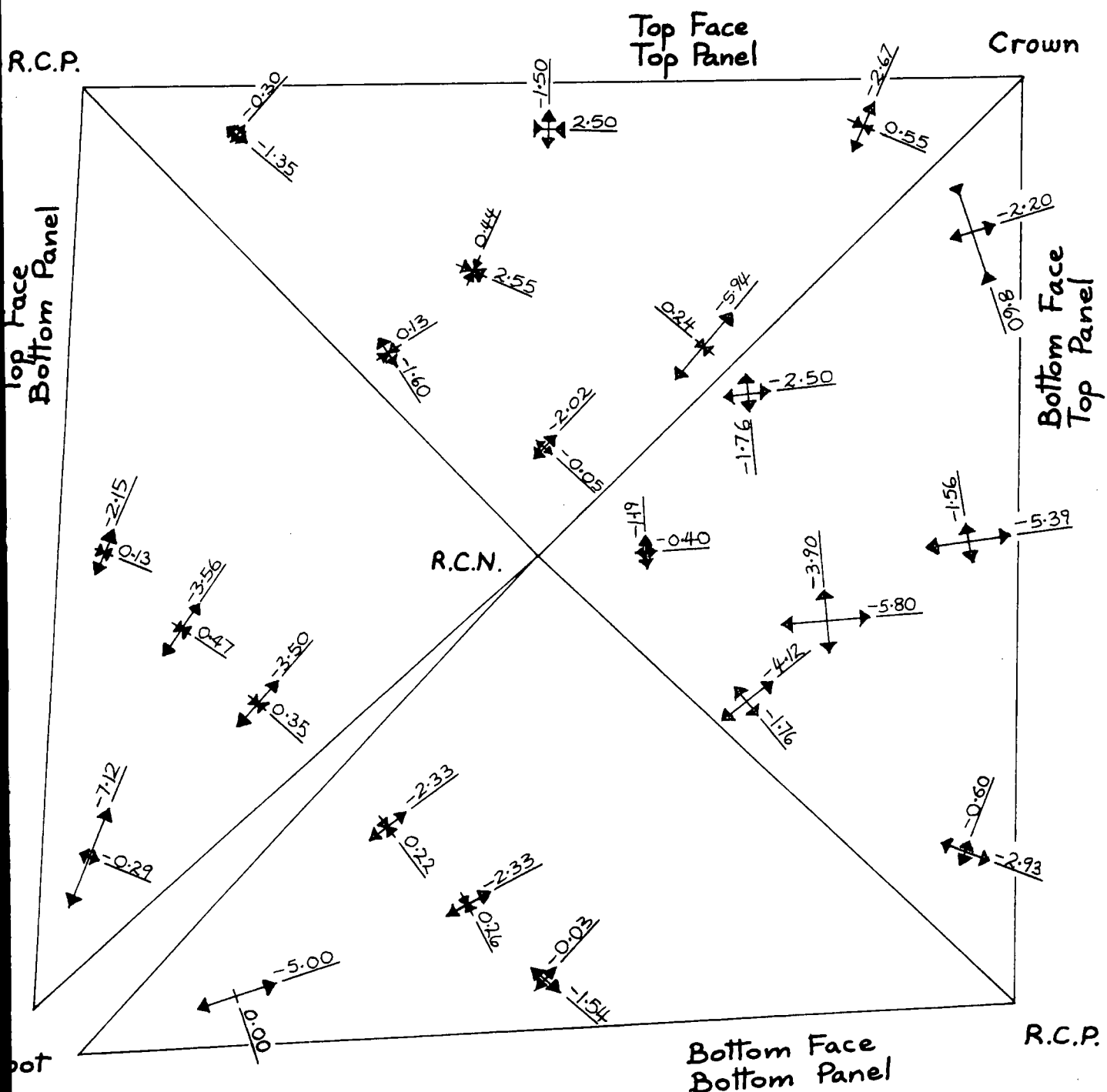

# Numerical Displacements and Forces in Edgebeams
## Load Series 3 Dome 2

FIG. 8.26-1
(1 OF 2)

# Numerical Displacements and Forces in Edgebeams
## Load Series 3 Dome 2

FIG. 8·26·2 (2 OF 2)

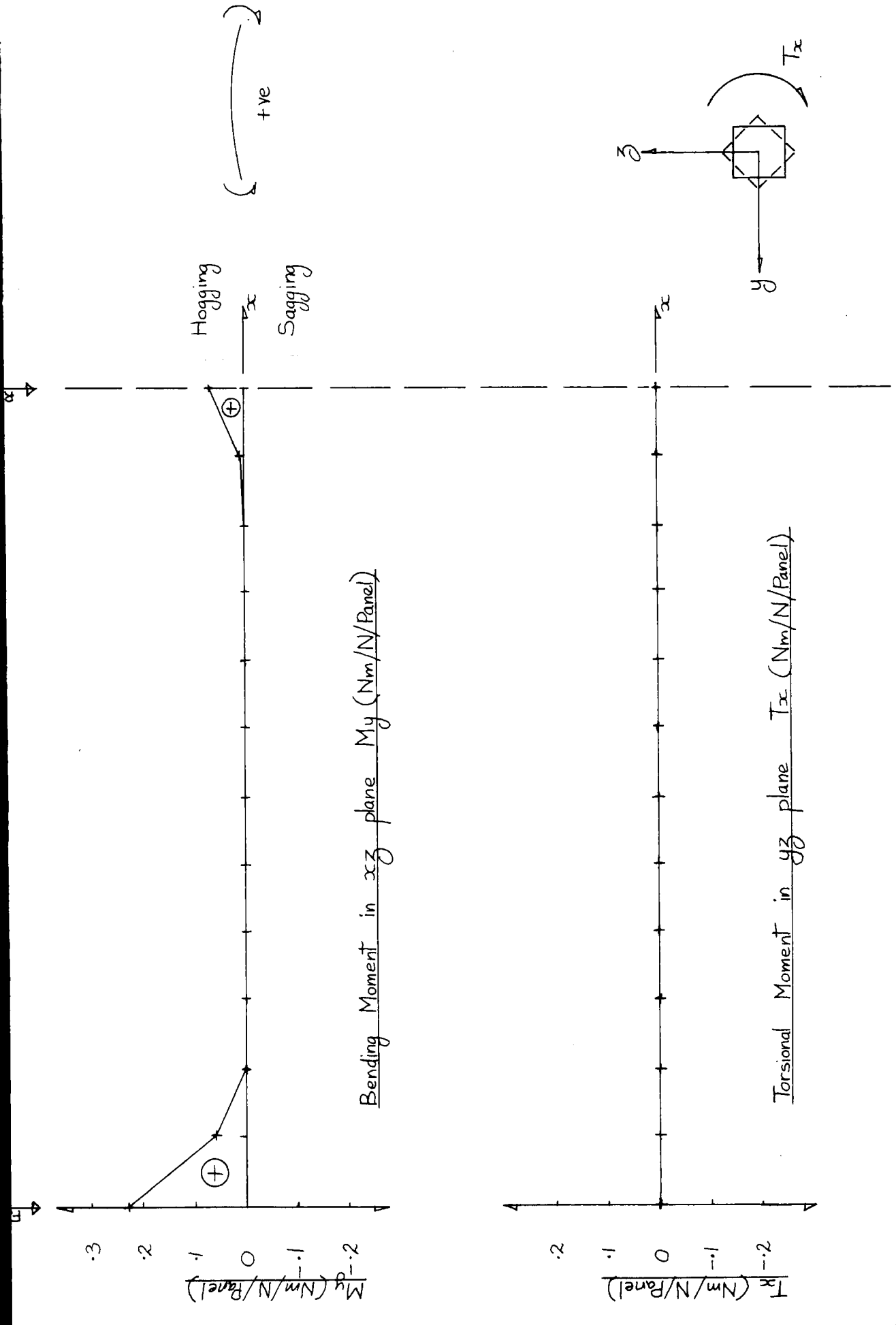

Section AA Dome 4 (Load Series 3)

⊙ Numerical Model

—⊡— Experimental Results

Displacements mm x $10^{-3}$/N/Panel

Displacement Scale 1000:1

All Displacements - Global

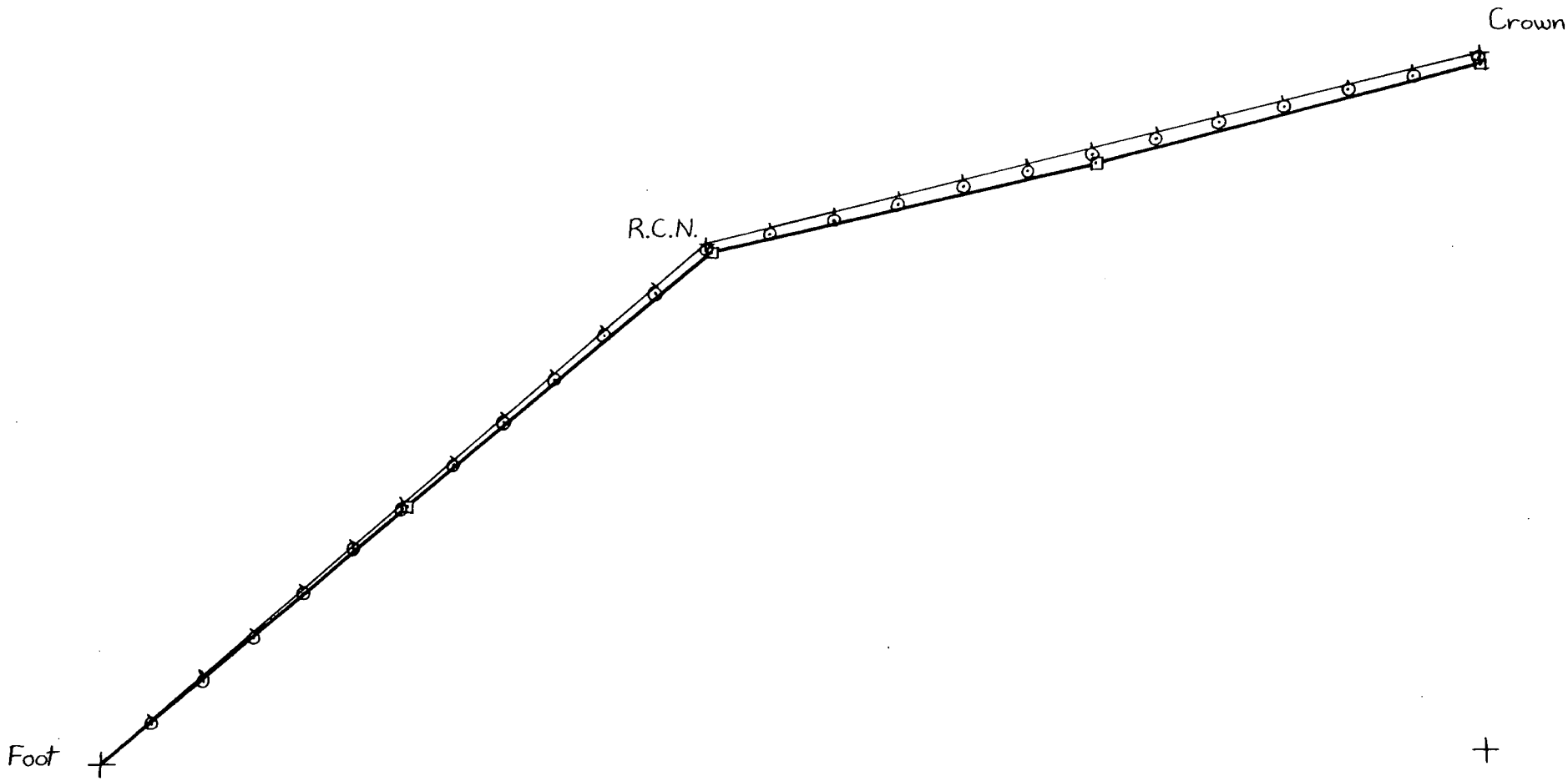


FIG. 8.27

Section BB Dome 4 (Load Series 3)

⊙ Numerical Model

—⊡— Experimental Results

Displacements mm x $10^{-3}$/N/Panel

Displacement Scale 1000:1

All Displacements - Local Coordinates
(except at panel edges - global)

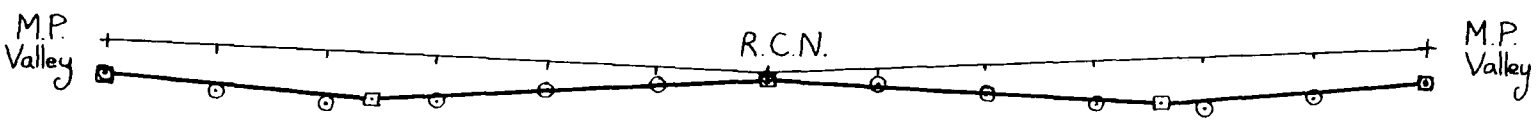


FIG.8.28

Section CC Dome 4 (Load Series 3)

Displacements mm x $10^{-3}$/N/Panel

Displacement Scale 1000:1

All Displacements - Global

⊙ Numerical Model

—⊡— Experimental Results

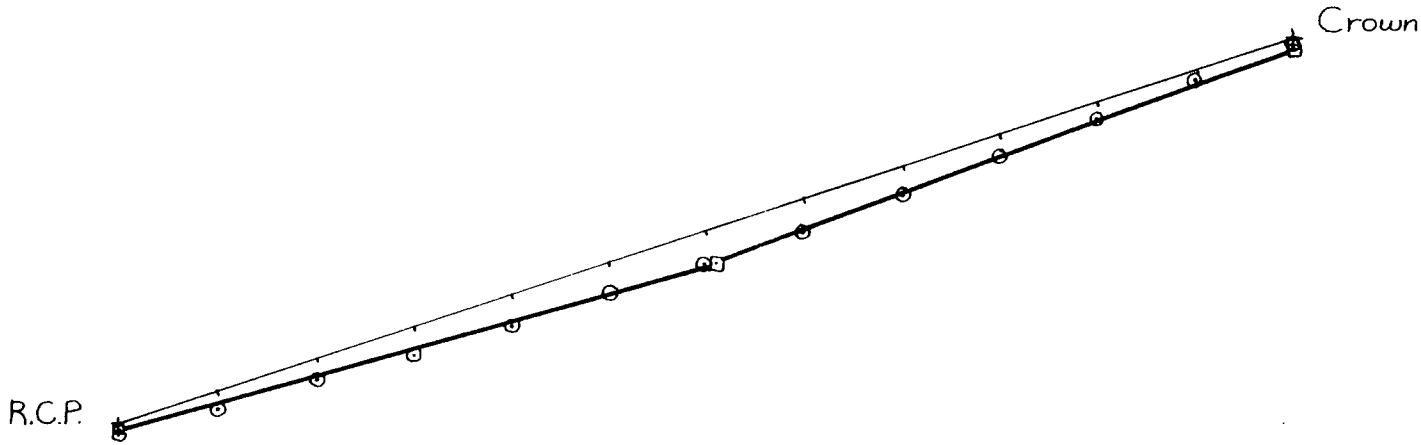


FIG. 8.29

FIG. 8·30

Dome 4

# Numerical Principal Stresses Load Series 3

Tension +ve

Compression -ve

$N \times 10^3/m^2/N/Panel$

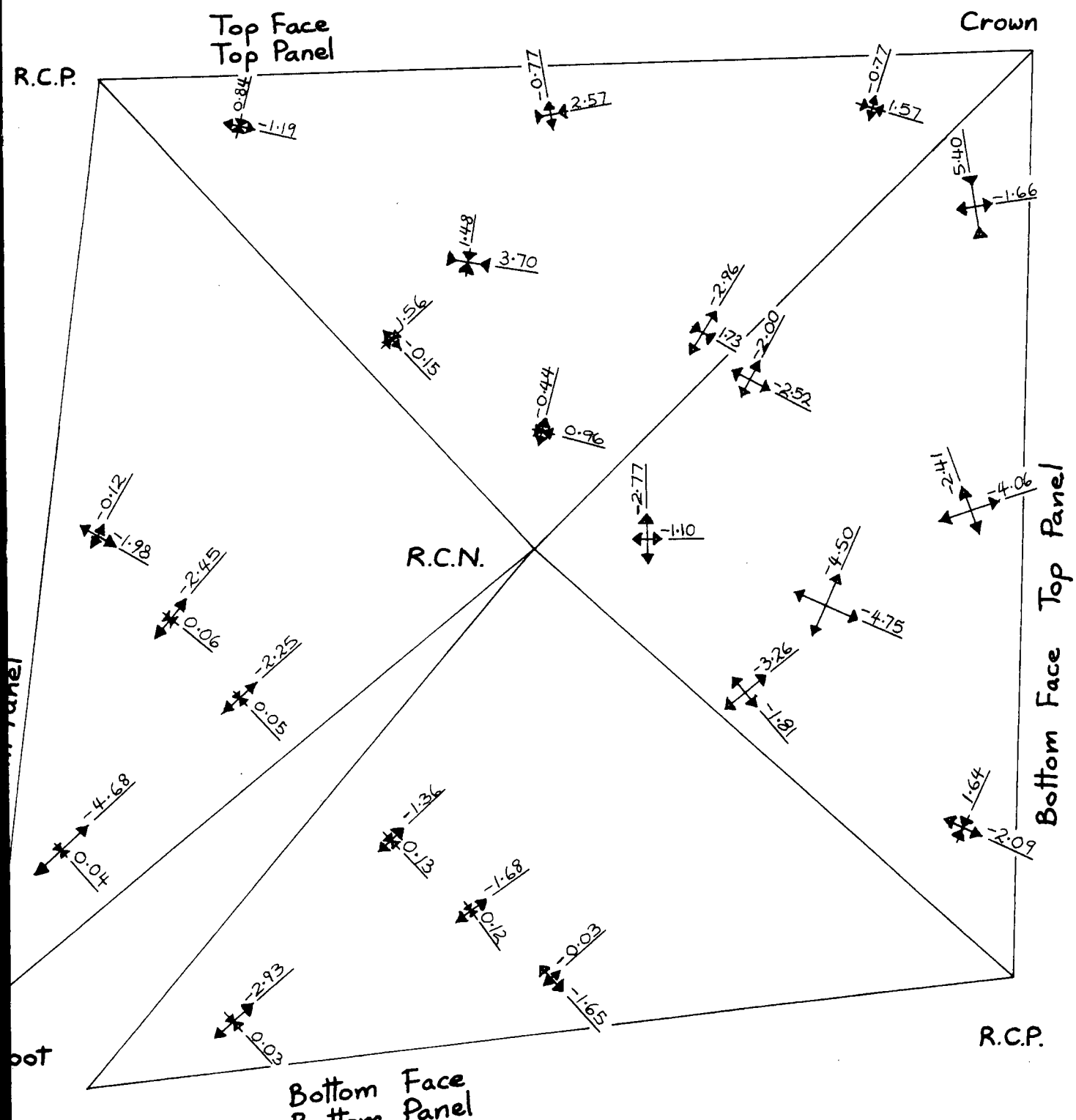

# Numerical Displacements and Forces in Edgebeams
## Load Series 3 Dome 4

FIG. 8.31.1
(1 OF 2)

# Numerical Displacements and Forces in Edgebeams
## Load Series 3 Dome 4



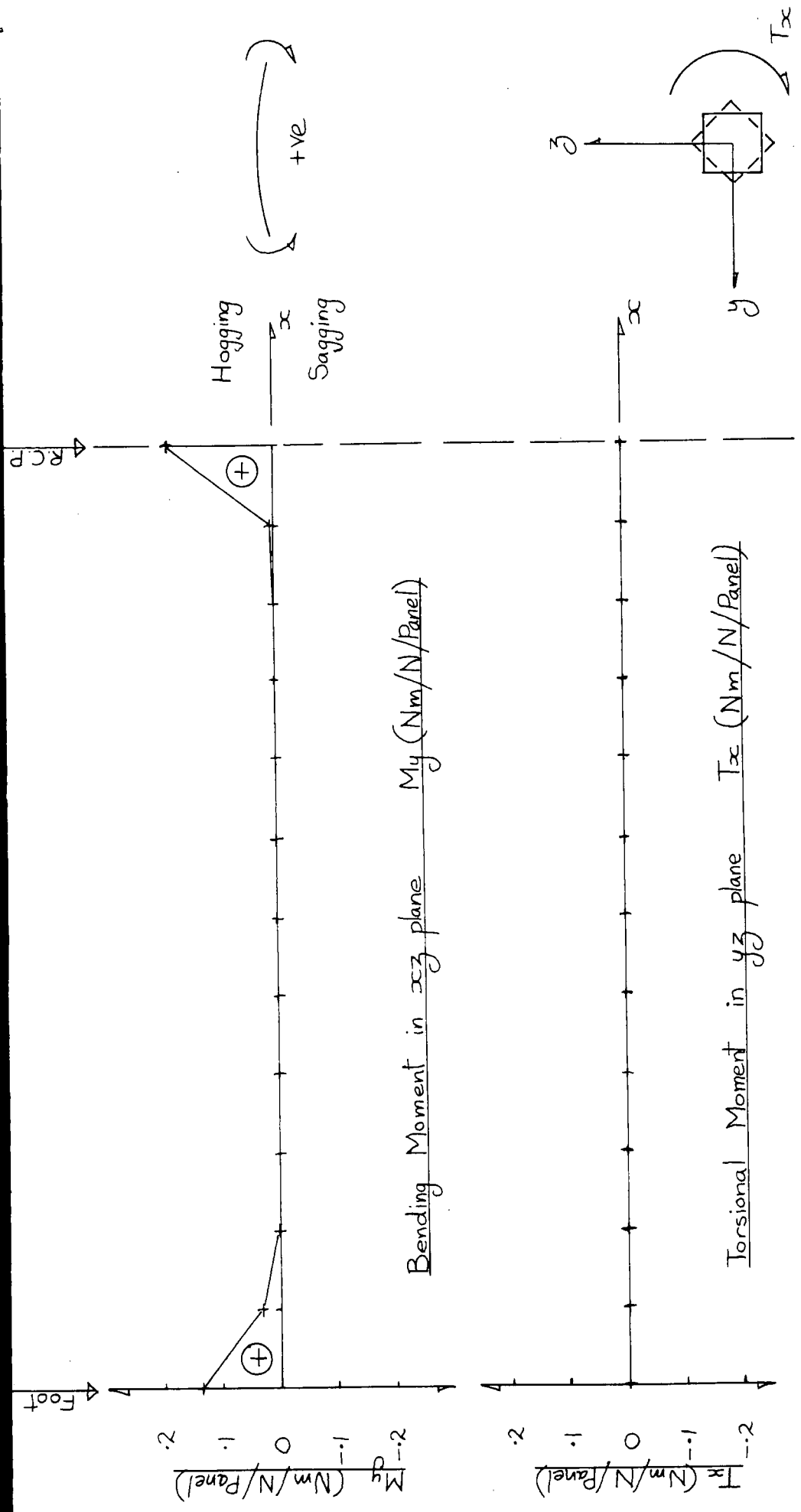

TABLE 8·1

Flexibility Influence Coefficients Dome 1
(Load Series 3)

+ve displacements and loads in towards centre of dome

| Displacement Point | Direction of Displacement | Experimental Flex. Infl. Coeff. mm x $10^{-3}$/N/Panel | Numerical Flex. Infl. Coeff. mm x $10^{-3}$/N/Panel | |
|---|---|---|---|---|
| | | | Unfactored Elastic Constants | Factored Elastic Constants |
| Load Point | Radial | 6·700 | 5·729 | 6·752 |
| Mid-point Valley joint | Radial | 6·205 | 5·825 | 6·340 |
| Crown | Radial | 2·185 | 0·529 | 0·728 |
| Rhomb Corner Projection | Vertical | 1·276 | 0·546 | 1·277 |
| | Horizontal | -0·276 | 0·013 | 0·179 |
| Rhomb Centre Node | Vertical | 2·720 | 0·231 | 0·584 |

TABLE 8.2

Flexibility Influence Coefficients Dome 2
(Load Series 3)

+ve displacements and loads in towards centre of dome

| Displacement Point | Direction of Displacement | Experimental Flex. Infl. Coeff. mm x $10^{-3}$/N/Panel | Numerical Flex. Infl. Coeff. mm x $10^{-3}$/N/Panel | |
|---|---|---|---|---|
| | | | Unfactored Elastic Constants | Factored Elastic Constants |
| Load Point | Radial | 8·560 | 6·203 | 8·559 |
| Mid-point Valley Joint | Radial | 7·030 | 4·813 | 7·106 |
| Crown | Radial | 4·140 | 1·748 | 3·147 |
| Rhomb Corner Projection | Vertical | 4·410 | 1·199 | 4·538 |
| | Horizontal | -0·200 | -0·072 | 0·279 |
| Rhomb Centre Node | Vertical | 3·060 | 1·084 | 3·226 |
| Centroid Bottom Panel | Normal to Panel | 2·250 | 0·712 | 2·563 |

TABLE 8.3

Flexibility Influence Coefficients Dome 3
(Load Series 3)

+ve displacements and loads in towards centre of dome

| Displacement Point | Direction of Displacement | Experimental Flex. Infl. Coeff. mm x $10^{-3}$/N/Panel | Numerical Flex. Infl. Coeff. mm x $10^{-3}$/N/Panel | |
|---|---|---|---|---|
| | | | Unfactored Elastic Constants | Factored Elastic Constants |
| Load Point | Radial | 14·500 | 7·522 | 13·636 |
| Mid-point Valley Joint | Radial | 13·180 | 6·375 | 12·235 |
| Crown | Radial | 8·140 | 3·744 | 8·502 |
| Rhomb Corner Projection | Vertical | 11·900 | 1·734 | 8·833 |
| | Horizontal | 0·000 | -0·175 | 0·121 |
| Rhomb Centre Node | Vertical | 7·840 | 2·244 | 8·061 |
| Centroid Bottom Panel | Normal to Panel | 6·780 | 1·412 | 6·199 |

TABLE 8.4

Flexibility Influence Coefficients (Load Series 3) Dome 4

+ve displacements and loads in towards centre of dome

| Displacement Point | Direction of Displacement | Experimental Flex. Infl. Coeff. mm x $10^{-3}$/N/Panel | Numerical Flex. Infl. Coeff. mm x $10^{-3}$/N/Panel | |
|---|---|---|---|---|
| | | | Unfactored Elastic Constants | Factored Elastic Constants |
| Load Point 1A | Radial | 4·800 | 4·770 | 5·316 |
| 1B | | 5·890 | 5·839 | 6·526 |
| 1C | | 6·870 | 5·471 | 5·964 |
| Average | | 5·850 | 5·360 | 5·935 |
| Mid-point Valley Joint | Radial | 4·310 | 3·827 | 4·419 |
| Crown | Radial | 1·670 | 0·622 | 0·868 |
| Rhomb Corner Projection | Vertical | 1·050 | 0·626 | 1·534 |
| | Horizontal | 0·000 | 0·000 | 0·182 |
| Rhomb Centre Node | Vertical | 1·000 | 0·368 | 0·821 |
| Mid-point Top Long. Ridge | Radial | 2·490 | 0·686 | 1·015 |
| Mid-point Bottom Long. Ridge | Radial | 0·550 | 0·604 | 0·940 |
| Mid-point Transverse Ridge | Radial | 0·820 | 0·318 | 1·134 |
| Centroid Bottom Panel | Normal to Panel | 0·450 | 0·202 | 0·531 |
| Mid-point Edgebeam | Normal to Panel | 0·090 | 0·272 | 0·687 |

TABLE 8.5

Factors Applied to Elastic Constants in Numerical Models Domes 1 to 4

| Element | Property | Multiplication Factor | | | |
|---|---|---|---|---|---|
| | | Dome 1 | Dome 2 | Dome 3 | Dome 4 |
| Top Panel Faces | Elastic Modulus | 0·85 | 0·85 | 0·75 | 0·85 |
| | Shear Modulus | 0·85 | 0·85 | 0·75 | 0·85 |
| Bottom Panel Faces | Elastic Modulus | 0·35 | 0·20 | 0·15 | 0·35 |
| | Shear Modulus | 0·35 | 0·20 | 0·15 | 0·35 |
| Edgebeams | Elastic Modulus | 0·40 | 0·20 | 0·15 | 0·35 |
| | Shear Modulus | 1·00 | 1·00 | 1·00 | 1·00 |
| Core Material | Shear Modulus | 1·00 | 1·00 | 1·00 | 1·00 |

## 9. DESIGN CONSIDERATIONS

The purpose of this section is not to provide a method for designing sixteen faced four segment polyhedral domes of the type tested by the author, but to outline the factors which must be taken into consideration when designing domes of this type.

Polyhedral sandwich domes are suitable for a mass production process in which the segments are manufactured in a factory and transported to site where they are combined to form the complete structure. The reason for developing these domes was to produce a cheap efficient type of roof structure, (12). It is therefore essential that as little non-standard material and equipment as possible is used during the manufacture, transportation and erection processes.

The dimensions of the standard size sheets of materials from which sandwich boards can be constructed limits the size of the individual panels and therefore the dimensions of the completed structure. Larger domes could be constructed if individual panels were made from more than one piece of sandwich board. A more attractive solution to the problem would be to use G.R.P. as a facing material, (8). A complete segment face could be manufactured in one piece. An additional improvement would result if a method could be found for injecting a foamed plastic core between the two faces of the sandwich. It would then be possible to produce relatively large domes, provided that the self-weight of the structure did not become excessive, as neither the core nor the faces would be limited to those sizes which were commercially available.

Already available?

Transportation and handling provide a constraint upon the size of the individual components of a dome.

It is envisaged that practical sizes for full size polyhedral sandwich domes would have base radii of between 3 m and 5 m.

In choosing a suitable geometry a designer must consider the effect of variation in the ratio h/r upon the overall stiffness of the dome and the stability of the ridges, (Section 7.6). Both these factors can be improved by moving the R.C.Ns. radially outward away from the centre of the dome, and/or moving the R.C.Ps. radially inward towards the centre of the dome. As a result the dome would no longer be spherically conformant. This has the effect of increasing the relative inclinations of the faces of the polyhedral dome .

Domes of this type should be designed to withstand the loading conditions specified in CP3: Chapter V : Parts I and II. Dead loads can be calculated from the known weights of the constituent materials used in the construction of the domes. The imposed loading conditions which must be designed for are snow loading, and a concentrated weight, (CP3 : Chapter V : Part I). Wind loading will be predominantly suctional, the direction, magnitude and distribution of the loading will depend upon the geometry of the dome, (CP3 : Chapter V : Part II). For a spherically conformant dome the wind loading will be approximately symmetrical (11). The design loads can be calculated using the procedure outlined in CP110 : Part 1 : 1972 : Section 2.3. The designer must design for both ultimate and serviceability limit states.

In addition to the above loads the designer must consider loads induced during the manufacture, transportation and erection of the dome.

When choosing the type and thickness of the sandwich materials the designer must consider the stresses and displacements caused by each of the above mentioned load conditions.

The panel core and face materials must be checked to ensure that the stresses at the design loads do not exceed their ultimate stresses. For dead and imposed loading conditions, panel shortening and time

dependent effects must be included, (Sections 5.0, 7.5 and 8.0). When calculating the effects due to a concentrated weight the designer should ensure that the load will not punch through the panel or cause permanent deformation of the core. Membrane action due to wind loading will be mainly tensile, and it is likely that it will be necessary to include for the in-plane deformation in the panels when calculating stresses and displacements induced by these loads, (Section 8.0). The panels must be checked against instability due to symmetric or antisymmetric wrinkling in the faces. Overall buckling of the panels is unlikely to be a critical design consideration under normal service loading (13). It is probable that the critical condition will be the 'displacement serviceability limit state'.

The adequacy of the adhesive must be checked against shearing and against failure due to tension normal to the plane of the panels caused by wrinkling, (Section 7.0,1).

The type and thicknesses of the core and faces must be balanced so as to achieve the most economic section for the panels (1). By using a thick core the faces need only be relatively thin, as a result of the increased resistance to transverse shear deformation and the reduction in the bending stesses in the faces.

For structures of this type it is possible that the resistance of the faces to abrasion will be the governing consideration in choosing the thickness of the panel faces, and that heat and sound insulation requirements will govern the core thickness.

The joints of a polyhedral sandwich dome must be able to resist the tensile and bending actions in the faces caused by the design loads. Joints with included angles in excess of $165^{o}$ should include some method for preventing core penetration, (Section 4.4). The valley joints should

be of a form which will facilitate site erection of the domes, (Section 4.2).

It was shown in Section 8.0 that a finite element method using an element such as the 'Parton Quadratic Shape Function Sandwich Element' is suitable for use in the design of polyhedral sandwich domes. When designing domes of this type it is important that the constraint conditions are accurately represented in the numerical model, and that any flexibility at the constraints is included in that model, (Section 7.2.1).

## 10. CONCLUSIONS

When the work described in this thesis was begun four objectives were defined, (Section 1.0). The remarks which follow are related to the requirements of those objectives.

The first objective was concerned with the effects upon the structural behaviour of sixteen faced four segment spherically conformant sandwich domes, due to changes in the ratio h/r.

It was found by the author that there was a non-linear relationship between the elastic deformation of the polyhedral sandwich domes which he tested and the ratio h/r, (Figs. 6.3 and 7.19). He also found that as the ratio h/r was reduced there was a reduction in local deformation around load points and an increase in the overall translation, (rigid body displacements), of the panels of the domes.

It was known from the work of other workers at the University of Durham, notably Parton (12) and Manos (10), that non-linear time dependent deformation was significant in polyhedral sandwich shells of the type tested by the author. As a result of the work described in this thresis two further significant non-linear effects on the structural behaviour of polyhedral sandwich domes , constructed from the type of sandwich materials used by the author, subjected to 'downward' loads, were identified as: non-linear variation in the flexibility of the dome with variation in the ratio h/r; and non-linear effects due to in-plane deformation in the panels. The extent of in-place deformation in the panels of polyhedral sandwich domes subjected to 'downward' loads was dependent upon the magnitude of the membrane action in the panel faces, and was consequently proportional to the ratio h/r, (Sections 7.0 and 8.0).

There are therefore a total of three significant non-linear effects upon the structural behaviour of polyhedral sandwich domes of the type tested by the author. These non-linear effects are discussed fully in Sections 5.0, 7.0 and 8.0.

The second objective was to compare the experimental elastic behaviour of the polyhedral sandwich domes tested by the author with that predicted by a numerical model using a finite element technique, and hence determine the extent to which that particular numerical model could be relied upon to predict the behaviour of those domes.

The numerical analyses for domes 1 to 4 were performed using the 'Parton Quadratic Shape Function Sandwich Element', (12). It was found that although the numerical model used gave an acceptable approximation for design purposes there was some room for improvement, particularly in the simulation of the stress situation in the panel faces. The results of the numerical analyses for domes 1 to 4 have been discussed fully in Section 8.0, which contains some suggestions for improvements to the numerical model.

The third objective was to determine the load carrying capacity, and modes of failure for each of the polyhedral domes tested by the author.

All the domes tested by the author failed as a result of a local failure, (Section 7.0). For domes 1 and 4, the ridges of which had the greatest geometric stability, the ultimate load depended upon the ultimate strength of the sandwich materials. For domes 2 and 3, the ridges of which had a relatively low geometric stability, the ultimate load depended upon the geometric stiffness of the dome. Section 7.0 gives a detailed account of the modes of failure for each of the domes tested by the author.

The fourth objective was to form some definite conclusions concerning the choice of an optimum ratio h/r.

Three factors effect the choice of an optimum ratio h/r for a spherically conformant polyhedral sandwich dome; the stresses induced in the dome materials at the design loads; the flexibility of the dome under design load conditions; and the stability of the ridges under design load conditions.

The first two of the above factors are inter-dependent to a great extent. In the design of polyhedral sandwich domes account should be taken of the interplay of these factors when selecting the geometry of the dome and the types and thicknesses of the face and core materials.

It has been shown in Section 8.0 that for a given load intensity the change in the general level of the stresses in the faces of a dome are not large if ratio h/r is varied. It is unlikely that the stress situation in the dome materials will be critical at the design loads, (Section 9.0).

Figs. 6.3 and 7.19 show that, when the ratio h/r was reduced below 0.3, the elastic displacements became excessive. It is therefore recommended that ratio h/r should not be reduced below 0.3.

The author found that,for the polyhedral sandwich domes which he tested, the ridges of the domes for which ratio $h/r < 0.5$ were relatively unstable. It is therefore recommended that the ridges should not have an included angle in excess of $157^{\circ}$, (dome 4: $h/r = 0.5$; included angle at the longitudinal ridge $156.53^{\circ}$), (Section 4.3).

It is unlikely that a spherically conformant polyhedral sandwich dome will produce the most structurally efficient sixteen faced four segment polyhedral sandwich dome. The most structurally efficient sixteen faced four segment sandwich dome would probably be a non-spherically conformant dome, the R.C.Ns. of which had been moved radially outward

away from the centre of the dome, and/or the R.C.Ps. of which had been moved radially inward towards the centre of the dome, (Section 9.0, 12). This would have the effect of increasing the relative inclinations of the dome faces, thus increasing the geometric stability of the ridges and increasing the geometric stiffness of the dome.

It can be concluded that the work described in this thesis has given an improved understanding of the elastic behaviour and ultimate failure of sixteen faced four segment spherically conformant polyhedral sandwich domes.

## BIBLIOGRAPHY


(1) Allen, H.G., "Analysis and design of structural sandwich panels," Pergamon 1969

(2) Bettess, P., "Analysis of polyhedral domed structures composed of flat plates of sandwich material ," Ph.D. Thesis, University of Durham, 1971

(3) Elliott, D.J., "The structural properties of flat sandwich panels", M.Sc. Thesis, University of Durham, 1970

(4) Finnie, I., and Heller, R. "Creep of Engineering Materials", McGraw-Hill, 1959

(5) Gibson, J.E., "Linear elastic theory of thin shells", Pergamon 1965

"The design of shell roofs", Spon,1968

(6) Holand, I., and Bell, K., "Finite element methods in stress analysis", Tapir, 1970

(7) Irons, B.M., "A frontal solution program for finite element analysis", International Journal for Numerical Methods in Engineering, Vol.2, 1970

(8) Leggatt, A.J., "G.R.P. in Buildings", The Structural Engineer, December 1976, No.12, Volume 54

(9) Madeiros, B., "Construction, testing and analysis of a geodesic dome", Final year honours project, University of Durham, 1976

(10) Manos, G.C., "Analysis of polyhedral domed sandwich structures", Ph.D. Thesis, University of Durham, 1975

(11) Newberry, C.W., and Eaton, K.J., "Wind loading handbook", H.M.S.O., 1974

(12) Parton, G.M., "The structural behaviour of polyhedral sandwich shells", Ph.D. Thesis, University of Durham, 1974

(13) Plantema, F.J., "Sandwich construction", Wiley, 1966

(14) Pryor, S.J., "A destructive test on a polyhedral dome", Final year honours project, University of Durham, 1976

# APPENDIX I

## Subroutine BSTIFF

### I.i Introduction

Subroutine BSTIFF can be used to incorporate beam elements at the edges of any of the sandwich panel elements in a finite element analysis which is performed using the 'Parton Quadratic Shape Function sandwich Element' (12). BSTIFF is called from the main subroutine STIFF which evaluates the stiffness matrix [STUCK] and the stress matrix [STICK] for the individual sandwich panel elements, (Section 8.0, 7). The sandwich panel element and beam element stiffness matrices are combined, by adding the stiffness contributions from the beam element to those of the sandwich panel element, to form a composite stiffness matrix for the sandwich panel element with stiffened edges.

### I.ii Beam Element

The beam element has five degrees of freedom; u, v, w, $\Theta y$ and $\Theta x$, (Fig. I.1). The orthogonal axes x and y lie in the plane of the panel, and the z axis is perpendicular to the plane of the panel. It is assumed that the sandwich panel provides infinite stiffness against bending about the z axis. Shear deformation in the beam is assumed to be negligible.

The stiffness matrix for the beam element, [k], is shown in Fig. I.ii, and was derived using cubic displacement shape functions. This stiffness matrix is in terms of the beam's local coordinates and degrees of freedom, and must therefore be transformed so that it is in terms of the sandwich panel element's local coordinates and degrees of freedom, before the stiffness matrices of the sandwich panel element and beam element can be combined. The beam element degrees of freedom are transformed to correspond to those

of the sandwich panel element using the following relationships:—

| Beam Element | | Sandwich Panel Element |
|---|---|---|
| $P_x$ | = | $P_{xTF} + P_{xBF}$ |
| $P_y$ | = | $P_{yTF} + P_{yBF}$ |
| $P_z$ | = | $P_z$ |
| $T_x$ | = | $P_{yBF} \times d$ |
| $M_y$ | = | $- P_{xBF} \times d$ |
| $\theta_x$ | = | $- \frac{V_{TF} - V_{BF}}{d}$ |
| $\theta_y$ | = | $\frac{U_{TF} - U_{BF}}{d}$ |

where TF = Top Face Node of the Sandwich Panel Element

BF = Bottom Face Node of the Sandwich Panel Element

d = Distance between Top and Bottom Face Nodes of the Sandwich Panel Element (i.e. core thickness + one face thickness).

The modified stiffness matrix for the beam element, $[K]$, for which the degrees of freedom correspond to those of the sandwich panel element, is shown in Fig. I.iii. The transformation matrix, $[T]$, which is used when transforming the beam elements local coordinates so that they correspond to those of the sandwich panel element, is shown in Fig. I.iv.

Once the beam element's stiffness matrix has been transformed, so that the stiffness matrices of the beam and sandwich panel elements are compatible, the stiffness contributions from the beam can be

posted directly into the appropriate locations in the stiffness matrix for the sandwich panel element [STUCK], to form the composite stiffness matrix for the sandwich panel element with stiffened edges.

Any transformations of the sandwich panel element, e.g. at plate boundaries are performed after the beam stiffness contributions have been added to the sandwich panel element stiffness matrix [STUCK].

I.iii Input (How to use BSTIFF)

All the information required to calculate the beam element stiffness and transformation matrices is either input in the form of 'stiffness sets', or derived from the data for the sandwich panel element which is to be stiffened. The 'stiffness sets' are read in by the main solution program, (Section 8.0, 2,7,12). INFO(18) is the information string which is specified in the data for each individual element in the finite element analysis.

The following information is input in the form of 'stiffness sets':-

| Stiffness Set (IN) | Beam Properties | |
|---|---|---|
| IN = INFO (15) | | |
| STIF(1,IN) = ABEAM | Area | ($m^2$) |
| STIF(2,IN) = EBEAM | Elastic Modulus | ($N/m^2$) |
| STIF(3,IN) = GBEAM | Shear Modulus | ($N/m^2$) |
| STIF(4,IN) = SMA | Second Moment of Area | ($m^4$) |
| STIF(5,IN) = J | Polar Second Moment of Area | ($m^4$) |
| Stiffness Set (IT) | Transformation Matrix Data | |
| IT = INFO(16) | | |
| STIF(1,IT) = Sin $\Theta$ | $\Theta$ = Transformation Angle | |
| STIF(2,IT) = Cos $\Theta$ | | |

The following information is derived from the panel element data:-

| | | |
|---|---|---|
| AD | Sandwich Thickness | (m) |
| F | Face Thickness | (m) |
| L | Beam Element Length | (m) |

All that is necessary to set BSTIFF into action, is to place, IN in location INFO(15), IT in location INFO(16), and 142, or 253, or 163 in location INFO(17), in the data for the element that is to be stiffened.

where: INFO(15) indicates the 'stiffness set' number

INFO(16) indicates the 'transformation set' number

INFO(17) indicates the element edge which is to be stiffened, where the numbers correspond to the node numbers at that edge, (Fig. I.i)

# Degrees of Freedom & Local Coordinate Systems

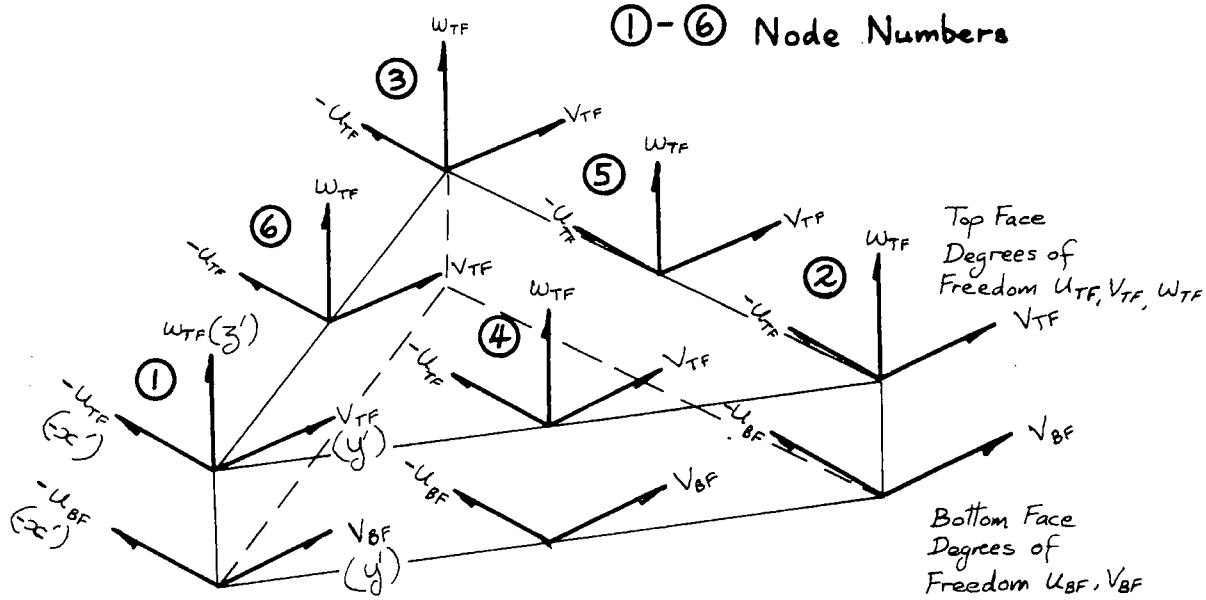


Sandwich Panel Element

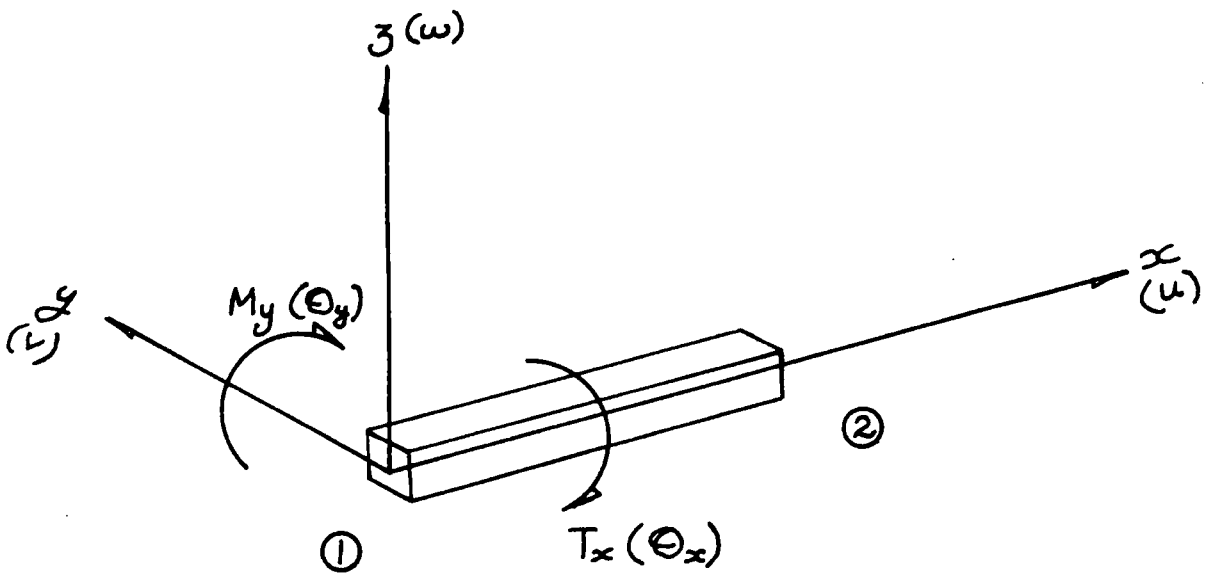


Beam Element

## Stiffness Matrix for Beam Element [k]
## (beam element's local coordinates and degrees of freedom)

$$
\begin{bmatrix} P_{x1} \\ P_{y1} \\ P_{z1} \\ M_{y1} \\ T_{x1} \\ P_{x2} \\ P_{y2} \\ P_{z2} \\ M_{y2} \\ T_{x2} \end{bmatrix} =
\begin{bmatrix}
\frac{EA}{L} & & & & & -\frac{EA}{L} & & & & \\
 & & & & & & & & & \\
 & & \frac{12EI}{L^3} & \frac{6EI}{L^2} & & & & -\frac{12EI}{L^3} & -\frac{6EI}{L^2} & \\
 & & \frac{6EI}{L^2} & \frac{4EI}{L} & & & & -\frac{6EI}{L^2} & -\frac{2EI}{L} & \\
 & & & & \frac{GJ}{L} & & & & & -\frac{GJ}{L} \\
-\frac{EA}{L} & & & & & \frac{EA}{L} & & & & \\
 & & & & & & & & & \\
 & & -\frac{12EI}{L^3} & -\frac{6EI}{L^2} & & & & \frac{12EI}{L^3} & \frac{6EI}{L^2} & \\
 & & -\frac{6EI}{L^2} & -\frac{2EI}{L} & & & & \frac{6EI}{L^2} & \frac{4EI}{L} & \\
 & & & & -\frac{GJ}{L} & & & & & \frac{GJ}{L}
\end{bmatrix}
\begin{bmatrix} u_1 \\ v_1 \\ w_1 \\ \theta_{y1} \\ \theta_{x1} \\ u_2 \\ v_2 \\ w_2 \\ \theta_{y2} \\ \theta_{x2} \end{bmatrix}
$$

## Stiffness Matrix for Beam Element [K]
(beam element's local coordinates, panel element's degrees of freedom)

| | | | | | | | | | | | |
|---|---|---|---|---|---|---|---|---|---|---|---|
| $P_{x1TF}$ | | A | | -B | -2C | | -D | | B | C | | $u_{1TF}$ |
| $P_{y1TF}$ | | | -E | | | E | | E | | | -E | $v_{1TF}$ |
| $P_{z1TF}$ | | -B | | F | B | | B | | -F | -B | | $w_{1TF}$ |
| $P_{x1BF}$ | | -2C | | B | 2C | | C | | -B | -C | | $u_{1BF}$ |
| $P_{y1BF}$ | = | | E | | | -E | | -E | | | E | $v_{1BF}$ |
| $P_{x2TF}$ | | -D | | B | C | | A | | -B | -2C | | $u_{2TF}$ |
| $P_{y2TF}$ | | | E | | | -E | | -E | | | E | $v_{2TF}$ |
| $P_{z2TF}$ | | B | | -F | -B | | -B | | F | B | | $w_{2TF}$ |
| $P_{x2BF}$ | | C | | -B | -C | | -2C | | B | 2C | | $u_{2BF}$ |
| $P_{y2BF}$ | | | -E | | | E | | E | | | -E | $v_{2BF}$ |

where: 1TF = Node 1 Top Face  1BF = Node 1 Bottom Face
2TF = Node 2 Top Face  2BF = Node 2 Bottom Face

$$A = \frac{EA}{L} + \frac{4EI}{d^2 L}$$

$$B = -\frac{6EI}{dL^2}$$

$$C = \frac{2EI}{d^2 L}$$

$$D = \frac{EA}{L} + \frac{2EI}{d^2 L}$$

$$E = -\frac{GJ}{d^2 L}$$

$$F = \frac{12EI}{L^3}$$

## Transformation from beam element's local coordinate system to panel element's local coordinate system

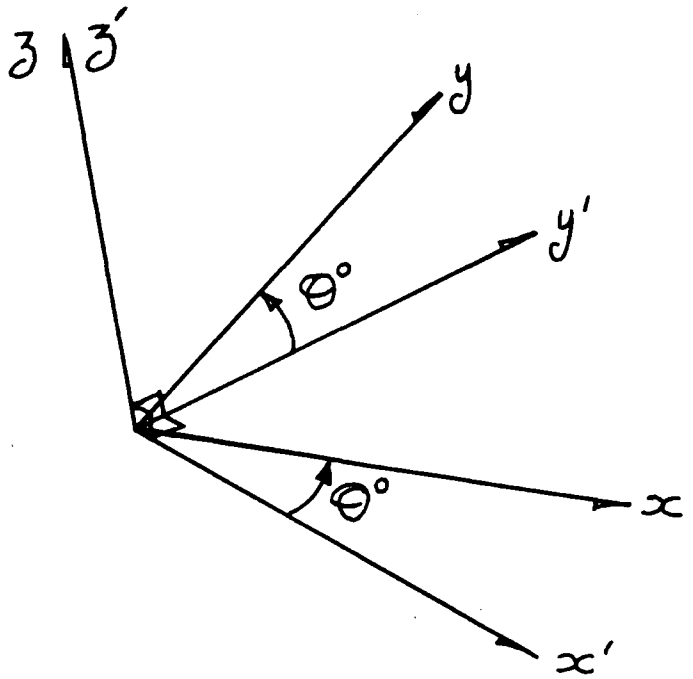


$x'y'z'$ panel element local coordinates
$x\ y\ z$ beam element local coordinates
$\theta^{\circ}$ transformation angle

## Transformation Matrix [T]

$$\{P'\} = [T] \times \{P\}$$

$$\begin{Bmatrix} P'_{x_{ITF}} \\ P'_{y_{ITF}} \\ P'_{z_{ITF}} \\ P'_{x_{IBF}} \\ P'_{y_{IBF}} \end{Bmatrix} = \begin{bmatrix} \cos\theta & -\sin\theta & & & \\ \sin\theta & \cos\theta & & & \\ & & 1 & & \\ & & & \cos\theta & -\sin\theta \\ & & & \sin\theta & \cos\theta \end{bmatrix} \begin{Bmatrix} P_{x_{ITF}} \\ P_{y_{ITF}} \\ P_{z_{ITF}} \\ P_{x_{IBF}} \\ P_{y_{IBF}} \end{Bmatrix}$$

where: $[K'] = [T][K][T]^T$

## I.iv Listing Subroutine STIFF

Parton Quadratic Shape Function Sandwich Element

with

Edge Stiffening Option

```
C     INCLUDING PLATE WINGING EDGE CONNECTION
C
      SUBROUTINE STIFF
      IMPLICIT REAL*8 (A-H,O-Z)
      COMMON / STOR / BLINT(2,36,36),BLUNT(2,36,36)
      COMMON / BEND / D(9),B(90)
      COMMON / SIZE / ALPHA,AA,AB,AD,F,C,FACE(144),COR(900)
      COMMON / SHAPE / W(3,6),E(3),AI(3,3),POINT(3,4),BB(36)
      COMMON / PROP / E1,E2,PR1,PR2,GF,GC
      COMMON / STI / X(3,20),YOUNG(12),STUCK(36,36),STICK(36,36),
     1FORCE(36),INFO(20),XY(3,3)
      COMMON / THREE / ELPA(1000) ,  EL(2000),FL(1000),VALUE(20),
     1 ELCOP(3,20),STIF(12,20)
C
C
C   THE ELEMENT DIMENSIONAL CHARACTERISTICS ARE AS:-
C
      DIMENSION SPY(30,30)
      DIMENSION PAT(3,4),XX(3,3),DIRCOS(3,3)
      KWEL = 1
  510 FORMAT(1HO,5X,'STAGE  ',I3,' COMPLETE')
  530 FORMAT(1H1,5X,'STIFFNESS MATRIX,  ELEMENT NO.   ',I3)
  531 FORMAT(1HO,(10D12.4/10D12.4/10D12.4),/)
  532 FORMAT(1H1,5X,'STRESS MATRIX, ELEMENT NO.    ',I3)
      KLOCK = INFO(18)
      IF((KLOCK.LT.10).AND.(KLOCK.NE.0)) GO TO 4000
      DO 3970 I=1,3
      DO 3970 J=1,3
 3970 XX(I,J) = X(J,I)
C
      CALL DIRECT(XX,DIRCOS)
C       CALCULATE COORDINATES IN THE LOCAL SYSTEM
      DO 680 I=1,3
      DO 680 J=1,3
      SUM = 0.
      DO 682 K=1,3
  682 SUM = SUM + DIRCOS(K,I) * XX(J,K)
  680 XY(J,I) = SUM
C
C          OPTIONAL DIAGNOSTIC WRITE STATEMENTS
C
      IF(INFO(17).EQ.999) WRITE(6,533) ((XY(I,J),J=1,3),I=1,3)
      IF(INFO(17).EQ.999) WRITE(6,533) ((DIRCOS(I,J),J=1,3),I=1,3)
  533 FORMAT(1HO,5X,3E15.5)
C
      AD = X(1,4)
      AB = 1.
      F = X(2,4)
      C = X(3,4)
C
C
      E1 = YOUNG(1)
      E2 = YOUNG(2)
      PR1 = YOUNG(3)
      PR2 = YOUNG(4)
      GF  = YOUNG(5)
      GC = YOUNG(6)
C
```

```
      IG= I + 1
      IF(IG.GT.3) IG = IG - 3
      IK = I + 2
      IF(IK.GT.3) IK = IK - 3
      A1(I,1)=(XY(IG,1)*XY(IK,2)-XY(IK,1)*XY(IG,2))
      AA = AA + A1(I,1)
      A1(I,2)=XY(IG,2)-XY(IK,2)
      A1(I,3)=XY(IK,1)-XY(IG,1)
 3540 CONTINUE
      DO 3550 I=1,3
      DO 3550 J=1,3
 3550 A1(I,J) = A1(I,J)/AA
      IF(INFO(17).EQ.999) WRITE(6,533)((A1(I,J),J=1,3),I=1,3)
C
      IF(INFO(17).EQ.999) WRITE(6,534) AA
  534 FORMAT(1HO,5X,'TWICE THE AREA OF THIS ELEMENT IS .... .. ',D12.3)
C
      IF(INFO(17).EQ.999) WRITE(6,510) KWEL
      KWEL=KWEL + 1
      CALL GADCOR
      IF(INFO(17).EQ.999) WRITE(6,510) KWEL
      KWEL = KWEL + 1
      CALL GADFAC
      IF(INFO(17).EQ.999) WRITE(6,510) KWEL
      KWEL = KWEL + 1
      CALL POST
      IF(INFO(17).EQ.999) WRITE(6,510) KWEL
      KWEL = KWEL + 1
C
C    OPTIONAL STORAGE AND RETEIVAL OF PAST STIFFNESS MATRICES
C
      IF(KLOCK.EQ.0) GO TO 405
      KLOCK = KLOCK - 10
      DO 401 I=1,30
      DO 401 J=1,30
  401 BLINT(KLOCK,I,J) = STUCK(I,J)
      DO 402 I=1,6
      DO 402 J=1,30
  402 BLINT(KLOCK,I,J) = STICK(I,J)
      GO TO 405
 4000 CONTINUE
      DO 403 I=1,30
      DO 403 J=1,30
  403 STUCK(I,J) = BLINT(KLOCK,I,J)
      DO 404 I=1,6
      DO 404 J=1,30
  404 STICK(I,J) = BLINT(KLOCK,I,J)
  405 CONTINUE
      IF(INFO(17).EQ.142) GOTO 110
      IF(INFO(17).EQ.253) GOTO 110
      IF(INFO(17).EQ.163) GOTO 110
      GOTO 113
  110 WRITE(6,533) ((CIRCOS(I,J),J=1,3),I=1,3)
C
      CALL PSTIFF
C
C    OPTIONAL LOCAL TRANSFORMATIONS AT PLATE INTERSECTIONS
  113 IF(INFO(1).EQ.0) GOTO 653
```

```
      652 SPY(IT,IS) = 0.
      654 SPY(IT,IT) = 1.
          KINK = INFO(1) + 1
          DO 651 K=2,KINK
          L = INFO(K)
          KK = (L-1) * 5
          DO 658 II=1,3
          DO 658 JJ=1,3
          SPY(KK+II,KK+JJ) = DIRCOS(JJ,II)
      658 CONTINUE
      651 CONTINUE
          CALL TIMES(STUCK,SPY,STUCK,36,36,30,30,36,36,30,30,30,0)
          CALL TIMES(STICK,SPY,STICK,36,36,30,30,36,36,30,30,30,0)
          CALL TIMES(SPY,STUCK,STUCK,30,30,36,36,36,36,30,30,30,1)
      653 CONTINUE
          IF(INFO(17).EQ.999) WRITE(6,510) KWEL
          IF(INFO(17).EQ.99) WRITE(6,510) KWEL
          IF(INFO(17).EQ.99) GOTO 601
          IF(INFO(17)-999) 602,601,602
      601 WRITE(6,530) INFO(20)
          WRITE(6,531) ((STUCK(I,J),J=1,30),I=1,30)
          WRITE(6,532) INFO(20)
          WRITE(6,531) ((STICK(I,J),J=1,30),I=1,6)
      602 CONTINUE
          RETURN
          END
          SUBROUTINE QADCOR
          IMPLICIT REAL*8 (A-H,O-Z)
          COMMON / BEND / D(9),B(90)
          COMMON / SIZE / ALPHA,AA,AB,AD,F,G,FACE(144),COR(900)
          COMMON / SHAPE / W(3,6),E(3),A1(3,3),PCINT(3,4),BB(36)
          COMMON / PROP / E1,E2,PR1,PR2,GF,GC
          COMMON / STI / X(3,20),YOUNG(12),STUCK(36,36),STICK(36,36),
         1FORCE(36),INFO(20)
          DIMENSION ED(2)
          DATA ED/0.211325,0.788675/
      504 FORMAT(1H0,5X,3F10.4)
          DO 2001 I=1,90
     2001 B(I) = 0.
C
      501 FORMAT(1H0,15I5)
C
          DO 200 I=1,900
      200 COR(I) = 0.
          DO 2 JJJ=1,3
          DO 3 I=1,3
        3 B(I) = PCINT(I,JJJ)
          CALL SHFR
          DO 4 IZ=1,2
          EM = ED(IZ)
          J=1
          N1 = 1
          N2 = 76
          DO 1 I=N1,N2,15
          B(I) = -W(1,J)/AD
          B(I+4) = B(I)
          B(I+9) = -B(I)
          B(I+13) = -B(I)
```

```
      E(I+5) = W(2,J)*(1.-EM)
      E(I+14) = W(2,J)*EM
      E(I+6) = W(2,J)
      E(I+7) = W(3,J)
      J=J+1
    1 CONTINUE
      DO 60 K=1,30
      KX = K*30 - 30
      DO 60 J=1,30
   10 IR = J + KX
      DO 60 I=1,3
      IA = 3*(J-1) + I
      IB = 3*(K-1) + I
   60 CCR(IR) = CCR(IR) + B(IA)*B(IB)*GC*AA*AB*AD/12.
    4 CONTINUE
    2 CONTINUE
  502 FORMAT(1H0,10D12.4)
  503 FORMAT(1H0,10F10.4)
  510 FORMAT(1H0,5X,'QUADRATIC CORE ELEMENT COMPLETE')
      WRITE(6,510)
      RETURN
      END
      SUBROUTINE SHER
      IMPLICIT REAL*8 (A-H,O-Z)
      COMMON / STI / X(3,20),YOUNG(12),STUCK(36,36),STICK(36,36),
     1FORCE(36),INFO(20)
      COMMON / SIZE / ALPHA,AA,AB,AD,F,CE,FACE(144),CCR(900)
      COMMON / SHAPE / W(3,6),E(3),A1(3,3),PCINT(3,4),BB(36)
      DO 1 I=1,3
      J=I+1
      K=I + 2
      IF(J.GT.3)J=J-3
      IF(K.GT.3) K=K-3
      II=I+3
      EI = E(I)
      EJ = E(J)
      EK = E(K)
  500 FORMAT(1H0,10F10.4)
      W(1,I) = (EI+EI-1.)*EI
      W(1,II) = 4.*EI*EJ
      W(2,I) = (4.*EI - 1.)*A1(I,2)
      W(2,II) = 4.*EI*A1(J,2) + 4.*EJ*A1(I,2)
      W(3,I) = (4.*EI - 1.)*A1(I,3)
      W(3,II) = 4.*EI*A1(J,3) + 4.*EJ*A1(I,3)
    1 CONTINUE
      RETURN
      END
      SUBROUTINE GAUFAC
      IMPLICIT REAL*8 (A-H,O-Z)
      COMMON / BEND / B(90),B(90)
      COMMON / STI / X(3,20),YOUNG(12),STUCK(36,36),STICK(36,36),
     1FORCE(36),INFO(20)
      COMMON/ PROP / E1,E2,PR1,PR2,GF,GC
      COMMON / SIZE / ALPHA,AA,AB,AD,F,C,FACE(144),CCR(900)
      COMMON / SHAPE / W(3,6),E(3),A1(3,3),PCINT(3,4),BB(36)
      DIMENSION BA(144)
      DO 40 I=1,90
   40 B(I) = 0.
```

```
      1 FACE(II) = 0.
        DO 12 JJJ=1,9
     12 D(JJJ) = 0.
        DEN = 1.-PR1*PR2
        EM = E1/E2
        DENCC = E2/DEN
        D(1) = EM*DENCC
        D(4) = PR1*DENCC
        D(2) = D(4)
        D(5) = 1.*DENCC
        D(9) = GF
C
C    ELASTIC TRANSFORMATION
C
        IF(YOUNG(7).NE.0.0) CALL DTRN
C
        DO 2 I=1,4
        DO 3 J=1,3
      3 E(J) = ECINT(J,I)
        CALL SHFR
        J=1
        DO 10 II=1,21,6
        B(II) = W(2,J)
        B(II+2) = W(3,J)
        B(II+4) = W(3,J)
        B(II+5) = W(2,J)
        J=J+1
     10 CONTINUE
        DO 11 IJK=1,144
     11 BA(144) = 0.
        CALL DMPRD(D,B,BB,3,3,0,0,12)
        IF(I.EQ.4) GO TO 30
        CALL DTPRD(B,BB,BA,3,12,0,0,12)
        DO 4 IJ=1,144
      4 FACE(IJ) = FACE(IJ) + BA(IJ)
      2 CONTINUE
     30 CONTINUE
        DO 6 IJ=1,144
      6 FACE(IJ) = FACE(IJ)*F*AA*AB/6.
        WRITE(6,504)
    504 FORMAT(1H0,10X,'QUADRATIC SHAPE FUNCTION FACE ELEMENT MADE UP')
     20 RETURN
        END
        SUBROUTINE PCST
        IMPLICIT REAL*8 (A-H,O-Z)
        DIMENSION JOG(2,6)
        DATA JOG/1,1,3,6,5,11,7,16,9,21,11,26/
        COMMON / STI / X(3,20),YOUNG(12),STUCK(36,36),STICK(36,36),
       1FORCE(36),INFO(20)
        COMMON / SIZE / ALPHA,AA,AB,AD,F,C,FACE(144),CCR(900)
        COMMON / SHAPE / W(3,6),E(3),A1(3,3),POINT(3,4),BB(36)
C
        DO 100 I=1,36
        DO 100 J=1,36
        STICK(I,J) = 0.
    100 STUCK(I,J) = 0.
C
        DO 1 KING=1,6
```

```
      DO 1 KONG=1,6
      K3 = JOG(1,KONG)
      K4 = K3 + 1
C
      DO 2 I=K1,K2
      DO 2 J=K3,K4
      IJ = 12*(J-1) + I
      II = (JOG(2,KING) + 1) - (K2-I)
      JJ = (JOG(2,KONG) + 1) - (K4-J)
      IIJ = 30*(JJ-1) + II
      IJJ = IIJ + 93
      COR(IIJ) = COR(IIJ) + FACE(IJ)
      COR(IJJ) = COR(IJJ) + FACE(IJ)
    2 CONTINUE
C
C
    1 CONTINUE
      WRITE(6,504)
  504 FORMAT(1HC,10X,'COMPOUND ELEMENT ASSEMBLED')
      DO 600 I=1,30
      DO 600 J=1,30
      IJ = I + (J-1)*30
  600 STICK(I,J) = COR(IJ)
C
      DO 3 KING = 1,3
      DO 3 KONG = 1,6
      K3 = JOG(1,KONG)
      K4 = K3 + 1
C
      DO 4 J = K3,K4
      IJ = 3*(J-1) + KING
      JJ = (JOG(2,KONG)+1) - (K4-J)
      JJJ = JJ + 3
      STICK(KING,JJ) = STICK(KING,JJ) + BB(IJ)
    4 STICK(KING+3,JJJ) = STICK(KING+3,JJJ) + BB(IJ)
C
    3 CONTINUE
      RETURN
      END
      BLOCK DATA
      IMPLICIT REAL*8 (A-H,O-Z)
      COMMON / SHAPE / W(3,6),E(3),A1(3,3),POINT(3,4),BB(36)
      REAL*8 POINT/0.0,0.5,0.5,0.5,0.0,0.5,0.5,0.5,0.0,
     1 0.33333,0.33333,0.33333/
      END
      SUBROUTINE TIMES(A,B,C,LI,LJ,MI,MJ,NI,NJ,L,M,N,MM)
      IMPLICIT REAL*8 (A-H,O-Z)
      DIMENSION A(LI,LJ),B(MI,MJ),C(NI,NJ),D(36,36)
      IF(MM.NE.0) GO TO 15
      DO 1 I=1,L
      DO 1 J=1,M
      SUM = 0.0
      DO 4 K=1,N
    4 SUM = SUM + A(I,K)*B(K,J)
      D(I,J) = SUM
    1 CONTINUE
   20 DO 7 I=1,L
      DO 7 J=1,M
```

```
      15 DO 16 I=1,L
         DO 16 J=1,M
         SUM = 0.
         DO 17 K=1,N
      17 SUM = SUM + A(K,I)*B(K,J)
         C(I,J) = SUM
      16 CONTINUE
         GO TO 20
         END
         SUBROUTINE DXCPY(A,R,L,NR,MR,NA,MA,MS)
         REAL*8 A(1),R(1)
C
C     INITIALISE
C
         IR = 0
         L2 = L + NR - 1
         K2 = K + MR - 1
C
         DO 5 J=K,K2
         DO 5 I=L,L2
         IR = IR + 1
         R(IR) = 0.
C
C           LOCATE ELEMENT FOR ANY MATRIX STORAGE MODE
C
         CALL LOC(I,J,IA,NA,MA,MS)
C
C           TEST FOR ZERO ELEMENT IN DIAGONAL STORAGE
C
         IF(IA) 4,5,4
      4  R(IR) = A(IA)
      5  CONTINUE
         RETURN
         END
C        DIRCOS
         SUBROUTINE DIRECT(X,DIRCOS)
         IMPLICIT REAL*8 (A-H,O-Z)
         DIMENSION X(3,20),DIRCOS(3,3)
         SQRT(AX) = DSQRT(AX)
C
C   FORMS MATRIX TRANSFORMATION FROM GLOBAL TO LOCAL CO-ORDINATES
C
C   (GLOBAL) = (DIRCOS)*(LOCAL)
C
         DO 1 I = 1,3
         DO 1 J = 1,3
      1  DIRCOS(I,J)=0.0
         AA=(X(2,2)-X(1,2))*(X(3,3)-X(1,3))
        1 -((X(3,2)-X(1,2))*(X(2,3)-X(1,3)))
         AB = -((X(2,1)-X(1,1))*(X(3,3)-X(1,3)))
        1  +(X(3,1)-X(1,1))*(X(2,3)-X(1,3))
         AC =  (X(2,1)-X(1,1))*(X(3,2)-X(1,2))
        1 -((X(3,1)-X(1,1))*(X(2,2)-X(1,2)))
         IF((AA.GT.-.1E-12.AND.AA.LT.0.1E-12).AND.(AB.GT.-.1E-12.AND.AB.
        1  LT.0.1E-12)) GOTO 2
         AD=SQRT(AA*AA+AB*AB+AC*AC)
         AE=SQRT(AA*AA+AB*AB)
         DIRCOS(1,3)=AA/AD
```

```
      DIRCOS(1,1)=-AE/AE
      DIRCOS(2,1)=AA/AE
      DIRCOS(1,2)=-AA*AC/(AE*AD)
      DIRCOS(2,2)=-AE*AC/(AE*AD)
      DIRCOS(3,2)=(AA*AA+AB*AB)/(AE*AC)
       RETURN
    2 DO 3 I = 1,3
    3 DIRCOS(I,I) = 1.0
      RETURN
      END
      SUBROUTINE DTRN
      IMPLICIT REAL*8 (A-H,O-Z)
      COMMON / BEND / D(9),B(90)
      COMMON / STI / X(3,20),YOUNG(12),STUCK(36,36),STICK(36,36),
     1FORCE(36),INFO(20)
      DIMENSION TS(9),TE(9),DUMMY(9)
      DATA DUMMY/9*0./
      THETA = YOUNG(7)*3.14159265359/180.
      CALL DSETTF(TE,TS,THETA)
      CALL DMPRD(D,TE,DUMMY,3,3,0,0,3)
      CALL DTPRD(TS,DUMMY,D,3,3,0,0,3)
      RETURN
      END
      SUBROUTINE DSETTF(TE,TS,THETA)
      IMPLICIT REAL*8 (A-H,O-Z)
      DIMENSION TS(9),TE(9)
C
      C = DCOS(THETA)
      S = DSIN(THETA)
      TE(1) = C*C
      TE(4) = S*S
      TE(7) = S*C
      TE(2) = S*S
      TE(5) = C*C
      TE(8) = -TE(7)
      TE(3) = -C*S
      TE(6) = -TE(3)
      TE(9) = (C*C - S*S)/2.
C
      DO 10 I=1,9
   10 TS(I) = TE(I)
C
      DO 30 I=3,9,3
   30 TE(I) = TE(I) * 2.
C
      DO 20 I=7,9
   20 TS(I) = 2.*TS(I)
C
C  SETS MATRICES FOR TS.D.TE TRANSFORMATION.
C   EXISTING MATRICES TRANSFORM ANTICLOCKWISE.
C     THETA MUST BE GIVEN ANTICLOCKWISE FROM THE ELEMENT AXES
C
      RETURN
      END
      SUBROUTINE BSTIFF
C
C
      IMPLICIT REAL*8 (J,L)
```

```
      COMMON / PROB / E1,E2,PR1,PR2,GF,GC
      COMMON / STI / X(3,20),YOUNG(12),STUCK(36,36),STICK(36,36),
     1FORCE(36),INFO(20),XY(3,3)
      COMMON / THREE / ELPA(10000) ,  EL(2000),FL(1000),VALUE(20),
     1 ELCOR(3,20),STIF(12,20)
      DIMENSION BST(10,10),TRN(10,10),ST(10,10)
      INTEGER IK,JK,KK,LK,IT,KKK,LLK
C
C
C
C   STIFFENING OF PANEL EDGE USING EDGE BEAM
C
C
C
C
      IN=INFO(15)
      IT=INFO(16)
      ABEAM=STIF(1,IN)
      EBEAM=STIF(2,IN)
      G=STIF(3,IN)
      SMA=STIF(4,IN)
      J=STIF(5,IN)
      D=AC-F
      XA=XY(2,1)-XY(1,1)
      XB=XY(2,2)-XY(1,2)
      XC=XY(3,1)-XY(2,1)
      XD=XY(3,2)-XY(2,2)
      XE=XY(3,1)-XY(1,1)
      XF=XY(3,2)-XY(1,2)
      IF(INFO(17).EQ.142) L=0.5*(XA*XA+XB*XB)**0.5
      IF(INFO(17).EQ.253) L=0.5*(XC*XC+XD*XD)**0.5
      IF(INFO(17).EQ.163) L=0.5*(XE*XE+XF*XF)**0.5
      WRITE(6,100) L,D,ABEAM,EBEAM,G,SMA,J
  100 FORMAT(1H0,3X,7D13.5)
C
C     CALCLLATE BEAM STIFFNESS CONTRIBUTIONS
C
      AS=EBEAM*ABEAM/L+(4.0*EBEAM*SMA)/(D*D*L)
      BS=-(6.0*EBEAM*SMA)/(D*L*L)
      CS=(2.0*EBEAM*SMA)/(D*D*L)
      DS=EBEAM*ABEAM/L+(2.0*EBEAM*SMA)/(D*D*L)
      ES=-(G*J)/(D*D*L)
      FS=(12.0*EBEAM*SMA)/(L*L*L)
      WRITE(6,101) AS,BS,CS,DS,ES,FS
  101 FORMAT(1HC,3X,6D13.5)
C
C     FORM BEAM STIFFNESS MATRIX
C
      DO 10 IK=1,10
      DO 10 JK=1,10
   10 BST(IK,JK)=0.0
      BST(1,1)=AS
      BST(1,3)=-BS
      BST(1,4)=-2.0*CS
      BST(1,6)=-DS
      BST(1,8)=BS
      BST(1,9)=CS
      DO 11 IK=3,9
```

```
      BST(2,5)=ES
      BST(2,7)=ES
      BST(2,10)=-ES
      DO 12 IK=5,10
   12 BST(IK,2)=BST(2,IK)
      BST(3,3)=FS
      BST(3,4)=BS
      BST(3,6)=BS
      BST(3,8)=-FS
      BST(3,9)=-BS
      DO 13 IK=4,9
   13 BST(IK,3)=BST(3,IK)
      BST(4,4)=2.0*CS
      BST(4,6)=CS
      BST(4,8)=-BS
      BST(4,9)=-CS
      DO 14 IK=6,9
   14 BST(IK,4)=BST(4,IK)
      BST(5,5)=-ES
      BST(5,7)=-ES
      BST(5,10)=ES
      BST(7,5)=-ES
      BST(10,5)=ES
      DO 15 IK=1,5
      JK=IK+5
      DO 15 KK=1,5
      LK=KK+5
   15 BST(JK,LK)=BST(IK,KK)
      WRITE(6,102) ((BST(IK,JK),JK=1,10),IK=1,10)
  102 FORMAT(/3X,10D13.5)
C
C     FORM TRANSFORMATION MATRIX
C
      IF(STIF(2,IT).EQ.1.0) GOTO 99
      DO 16 IK=1,10
      DO 16 JK=1,10
   16 TRN(IK,JK)=0.0
C     SINE THETA=STIF(1,IT) , COSINE THETA=STIF(2,IT)
      TRN(1,1)=STIF(2,IT)
      TRN(1,2)=-STIF(1,IT)
      TRN(2,1)=STIF(1,IT)
      TRN(2,2)=STIF(2,IT)
      TRN(3,3)=1.0
      TRN(4,4)=TRN(1,1)
      TRN(4,5)=TRN(1,2)
      TRN(5,4)=TRN(2,1)
      TRN(5,5)=TRN(2,2)
      DO 18 IK=1,5
      DO 18 JK=1,5
      KK=IK+5
      LK=JK+5
   18 TRN(KK,LK)=TRN(IK,JK)
      WRITE(6,102) ((TRN(IK,JK),JK=1,10),IK=1,10)
C
C     TRANSFORMATION OF BEAM STIFFNESS MATRIX TO PANEL COORDINATES
C
      DO 19 IK=1,10
      DO 19 JK=1,10
```

```
      DO 21 JK=1,10
      SUM=0.0
      DO 22 KK=1,10
   22 SUM=SUM+TRN(IK,KK)*BST(KK,JK)
   21 ST(IK,JK)=SUM
   20 CONTINUE
      DO 23 IK=1,10
      DO 23 JK=1,10
   23 BST(IK,JK)=0.0
      DO 24 IK=1,10
      DO 25 JK=1,10
      SUM=0.0
      DO 26 KK=1,10
   26 SUM=SUM+ST(IK,KK)*TRN(JK,KK)
   25 BST(IK,JK)=SUM
   24 CONTINUE
      WRITE(6,102) ((BST(IK,JK),JK=1,10),IK=1,10)
   99 CONTINUE
C
CC    POST BEAM STIFFNESSES INTO STUCK
C
      IF(INFO(17).EQ.142) GOTO 27
      IF(INFO(17).EQ.253) GOTO 28
      IF(INFO(17).EQ.163) GOTO 29
C
CC    EDGE 1-4-2 STIFFENED
C
   27 DO 30 IK=1,5
      DO 30 JK=1,5
      KK=IK+5
      LK=JK+5
      KKK=IK+15
      LLK=JK+15
      STUCK(IK,JK)=STUCK(IK,JK)+BST(IK,JK)
      STUCK(IK,LLK)=STUCK(IK,LLK)+BST(IK,LK)
      STUCK(KK,LK)=STUCK(KK,LK)+BST(KK,LK)
      STUCK(KK,LLK)=STUCK(KK,LLK)+BST(KK,JK)
      STUCK(KKK,JK)=STUCK(KKK,JK)+BST(KK,JK)
      STUCK(KKK,LK)=STUCK(KKK,LK)+BST(IK,LK)
   30 STUCK(KKK,LLK)=STUCK(KKK,LLK)+BST(IK,JK)+BST(KK,LK)
      GOTO 31
   28 CONTINUE
C
CC    EDGE 2-5-3 STIFFENED
C
      DO 32 IK=1,5
      DO 32 JK=1,5
      KI=IK+5
      KJ=JK+5
      KK=IK+10
      LK=JK+10
      KKK=IK+20
      LLK=JK+20
      STUCK(KI,KJ)=STUCK(KI,KJ)+BST(IK,JK)
      STUCK(KI,LLK)=STUCK(KI,LLK)+BST(IK,KJ)
      STUCK(KK,LK)=STUCK(KK,LK)+BST(KI,KJ)
      STUCK(KK,LLK)=STUCK(KK,LLK)+BST(KI,JK)
      STUCK(KKK,KJ)=STUCK(KKK,KJ)+BST(KI,JK)
```

```
      GOTO 31
   29 CONTINUE
C
C     EDGE 1-6-3 STIFFENED
C
      DO 32 IK=1,5
      DO 33 JK=1,5
      KI=IK+5
      KJ=JK+5
      KL=IK+10
      KM=JK+10
      KK=IK+15
      LK=JK+15
      KKK=IK+25
      LLK=JK+25
      STUCK(IK,JK)=STUCK(IK,JK)+BST(KI,KJ)
      STUCK(IK,LLK)=STUCK(IK,LLK)+BST(KI,JK)
      STUCK(KL,KM)=STUCK(KL,KM)+BST(IK,JK)
      STUCK(KL,LLK)=STUCK(KL,LLK)+BST(IK,KJ)
      STUCK(KKK,JK)=STUCK(KKK,JK)+BST(IK,KJ)
      STUCK(KKK,KM)=STUCK(KKK,KM)+BST(KI,JK)
   33 STUCK(KKK,LLK)=STUCK(KKK,LLK)+BST(IK,JK)+BST(KI,KJ)
   31 CONTINUE
      WRITE(6,103) ((STUCK(IK,JK),JK=1,30),IK=1,30)
      WRITE(6,103) ((STICK(IK,JK),JK=1,30),IK=1,6)
  103 FORMAT(1HO,3(/3X,10D13.5))
      RETURN
      END
END OF FILE
```

## APPENDIX II

### Program for the Solution of Forces and Strains in Edgebeams

#### II.i Introduction

Having determined the displacements for the various elements used in the finite element analysis of a dome, section 8.0, it was required to determine the forces in the edgebeams used to stiffen that dome's gable edges.

Program BFORCE solves for the forces and strains in the edgebeams using the displacements derived during the finite element analysis of the dome.

Strains:- $\frac{\partial u}{\partial x}$ , $-\frac{\partial^2 w}{\partial x^2}$ , $-\frac{\partial^2 w}{\partial y \partial x}$

Forces:- $P_x$ , $M_y$ , $T_x$

where; x, y and z are the axes of the beam's local coordinate system (Fig. I.i).

The above forces and strains are calculated from the global displacements $U_{TF}$, $V_{TF}$, $W_{TF}$, $U_{BF}$, $V_{BF}$ at the two nodes of each beam element in the overall finite element analysis, (Fig. I.i, Section 8.0), (i.e. global displacements are taken to be in terms of the sandwich panel element's degrees of freedom and local coordinate system).

The forces and strains for the edgebeams are calculated using the following relationships:-

$$\{\varepsilon\} = [B]\{q\}$$

$$\{\sigma\} = [C][B]\{q\}$$

where $\{\varepsilon\}$ Vector of strains at any point within the element

$\{\sigma\}$ Vector of stresses at any point within the element

$\{q\}$ Vector of nodal displacements

$[B]$ Strain-displacement matrix for interpolation models

$[C]$ Stress-Strain matrix

II.ii Input

The data input to the program is contained on the following set of cards:

Card 1 reads in the length of each beam element, the sandwich panel thickness, the area of the beam section, the second moment of area of the beam, the polar second moment of area of the beam, the elastic modulus of the beam, and the modulus of rigidity of the beam, (all beam elements are assumed to have the same geometric and elastic properties).

[Format 7D10.6]

Card 2 reads in the element number and the element type, of the individual panel element

[Format 2I5]

Notes: 1. The first element in a new panel is element type (ELTYP) 1,
all subsequent elements in that panel are element type (ELTYP) 2

2. To terminate the execution of the program both element number (ELNO), and element type (ELTYP) are set to 0

Cards 3, 4 and 5 read in the transformation matrix $[T]$ for the element, (Fig. II.i). These cards are only required if the element is element

type 1, [ELTYP = 1].

[Format 3D10.6]

Cards 6,7 and 8 read in the global displacements, (Fig. II.ii), of the individual panel element.

[Format (2(6D10.6/), 3D10.6)]

Example of the data that would be input, if the edge of a sandwich panel element which contained node numbers 1, 7 and 3, was stiffened by an edgebeam:

$U_1$, $U_2$, $U_3$, $U_4$, $U_7$, $U_8$

$V_1$, $V_2$, $V_3$, $V_4$, $V_7$, $V_8$

$W_1$, $W_3$, $W_7$

II.iii Output

The data that would be output by the program is shown below for an example, where the edge of a sandwich panel element which contained node numbers 1, 7 and 3, was stiffened by an edgebeam:

Strains

$$\frac{\partial u}{\partial x_{17}}, -\frac{\partial^2 w}{\partial x_{17}^2}, -\frac{\partial^2 w}{\partial y \partial x_{17}}, \quad \frac{\partial u}{\partial x_{71}}, -\frac{\partial^2 w}{\partial x_{71}^2}, -\frac{\partial^2 w}{\partial y \partial x_{71}}$$

$$\frac{\partial u}{\partial x_{73}}, -\frac{\partial^2 w}{\partial x_{73}^2}, -\frac{\partial^2 w}{\partial y \partial x_{73}}, \quad \frac{\partial u}{\partial x_{37}}, -\frac{\partial^2 w}{\partial x_{37}}, -\frac{\partial^2 w}{\partial y \partial x_{37}}$$

Forces

$$P_{x_{17}}, \quad M_{y_{17}}, \quad T_{x_{17}}, \quad P_{x_{71}}, \quad M_{y_{71}}, \quad T_{x_{71}}$$

$$P_{x_{73}}, \quad M_{y_{73}}, \quad T_{x_{73}}, \quad P_{x_{37}}, \quad M_{y_{37}}, \quad T_{x_{37}}$$

FIG. II·i

## Transformation from beam element's local coordinate system to panel element's local coordinate system

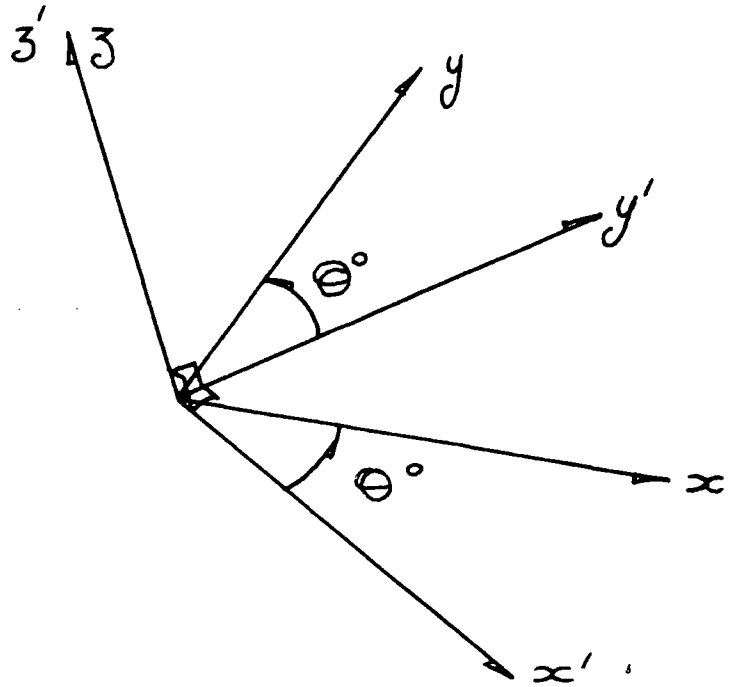


$x'y'z'$ panel element local coordinates
$xyz$ beam element local coordinates
$\Theta^\circ$ transformation angle

## Transformation Matrix [T]

$$\{P'\} = [T] \times \{P\}$$

$$\begin{bmatrix} P_x' \\ P_y' \\ P_3' \end{bmatrix} = \begin{bmatrix} \cos\Theta & -\sin\Theta & \\ \sin\Theta & \cos\Theta & \\ & & 1.0 \end{bmatrix} \begin{bmatrix} P_x \\ P_y \\ P_3 \end{bmatrix}$$

## Global Displacements

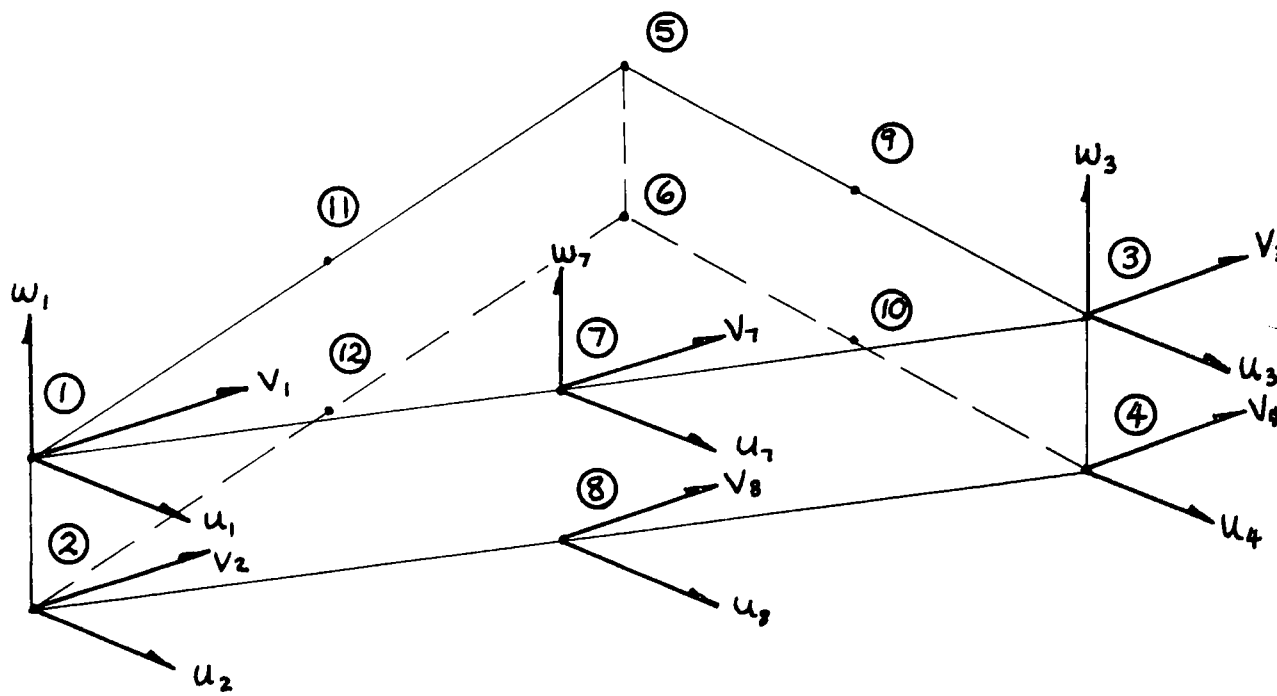


① - ⑫ Node Numbers

## II.iv Listing Program BFORCE

### Program for the Solution of Forces and Strains in Edgebeams

```
      C       PROGRAM FOR THE SOLUTION OF FORCES AND STRAINS IN EDGEBEAMS
      C       TO BE USED IN CONJUNCTION WITH QUADIS AND IRONSEIS
      C
              IMPLICIT REAL*8 (A-H,O-Z)
              DIMENSION T1(3,3),T2(15,15),T3(15,15),E(12,15),X(15),XL(15),XB(15)
             1,E(12),P(12),C(12,12)
              INTEGER ELNO,ELTYP
              WRITE(6,110)
      110     FORMAT(1HO,5X,'STRAINS AND FORCES IN EDGEBEAMS',///)
      C
      C       READS IN BEAM PROPTIES
      C
              READ(5,99) S17,C,AREA,SMA,BJ,EE,GE
       99     FORMAT(7D10.6)
       30     READ(5,100) ELNO,ELTYP
      100     FORMAT(2I5)
              IF(ELNO.EQ.0.AND.ELTYP.EQ.0) GOTO 40
              IF(ELTYP.EQ.2) GOTO 1
      C
      C       READ IN TRANSFORMATION MATRIX FOR EACH NEW PANEL
      C
              READ(5,101) ((T1(I,J),I=1,3),J=1,3)
      101     FORMAT(3D10.6)
      C
      C       SET 'B' MATRIX UP FOR NEW PANEL
      C
              DO 15  I=1,12
              DO 15  J=1,15
       15     B(I,J)=0.0
              AA=1.0/S17
              B(1,1)=AA
              B(1,3)=-AA
              B(2,7)=6.0*AA*AA
              B(2,9)=-6.0*AA*AA
              B(2,13)=-4.0*AA*AA
              B(2,15)=2.0*AA*AA
              B(3,10)=-AA
              B(3,12)=AA
              B(7,2)=-AA
              B(7,3)=AA
              B(8,9)=6.0*AA*AA
              B(8,8)=-6.0*AA*AA
              B(8,14)=2.0*AA*AA
              B(8,15)=-4.0*AA*AA
              B(9,11)=AA
              B(9,12)=-AA
              B(4,1)=-AA
              B(4,2)=AA
              B(5,7)=-6.0*AA*AA
              B(5,9)=6.0*AA*AA
              B(5,13)=2.0*AA*AA
              B(5,15)=-4.0*AA*AA
              B(6,10)=AA
              B(6,12)=-AA
              B(10,2)=AA
              B(10,3)=-AA
              B(11,8)=6.0*AA*AA
              B(11,9)=-6.0*AA*AA
              B(11,14)=-4.0*AA*AA
```

```
      E(12,12)=AA
      WRITE(6,112) ((E(I,J),J=1,15),I=1,12)
C
C     SET 'C' MATRIX UP FOR NEW PANEL
C
      DO 20 I=1,12
      DO20 J=1,12
   20 C(I,J)=0.0
      C(1,1)=EE*AREA
      C(2,2)=EB*SMA
      C(3,3)=GB*BJ
      DO 50 I=4,10,3
      J=I+1
      K=I+2
      C(I,I)=C(1,1)
      C(J,J)=C(2,2)
   50 C(K,K)=C(3,3)
    1 CONTINUE
C
C     READ IN GLOBAL DISPLACEMENTS
C
      READ(5,102) (X(I),I=1,15)
  102 FORMAT(2(6D10.6/),3D10.6)
      DO 2 I=1,15
      DO 2 J=1,15
    3 T2(I,J)=0.0
    2 T2(I,I)=1.0
      DO 4 I=1,5,2
      T2(I,I)=T1(1,1)
    4 T2(I+1,I+1)=T1(1,1)
      DO 5 I=7,11,2
      T2(I,I)=T1(2,2)
    5 T2(I+1,I+1)=T1(2,2)
      DO 6 I=1,5,2
      J=I+6
      T2(I,J)=T1(1,2)
      T2(I+1,J+1)=T1(1,2)
      T2(J,I)=T1(2,1)
    6 T2(J+1,I+1)=T1(2,1)
      J=13
      DO 7 I=1,5,2
      K=I+6
      T2(I,J)=T1(1,3)
      T2(I+1,J)=T1(1,3)
      T2(K,J)=T1(2,3)
      T2(K+1,J)=T1(2,3)
    7 J=J+1
C
C     CALCULATE DISPLACEMENTS IN ELEMENT'S LOCAL COORDINATES
C
      DO 8 J=1,15
      SUM=0.0
      DO 9 K=1,15
    9 SUM=SUM+T2(J,K)*X(K)
    8 XL(J)=SUM
      WRITE(6,112) (XL(I),I=1,15)
  112 FORMAT(//5X,6E15.5/,5X,6E15.5/,5X,3E15.5/)
C
```

```
      C
            DO 13 I=1,15
            DO 13 J=1,15
            T3(I,J)=0.0
         13 CONTINUE
            DO 14 I=1,6
            K=I*2
            L=K-1
            T3(I,L)=0.5
         14 T3(I,K)=0.5
            T3(7,13)=1.0
            T3(8,14)=1.0
            T3(9,15)=1.0
            AD=-1.0/D
            T3(10,7)=AD
            T3(10,8)=-AD
            T3(11,9)=AD
            T3(11,10)=-AD
            T3(12,11)=AD
            T3(12,12)=-AD
            T3(13,1)=-AD
            T3(13,2)=AD
            T3(14,3)=-AD
            T3(14,4)=AD
            T3(15,5)=-AD
            T3(15,6)=AD
            IF(ELTYP.EQ.1) WRITE(6,112) ((T3(I,J),J=1,15),I=1,15)
      C
      C     CALCULATE  DEFLECTIONS IN TERMS OF BEAMS DEGREES OF FREEDOM
      C
            DO 18 I=1,15
            SUM=0.0
            DO 19 J=1,15
         19 SUM=SUM+T3(I,J)*XL(J)
         18 XB(I)=SUM
            WRITE(6,112) (XB(I),I=1,15)
      C
      C     CALCULATE AND WRITE STRAINS
      C
            DO 16 I=1,12
            SUM=0.0
            DO 17 J=1,15
         17 SUM=SUM+E(I,J)*XE(J)
         16 E(I)=SUM
            WRITE(6,103) ELNO
        103 FORMAT(///,5X,'ELEMENT NO. .. ',I5///,5X,'STRAINS IN EDGEBEAMS')
            WRITE(6,104) (E(I),I=1,12)
        104 FORMAT(///5X,6E15.5/,5X,6E15.5)
      C
      C     CALCULATE AND WRITE FORCES
      C
            DO 21 I=1,12
         21 F(I)=C(I,I)*E(I)
            WRITE(6,105) (F(I),I=1,12)
        105 FORMAT(///5X,'FORCES IN EDGEBEAMS',///5X,6E15.5/,5X,6E15.5)
            GOTO 30
         40 CONTINUE
            END
END OF FILE
```